Unstructured Adiabatic Quantum Optimization

Thesis submitted in partial fulfillment
of the requirements for the degree of

Master of Science in Computer Science and Engineering by Research

by

Alapan Chaudhuri
2019111023
alapan.chaudhuri@research.iiit.ac.in

Centre for Quantum Science and Technology (CQST)
International Institute of Information Technology (IIIT)
Hyderabad - 500032, India
February 2026

International Institute of Information Technology
Hyderabad, India

CERTIFICATE

It is certified that the work contained in this thesis, titled "Unstructured Adiabatic Quantum Optimization" by Alapan Chaudhuri, has been carried out under my supervision and is not submitted elsewhere for a degree.

_____ _____

Date Adviser: Prof. Indranil Chakrabarty

_____ _____

Date Co-Adviser: Prof. Shantanav Chakraborty

To a world that feels like it's splitting apart.
May we keep repairing what we can.

Abstract

Acknowledgement

Contents

List of Theorems

List of Algorithms

List of Figures

Chapter 1

Introduction

Chapter 2

Physics and Computation

Three people walk into a room with the same problem. A logistics manager needs the shortest route through a hundred cities. A physicist needs the lowest energy state of a hundred interacting spins. A computer scientist needs to prove that no algorithm can find the answer faster than brute search. They are all navigating the same exponentially large space of configurations, and they will all get stuck in the same ways. But they will formalize the problem differently, and that difference will determine what each of them can prove.

This chapter builds the vocabulary that makes that claim precise. The path runs from physics through complexity theory to the adiabatic mechanism, and each piece earns its place by answering a question the previous piece leaves open.

2.1 Reality

The reach of a proof is bounded by the formalization behind it. Choosing a formalization means committing to which aspects of physical reality the mathematics captures. This thesis needs one such commitment. Mathematics models regularities in the physical world but does not replace the world itself.

The consequence is immediate. A complexity claim is meaningful only after the computational model and the resource accounting are fixed. If access to the input changes, if precision demands change, or if the available control primitives change, the same task can move from easy to hard. Hardness is not an intrinsic property of a problem. It is a joint property of the problem, the model, and the resources being counted.

A concrete example makes this vivid. Finding the minimum of a function $f : \{0,1\}^n \to \mathbb{R}$ with no promise about its structure requires checking nearly every input in the worst case. In a classical query model this costs $\Theta(2^n)$ evaluations. In a quantum query model the same task costs $\Theta(2^{n/2})$ evaluations [1, 2]. The function did not change. The counting of resources did not change. Only the model of computation changed, and with it the sharp boundary between efficient and inefficient.

The dependence on model choice will recur throughout this thesis. Physical assumptions determine a computational model. The model determines a resource accounting. And the resource accounting supports, or fails to support, a complexity claim. Chapters 3 and 4 will put this chain under pressure. The optimization objective stays fixed while the computational model shifts from query circuits to continuous Hamiltonian evolution.

2.2 Physics

The modeling chain begins with physics, and physics contributes a single object that will persist through every chapter of this thesis: the Hamiltonian. Energy plays a double role. It generates the dynamics of a system, and it simultaneously defines what it means for a configuration to be preferred. This double role is what connects physics to optimization.

In classical mechanics, a system with f degrees of freedom lives in a phase space of generalized coordinates $q_1, \ldots, q_f$ and conjugate momenta $p_1, \ldots, p_f$. The Hamiltonian $H_{\mathrm{cl}}(q,p)$ determines the full time evolution through Hamilton's equations

$$\dot{q}_j = \frac{\partial H_{\mathrm{cl}}}{\partial p_j}, \qquad \dot{p}_j = -\frac{\partial H_{\mathrm{cl}}}{\partial q_j}. \tag{2.2.1}$$

The rate of change of each variable is set by how the energy depends on its conjugate. The Hamiltonian does not merely label states by their energy. It generates the flow that carries one state to the next.

Statistical mechanics introduces the second role. When a system is coupled to a heat bath at temperature T, the probability of finding it in configuration z is not uniform. Low-energy configurations are exponentially preferred. For a cost profile $C(z)$ and inverse temperature $\beta = 1/(k_B T)$, the Gibbs distribution assigns probabilities

$$\pi_\beta(z) = \frac{e^{-\beta C(z)}}{Z_\beta}, \qquad Z_\beta = \sum_z e^{-\beta C(z)}. \tag{2.2.2}$$

As $\beta \to \infty$, mass concentrates on the minimizers of C. The mechanism is direct. For any non-optimal configuration z, the ratio $\pi_\beta(z)/\pi_\beta(z^*) = e^{-\beta(C(z)-C_{\min})}$ vanishes exponentially as β grows. Finding the ground state is what thermal equilibrium does at zero temperature. The partition function Z_β encodes the full thermodynamic content of the system, and evaluating it turns out to be, in general, computationally hard. Section 2.4 will make that precise.

Quantum mechanics preserves the Hamiltonian as generator but changes the arena. The state is now a unit vector $|\psi\rangle$ in a Hilbert space, the Hamiltonian is a Hermitian operator, and with $\hbar = 1$ the evolution law is

$$i\frac{d}{dt}|\psi(t)\rangle = H(t)\,|\psi(t)\rangle\,. \tag{2.2.3}$$

The ground state of H is its minimum-energy eigenstate, and finding it is the quantum analogue of minimizing a cost function. The eigenvalue structure of the Hamiltonian, specifically the spectral gap between the ground state and the first excited state, will turn out to control how long an adiabatic algorithm must run. Sections 2.5 and 2.7 develop this connection.

2.3 Computation

The spectral gap determines how long the adiabatic algorithm runs. But "long" needs a yardstick, and that yardstick comes from complexity theory, the precise framework for measuring hardness across computational models. Without it, saying that an adiabatic algorithm is fast or slow would be meaningless.

The baseline model is the Turing machine [3]. A language $L \subseteq \{0,1\}^*$ is decidable if some Turing machine halts on every input and accepts exactly the strings in L. Decidability separates what can be computed from what cannot. The Church–Turing thesis asserts that every physically realizable computation can be performed by a Turing machine. The extended Church–Turing thesis goes further, adding an efficiency claim that every physically realizable computation can be simulated by a probabilistic classical machine with at most polynomial overhead [3]. Quantum computation challenges this efficiency claim while leaving computability untouched [4, 5]. Whether the challenge succeeds is the question this thesis addresses in the setting of unstructured optimization.

With the model fixed, "efficient" means polynomial time.

Definition 2.3.1 (Class P)**.** *A decision problem is in* P *if a deterministic Turing machine solves it in time polynomial in input length.*

Evaluating a cost function $C(z)$ at a given z is typically in P by direct substitution. But minimizing C over all of $\{0,1\}^n$ appears to require searching an exponentially large space. Boolean satisfiability makes the difficulty concrete. A 3-SAT formula has the form

$$F(x_1, \ldots, x_n) = \bigwedge_{j=1}^{m} (\ell_{j,1} \vee \ell_{j,2} \vee \ell_{j,3}), \tag{2.3.1}$$

with each literal $\ell_{j,k}$ being either x_i or $\overline{x}_i$. Given a candidate assignment x, checking whether $F(x) = 1$ takes time linear in the formula, since one need only evaluate each clause and confirm all are satisfied. A first-year student can verify a solution. But finding a satisfying assignment from scratch, or proving that none exists, appears to require effort that grows exponentially with n. This asymmetry between finding and checking is not an accident of 3-SAT. It is the heart of the P versus NP question.

Definition 2.3.2 (Class NP)**.** *A decision problem is in* NP *if every yes-instance has a certificate of length polynomial in the input that can be verified in polynomial time by a deterministic Turing machine.*

Every problem in P is also in NP, since an efficient algorithm can serve as its own verifier. The converse, whether P = NP, is the most famous open problem in theoretical computer science. The strong consensus is that P $\neq$ NP, but this remains unproved after more than fifty years.

What makes 3-SAT remarkable is not just that it appears hard, but that it captures the full difficulty of NP. Cook proved that every efficiently verifiable problem can be translated into an instance of SAT through

a polynomial-time computable function that preserves yes and no answers [6]. Such a function is called a reduction. It converts one problem into another while preserving the answer.

Definition 2.3.3 (Polynomial-time many-one reduction)**.** *For decision problems A and B, write $A \leq_p B$ if there exists a polynomial-time computable function r such that*

$$x \in A \iff r(x) \in B. \tag{2.3.2}$$

A reduction from A to B means that B is at least as hard as A. Any algorithm for B immediately yields one for A by composing with r, so hardness flows upward through a hierarchy of problems. A problem to which all of NP reduces is NP-hard; if it also lies in NP, it is NP-complete. Cook proved that SAT is NP-complete; Karp then showed that many combinatorial problems, including 3-SAT, are NP-complete through polynomial reductions [7]. Solving any one of them in polynomial time would collapse the entire class. The hardness reductions in Chapter 8 of this thesis begin from exactly this problem.

The point of contact with optimization is threshold decision. Given a cost function C and a threshold τ, ask whether there exists z with $C(z) \leq \tau$. For 3-SAT, this asks whether the minimum number of violated clauses is at most τ. If this threshold language is NP-hard, no generic polynomial-time algorithm can minimize C over all instances, unless P = NP. The adiabatic algorithm's task is precisely this minimization. The complexity classes just defined measure how hard that task is.

2.4 The #P Complexity Class

There is a subtlety the decision framework misses. The spectral parameters that control adiabatic runtime in Chapters 5 through 8 depend on the degeneracies $\{d_k\}$ and energy gaps $\{E_k - E_0\}$ of the problem Hamiltonian. Computing these parameters to the precision the algorithm requires can be #P-hard (Chapter 8). The issue is not just whether a solution exists, but how many solutions exist. For the spectral quantities that govern this thesis, counting is the operative difficulty.

Two Boolean formulas might both be satisfiable, but one could have a single satisfying assignment while the other has exponentially many. A decision algorithm cannot distinguish the two cases. A counting algorithm must, and counting turns out to be a fundamentally harder task.

Definition 2.4.1 (Class #P)**.** *A function $f : \{0,1\}^* \to \mathbb{N}$ is in #P if there exists a nondeterministic polynomial-time Turing machine M such that $f(x)$ equals the number of accepting branches of M on input x.*

Valiant introduced #P and established the hardness of canonical counting problems [8]. The standard example is

$$\#\mathrm{SAT}(F) = \left|\{x \in \{0,1\}^n : F(x) = 1\}\right|. \tag{2.4.1}$$

Decision SAT asks whether this count is nonzero. But computing the exact count is far harder. #P is at least as hard as every class in the polynomial hierarchy [9, 3], placing counting strictly above NP-hard decision problems in a strong structural sense. The permanent of a 0-1 matrix is the canonical example. Computing it is #P-complete [8], yet the closely related determinant is computable in polynomial time. A single sign change in the summation separates efficient computation from intractability.

The ground-state degeneracy $d_0 = |\{z : C(z) = C_{\min}\}|$ is exactly such a counting object. Adiabatic runtime depends on the full degeneracy spectrum through spectral parameters defined in Chapter 5. Chapter 8 proves that approximating the key parameter A_1 to additive precision $\varepsilon < 1/(72(n-1))$ is NP-hard. The #P-hardness result is stronger. Given $O(\mathrm{poly}(n))$ exact oracle queries to the spectral parameter, polynomial interpolation suffices to extract the degeneracy d_0. Since computing d_0 is #P-hard, near-exact estimation at precision $\varepsilon \in O(2^{-\mathrm{poly}(n)})$ inherits #P-hardness [10].

2.5 Spectral Complexity

Counting complexity enters quantum dynamics not through the evolution equation but through the spectrum. The Schrödinger equation (2.2.3) is linear in the state vector, without approximation. For a time-independent Hamiltonian it has the explicit solution $|\psi(t)\rangle = e^{-iHt}|\psi(0)\rangle$, and even for time-dependent Hamiltonians the evolution remains a linear map on $\mathcal{H}$. One might expect that linearity implies computational simplicity. It does not.

The difficulty resides not in the evolution equation but in the spectrum. Consider an interpolation $H(s) = (1-s)H_0 + sH_z$ between an initial Hamiltonian H_0 (whose ground state is easy to prepare; Chapter 4 specifies

the concrete choice) and a problem Hamiltonian H_z diagonal in the computational basis, with s ranging from 0 to 1. As s varies, the eigenvalues of $H(s)$ trace curves. When two of these curves approach each other, they generically do not cross. Instead they undergo an avoided crossing. The curves repel, reaching a minimum separation before diverging again (Figure 2.1). The width of this avoided crossing and the value of s at which it occurs depend on the global structure of both Hamiltonians. For an n-qubit problem Hamiltonian with up to 2^n eigenvalues, the crossing geometry is determined by the full set of energies and degeneracies.

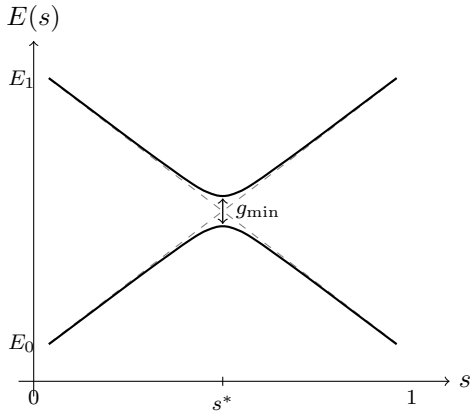

Figure 2.1: Avoided crossing in the spectrum of $H(s) = (1-s)H_0 + sH_z$. Dashed lines show the eigenvalues that would result if the two Hamiltonians did not couple; they cross at $s = s^*$. Solid curves show the actual eigenvalues, which repel near the would-be crossing. The minimum gap $g_{\min}$ sets the internal timescale of the quantum system: Section 2.7 makes precise how it controls runtime.

This is where computational hardness enters. Small perturbations to a Hamiltonian can rearrange its eigenvalue structure entirely. Spectral gaps can close exponentially, avoided crossings can narrow or widen, degenerate subspaces can split. These spectral rearrangements control algorithmic runtime, and predicting them is NP-hard in general (Chapter 8). The interpolation between two Hamiltonians can be written in a single line. The location and width of the avoided crossing that controls the adiabatic algorithm's runtime depends on the full eigenvalue structure of the problem Hamiltonian, a structure that can itself be computationally hard to characterize. The evolution is simple. The geometry it must navigate is not.

2.6 Optimization

The translation from combinatorial cost function to energy spectrum is exact. It requires no relaxation or rounding, and preserves every feature that makes the problem hard.

Write the optimization objective as

$$\min_{z\in\{0,1\}^n} C(z), \tag{2.6.1}$$

and define the diagonal Hamiltonian

$$H_z = \sum_{z\in\{0,1\}^n} C(z)\,|z\rangle\langle z|\,. \tag{2.6.2}$$

The ground states of H_z are exactly the minimizers of C. The combinatorial objective has become an energy spectrum, and finding the optimum has become finding the ground state.

For SAT, the encoding is explicit. Let $\chi_j(x) \in \{0,1\}$ indicate whether assignment x satisfies clause j, and define the penalty function

$$C_F(x) = \sum_{j=1}^{m}\big(1-\chi_j(x)\big). \tag{2.6.3}$$

Then F is satisfiable if and only if $\min_x C_F(x) = 0$. Each unsatisfied clause contributes a unit penalty, so C_F counts the number of violations.

Counting resurfaces at the optimum. If $C_{\min}$ denotes the minimum cost, the ground-state degeneracy is

$$d_0 = \left|\{z \in \{0,1\}^n : C(z) = C_{\min}\}\right|. \tag{2.6.4}$$

Even an algorithm that outputs a single optimizer has runtime that depends, through the spectral structure of H_z, on how many optimizers exist. The spectral parameters controlling adiabatic runtime (defined in Chapter 5)

are functions of the complete set of degeneracies $\{d_k\}$ and energy gaps $\{E_k - E_0\}$. A single-solution algorithm cannot escape the influence of a counting object.

A canonical hard family illustrating the encoding is the Ising model on a graph $G = (V, E)$

$$H_\sigma = \sum_{(i,j)\in E} J_{ij}\sigma_z^i\sigma_z^j + \sum_{j=1}^{n} h_j\sigma_z^j, \tag{2.6.5}$$

where σ_z^j is the Pauli-Z operator on site j (Chapter 3 develops the formalism), the first sum runs over edges of G with couplings J_{ij}, and the second sum includes local fields h_j. Many NP-hard combinatorial objectives map directly to this form [11, 12]. Weighted MaxCut provides a transparent example. For $x_i \in \{0, 1\}$, the cut value is

$$C_{\text{cut}}(x) = \sum_{(i,j)\in E} w_{ij}(x_i \oplus x_j), \tag{2.6.6}$$

and under the spin substitution $\sigma_i = (-1)^{x_i}$ this becomes

$$C_{\text{cut}}(\sigma) = \frac{1}{2}\sum_{(i,j)\in E} w_{ij}(1 - \sigma_i\sigma_j). \tag{2.6.7}$$

Under the correspondence $J_{ij} = -w_{ij}/2$ and $h_j = 0$, the total weight of edges crossing the cut becomes an antiferromagnetic Ising interaction energy. Any graph optimization objective expressible as pairwise interactions maps to an Ising model with no auxiliary variables, making the spectral analysis of Chapter 5 directly applicable. Combinatorial objectives and spin Hamiltonians are the same mathematical object. The encoding was introduced in the adiabatic context by Farhi et al. [13, 14], and it means that any NP-hard optimization objective can be attacked with Hamiltonian methods. Runtime analysis then reduces entirely to the spectral analysis of H_z, which is the subject of Sections 2.7 and 2.8.

2.7 Adiabaticity

The Hamiltonian H_z encodes the cost function. What remains is a mechanism for finding its ground state without knowing the answer in advance. The mechanism this thesis studies is adiabatic evolution, and understanding it requires understanding what "slow" means in quantum mechanics.

The word adiabatic comes from the Greek *adiabatos*, meaning "impassable," and entered physics through Clausius for processes with no heat exchange across system boundaries. The meaning in quantum mechanics differs from the thermodynamic original, but both rest on a shared structure: two competing timescales. Every adiabatic process has an external timescale, set by how rapidly conditions change, and an internal timescale, set by how rapidly the system can respond. Adiabaticity holds when external change is slow relative to internal response. In thermodynamics, the internal timescale is the relaxation time to local equilibrium. If a gas is compressed slowly enough, it remains in equilibrium throughout. In quantum mechanics, the internal timescale is the inverse spectral gap. There is no absolute meaning of "slow." Slow is always slow compared to something.

For a quantum system governed by a time-dependent Hamiltonian $H(t)$, the internal timescale is set by the energy gap between eigenstates. At each instant, $H(t)$ has a spectrum of eigenstates and eigenvalues. If the system begins in an eigenstate and the Hamiltonian changes slowly enough, the state tracks the instantaneous eigenstate. It remains an eigenstate of $H(t)$ at every moment, even as the eigenstate itself changes character. If the Hamiltonian changes too rapidly, the state develops overlap with other eigenstates and the system has made a transition [15, 16]. In the context of an algorithm, this transition is a failure.

The mechanism is visible in first-order time-dependent perturbation theory. When the Hamiltonian changes, the amplitude for transitioning from the instantaneous ground state $|e_0(t)\rangle$ to an excited state $|e_n(t)\rangle$ acquires a factor

$$\frac{\langle e_n(t)|\,\dot{H}(t)\,|e_0(t)\rangle}{E_n(t) - E_0(t)}. \tag{2.7.1}$$

The energy denominator tells the story. Transitions to nearby energy levels are enhanced while transitions to distant levels are suppressed. The dominant leakage channel is the nearest excited state, and the gap $g(t) = E_1(t) - E_0(t)$ sets the relevant scale. The inverse gap $1/g(t)$ is the internal response timescale. It sets the natural oscillation period between the two lowest eigenstates. For the Hamiltonian to change negligibly over this period, the fractional change per oscillation must be small compared to the gap itself.

This reasoning yields the adiabatic heuristic condition [17]

$$\frac{\|\dot{H}(t)\|}{g(t)^2} \ll 1, \tag{2.7.2}$$

where $\|\cdot\|$ denotes the spectral norm. This is the physical motivation behind every runtime bound in this thesis. Total evolution time T must be large enough that the sweep rate $\|\dot{H}(t)\|$ remains small relative to $g(t)^2$ at every point along the Hamiltonian path, requiring at minimum $T = \Omega(1/g_{\min}^2)$. The minimum gap along the path is the bottleneck. Small gaps force slowness, and that forced slowness is the computational cost. The heuristic captures the right qualitative scaling, but the rigorous version of the adiabatic theorem [17, 18] involves additional terms: the degeneracy of the ground state, norms of higher derivatives of $H(s)$, and an integral bound rather than a pointwise one. Chapter 4 states the precise result and derives the runtime from it.

The Landau–Zener formula makes the cost quantitative. For a two-level system with a linearly varying energy splitting near an avoided crossing, the probability of a diabatic transition is

$$P_{\mathrm{LZ}} \approx \exp\left(-\frac{\pi g_{\min}^2}{2v}\right), \tag{2.7.3}$$

where $g_{\min}$ is the minimum gap and v is the effective sweep rate [19, 20]. The formula is exact for an isolated two-level system with linear sweep and serves as the leading approximation whenever a crossing is traversed at approximately constant speed. A fast sweep through a narrow gap gives transition probability close to 1. The system jumps levels and the algorithm fails. A slow sweep gives exponentially suppressed transition probability. The system tracks the ground state and the algorithm succeeds.

One caveat belongs here, and it is not minor. For generic families of local Hamiltonians, even the ground-energy promise problem is QMA-complete [21]. The adiabatic quantum optimization regime studied in later chapters restricts to a rank-one driver Hamiltonian, a diagonal problem Hamiltonian, and a spectral condition on gaps and degeneracies (Chapter 4 specifies all three). The restriction is not a weakness of the analysis. It is what makes the analysis possible at all.

The deliverables of this section are the adiabatic heuristic condition (2.7.2) and the Landau–Zener formula (2.7.3). Together they determine how long any adiabatic algorithm must run as a function of the spectral gap profile along the interpolation path.

2.8 Energy Landscapes

Encoding a cost function into a Hamiltonian is exact, but the encoding does not solve the problem. What makes optimization hard is the geometry of the energy landscape, and the nature of that geometry differs between classical and quantum algorithms in a revealing way.

A classical landscape is rugged when it has many local minima separated by energy barriers. Escaping a local basin to explore deeper ones requires crossing the intervening barrier. At inverse temperature β, a barrier of height E_b costs time scaling like $\exp(\beta E_b)$: the Arrhenius bottleneck [22]. Simulated annealing navigates this landscape by cooling. The Metropolis acceptance rule [23] for moving from configuration z to z' is

$$P_{\mathrm{accept}}(z \to z') = \min\{1, e^{-\beta(C(z')-C(z))}\}. \tag{2.8.1}$$

At high temperature the walk moves freely but does not concentrate on the minimum. At low temperature it concentrates near low-energy configurations but takes exponentially long to cross barriers. In worst cases no polynomial cooling schedule suffices [22].

For an adiabatic quantum algorithm, the bottleneck is different. The system does not hop over barriers. It follows a continuous eigenstate trajectory through Hilbert space, and the obstacle is an avoided crossing where the spectral gap narrows. At the crossing, the ground state changes character rapidly over a small interval of the interpolation parameter. The eigenstate that was spread uniformly must concentrate on a small set of computational basis states, and the gap measures how abruptly this rearrangement occurs. The barrier height that governs classical runtime is replaced by the minimum gap that governs quantum runtime through condition (2.7.2). The two bottlenecks are structurally analogous but physically distinct, and instances where one is severe while the other is mild do exist [24].

Unstructured search calibrates the stakes. Among $N = 2^n$ configurations with a single marked item, classical query complexity is $\Theta(N)$, with essentially no shortcut beyond exhaustive evaluation. Quantum query complexity is $\Theta(\sqrt{N})$ [1, 2]. This quadratic gap is the benchmark. The question is not whether quantum methods outperform all classical heuristics on all instances, but whether they achieve better worst-case scaling on specific, well-defined families. For unstructured optimization, the quadratic gap is the target against which everything in this thesis is measured.

2.9 Bridge to Quantum Computation

The vocabulary is now in place. The modeling chain makes explicit that complexity claims depend on the computational model. Energy plays a double role as generator of dynamics and as optimization objective, and the diagonal Hamiltonian H_z encodes any combinatorial cost function exactly. The complexity classes P, NP, and #P measure the difficulty of deciding, verifying, and counting, and the spectral parameters that control adiabatic runtime live in the counting regime. The spectral gap is the bottleneck parameter. It sets the internal timescale of the quantum system and determines, through condition (2.7.2), how long the algorithm must run.

Writing down the Hamiltonian, however, does not reveal its ground state. A computational model must specify how the ground state is found, and a resource accounting must determine how long it takes.

Chapter 3 fixes the circuit and query baseline. It develops the quantum formalism, defines BQP, and establishes the unstructured frontier through Grover's algorithm and the BBBV lower bound. Chapter 4 holds the optimization objective fixed and changes the model from discrete oracle calls to continuous Hamiltonian evolution. Whether these two models achieve the same scaling for unstructured optimization, and what spectral information the adiabatic model demands, is the question that drives the remainder of this thesis.

Chapter 3

Quantum Computation

Chapter 2 translated combinatorial optimization into ground-state energy minimization. The translation is exact and natural. A cost function becomes a diagonal Hamiltonian, and the optimal solutions become its lowest-energy eigenstates. But a Hamiltonian that encodes an answer is not a procedure that finds it. For that, one needs a computational model with definite operations and countable resources.

Quantum mechanics provides such a model, and it provides it with a distinctive tension. A system of n qubits carries 2^n complex amplitudes, an exponentially large internal description. Yet measurement returns a single sampled outcome, and the superposition that supported the computation is destroyed. The entire theory of quantum algorithms lives in the gap between what the system maintains privately and what it reveals upon observation. Bridging that gap for a specific computational task by arranging interference so that the measured outcome is likely to be useful is what algorithm design amounts to.

This chapter builds the computational baseline and derives its sharpest consequence for unstructured problems. The main result is a tight characterization: finding a marked item among N unstructured alternatives has quantum query complexity $\Theta(\sqrt{N})$. Grover's algorithm achieves the upper bound; the lower bound of Bennett, Bernstein, Brassard, and Vazirani proves nothing can do better. That characterization is the floor against which every later adiabatic claim must be measured.

3.1 States and Measurement

The simplest quantum system distinguishes two states. Call them $|0\rangle$ and $|1\rangle$, the two basis states of a quantum bit, or qubit. The state space of a single qubit is

$$\mathcal{H}_1 = \mathbb{C}^2 = \mathrm{span}\{|0\rangle, |1\rangle\}. \tag{3.1.1}$$

A qubit can be in either basis state, or in any normalized linear combination $\alpha|0\rangle + \beta|1\rangle$ with $|\alpha|^2 + |\beta|^2 = 1$. The coefficients α and β are complex numbers called amplitudes. Their squared moduli are probabilities, but the amplitudes themselves carry phase information that has no classical analogue and that will turn out to be the source of computational advantage.

For n qubits, the state space is the tensor product

$$\mathcal{H}_n = (\mathbb{C}^2)^{\otimes n}, \qquad \dim \mathcal{H}_n = N = 2^n. \tag{3.1.2}$$

The computational basis is $\{|x\rangle : x \in \{0,1\}^n\}$, one vector for each binary string of length n. Every pure state of n qubits admits an amplitude expansion

$$|\psi\rangle = \sum_{x\in\{0,1\}^n} \alpha_x |x\rangle, \qquad \sum_x |\alpha_x|^2 = 1. \tag{3.1.3}$$

The normalization condition ensures that the amplitudes define a valid probability distribution upon measurement. Dirac and von Neumann gave the canonical operator-state formalism used here [25, 26]; Nielsen and Chuang [27] provide a modern computational treatment.

The culprit is the tensor product. A two-qubit system does not merely carry the state of qubit A and the state of qubit B side by side; it carries every possible correlation between them. Some of these correlations have no classical counterpart. A bipartite state $|\psi_{AB}\rangle$ is called entangled when it cannot be written as a product

$$|\psi_{AB}\rangle \neq |\psi_A\rangle \otimes |\psi_B\rangle \tag{3.1.4}$$

for any choice of single-system states. The Bell state $(|00\rangle + |11\rangle)/\sqrt{2}$ is the canonical example. Measuring one qubit determines the outcome of measuring the other, regardless of spatial separation. Entanglement is not, by itself, a speedup theorem. But it expands the reachable space of correlations, and therefore the space of algorithmic strategies.

Not all features of a quantum state are physical. A global phase $e^{i\phi}$ multiplying the entire state vector is unobservable:

$$|\psi\rangle \equiv e^{i\phi} |\psi\rangle . \tag{3.1.5}$$

Relative phases between components are a different matter entirely. The states $(|0\rangle + |1\rangle)/\sqrt{2}$ and $(|0\rangle - |1\rangle)/\sqrt{2}$ produce identical statistics when measured in the $\{|0\rangle, |1\rangle\}$ basis. Both yield 0 or 1 with probability 1/2. Yet they are perfectly distinguishable in the $\{|+\rangle, |-\rangle\}$ basis. The sign between components is physical, and it is the mechanism through which quantum amplitudes interfere constructively or destructively. Interference is where quantum algorithms get their non-classical behavior, and relative phase is what makes interference possible.

Measurement connects the amplitude world to observable outcomes. A projective measurement is specified by a collection of orthogonal projectors $\{P_m\}$ satisfying $P_m P_{m'} = \delta_{m,m'} P_m$ and $\sum_m P_m = I$. The Born rule gives the probability of outcome m:

$$\Pr[m] = \langle\psi| P_m |\psi\rangle . \tag{3.1.6}$$

For a rank-one measurement onto some state $|\phi\rangle$, this simplifies to

$$\Pr[\phi] = |\langle\phi|\psi\rangle|^2, \tag{3.1.7}$$

and the post-measurement state, conditioned on outcome m occurring, is $P_m |\psi\rangle / \sqrt{\Pr[m]}$.

The thesis works primarily with pure-state dynamics, but adiabatic evolution through a small gap can leak probability into excited states, making the pure-state description insufficient. The overlap $\langle\psi(s)| P(s) |\psi(s)\rangle$ between the evolved state and the instantaneous ground-state projector (the central figure of merit in later chapters) generalizes naturally to mixed states. The appropriate description of a system that has interacted with an unmonitored environment is a density operator

$$\rho = \sum_j p_j |\psi_j\rangle \langle\psi_j| , \qquad p_j \geq 0, \quad \sum_j p_j = 1, \tag{3.1.8}$$

with measurement rule $\Pr[m] = \mathrm{Tr}(P_m \rho)$. Pure states correspond to $\rho = |\psi\rangle \langle\psi|$ with $\mathrm{Tr}(\rho^2) = 1$.

The Born rule has a computational consequence that deserves emphasis. Eq. (3.1.3) describes a vector with 2^n complex entries, but a computational-basis measurement returns a single sampled string x, drawn with probability $|\alpha_x|^2$. There is no physical operation that reads out the full amplitude table. A quantum computer is not a device that explores 2^n possibilities in parallel and then reports all the answers. It is a device that, through controlled unitary evolution, arranges constructive interference on desired outcomes and destructive interference on the rest, and then bets everything on a single measurement. Algorithmic advantage is the art of making that bet pay off with high probability.

3.2 Dynamics

Between preparation and measurement, quantum mechanics is entirely deterministic. The state vector evolves by a norm-preserving rotation in Hilbert space. This rotation acts not in physical space but in the abstract space of amplitudes. The generator of this rotation is the Hamiltonian.

The fundamental single-qubit operators are the Pauli matrices

$$\sigma_x = \begin{pmatrix} 0 & 1 \\ 1 & 0 \end{pmatrix}, \quad \sigma_y = \begin{pmatrix} 0 & -i \\ i & 0 \end{pmatrix}, \quad \sigma_z = \begin{pmatrix} 1 & 0 \\ 0 & -1 \end{pmatrix}. \tag{3.2.1}$$

Each is Hermitian, unitary, and has eigenvalues ± 1. On an n-qubit system, σ_α^j denotes the Pauli-α operator acting on qubit j with identity on all other qubits. Tensor products of Pauli operators generate the full algebra of observables on $\mathcal{H}_n$, and every Hamiltonian in this thesis (Ising couplings, diagonal cost functions, transverse-field drivers) is expressed in this language.

A Hamiltonian H is a Hermitian operator on $\mathcal{H}_n$. Hermiticity guarantees real eigenvalues and a complete orthonormal eigenbasis. The spectral decomposition reads

$$H = \sum_k E_k P_k, \tag{3.2.2}$$

where P_k projects onto the eigenspace at energy E_k, with $P_k P_{k'} = \delta_{k,k'} P_k$ and $\sum_k P_k = I$. In non-degenerate form, this becomes $H = \sum_j \lambda_j |\phi_j\rangle \langle\phi_j|$ with $H|\phi_j\rangle = \lambda_j |\phi_j\rangle$. The spectral decomposition immediately yields a natural operator norm: $\|H\| = \max_k |E_k|$, the largest eigenvalue in absolute value.

Two quantities from this decomposition will recur throughout the thesis. Order the distinct eigenvalues as $E_0 < E_1 < \cdots$. The ground energy E_0 is the smallest eigenvalue; if the ground space is d_0-fold degenerate, its projector is

$$P_0 = \sum_{j=1}^{d_0} |\phi_{0,j}\rangle \langle\phi_{0,j}| . \tag{3.2.3}$$

The spectral gap is the distance from the ground level to the first excited level:

$$\Delta = E_1 - E_0. \tag{3.2.4}$$

For now, Δ is a property of a single static Hamiltonian. In the adiabatic setting of Chapter 4, the Hamiltonian varies with a schedule parameter s, and the relevant quantity becomes $g(s) = E_1(s) - E_0(s)$ along the full interpolation path. The distinction between a static gap and a path-dependent gap profile is where much of the later complexity resides.

The spectral decomposition extends to a functional calculus: for any function f defined on the spectrum,

$$f(H) = \sum_k f(E_k) P_k. \tag{3.2.5}$$

Setting $f(E) = E$ gives the energy expectation $\langle H\rangle_\psi = \sum_k E_k \langle\psi| P_k |\psi\rangle$. Setting $f(E) = e^{-iEt}$ produces the time-evolution operator. The spectral projections P_k themselves reappear in adiabatic error bounds, where the overlap between the evolving state and the instantaneous ground projector is the central diagnostic.

When a Hamiltonian depends on a parameter λ, the spectral decomposition gives eigenvalue derivatives without differentiating eigenvectors. If $E_k(\lambda)$ is a non-degenerate eigenvalue with eigenstate $|\phi_k(\lambda)\rangle$, the Hellmann–Feynman theorem states

$$\frac{dE_k}{d\lambda} = \langle\phi_k(\lambda)| \frac{\partial H}{\partial \lambda} |\phi_k(\lambda)\rangle . \tag{3.2.6}$$

The eigenvalue derivative is the expectation value of the Hamiltonian derivative in the current eigenstate. For the adiabatic Hamiltonians of Chapter 4, λ is the schedule parameter s, and Eq. (3.2.6) converts spectral gap derivatives into matrix elements of the fixed operator $H_z - H_0$.

Closed-system dynamics obeys the Schrödinger equation. In units where $\hbar = 1$, a time-independent Hamiltonian generates

$$i\frac{d}{dt}|\psi(t)\rangle = H|\psi(t)\rangle , \tag{3.2.7}$$

with solution

$$|\psi(t)\rangle = U(t)|\psi(0)\rangle , \qquad U(t) = e^{-iHt} = \sum_k e^{-iE_k t} P_k. \tag{3.2.8}$$

The operator $U(t)$ is unitary, $U^\dagger U = I$, which is exactly the statement that total measurement probability is preserved. Unitarity is to quantum dynamics what conservation of probability is to classical stochastic processes, except that it acts on amplitudes rather than probabilities, and therefore permits interference.

When the Hamiltonian varies in time, the solution involves a time-ordered exponential:

$$|\psi(t)\rangle = \mathcal{T} \exp\left(-i \int_0^t H(\tau)\, d\tau\right) |\psi(0)\rangle . \tag{3.2.9}$$

The time ordering $\mathcal{T}$ is necessary because $H(\tau_1)$ and $H(\tau_2)$ need not commute at different times. For adiabatic algorithms, $H(t)$ interpolates slowly between an initial Hamiltonian whose ground state is easy to prepare and a final Hamiltonian whose ground state encodes the answer. The relevant question will be how slowly the interpolation must proceed to keep the evolving state near the instantaneous ground state.

Two normalizations deserve mention now to prevent confusion later. Adding a constant cI to any Hamiltonian shifts all energy levels by c without changing eigenvectors, the spectral gap, or any transition amplitude. Under unitary evolution, this shift contributes only a global phase e^{-ict}, which is physically unobservable. Setting the ground energy to zero is therefore a computationally harmless convention, used freely in the chapters that follow.

3.3 The Circuit Model

Quantum mechanics provides the physical substrate. To do computer science with it, one needs a formal model of computation that specifies what counts as an algorithm, what counts as a step, and what counts as efficient. The circuit model serves this role for quantum computation, just as the Turing machine serves it for classical computation.

A quantum circuit is a sequence of elementary unitary operations, called gates, drawn from a finite set. Each gate acts on one or two qubits; universality means that any unitary on n qubits can be approximated to arbitrary precision by a sufficiently long sequence of such gates. Barenco et al. established that the controlled-NOT gate together with arbitrary single-qubit rotations form a universal set [28]. The Solovay-Kitaev theorem guarantees that the overhead of approximating a target unitary to precision ε is only polylogarithmic in $1/\varepsilon$, so the choice of finite gate set does not affect the complexity class [29, 30].

The complexity class BQP (bounded-error quantum polynomial time) captures what polynomial-size quantum circuits can decide with high confidence. A promise problem is a pair $(L_{\text{yes}}, L_{\text{no}})$ of disjoint subsets of $\{0,1\}^*$; the promise is that inputs come from $L_{\text{yes}} \cup L_{\text{no}}$, and behavior on other inputs is unconstrained. A promise problem is in BQP if there exists a uniform family of polynomial-size quantum circuits that accepts every $x \in L_{\text{yes}}$ with probability at least $2/3$ and rejects every $x \in L_{\text{no}}$ with probability at least $2/3$. Uniformity means a classical polynomial-time algorithm can output the circuit description for input length n. The choice of $2/3$ is arbitrary in the sense that any constant bounded away from $1/2$ defines the same class. Standard repetition with majority vote amplifies success probability to $1 - 2^{-p(n)}$ for any polynomial p [5, 31].

Promise formulations are more than a technicality. Optimization problems naturally arrive as promise problems, and the adiabatic results of later chapters are stated in this form. For orientation in the complexity landscape: $\mathrm{P} \subseteq \mathrm{BQP} \subseteq \mathrm{PSPACE}$, with the intermediate inclusion passing through PP [5, 31]. Whether any of these containments is strict remains open, and for this thesis the relevant point is simply that BQP is a well-defined class with known relationships to classical complexity.

Many of the sharpest results in quantum algorithms are proved not in the full circuit model but in a restriction that isolates information acquisition from computational overhead. In the query model, an algorithm accesses the problem instance only through calls to an oracle O_f, and the counted resource is the number of such calls. For a Boolean oracle $f : \{0,1\}^n \to \{0,1\}$, the standard query acts as

$$O_f \,|x, y\rangle = |x,\, y \oplus f(x)\rangle \,. \tag{3.3.1}$$

An equivalent phase-oracle form, obtained by preparing the target register in the $|-\rangle$ state, acts as

$$O_f \,|x\rangle = (-1)^{f(x)} \,|x\rangle \,. \tag{3.3.2}$$

These forms are interconvertible with one ancilla qubit, so lower bounds and upper bounds transfer freely between them.

A T-query quantum algorithm has the interleaved structure

$$|\psi^{(T)}\rangle = U_T \, O_f \, U_{T-1} \, O_f \cdots O_f \, U_1 \, O_f \, U_0 \, |0^m\rangle \,, \tag{3.3.3}$$

where the U_j are input-independent unitaries and O_f carries the instance information. The bounded-error quantum query complexity $Q_2(f_n)$ is the minimum T over all algorithms of this form that succeed with probability at least $2/3$ on every valid input of size n. The classical randomized query complexity $R_2(f_n)$ is defined analogously with randomized decision trees [3, 27].

Query complexity isolates information-theoretic content from computational overhead. When a query lower bound holds, it holds regardless of how cleverly the intermediate unitaries U_j are designed. No circuit-level ingenuity can circumvent an information-theoretic barrier. This is why the Grover frontier, proved in the query model, is so robust.

One further connection completes the bridge from decision to optimization. Given a cost function $C : \{0,1\}^n \to \mathbb{R}$ accessed by oracle, define the threshold decision problem

$$D_\tau(C) = \mathbf{1}[\exists\, x : \, C(x) \le \tau]. \tag{3.3.4}$$

Optimization (finding $\arg\min_x C(x)$ in this context) reduces to repeated calls to D_τ with varying threshold τ. Dürr and Høyer exploited this reduction with Grover subroutines, achieving unstructured minimum finding in $\Theta(\sqrt{N/d_0})$ queries, where d_0 is the number of minimizers [32, 33, 34]. The query complexity of unstructured search therefore transfers directly to unstructured optimization. The underlying primitive is amplitude estimation: given a quantum subroutine whose output qubit has probability p of being measured as $|1\rangle$, the algorithm of Brassard, Høyer, Mosca, and Tapp estimates p to additive precision ε using $O(1/\varepsilon)$ applications of the subroutine and its inverse, quadratically faster than the $O(1/\varepsilon^2)$ samples required classically [34].

3.4 Grover's Algorithm

Strip away all structure. A Boolean function $f : \{0,1\}^n \to \{0,1\}$ marks a subset $W \subseteq \{0,1\}^n$ of solutions, and the goal is to find any $x \in W$ using as few oracle queries as possible. No regularity in the labels is promised or assumed. Classically, the best one can do is query inputs one by one; with $|W| = d_0$ solutions among $N = 2^n$ candidates, the expected number of queries is $\Theta(N/d_0)$. Grover showed that a quantum algorithm needs only $\Theta(\sqrt{N/d_0})$, a quadratic improvement driven by a genuinely quantum mechanism [1].

The mechanism is geometric, and it unfolds in a two-dimensional subspace of the full N-dimensional Hilbert space. This is the essential surprise: a problem defined on 2^n items reduces to a rotation in the plane.

Define the normalized marked and unmarked superpositions

$$|w\rangle = \frac{1}{\sqrt{d_0}} \sum_{x \in W} |x\rangle , \qquad |r\rangle = \frac{1}{\sqrt{N - d_0}} \sum_{x \notin W} |x\rangle . \tag{3.4.1}$$

These are orthogonal unit vectors spanning a two-dimensional subspace $\mathcal{V} = \text{span}\{|w\rangle , |r\rangle\}$. The uniform superposition over all basis states decomposes in $\mathcal{V}$ as

$$|s\rangle = \frac{1}{\sqrt{N}} \sum_{x} |x\rangle = \sin\theta \; |w\rangle + \cos\theta \; |r\rangle , \qquad \sin\theta = \sqrt{\frac{d_0}{N}}. \tag{3.4.2}$$

When $d_0 \ll N$, the initial state $|s\rangle$ is nearly orthogonal to the target $|w\rangle$, tilted toward it by an angle θ of order $\sqrt{d_0/N}$.

The oracle provides a phase-flip on marked states, which in $\mathcal{H}_n$ is a reflection through the hyperplane orthogonal to $|w\rangle$:

$$O_w = I - 2\,|w\rangle\,\langle w| . \tag{3.4.3}$$

Grover's iterate combines this oracle reflection with a reflection through the initial state:

$$G = D\,O_w, \qquad D = 2\,|s\rangle\,\langle s| - I. \tag{3.4.4}$$

The diffusion operator D is itself implementable as $H^{\otimes n}(2\,|0^n\rangle\,\langle 0^n| - I)H^{\otimes n}$, so each application of G costs one oracle query and $O(n)$ elementary gates.

A product of two reflections in a plane is a rotation by twice the angle between their reflection axes. In the basis $(|w\rangle , |r\rangle)$, the iterate acts as

$$G = \begin{pmatrix} \cos 2\theta & \sin 2\theta \\ -\sin 2\theta & \cos 2\theta \end{pmatrix}, \tag{3.4.5}$$

rotating the state toward $|w\rangle$ by 2θ per application. After k iterations,

$$G^k\,|s\rangle = \sin\big((2k+1)\theta\big) \; |w\rangle + \cos\big((2k+1)\theta\big) \; |r\rangle , \tag{3.4.6}$$

so the probability of observing a marked item is $\sin^2\big((2k+1)\theta\big)$. This reaches its first maximum near 1 when $(2k+1)\theta \approx \pi/2$, giving an optimal iteration count of

$$k^* \approx \left\lfloor \frac{\pi}{4\theta} - \frac{1}{2} \right\rfloor . \tag{3.4.7}$$

For $d_0 \ll N$, $\theta \approx \sqrt{d_0/N}$, and $k^* = \Theta(\sqrt{N/d_0})$. Each iteration uses one query, so the total query complexity is

$$Q_{\text{Grover}} = \Theta\left(\sqrt{\frac{N}{d_0}}\right) . \tag{3.4.8}$$

When d_0 is unknown in advance, Boyer, Brassard, Høyer, and Tapp showed that a randomized schedule of iteration counts achieves the same asymptotic scaling in expectation [33].

The two-dimensional picture deserves a moment of reflection, because it is a structural motif that will reappear in a different guise. A problem defined over 2^n basis states might seem to require 2^n-dimensional analysis. But the symmetry of the unstructured oracle (treating all marked items equally and all unmarked items equally) collapses the relevant dynamics to a plane. The full Hilbert space serves as a stage, but only two directions participate in the performance. The runtime is determined entirely by the angular geometry in $\mathcal{V}$: how far the initial state is from the target, and how fast the iterate rotates.

The same dimensional reduction occurs in adiabatic search. In Chapter 4, the avoided crossing between the two lowest energy levels of an interpolating Hamiltonian plays the role that $\text{span}\{|w\rangle , |r\rangle\}$ plays here. The minimum spectral gap at the crossing replaces the angle θ. The local schedule speed replaces the iteration count. The structural lesson is the same: effective low-dimensional dynamics, embedded in an exponentially large state space, controls the computational outcome.

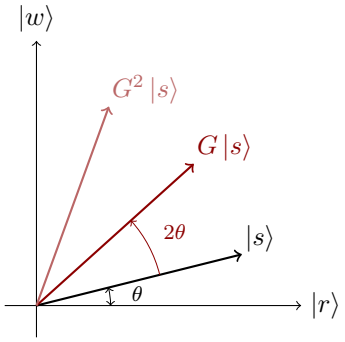

Figure 3.1: Grover's algorithm as rotation in the plane $\mathcal{V} = \text{span}\{|w\rangle, |r\rangle\}$. The initial state $|s\rangle$ makes angle $\theta = \arcsin\sqrt{d_0/N}$ with the $|r\rangle$ axis. Each Grover iterate G rotates the state by 2θ toward the marked-state axis. After $k^* \approx \pi/(4\theta)$ iterations the state is near $|w\rangle$.

3.5 The Search Frontier

Grover's algorithm demonstrates that $\sqrt{N/d_0}$ queries suffice for unstructured search. Bennett, Bernstein, Brassard, and Vazirani showed that no quantum algorithm can do better [2].

The argument rests on a hybrid distinguishability bound. Consider a quantum algorithm that makes T queries to a single-marked-item oracle. Let $|\psi_T^{(w)}\rangle$ denote the algorithm's final state when item w is marked, and let $|\psi_T^{(\varnothing)}\rangle$ denote the final state under the null oracle, which marks nothing. Each oracle query perturbs the state by an amount that depends on how much amplitude currently sits on the queried location. A careful accounting of these perturbations, averaged over all possible marked items, yields the bound

$$\frac{1}{N}\sum_{w=1}^{N}\left\||\psi_T^{(w)}\rangle - |\psi_T^{(\varnothing)}\rangle\right\| \leq \frac{2T}{\sqrt{N}}. \tag{3.5.1}$$

The right-hand side grows linearly in T. When $T \ll \sqrt{N}$, it remains $o(1)$: the average distance between the final state under a random single-marked oracle and the final state under the null oracle is negligible. In this regime, no measurement can reliably distinguish the two cases, because states that are close in norm produce nearly identical measurement statistics. For an algorithm to identify the marked item with constant success probability, the final states must be well separated, forcing $T = \Omega(\sqrt{N})$.

The extension to $d_0 > 1$ marked items follows by a standard averaging argument, yielding $\Omega(\sqrt{N/d_0})$. Nayak and Wu give a complementary polynomial-method perspective on related bounds [35].

Combining the upper bound from Grover with the BBBV lower bound closes the frontier for unstructured quantum search:

$$Q_{\text{search}} = \Theta\left(\sqrt{\frac{N}{d_0}}\right). \tag{3.5.2}$$

This is not merely a known algorithm paired with a known lower bound. The quantum query complexity of unstructured search is now determined up to constant factors. No future algorithm can improve the exponent.

The same $\Omega(\sqrt{N})$ barrier survives the transition from discrete queries to continuous-time Hamiltonian evolution. Farhi, Goldstone, and Gutmann proved that any adiabatic algorithm using a rank-one projector driver (the driver $H_0 = -|\psi_0\rangle\langle\psi_0|$ used throughout Chapter 4) for unstructured search requires time $\Omega(\sqrt{N/d_0})$, matching the BBBV bound in the circuit-query model [36]. Changing the physical implementation from gates to Hamiltonians does not remove the information-theoretic barrier.

The word "unstructured" carries precise but different meanings in the two settings. In the circuit model, it means black-box oracle access. The only way to learn about f is to query it, and no exploitable regularity in the labels is promised or assumed. In the adiabatic model, it means that the problem Hamiltonian is a diagonal cost map $z \mapsto E_z$ with no additional promised structure and no locality, sparsity, or algebraic pattern that an algorithm could exploit. The two models enforce the same absence of exploitable information through different physical primitives.

The frontier is now closed. Unstructured quantum search has query complexity $\Theta(\sqrt{N/d_0})$, and this holds regardless of whether the algorithm uses discrete oracle queries or continuous Hamiltonian evolution. The question that remains is subtler. In the circuit model, achieving the optimal scaling requires only knowledge of N and d_0. The algorithm runs k^* iterations of a fixed two-reflection circuit, and k^* depends on nothing else. In

the adiabatic model, matching the same scaling requires a schedule that is adapted to the spectral gap profile along the interpolation path. Whether the information needed for that adaptation is easier or harder to obtain than the information implicit in a single oracle query is not settled by BBBV alone. Chapter 4 introduces the adiabatic framework and makes this question precise.

Chapter 4

Adiabatic Quantum Computation

Chapter 3 closed the circuit-query model cleanly. Unstructured search among N alternatives has quantum query complexity $\Theta(\sqrt{N/d_0})$, with Grover achieving the upper bound and BBBV proving the lower. That characterization is tight and model-independent. Farhi, Goldstone, Gutmann, and Nagaj showed that the same $\Omega(\sqrt{N/d_0})$ barrier persists under continuous-time Hamiltonian evolution [36]. The exponent is settled.

But the exponent is not the whole story. Grover's algorithm requires knowledge of N and d_0 to set its iteration count, and nothing else. The algorithm is a fixed two-reflection circuit repeated a computable number of times. An adiabatic algorithm matching the same scaling faces a different challenge. It requires a schedule adapted to the spectral gap profile along a Hamiltonian interpolation path. Whether the information needed for that adaptation is easy or hard to obtain is a question the circuit model never had to face.

This chapter builds the adiabatic framework and makes that question precise. What is the adiabatic idea, and what does it formalize? How slow must "slow" be, in quantitative terms and not just qualitative ones? Can the resulting algorithm match the circuit-model frontier? And if it can, what does the matching cost?

4.1 The Model

The adiabatic idea begins with a physical observation. A quantum system in the ground state of a Hamiltonian will remain near the ground state if the Hamiltonian is deformed sufficiently slowly. This is the adiabatic theorem, known since Born and Fock [15] and formalized in modern operator language by Kato [16]. It was not, for most of its history, thought of as a computational primitive.

Farhi, Goldstone, Gutmann, and Sipser changed that perspective. They proposed encoding the solution to an optimization problem in the ground state of a "problem" Hamiltonian H_P, then reaching that ground state by slow interpolation from an initial Hamiltonian H_0 whose ground state is known and easy to prepare [13]. The algorithm requires no gates, no oracles, no discrete iteration count. It requires only a Hamiltonian path and enough time.

The standard interpolation is

$$H(s) = (1-s)H_0 + sH_P, \qquad s \in [0,1], \tag{4.1.1}$$

where the schedule parameter s maps to physical time $t \in [0,T]$ through an increasing function $s(t)$. The choice of $s(t)$ determines how the evolution distributes its time budget across the interpolation path. Reparameterizing the Schrödinger equation from Chapter 3 in terms of s gives

$$\frac{i}{T}\frac{d}{ds}\left|\psi(s)\right\rangle = H(s)\left|\psi(s)\right\rangle. \tag{4.1.2}$$

The factor $1/T$ in front makes the dependence on total runtime explicit. Larger T slows the effective rate of change and improves adiabatic tracking. The algorithm prepares the ground state of H_0 at $s=0$ and evolves under $H(s)$ until $s=1$, then measures. Success means the final state has large overlap with the ground space of H_P.

This much defines adiabatic quantum computation (AQC) in its broadest form. Aharonov, van Dam, Kempe, Landau, Lloyd, and Regev showed that AQC with two-body Hamiltonians is polynomially equivalent to the circuit model [37]. Any problem solvable by one model is solvable by the other with at most polynomial overhead. That equivalence resolves a model-power question. It does not resolve the algorithm-design question that this thesis addresses: for a fixed interpolation family, can one achieve the target speedup with feasible spectral information?

Adiabatic quantum optimization (AQO) is the specialization where H_P is a classical cost Hamiltonian, diagonal in the computational basis:

$$H(s) = (1-s)H_0 + sH_z. \tag{4.1.3}$$

This is the regime analyzed in Chapters 5 through 9. The word "unstructured" needs pinning down across models. In the circuit setting, unstructured search means black-box oracle access with no exploitable regularity. In this thesis, "unstructured adiabatic" refers to a specific driver design: a uniform initial state, a rank-one driver, and no instance-specific structure injected into H_0 [38, 36, 10]. It does not mean that the problem Hamiltonian H_z itself lacks combinatorial structure. The restriction is on what the algorithm's starting point knows, not on what the problem contains.

The concrete driver used throughout the later chapters is

$$H_0 = -\left|\psi_0\right\rangle\left\langle\psi_0\right|, \qquad \left|\psi_0\right\rangle = \left|+\right\rangle^{\otimes n} = \frac{1}{\sqrt{N}} \sum_{z\in\{0,1\}^n} \left|z\right\rangle. \tag{4.1.4}$$

The ground state of H_0 is the uniform superposition $|\psi_0\rangle$ with eigenvalue -1; all orthogonal states have eigenvalue 0. This is the adiabatic analogue of Grover's initial state, and the choice is not incidental. With diagonal H_z and rank-one H_0, the low-energy spectrum of $H(s)$ is dominated by a single avoided crossing that admits explicit analysis [10]. The entire runtime of the algorithm is controlled by the geometry of that crossing. By contrast, transverse-field drivers, which are the standard choice in quantum annealing hardware, can produce cascades of narrow crossings and Anderson-localization effects that obstruct generic runtime control [39, 40]. The rank-one restriction buys analytical tractability at the cost of generality, and that tradeoff is deliberate.

4.2 The Adiabatic Theorem and Schedule Design

The qualitative adiabatic theorem is simple. Go slowly enough and you stay near the ground state. For algorithm design, "slowly enough" must be a number, not an aspiration. The quantitative version needed here is due to Jansen, Ruskai, and Seiler [17], with complementary bounds from Elgart and Hagedorn [18]. The JRS formulation makes the gap dependence fully explicit.

Let $P(s)$ project onto the followed eigenspace of $H(s)$. In the AQO application, this is the instantaneous ground-state subspace. Assume it has dimension d and is separated from the rest of the spectrum by a gap $g(s) > 0$ for all $s \in [0,1]$. Assume H is twice differentiable as a function of s and that the initial state satisfies $|\psi(0)\rangle \in \mathrm{range}(P(0))$. The Jansen-Ruskai-Seiler bound controls the leakage out of the followed subspace:

$$\left|1 - \left\langle\psi(s)\right| P(s) \left|\psi(s)\right\rangle\right| \le \nu^2(s), \tag{4.2.1}$$

with

$$\nu(s) = C\left\{\frac{1}{T}\frac{d\|H'(0)\|}{g(0)^2} + \frac{1}{T}\frac{d\|H'(s)\|}{g(s)^2} + \frac{1}{T}\int_0^s \left(\frac{d\|H''(s')\|}{g(s')^2} + \frac{d^{3/2}\|H'(s')\|}{g(s')^3}\right) ds'\right\}, \tag{4.2.2}$$

where C is a universal constant independent of s, T, and the specific Hamiltonian family.

The formula is elaborate, but the controlling mechanism is simple. Every term involves a ratio of derivative norms to powers of the gap. Small gaps amplify adiabatic error. The integral term accumulates contributions from the entire path traversed so far, weighted by inverse gap powers. Where the gap is large, these contributions are negligible. Where the gap shrinks, they dominate.

This structure converts the spectral gap from a descriptive property of the Hamiltonian into a computational bottleneck. The minimum gap along the path is not the only quantity that matters. The full gap profile enters through the integral. But the minimum gap sets the scale. If $g_{\min} = \min_s g(s)$ is the bottleneck, then a linear schedule requires $T = \Omega(1/g_{\min}^2)$ for constant fidelity, and this scaling is tight for the worst case over gap profiles. Faster schedules leak probability into excited states; slower schedules waste time where the gap is wide.

Schedule design is the art of distributing the time budget $T = \int_0^1 ds/\dot{s}$ across the interpolation path to match the gap profile. A linear schedule sets $\dot{s} = 1/T$, spending equal time per unit s regardless of spectral structure. This is the choice Farhi et al. used in their original adiabatic search construction, and it yields runtime $O(N)$. This is no better than classical exhaustive search. The linear schedule wastes most of its budget in regions where the gap is wide and starves the narrow bottleneck near $s = 1/2$ [13].

A local schedule adapts the sweep rate to the instantaneous gap. The standard local control law, used by Roland and Cerf and by subsequent work [41, 38], sets the rate proportional to the squared gap:

$$\left|\frac{ds}{dt}\right| \lesssim \frac{\varepsilon\, g(s)^2}{\chi(s)}, \qquad \chi(s) = \left|\left\langle e_1(s)\right| \frac{dH}{ds} \left|e_0(s)\right\rangle\right|, \tag{4.2.3}$$

where $|e_0(s)\rangle$ and $|e_1(s)\rangle$ are the instantaneous ground and first excited states, ε is the target adiabatic error, and $\chi(s)$ is the matrix element of the Hamiltonian derivative between them. This law is derived from the adiabatic condition applied locally at each s. The transition amplitude from ground to first excited state, accumulated over an infinitesimal interval ds, must remain below ε. The general AQO analysis in Chapters 6 and 7 uses a simplified adiabatic theorem where the schedule derivative scales with $g(s)$ rather than $g(s)^2/\chi(s)$ [10]; the two forms agree in scaling for the Roland-Cerf benchmark but differ in how the schedule is parameterized for general problem Hamiltonians.

The physical content is immediate. Near gap bottlenecks, $g(s)$ is small and $\dot{s}$ must be small. The evolution crawls through the dangerous region. Where the gap is wide, $\dot{s}$ can be large. The evolution sprints through safe territory. The total runtime is then

$$T = \int_0^1 \frac{ds}{\dot{s}(s)} \sim \frac{1}{\varepsilon} \int_0^1 \frac{\chi(s)}{g(s)^2}\, ds. \tag{4.2.4}$$

The runtime integral concentrates its weight at the gap minimum. If the bottleneck is a narrow avoided crossing of width δ_s where $g(s)$ dips to $g_{\min}$, then the integral is dominated by the contribution from that region, and the rest of the path contributes lower-order terms.

Guo and An have recently placed this local-gap logic in a broader framework, showing that power-law schedule families $u'(s) \propto g(u(s))^p$ can improve the gap dependence from inverse-square to inverse-linear, provided the Lebesgue measure of $\{s : g(s) \leq t\}$ grows at most linearly in t [42]. The later chapters take a different route, exploiting explicit spectral formulas for the rank-one AQO family.

One consequence of the JRS bound deserves emphasis before proceeding. Gap-aware schedules require gap information. The local control law (4.2.3) uses $g(s)$ and $\chi(s)$ as functions of s, and these are not free. Computing the gap of a general local Hamiltonian at a single point is QMA-hard [21]. Schedule design and spectral inference are therefore entangled problems. The sequential approach of first computing the gap and then designing the schedule is valid only when the spectral structure is analytically known or efficiently computable. For the rank-one AQO family, it happens to be analytically known. For general problem Hamiltonians, it is not.

4.3 Avoided Crossings and the Roland-Cerf Benchmark

In the rank-one AQO setting, the gap profile along the interpolation path is wide at both endpoints and pinches to a minimum at a single avoided crossing between the two lowest energy levels. Near that crossing, the dynamics is effectively two-dimensional, and the physics is captured by the Landau-Zener model from the theory of atomic collisions [19, 20].

The Landau-Zener formula describes what happens when a system is swept linearly through a two-level anticrossing. If the minimum gap is $g_{\min}$ and the effective sweep rate is v, the probability of a diabatic transition is

$$P_{\mathrm{LZ}} \approx \exp\left(-\frac{\pi g_{\min}^2}{2v}\right). \tag{4.3.1}$$

The formula makes precise what "too fast" means. The exponent is the ratio of the gap squared to the sweep rate. When $v \gg g_{\min}^2$, the exponential is near one and the system leaks into the excited state. When $v \ll g_{\min}^2$, the exponential is near zero and the system tracks the ground state through the crossing. The transition between these regimes is exponentially sharp.

This is the same dimensional reduction that appeared in Grover's algorithm, now in a continuous-time setting. In Chapter 3, the full N-dimensional Hilbert space collapsed to the two-dimensional plane $\mathrm{span}\{|w\rangle, |r\rangle\}$, and the algorithm was a rotation in that plane. Here, the effective dynamics collapses to the two-dimensional subspace spanned by the instantaneous ground and first excited states of $H(s)$, and the algorithm is a slow traversal of an avoided crossing in that subspace. The structural motif is the same. In both settings, low-dimensional effective dynamics controls an exponentially large system. The parameterization changes from a discrete iteration count k to a continuous schedule variable s.

Roland and Cerf were the first to convert this physical picture into an adiabatic algorithm matching Grover's scaling [38]. Their construction uses the simplest possible instance: one marked state $|w\rangle$ among $N = 2^n$ basis states. The Hamiltonian path is

$$H_{\mathrm{RC}}(s) = -(1-s)\,|\psi_0\rangle\langle\psi_0| + s\,(I - |w\rangle\langle w|), \qquad |\psi_0\rangle = \frac{1}{\sqrt{N}} \sum_x |x\rangle. \tag{4.3.2}$$

At $s = 0$, the ground state is $|\psi_0\rangle$ with eigenvalue -1; at $s = 1$, the problem Hamiltonian $H_P = I - |w\rangle\langle w|$ has ground state $|w\rangle$ with eigenvalue 0 and all other states at energy 1. The interpolation lives in a two-dimensional

invariant subspace spanned by $|w\rangle$ and the component of $|\psi_0\rangle$ orthogonal to $|w\rangle$, reproducing the geometric simplification behind Grover.

The spectral gap along this path is

$$g(s) = \sqrt{(2s-1)^2 + \frac{4s(1-s)}{N}}. \tag{4.3.3}$$

At $s = 0$ and $s = 1$, the gap is 1. At $s = 1/2$, it reaches its minimum $g_{\min} = 1/\sqrt{N}$. The gap profile is a smooth arch with a single narrow dip. The location, width, and minimum value of the crossing are all determined by N alone. No instance-specific information is needed.

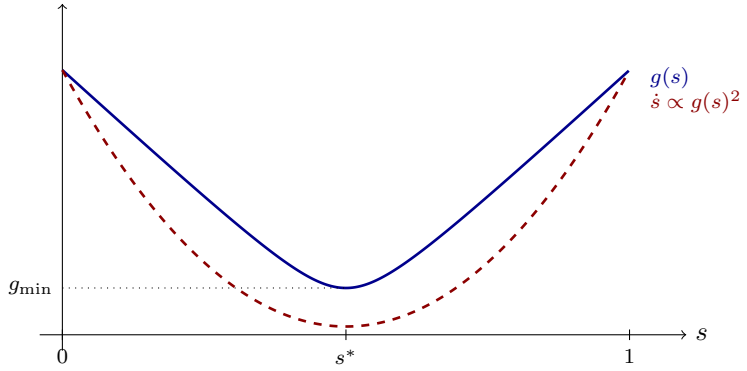

Figure 4.1: Gap profile $g(s)$ (solid) and local schedule speed $\dot{s} \propto g(s)^2$ (dashed) for the Roland-Cerf Hamiltonian. Both reach their minimum at the avoided crossing $s^* = 1/2$. The schedule crawls through the narrow-gap bottleneck and sprints through the wide-gap regions on either side. The runtime is dominated by the integral of $1/g(s)^2$ near s^*.

Roland and Cerf applied the local schedule $\dot{s} = \varepsilon\, g(s)^2$, which crawls through the bottleneck near $s = 1/2$ and sprints through the wide-gap regions on either side. The resulting runtime is

$$T = \frac{1}{\varepsilon}\int_0^1 \frac{ds}{g(s)^2} = \frac{N}{\varepsilon\sqrt{N-1}}\arctan\sqrt{N-1} = \Theta\left(\frac{\sqrt{N}}{\varepsilon}\right). \tag{4.3.4}$$

The integral evaluates in closed form because the gap profile (4.3.3) has an explicit algebraic expression. The $\Theta(\sqrt{N})$ scaling matches Grover exactly.

Two facts about this result are as important as the result itself.

First, the matching is optimal. Farhi et al. proved that for any rank-one projector driver, any diagonal problem Hamiltonian with d_0 ground states, and any schedule, the adiabatic runtime satisfies $T = \Omega(\sqrt{N/d_0})$ [36]. Their proof adapts the BBBV argument from Chapter 3 to continuous time, introducing N auxiliary Hamiltonians related by diagonal phase shifts and bounding the average distinguishability of the resulting final states. The Roland-Cerf construction saturates this lower bound for $d_0 = 1$, so the adiabatic frontier for one-marked-item search is closed.

Second, the success depends entirely on explicit spectral knowledge. The local schedule $\dot{s} = \varepsilon\, g(s)^2$ requires $g(s)$ as a known function. For the Roland-Cerf Hamiltonian, $g(s)$ has the closed form (4.3.3), determined by N alone. The algorithm designer does not need to solve any hard problem to implement the schedule. This is the feature that will not survive generalization.

4.4 The Information Cost

The Roland-Cerf construction is a proof of concept. Adiabatic evolution can match the circuit-model speedup for unstructured search. The question for the rest of the thesis is whether this matching extends to general diagonal problem Hamiltonians, and at what cost.

The polynomial equivalence between AQC and the circuit model (Section 4.1) resolves a model-power question but not an algorithm-design question. The equivalence proof encodes circuits into Hamiltonians with carefully designed spectral properties. It does not say that a natural interpolation between a simple initial Hamiltonian and a problem Hamiltonian will achieve the optimal runtime with a feasible schedule.

The distinction is visible throughout the literature. One line of work uses adiabatic evolution beyond optimization, applying it to state generation, Markov-chain speedups, and ranking [43, 44, 45, 46]. A second line connects adiabatic reasoning to gate-model primitives through Hamiltonian simulation and discretization [47, 48, 49]. Both exploit structure in the Hamiltonian that goes beyond the AQO setting.

The same literature also displays the failure modes of naive adiabatic optimism. Filtering and endpoint strategies can outperform strictly gap-limited adiabatic paths [50, 51, 52]. Anderson-localization effects can create exponentially small gaps in transverse-field models [39, 53]. Practical annealing studies consistently find that path design and spectral structure dominate time-to-solution scaling, and that the abstract promise of universality offers little guidance for specific instances [54, 55, 56, 57, 58, 59].

The rank-one AQO family used in this thesis is deliberately narrower than general AQC:

$$H(s) = -(1-s)\left|\psi_0\right\rangle\left\langle\psi_0\right| + sH_z, \qquad H_z \text{ diagonal in the computational basis.} \tag{4.4.1}$$

The restriction is natural for classical cost functions. With diagonal H_z and rank-one H_0, the spectrum decomposes into a symmetric subspace of dimension M (the number of distinct eigenvalues of H_z) and an orthogonal complement where eigenvalues track trivially. Chapter 6 develops this decomposition in full, deriving the secular equation whose roots are the eigenvalues of $H(s)$ within the symmetric subspace. The low-energy dynamics is controlled by a single avoided crossing between the two lowest levels of this subspace.

The crossing geometry has explicit formulas. The eigenvalues of $H(s)$ satisfy a secular equation involving the resolvent of the diagonal part H_z, and expanding that resolvent produces weighted sums over the excited spectrum that control the crossing. Write the distinct eigenvalues of H_z as $E_0 < E_1 < \cdots < E_{M-1}$ with degeneracies d_k, and define the spectral moments

$$A_p = \frac{1}{N}\sum_{k=1}^{M-1}\frac{d_k}{(E_k - E_0)^p}, \qquad p \in \mathbb{N}. \tag{4.4.2}$$

Higher-p moments weight eigenvalues closer to the ground energy more heavily. The moment A_1 controls the crossing location; A_2 controls the crossing width and the minimum gap. These formulas hold under a spectral regularity condition

$$\frac{1}{\Delta}\sqrt{\frac{d_0}{A_2 N}} < c \tag{4.4.3}$$

for a sufficiently small constant $c > 0$ [10], which ensures the avoided crossing is well separated from higher spectral features. Under this condition, the crossing geometry is governed by three quantities:

$$s^* = \frac{A_1}{A_1 + 1}, \tag{4.4.4}$$

$$\delta_s = \frac{2}{(A_1+1)^2}\sqrt{\frac{d_0 A_2}{N}}, \tag{4.4.5}$$

$$g_{\min} = \frac{2A_1}{A_1+1}\sqrt{\frac{d_0}{A_2 N}}. \tag{4.4.6}$$

These are crossing location, crossing width scale, and minimum-gap scale, respectively. Each has a clear physical reading. The crossing sits at s^*, which is close to 1 when A_1 is large. The crossing region has width δ_s around s^*, shrinking as N grows and as A_1 increases. The minimum gap $g_{\min}$ decreases with N as $1/\sqrt{N}$ up to spectral prefactors, reproducing the Roland-Cerf scaling when the prefactors are $O(1)$.

The parameter dependencies reveal the physics. A larger d_0 means more states share the ground energy, which widens the crossing and increases $g_{\min}$ by concentrating more amplitude in the ground subspace. A larger A_2 means excited eigenvalues sit closer to the ground energy, which narrows the gap as $1/\sqrt{A_2}$ because near-degenerate levels create a tighter pinch. Increasing A_1 pushes s^* toward 1 and compresses δ_s through the $(A_1+1)^{-2}$ factor, concentrating the dangerous region into a narrower interval that the schedule must target more precisely.

Now the cost becomes visible. An optimal local schedule must slow down in the crossing window $[s^* - \delta_s,\, s^* + \delta_s]$ and can sprint elsewhere. To implement this schedule, s^* must be known to additive precision $O(\delta_s)$. For $d_0 = O(1)$ with polynomial spectral prefactors, this precision is roughly $2^{-n/2}$ up to polynomial factors [10]. Computing s^* to this precision requires computing A_1 to comparable precision, and that computation involves the full spectrum of H_z.

This is the thesis's central tension, and it splits into two hardness results that Chapters 5 through 8 develop in full. Approximating A_1 to additive precision $\varepsilon < 1/(72(n-1))$ is NP-hard, by reduction from satisfiability.

The construction encodes 3-SAT instances into the spectral moments of a diagonal Hamiltonian. Approximating A_1 to exponential precision $\varepsilon = 2^{-\mathrm{poly}(n)}$ is #P-hard [10]. The first result says that even moderate-precision schedule design is as hard as NP. The second says that the high-precision regime needed for asymptotically optimal schedules is as hard as counting.

Combined with the lower bound $T = \Omega(\sqrt{N/d_0})$ from Farhi et al. [36], these hardness results give a precise picture. The Grover-like scaling $\Theta(\sqrt{N/d_0})$ is achievable in principle: there exists a schedule that realizes it, and the spectral formulas above describe its structure. But the spectral moments A_1 and A_2 that the schedule requires can themselves be computationally hard to obtain. The adiabatic model relocates the difficulty from algorithm execution to algorithm specification.

This is where the parallel with Grover breaks down most sharply. Grover's algorithm is specified by two integers, N and d_0. Its iteration count $k^* \approx (\pi/4)\sqrt{N/d_0}$ depends on nothing else. The adiabatic algorithm matching the same runtime requires the gap profile, the crossing location, and the schedule, all of which depend on the full spectrum of the problem Hamiltonian. The circuit model achieves its frontier with minimal information. The adiabatic model achieves the same frontier with maximal information.

That is the handoff to Chapter 5. The circuit model closes unstructured search with a self-contained algorithm. The adiabatic model matches the scaling law but embeds an information problem in the schedule design. Chapter 5 formalizes the AQO problem around the rank-one path (4.4.1). Chapter 6 derives the global gap bounds outside and near the crossing window. Chapter 7 constructs the optimal local schedule and its runtime. Chapter 8 proves the hardness of the spectral estimation that the schedule requires. Together, they fill in the full quantitative picture that this chapter has outlined.

Chapter 5

Adiabatic Quantum Optimization

In the circuit model, unstructured optimization is already understood. Given a black-box cost function on $N = 2^n$ bit-strings, Grover's algorithm and its generalizations find a minimizer in $O(\sqrt{N/d_0})$ queries, where d_0 is the number of optima [1, 33]. The algorithm needs no prior knowledge of the cost function's structure. Amplitude amplification gathers what it needs adaptively, one oracle query at a time. No spectral parameter is computed in advance, no schedule is tuned to a gap profile, and no preprocessing competes with the search cost itself.

Adiabatic quantum computation is polynomially equivalent to the circuit model [37], so the same speedup exists in principle. The obstruction is different. The evolution Hamiltonian $H(s)$ interpolates continuously between an initial Hamiltonian H_0 and the problem Hamiltonian H_z, and the runtime is controlled by the spectral gap of $H(s)$ along the entire path. The location of the avoided crossing, the sharpness of the minimum gap, and the reopening rate all matter. Matching the Grover speedup now requires controlling spectral features that depend on the full degeneracy structure of H_z.

The adiabatic version of Grover's algorithm, due to Roland and Cerf [60], finds a single marked item among $N = 2^n$ by slowly interpolating between a uniform superposition and a problem Hamiltonian that penalizes all unmarked items. The crossing between the two lowest energy levels occurs at $s = 1/2$, its position independent of the Hamiltonian's spectrum. The minimum spectral gap scales as $1/\sqrt{N}$, and a schedule that slows near the crossing achieves the optimal $O(\sqrt{N})$ runtime.

Consider a cost function encoded in an n-qubit Hamiltonian diagonal in the computational basis, with M distinct energy levels, arbitrary degeneracies, and a spectral gap that may vary with the number of qubits. The ground states encode solutions to a combinatorial optimization problem. Can the adiabatic approach still match the $\Theta(\sqrt{N})$ lower bound for unstructured search [36]?

The bound applies directly to our setup. Farhi et al. proved that when H_0 is a rank-one projector onto the uniform superposition, no schedule can find the ground state in time $o(\sqrt{N/d_0})$, regardless of the cost function. Their proof constructs N equivalent Hamiltonians related by Fourier shifts and applies a continuous-time analogue of the BBBV argument [2]. Partial answers came first. Žnidarič and Horvat [61] showed via analytical and heuristic arguments that the minimum gap scales as $\sqrt{d_0/2^n}$ for 3-SAT instances and identified the crossing position, but did not rigorously bound the runtime. Hen [62] proved a quadratic speedup for a random Hamiltonian whose energy distribution makes the crossing position spectrum-independent, sidestepping the central difficulty.

The answer in full generality is yes, and in our view that is the surprising part. But it comes with a sharp caveat. The spectrum of the interpolated Hamiltonian is much richer than in the Grover case. Instead of a two-level system plus a degenerate bulk, one gets M interacting energy levels in a symmetric subspace, with higher-state avoided crossings that obscure the lowest gap. The ground-state crossing position depends nontrivially on the degeneracy structure of H_z. The minimum gap still scales as $\Theta(1/\sqrt{N})$ up to spectral factors, but it occurs at a position that must be known to exponential precision for the schedule to be correct.

For a general diagonal problem Hamiltonian, $H(s)$ has a single avoided crossing at position $s^* = A_1/(A_1+1)$, where A_1 is a spectral parameter determined by the degeneracy structure. The minimum spectral gap at the crossing scales as $\Theta(\sqrt{d_0/(NA_2)})$, and the gap grows linearly on both sides. Chapter 6 proves the gap bounds outside the crossing window, and Chapter 7 derives the optimal runtime. Chapter 8 then shows where the edge comes from. Computing s^* is NP-hard.

5.1 From Cost Function to Adiabatic Path

The adiabatic path is determined entirely by the spectrum of the problem Hamiltonian, specifically its distinct energy levels and their degeneracies. Because $H_0 = -|\psi_0\rangle\langle\psi_0|$ is a rank-one projector onto the uniform superposition, it treats all computational basis states symmetrically, and only the energy values and the number of states at each energy affect the crossing structure. The definitions below parameterize this spectral data. Permutation symmetry then confines the dynamics to a polynomial-dimensional subspace indexed by these levels (Section 5.3), making the full analysis tractable.

Consider an n-qubit Hamiltonian H_z that is diagonal in the computational basis.

$$H_z = \sum_{z\in\{0,1\}^n} E_z |z\rangle\langle z|, \tag{5.1.1}$$

where E_z is the energy assigned to bit-string z. Since H_z acts diagonally, it encodes a classical cost function. The energy E_z is the cost of configuration z, and the ground states are the optimal solutions. Without loss of generality, we rescale and shift so that all eigenvalues lie in $[0, 1]$.

Suppose H_z has M distinct energy levels with eigenvalues

$$0 \le E_0 < E_1 < \cdots < E_{M-1} \le 1. \tag{5.1.2}$$

For each level k, the set of bit-strings at that energy is

$$\Omega_k = \{z \in \{0,1\}^n : H_z|z\rangle = E_k|z\rangle\}, \tag{5.1.3}$$

with degeneracy $d_k = |\Omega_k|$. The degeneracies partition the full Hilbert space, so $\sum_{k=0}^{M-1} d_k = 2^n = N$. The spectral gap of the problem Hamiltonian is $\Delta = E_1 - E_0$, the energy difference between the ground state and the first excited level.

NP-hard optimization problems such as MaxCut and QUBO encode directly as ground states of the 2-local Ising Hamiltonian [11, 12].

$$H_\sigma = \sum_{\langle i,j\rangle} J_{ij}\sigma_z^i\sigma_z^j + \sum_{j=1}^{n} h_j\sigma_z^j, \tag{5.1.4}$$

where $J_{ij}, h_j \in \{-m, -m+1, \ldots, m\}$ for some constant positive integer m. Since each eigenvalue is an integer linear combination of at most $\binom{n}{2} + n$ couplings bounded by m, the eigenvalues lie in $\{-L, -L+1, \ldots, L\}$ for $L = O(mn^2)$, giving at most $2L+1 \in \text{poly}(n)$ distinct energy levels. After normalization to unit operator norm, consecutive eigenvalues differ by at least $1/(2L) \ge 1/\text{poly}(n)$, so the spectral gap satisfies $\Delta \ge 1/\text{poly}(n)$.

Unstructured search also fits this framework. It has $M = 2$ energy levels, a single ground state ($d_0 = 1$) with energy $E_0 = 0$, and $N-1$ excited states ($d_1 = N-1$) at energy $E_1 = 1$. The ground state is the "marked item." Classical search requires $\Theta(N)$ queries, while Grover's circuit algorithm requires $\Theta(\sqrt{N})$ [1, 2].

The adiabatic Hamiltonian interpolates between a rank-one projector and H_z. The initial Hamiltonian is

$$H_0 = -|\psi_0\rangle\langle\psi_0|, \qquad |\psi_0\rangle = |+\rangle^{\otimes n} = \frac{1}{\sqrt{N}}\sum_{z\in\{0,1\}^n} |z\rangle. \tag{5.1.5}$$

Every computational basis state receives equal amplitude, so $|\psi_0\rangle$ introduces no bias toward any particular solution.

The adiabatic Hamiltonian is the linear interpolation

$$H(s) = -(1-s)|\psi_0\rangle\langle\psi_0| + sH_z, \qquad s \in [0,1]. \tag{5.1.6}$$

At $s = 0$, the ground state is $|\psi_0\rangle$ with energy -1, and all other states have energy 0. At $s = 1$, the Hamiltonian is H_z itself, and its ground states encode the solutions. The adiabatic theorem guarantees that if the schedule $s(t)$ traverses $[0, 1]$ slowly enough, the evolved state remains close to the instantaneous ground state throughout, arriving at the end in a state with high overlap with the ground space of H_z.

A rank-one H_0 produces exactly one avoided crossing between the two lowest energy levels. At $s = 0$, the spectrum has a non-degenerate ground state at -1 and an $(N-1)$-fold degenerate level at 0. As s increases, the degeneracy splits according to H_z. Because $H_0 = -|\psi_0\rangle\langle\psi_0|$ has rank one, all coupling between eigenstates of sH_z factors through $|\psi_0\rangle$. The matrix element $\langle k|H_0|j\rangle = -\sqrt{d_k d_j}/N$ is nonzero for all pairs, yet the perturbation has only one degree of freedom, so eigenvalues repel through a single channel. That single crossing is what makes the spectral analysis of Chapters 5–7 possible.

The standard alternative is the transverse-field driver $H_0 = -\sum_{j=1}^{n} \sigma_x^j$, the default in quantum annealing hardware [40]. It couples every pair of computational basis states that differ in a single qubit, producing a dense web of avoided crossings throughout the interpolation. For random instances of NP-complete problems, Altshuler, Krovi, and Roland [39] showed that the resulting spectrum exhibits Anderson localization: exponentially many avoided crossings with exponentially small gaps, and no known analytical technique yields tight gap bounds in that regime [63, 56]. Whether comparable results can be obtained for the transverse-field driver remains open [10].

In the unstructured case, $H(s) = -(1-s)\,|\psi_0\rangle\langle\psi_0| + s(I - |w\rangle\langle w|)$, where $|w\rangle$ is the marked item. Up to a global energy shift of s, this is the Roland-Cerf Hamiltonian [60]. The spectrum has $N-2$ states at energy s (degenerate, orthogonal to both $|\psi_0\rangle$ and $|w\rangle$) and two states whose energies depend on s and undergo an avoided crossing near $s = 1/2$.

5.2 Spectral Parameters

In the Roland-Cerf setting, the crossing position ($s^* = 1/2$), its width, and the minimum gap are all determined by a single quantity, N. For a general problem Hamiltonian H_z with M energy levels and arbitrary degeneracies, no single number suffices. The crossing position depends on the full eigenvalue structure of H_z, not only on E_0 and E_1. We therefore need quantities that compress this M-dimensional information into parameters that directly control the algorithm, namely the crossing location, the sharpness of the minimum gap, and the reopening rate.

Definition 5.2.1 (Spectral parameters)**.** *For the problem Hamiltonian H_z with eigenvalues $E_0 < E_1 < \cdots < E_{M-1}$ and degeneracies d_k, define*

$$A_p = \frac{1}{N} \sum_{k=1}^{M-1} \frac{d_k}{(E_k - E_0)^p}, \qquad p \in \mathbb{N}. \tag{5.2.1}$$

Each excited level contributes its degeneracy d_k weighted by the inverse p-th power of its distance to the ground energy. Larger p gives more weight to near-ground levels. Concretely, A_1 uses weight $1/(E_k - E_0)$, while A_2 uses $1/(E_k - E_0)^2$. A level at energy $E_0 + \varepsilon$ therefore contributes $O(1/\varepsilon)$ to A_1 but $O(1/\varepsilon^2)$ to A_2. The parameter A_1 determines the crossing position, and A_2 determines how sharp the crossing is. Normalization by $N = 2^n$ makes A_p an average over the full Hilbert space.

When $M = 2$, $d_0 = 1$, $d_1 = N - 1$, $E_0 = 0$, and $E_1 = 1$, we get

$$A_p = \frac{N-1}{N} \approx 1 \quad \text{for all } p, \tag{5.2.2}$$

since $E_1 - E_0 = 1$. The spectral parameters are trivial in this case, which is precisely why the Roland-Cerf analysis is simple.

For a general Ising Hamiltonian with $\Delta \geq 1/\mathrm{poly}(n)$ and $M \in \mathrm{poly}(n)$, the bound $A_1 \leq (1 - d_0/N)/\Delta$ gives $A_1 = O(\mathrm{poly}(n))$. The bound $A_2 \geq 1 - d_0/N$ then guarantees A_2 stays constant-order whenever $d_0 \ll N$.

A_1 determines the crossing position, $s^* = A_1/(A_1+1)$. The parameter A_2 enters the minimum spectral gap, $g_{\min} = \Theta(\sqrt{d_0/(NA_2)})$. The gap scales as $\sqrt{d_0/N}$, so more ground states strengthen the coupling and widen the crossing. Both parameters appear in the runtime:

$$T = O\left(\frac{\sqrt{A_2}}{A_1(A_1+1)\Delta^2} \sqrt{\frac{N}{d_0}} \right).$$

Since every eigenvalue gap satisfies $E_k - E_0 \leq 1$ and the total excited degeneracy is $\sum_{k \geq 1} d_k = N - d_0$, we have

$$A_2 \geq \frac{1}{N} \sum_{k=1}^{M-1} d_k = 1 - \frac{d_0}{N}. \tag{5.2.3}$$

For $d_0 \ll N$ (few solutions), $A_2 \geq 1 - 1/N$ is close to 1. We also have $A_1 \leq (1 - d_0/N)/\Delta$, since $(E_k - E_0)^{-1} \leq \Delta^{-1}$ for all $k \geq 1$. A lower bound follows by the same comparison: because $E_k - E_0 \geq \Delta$, termwise comparison gives $A_1 \geq A_2\Delta$. Since $E_k - E_0 \leq 1$, we also have $A_1 \leq A_2$. Hence

$$A_2\Delta \leq A_1 \leq A_2.$$

The two-level approximation near the crossing is accurate only when the crossing window $\delta_s = O(\sqrt{d_0 A_2/N})$ is narrow compared to s^*. Since $\delta_s/s^* = O((1/\Delta)\sqrt{d_0/(A_2 N)})$, this requires the spectral parameters to be polynomially bounded relative to N.

Definition 5.2.2 (Spectral condition)**.** *The problem Hamiltonian H_z satisfies the spectral condition if there exists a constant $c < 1$ (choosing $c \approx 0.02$ suffices; see the monotonicity proof in Chapter 6) such that*

$$\frac{1}{\Delta}\sqrt{\frac{d_0}{A_2 N}} < c. \tag{5.2.4}$$

The quantity on the left is, up to constants, the ratio between the crossing-window width and the problem-Hamiltonian spectral gap Δ. When this ratio is small, the two-level approximation near the crossing is accurate. Higher levels stay perturbative, and the window occupies only a small part of $[0, 1]$. The appendix of [10] shows that $c \approx 0.02$ is sufficient. The specific value emerges from tracking error terms through the eigenvalue approximation and the gap bounds. The quadratic truncation of the eigenvalue equation (Eq. (5.4.3)) introduces relative errors of order c^2. When c is small, these errors remain negligible, and the approximate crossing position s^* and minimum gap $g_{\min}$ match their exact values to within $O(c^2)$ corrections. The monotonicity proof in Chapter 6 inherits this precision, and the constant c propagates into the spectral gap lower bounds through a factor $(1 - O(c^2))$. When the condition fails, the argument breaks in a specific place. The eigenvalue equation is still valid, but the quadratic truncation in δ (Eq. (5.4.3)) requires $|\delta| \ll s\Delta$. That fails when many excited levels crowd near E_0. The result is a genuine multi-crossing regime, exemplified by transverse-field dynamics on random NP-complete instances [39]. The spectral condition therefore marks the boundary between the single-crossing regime of Chapters 5–7 and a regime that remains analytically intractable [63].

For any H_z with $\Delta > (1/c)\sqrt{d_0/N}$, the condition holds, using $A_2 \geq 1 - d_0/N$. For the Ising Hamiltonian with $\Delta \geq 1/\text{poly}(n)$ and d_0 not scaling with N, the left side is exponentially small in n, so the condition is easily satisfied. With $\Delta = 1$ and $d_0 = 1$ (unstructured search), the left side is $1/\sqrt{N}$, well below any constant c for $N \geq 2$.

5.3 Symmetry Reduction

The Hilbert space of $H(s)$ has dimension $N = 2^n$, exponentially large in the number of qubits. Direct spectral analysis is intractable. But the problem Hamiltonian H_z has only M distinct energy levels, and the initial state $|\psi_0\rangle$ treats all bit-strings at the same energy identically. This permutation symmetry within each degenerate subspace reduces the eigenvalue problem from N dimensions to M.

For each energy level k, define the symmetric state

$$|k\rangle = \frac{1}{\sqrt{d_k}} \sum_{z \in \Omega_k} |z\rangle\,, \qquad 0 \leq k \leq M-1. \tag{5.3.1}$$

These M states are orthonormal: $\langle j\,|\,k\rangle = \delta_{jk}$. They span the M-dimensional symmetric subspace

$$\mathcal{H}_S = \text{span}\,\{|k\rangle : 0 \leq k \leq M-1\}\,. \tag{5.3.2}$$

In this basis, the problem Hamiltonian has M non-degenerate eigenvalues.

$$H_z = \sum_{k=0}^{M-1} E_k\,|k\rangle\langle k| \quad \text{on } \mathcal{H}_S, \tag{5.3.3}$$

and the initial state decomposes as

$$|\psi_0\rangle = \sum_{k=0}^{M-1} \sqrt{\frac{d_k}{N}}\,|k\rangle\,. \tag{5.3.4}$$

Since $|\psi_0\rangle \in \mathcal{H}_S$ and both H_z and $|\psi_0\rangle\langle\psi_0|$ map $\mathcal{H}_S$ to itself, the adiabatic Hamiltonian $H(s)$ leaves $\mathcal{H}_S$ invariant. The time evolution starting from $|\psi_0\rangle$ remains in $\mathcal{H}_S$ for all s.

The complement $\mathcal{H}_S^{\perp}$ has dimension $N-M$ and is spanned by states orthogonal to $|\psi_0\rangle$ within each degenerate subspace. Since $|\psi_0\rangle$ is a uniform superposition, its projection onto each degenerate subspace is proportional to $|k\rangle$. Any state in that subspace orthogonal to $|k\rangle$ therefore has zero inner product with $|\psi_0\rangle$, and the rank-one term $|\psi_0\rangle\langle\psi_0|$ in $H(s)$ cannot couple it to anything. Fourier states provide a canonical orthogonal basis with this property. For each level k, order the bit-strings in Ω_k as $z_k^{(1)}, \ldots, z_k^{(d_k)}$ and define the Fourier basis

$$|k^{(\ell)}\rangle = \frac{1}{\sqrt{d_k}} \sum_{\ell'=1}^{d_k} \exp\left[\frac{i2\pi\ell\ell'}{d_k}\right] |z_k^{(\ell')}\rangle\,, \qquad 1 \leq \ell \leq d_k - 1. \tag{5.3.5}$$

Note that $|k^{(0)}\rangle = |k\rangle$ is the symmetric state already in $\mathcal{H}_S$. The remaining $d_k - 1$ states for each level k form a basis for $\mathcal{H}_S^\perp$.

$$\mathcal{H}_S^\perp = \text{span}\left\{|k^{(\ell)}\rangle : 0 \le k \le M-1,\ 1 \le \ell \le d_k - 1\right\}. \tag{5.3.6}$$

Each $|k^{(\ell)}\rangle$ is an eigenstate of $H(s)$ with eigenvalue sE_k:

$$H(s)\,|k^{(\ell)}\rangle = -(1-s)\,|\psi_0\rangle \underbrace{\langle\psi_0|\,k^{(\ell)}}_{=0} + sE_k\,|k^{(\ell)}\rangle = sE_k\,|k^{(\ell)}\rangle\,. \tag{5.3.7}$$

The inner product vanishes because $|k^{(\ell)}\rangle$ is orthogonal to $|k\rangle = |k^{(0)}\rangle$ by construction, and $|\psi_0\rangle$ is a linear combination of the $|k\rangle$ states. Thus, out of the full 2^n-dimensional Hilbert space, only M dimensions participate in the adiabatic evolution. The remaining $N - M$ states are spectators. They are exact eigenstates with known eigenvalues sE_k and have zero overlap with the initial state. For Ising Hamiltonians, $M = O(\text{poly}(n))$, so the full dynamics lives in a polynomial-dimensional subspace.

Henceforth, $H(s)$ denotes its restriction to the symmetric subspace $\mathcal{H}_S$:

$$H(s) = -(1-s)\,|\psi_0\rangle\langle\psi_0| + s\sum_{k=0}^{M-1} E_k\,|k\rangle\langle k|\,. \tag{5.3.8}$$

This is a rank-one perturbation of the diagonal matrix sH_z, the setting of the Golub eigenvalue interlacing results [64].

Lemma 5.3.1 (Eigenvalue equation)**.** *Let $H(s)$ be the adiabatic Hamiltonian restricted to $\mathcal{H}_S$ as in Eq. (5.3.8). Then $\lambda(s)$ is an eigenvalue of $H(s)$ if and only if*

$$\frac{1}{1-s} = \frac{1}{N}\sum_{k=0}^{M-1}\frac{d_k}{sE_k - \lambda(s)}. \tag{5.3.9}$$

Proof. Let $|\psi\rangle = \sum_{k=0}^{M-1}\alpha_k\,|k\rangle$ be an eigenstate of $H(s)$ with eigenvalue λ, and set $\gamma = \langle\psi_0|\,\psi$. Acting with $H(s)$ on $|\psi\rangle$ gives

$$H(s)\,|\psi\rangle = s\sum_{k=0}^{M-1} E_k\alpha_k\,|k\rangle - (1-s)\gamma\,|\psi_0\rangle = \lambda\sum_{k=0}^{M-1}\alpha_k\,|k\rangle\,. \tag{5.3.10}$$

Comparing coefficients of $|k\rangle$ and using $\langle\psi_0|\,k = \sqrt{d_k/N}$ gives

$$\alpha_k = \frac{(1-s)\gamma\sqrt{d_k/N}}{sE_k - \lambda}. \tag{5.3.11}$$

Since $\gamma = \langle\psi_0|\,\psi = (1/\sqrt{N})\sum_k \alpha_k\sqrt{d_k}$, substituting Eq. (5.3.11) yields

$$1 = \frac{1-s}{N}\sum_{k=0}^{M-1}\frac{d_k}{sE_k - \lambda}, \tag{5.3.12}$$

which is equivalent to Eq. (5.3.9). Each step is reversible: given a solution λ of Eq. (5.3.9), the coefficients in Eq. (5.3.11) define an eigenstate (after normalization), provided $\gamma \neq 0$. The case $\gamma = 0$ corresponds to $\lambda = sE_k$ for some k, which are the eigenvalues in $\mathcal{H}_S^\perp$ already accounted for. □

Viewed as a function of λ, the right-hand side of Eq. (5.3.9) is a sum of M terms, each decreasing with a vertical asymptote at $\lambda = sE_k$. Between consecutive poles sE_{k-1} and sE_k, the function decreases monotonically from $+\infty$ to $-\infty$, producing exactly one root per interval. Below the lowest pole sE_0, there is one additional root. The total count is M eigenvalues in $\mathcal{H}_S$, consistent with the dimension.

The two lowest eigenvalues are $\lambda_0(s) < sE_0$ (ground state) and $\lambda_1(s) \in (sE_0, sE_1)$ (first excited state). The spectral gap is $g(s) = \lambda_1(s) - \lambda_0(s) > 0$. However, this ordering information alone does not yield a useful quantitative upper bound on $g(s)$ uniformly over $s \in [0,1]$. Extracting tight bounds requires analyzing the eigenvalue equation in the vicinity of the crossing.

For $M = 2$, Eq. (5.3.9) becomes

$$\frac{1}{1-s} = \frac{1}{N}\cdot\frac{1}{-\lambda} + \frac{N-1}{N}\cdot\frac{1}{s-\lambda}, \tag{5.3.13}$$

where we set $E_0 = 0$ and $E_1 = 1$. Clearing denominators produces the quadratic $N\lambda^2 - N(2s-1)\lambda - s(1-s) = 0$, whose two roots give the ground and first excited energies:

$$\lambda_\pm(s) = \frac{2s-1}{2} \pm \frac{1}{2}\sqrt{(2s-1)^2 + \frac{4s(1-s)}{N}}. \tag{5.3.14}$$

At $s = 0$, the ground energy is $\lambda_- = -1$ and the first excited energy is $\lambda_+ = 0$, consistent with the spectrum of $H(0) = -|\psi_0\rangle\langle\psi_0|$. The gap $g(s) = \lambda_+(s) - \lambda_-(s)$ simplifies to

$$g(s) = \sqrt{(2s-1)^2 + \frac{4s(1-s)}{N}}, \tag{5.3.15}$$

which is minimized at $s = 1/2$ exactly, giving $g_{\min} = 1/\sqrt{N}$. This is the Roland-Cerf gap. The general theory of the next section reproduces this scaling as a special case.

5.4 The Avoided Crossing

The eigenvalue equation (Lemma 5.3.1) characterizes the spectrum of $H(s)$ implicitly. To extract explicit formulas for s^*, δ_s, and $g_{\min}$, we analyze it near the ground-state energy. Near the crossing, the ground and first excited states behave like a two-level system, while higher levels enter as a perturbation controlled by the spectral condition.

The two lowest eigenvalues have the form $\lambda(s) = sE_0 + \delta(s)$, where $\delta(s)$ is a correction to the trivial energy sE_0. Writing the eigenvalue as a perturbation of the nearest pole isolates the ground-state contribution and converts the implicit equation into an explicit power series. This is a standard technique for rank-one updates of diagonal eigenvalue problems [64]. Substituting into Eq. (5.3.9) gives

$$-\frac{d_0}{N\delta} + \frac{1}{N}\sum_{k=1}^{M-1} \frac{d_k}{s(E_k - E_0) - \delta} = \frac{1}{1-s}. \tag{5.4.1}$$

The first term has a pole at $\delta = 0$. The sum has poles at $\delta = s(E_k - E_0)$ for $k \geq 1$. When $|\delta| \ll s\Delta$ (guaranteed by the spectral condition), the sum can be expanded in powers of $\delta/(s(E_k - E_0))$:

$$\frac{1}{N}\sum_{k=1}^{M-1} \frac{d_k}{s(E_k - E_0) - \delta} = \frac{1}{s}\left(A_1 + \frac{\delta}{s}A_2 + \frac{\delta^2}{s^2}A_3 + \cdots\right). \tag{5.4.2}$$

Truncating at the A_2 term and rearranging Eq. (5.4.1) gives a quadratic in δ whose two roots are the corrections $\delta_0^+(s)$ and $\delta_0^-(s)$ for the first excited and ground states, respectively:

$$\delta_0^\pm(s) = \frac{s(A_1+1)}{2A_2(1-s)}\left[(s-s^*) \pm \sqrt{(s^*-s)^2 + \frac{4A_2 d_0}{N(A_1+1)^2}(1-s)^2}\right], \tag{5.4.3}$$

Here $\delta_0^+(s) > 0$ corresponds to the first excited state and $\delta_0^-(s) < 0$ to the ground state. The superscript indicates the sign of the correction relative to sE_0. The crossing position is

$$s^* = \frac{A_1}{A_1 + 1}. \tag{5.4.4}$$

The problem Hamiltonian has M eigenvalues and M degeneracies, so in principle there are $2M$ free spectral parameters. Yet the crossing location depends on one weighted average, A_1. This reduction is what makes a closed-form schedule possible despite rich spectral structure. For Ising Hamiltonians with $\Delta \geq 1/\text{poly}(n)$, A_1 is polynomially bounded above. In the hard-search regime $d_0 \ll N$, one also has $A_1 = \Omega(1)$, so s^* stays away from 0. As $A_1 \to \infty$ (many levels close to the ground state), $s^* \to 1$. For small A_1, s^* moves toward 0.

The crossing position is the balance point in the eigenvalue equation, $A_1/s^* = 1/(1-s^*)$. The left side is the aggregate pull of the excited spectrum toward sE_0, and the right side is the projector contribution. At $s = s^*$, the linear coefficient in the quadratic for δ (Eq. (5.4.3)) vanishes, so the roots $\delta_0^\pm$ are symmetric about zero. The minimum gap is then set by the constant term d_0/N, which is why ground-state degeneracy controls the opening size.

The truncation is remarkably accurate. The actual roots $\delta_\pm(s)$ of the full equation differ from $\delta_0^\pm(s)$ by a relative error controlled by the spectral condition. The next result makes this precise. Its proof uses the

intermediate value theorem on the full equation after bounding the remainder with A_3 and the spectral condition. The technique was developed for optimal spatial search via continuous-time quantum walks [65], where the same rank-one perturbation structure appears with a graph Laplacian replacing the diagonal Hamiltonian. The adaptation to the AQO setting appears in [10].

Lemma 5.4.1 (Validity of approximation)**.** *Let H_z satisfy the spectral condition (Definition 5.2.2) with constant $c \approx 0.02$, and define*

$$\delta_s = \frac{2}{(A_1+1)^2}\sqrt{\frac{d_0 A_2}{N}}. \tag{5.4.5}$$

Then for any $s \in \mathcal{I}_{s^*} = [s^* - \delta_s,\ s^* + \delta_s]$, there exists a constant $\eta \ll 1$ such that the two lowest eigenvalues of $H(s)$ satisfy

$$\delta_+(s) \in \left((1-\eta)\,\delta_0^+(s),\ (1+\eta)\,\delta_0^+(s)\right), \tag{5.4.6}$$

$$\delta_-(s) \in \left((1+\eta)\,\delta_0^-(s),\ (1-\eta)\,\delta_0^-(s)\right), \tag{5.4.7}$$

where $\delta_0^\pm(s)$ are given by Eq. (5.4.3).

The proof evaluates the full equation (5.4.1) at $\delta_0^\pm(1\pm\eta)$ and shows, using the spectral condition to bound the truncated Taylor remainder, that the full equation changes sign between these points. The intermediate value theorem then guarantees a root in the interval. The spectral condition enters through the bound $|\delta_0^\pm(s)|/(s\Delta) \leq \kappa c < 1$, where κ is a constant depending on c, ensuring the geometric series in the Taylor expansion converges. The constant $c \approx 0.02$ is sufficient for $\eta \leq 0.1$. The complete calculation appears in the appendix of [10].

Since both corrections are approximated to within $1 \pm \eta$, the spectral gap $g(s) = \delta_+(s) - \delta_-(s)$ is within a factor of $1 \pm 2\eta$ of $\delta_0^+(s) - \delta_0^-(s)$, which evaluates to

$$g(s) = (1 \pm 2\eta) \cdot \frac{s(A_1+1)}{A_2(1-s)}\sqrt{(s^*-s)^2 + \frac{4A_2 d_0}{N(A_1+1)^2}(1-s)^2}. \tag{5.4.8}$$

At $s = s^*$, the first term under the square root vanishes, leaving only the second:

$$g_{\min} = g(s^*) \geq (1-2\eta) \cdot \frac{2A_1}{A_1+1}\sqrt{\frac{d_0}{NA_2}}. \tag{5.4.9}$$

The gap scales as $\sqrt{d_0/N}$ with corrections from spectral structure. The factor $2A_1/(A_1+1)$ captures crossing position. A crossing near the boundary ($s^* \to 0$ or $s^* \to 1$) reduces the gap. The factor $\sqrt{d_0/N}$ is the Grover-like contribution. More solutions (larger d_0) increase the gap and reduce runtime. The factor $1/\sqrt{A_2}$ encodes spectral structure beyond the simplest two-level case.

An exact algebraic identity connects s^*, δ_s, and the leading-order minimum gap. Writing $\hat{g} = \frac{2A_1}{A_1+1}\sqrt{\frac{d_0}{NA_2}}$ for the leading-order expression, direct substitution gives

$$\frac{s^*(A_1+1)^2}{A_2} \cdot \delta_s = \hat{g}, \tag{5.4.10}$$

and by Eq. (5.4.9), $g_{\min} \geq (1-2\eta)\hat{g}$. This relation will be used in Chapter 7 to verify the runtime calculation.

Three regions partition $[0,1]$ based on the crossing.

$$\mathcal{I}_{s^\leftarrow} = [0,\ s^* - \delta_s), \qquad \mathcal{I}_{s^*} = [s^* - \delta_s,\ s^* + \delta_s], \qquad \mathcal{I}_{s^\rightarrow} = (s^* + \delta_s,\ 1]. \tag{5.4.11}$$

Lemma 5.4.2 (Gap within the crossing window)**.** *Let H_z satisfy the spectral condition with constant c, and define*

$$\kappa' = \frac{(1+2\eta)(1+2c)}{(1-2\eta)(1-2c)}\sqrt{1+(1-2c)^2}. \tag{5.4.12}$$

Then for any $s \in \mathcal{I}_{s^*}$,

$$g_{\min} \leq g(s) \leq \kappa' \cdot g_{\min}. \tag{5.4.13}$$

Proof. The lower bound is immediate from the definition of $g_{\min}$ as the minimum over $\mathcal{I}_{s^*}$. For the upper bound, start from Eq. (5.4.8) with $|s - s^*| \leq \delta_s$:

$$g(s) \leq \frac{s(A_1+1)}{A_2(1-s)}\sqrt{\delta_s^2 + \frac{4A_2 d_0}{N(A_1+1)^2}(1-s)^2}. \tag{5.4.14}$$

Factoring out $(A_1+1)\delta_s(1-s)$ under the square root and using $s/s^* \leq 1 + \delta_s/s^*$:

$$g(s) \leq \frac{s^*(A_1+1)^2}{A_2}\delta_s \cdot \frac{s}{s^*} \cdot \sqrt{\frac{1}{(1-s)^2(A_1+1)^2} + 1}. \tag{5.4.15}$$

The first factor equals $\hat{g}$ by Eq. (5.4.10). The spectral condition gives $\delta_s/(1-s^*) \leq 2c$ and $\delta_s/s^* \leq 2c$. To see the first, compute

$$\frac{\delta_s}{1-s^*} = \frac{2}{1+A_1}\sqrt{\frac{d_0 A_2}{N}} = \frac{2A_2\Delta}{1+A_1} \cdot \frac{1}{\Delta}\sqrt{\frac{d_0}{A_2 N}} \leq 2s^* c \leq 2c, \tag{5.4.16}$$

where we used $A_2\Delta/(1+A_1) \leq A_1/(1+A_1) = s^*$. The bound $\delta_s/s^* \leq 2c$ follows similarly. Substituting into the upper bound:

$$g(s) \leq (1+2\eta)\hat{g} \cdot (1+2c)\sqrt{1+(1-2c)^2} \leq \kappa' \cdot g_{\min}, \tag{5.4.17}$$

where the factor $(1+2\eta)$ comes from the upper approximation in Eq. (5.4.8), and the last step uses $\hat{g} \leq g_{\min}/(1-2\eta)$. □

Inside $\mathcal{I}_{s^*}$, the gap is $\Theta(g_{\min})$. Outside, it is strictly larger, as the next section establishes. The avoided crossing is localized.

Specializing to unstructured search, with $A_1 = A_2 = (N-1)/N$:

$$s^* = \frac{(N-1)/N}{(N-1)/N + 1} = \frac{N-1}{2N-1} \approx \frac{1}{2}, \tag{5.4.18}$$

$$g_{\min} = \frac{2(N-1)/(2N-1)}{\sqrt{N \cdot (N-1)/N}} = \frac{2(N-1)}{(2N-1)\sqrt{N-1}} \approx \frac{1}{\sqrt{N}}, \tag{5.4.19}$$

$$\delta_s = \frac{2N^2}{(2N-1)^2}\sqrt{\frac{N-1}{N^2}} \approx \frac{1}{2\sqrt{N}}. \tag{5.4.20}$$

The crossing is at $s^* \approx 1/2$, the minimum gap scales as $1/\sqrt{N}$, and the window width scales as $1/\sqrt{N}$. These agree asymptotically with the exact quadratic solution in Eq. (5.3.15), confirming the general theory reproduces the known scaling. The small discrepancy between $s^* = (N-1)/(2N-1)$ and the exact minimum at $s = 1/2$ is a higher-order effect of the two-level truncation, vanishing as $O(1/N)$.

5.5 Gap Structure

The adiabatic schedule requires the gap everywhere, not just near the crossing. The local adaptive schedule speeds up where the gap is large and slows where it is small, so the runtime depends on the gap profile across the full interval $[0,1]$. Inside $\mathcal{I}_{s^*}$, the gap is $\Theta(g_{\min})$. Outside it, the gap grows linearly. Proving this split requires different techniques on the two sides, and that split drives the structure of Chapter 6.

Lemma 5.5.1 (Gap to the left of the crossing)**.** *For any $s \in \mathcal{I}_{s\leftarrow} = [0,\, s^* - \delta_s)$, the spectral gap of $H(s)$ satisfies*

$$g(s) \geq \frac{A_1(A_1+1)}{A_2}(s^* - s). \tag{5.5.1}$$

The bound admits two proofs. One route uses the variational principle. An explicit ansatz $|\phi\rangle$ gives an upper bound $\lambda_0(s) \leq \langle\phi|\, H(s)\, |\phi\rangle$, while the eigenvalue equation gives the lower bound $\lambda_1(s) \geq sE_0$. The ansatz is

$$|\phi\rangle = \frac{1}{\sqrt{A_2 N}} \sum_{k=1}^{M-1} \frac{\sqrt{d_k}}{E_k - E_0} |k\rangle\,. \tag{5.5.2}$$

This ansatz concentrates amplitude near the ground energy and yields a tight upper bound on $\lambda_0(s)$. A second route uses concavity. Because $\lambda_0(s) = \min_{|\psi\rangle} \langle\psi|\, H(s)\, |\psi\rangle$ is the pointwise minimum of linear functions in s, it is concave. The tangent line at s^* therefore lies above $\lambda_0(s)$. Combining that tangent bound with $\lambda_1(s) \geq sE_0$ reproduces Eq. (5.5.1). Chapter 6 develops both arguments in detail.

Lemma 5.5.2 (Gap to the right of the crossing). *Assume $A_1 \geq 1/2$ (equivalently $s^* \geq 1/3$). Let $k = 1/4$, $a = 4k^2\Delta/3$, and*

$$s_0 = s^* - \frac{k\, g_{\min}(1-s^*)}{a - k\, g_{\min}}. \tag{5.5.3}$$

Then for all $s \geq s^*$, the spectral gap of $H(s)$ satisfies

$$g(s) \geq \frac{\Delta}{30} \cdot \frac{s - s_0}{1 - s_0}. \tag{5.5.4}$$

This bound is linear in $s - s_0$, with slope proportional to Δ. The proof strategy differs from the left side. One places a line $\gamma(s) = sE_0 + \beta(s)$ between the two lowest eigenvalues and then uses Sherman-Morrison [66] to control the resolvent norm $\|R_{H(s)}(\gamma)\|$. This yields $g(s) \geq 2/\|R_{H(s)}(\gamma)\|$. The constants $k = 1/4$ and $a = 4k^2\Delta/3$ are chosen so that the auxiliary function $f(s)$ decreases monotonically on $[s^*, 1]$, producing the clean slope constant $\Delta/30$.

At the window boundary, both bounds match $g_{\min}$ in order. At $s = s^* - \delta_s$, the left bound gives

$$g(s^* - \delta_s) \geq \frac{A_1(A_1+1)}{A_2} \cdot \delta_s = \frac{2A_1}{A_1+1}\sqrt{\frac{d_0}{NA_2}} = \hat{g}, \tag{5.5.5}$$

which satisfies $\hat{g} = \Theta(g_{\min})$ by Eq. (5.4.9). At $s = s^*$ (right boundary start), $\beta(s^*) \geq k\, g_{\min}$, so $g(s^*) \geq 2k\, g_{\min}/(1 + f(s^*)) = O(g_{\min})$ since $f(s^*) = \Theta(1)$. The gap profile is therefore continuous across region boundaries. It dips to $g_{\min}$ at s^* and rises linearly on both sides.

With the gap profile in hand, runtime follows from the optimal local adaptive schedule [41, 60], where $ds/dt \propto g(s)^2$. Evolution therefore slows quadratically as the gap decreases. The total runtime is

$$T \propto \int_0^1 \frac{ds}{g(s)^2}, \tag{5.5.6}$$

split across the three regions. In the left and right regions, linear gap growth gives $1/g(s)^2 \propto 1/(s-s^*)^2$, so each outer contribution scales like $1/\delta_s$ at the window boundary. Inside the window, the gap is approximately constant at $g_{\min}$ and contributes $2\delta_s/g_{\min}^2$. This window term dominates. The bottleneck is therefore a $\Theta(1/\sqrt{N})$-wide interval around s^*.

$$\frac{\delta_s}{g_{\min}^2} \propto \frac{\sqrt{A_2}}{A_1(A_1+1)\Delta^2}\sqrt{\frac{N}{d_0}}, \tag{5.5.7}$$

yielding the optimal runtime [10]. For the Ising Hamiltonian with $A_1, A_2 = O(\text{poly}(n))$ and $\Delta \geq 1/\text{poly}(n)$, this gives $T = \widetilde{O}(\sqrt{N/d_0})$, matching the Grover lower bound up to polylogarithmic factors. Chapter 7 carries out this calculation rigorously.

5.6 What Remains

At this point, the structure is in place and the remaining steps are focused. Chapter 6 proves the outer-region gap bounds. Chapter 7 converts those bounds into the optimal runtime. Chapter 8 accounts for the pre-computation cost required to realize that schedule.

Given the complete gap profile, the optimal runtime is

$$T = O\left(\frac{1}{\varepsilon} \cdot \frac{\sqrt{A_2}}{A_1(A_1+1)\Delta^2} \cdot \sqrt{\frac{N}{d_0}}\right), \tag{5.6.1}$$

where ε is the target error. For Ising Hamiltonians, this is $\widetilde{O}(\sqrt{N/d_0})$, matching the lower bound of Farhi, Goldstone, and Gutmann [36]. Adiabatic quantum optimization achieves the Grover speedup.

The local adaptive schedule requires s^* to precision $O(\delta_s) = O(2^{-n/2})$, so A_1 must be known at comparable precision. Approximating A_1 is already hard much earlier on this scale. At additive error $1/\text{poly}(n)$, two oracle queries suffice to solve 3-SAT, so the task is NP-hard. Exact computation of A_1, or approximation to $O(2^{-\text{poly}(n)})$, is #P-hard because polynomial interpolation recovers all degeneracies d_k from $O(\text{poly}(n))$ exact queries. Chapter 8 proves both statements and quantifies the resulting precision gap.

In the circuit model, Grover's algorithm reaches $\widetilde{O}(\sqrt{N/d_0})$ without pre-computing any spectral parameter. Oracle queries gather the needed information during execution. In the adiabatic framework, by contrast, the schedule is fixed before evolution starts, which forces NP-hard pre-computation. In our view, this asymmetry

is not a proof artifact. It reflects a genuine model-level difference. The adiabatic speedup is real, but it is conditional on solving a hard preprocessing problem first [10]. Chapter 9 makes this tradeoff explicit through an uninformed-schedule separation, an interpolation theorem for partial information, and an adaptive measurement protocol that bypasses classical hardness.

In the unstructured case, the limitation vanishes: $A_1 = (N-1)/N \approx 1$ is trivially known, so $s^* \approx 1/2$ requires no hard computation. The complexity arises only for problem Hamiltonians with rich spectral structure, where the degeneracies d_k and energy gaps $E_k - E_0$ are not known in advance. The Ising Hamiltonian encoding an NP-hard problem is precisely such a case.

Chapter 6

Spectral Analysis

Chapter 5 established the crossing window $\mathcal{I}_{s^*}$ where the spectral gap satisfies $g(s) = \Theta(g_{\min})$, and it stated the outer-region bounds: a linear lower bound on the left (Lemma 5.5.1) and on the right (Lemma 5.5.2). What remains is to prove them.

The two proofs use different tools because the spectrum behaves differently on the two sides of the crossing. To the left of s^*, the ground energy $\lambda_0(s)$ sits below sE_0 while the first excited energy $\lambda_1(s)$ sits above it. A variational argument gives a sharp linear gap bound. To the right of s^*, eigenvalues of sH_z crowd the interval $[sE_0, sE_1]$, and that variational strategy loses traction. There we switch to a resolvent argument plus Sherman-Morrison for rank-one perturbations. The resulting profile is steep on the left, flatter on the right, and nearly flat inside the window.

6.1 Gap to the Left of the Crossing

The eigenvalue equation (Lemma 5.3.1) places the ground state energy at $\lambda_0(s) < sE_0$ and the first excited energy at $\lambda_1(s) \in (sE_0, sE_1)$. This already proves $g(s) > 0$. It does not yet give the quantitative lower bound needed for the runtime integral. What we need is a bound that makes the left-side linear reopening explicit.

The strategy is to tighten the upper bound on $\lambda_0(s)$. Two routes give the same linear form. The first uses the variational principle. For any normalized state $|\phi\rangle$, the ground energy satisfies $\lambda_0(s) \le \langle\phi| H(s) |\phi\rangle$, so a carefully chosen ansatz directly yields a bound. The second uses concavity. Because $\lambda_0(s) = \min_{|\psi\rangle} \langle\psi| H(s) |\psi\rangle$ is the pointwise minimum of affine functions in s, it is concave, and every tangent line lies above it. We start with the variational route because it keeps the constants explicit.

Lemma 6.1.1 (Gap to the left of the crossing)**.** *For any $s \in \mathcal{I}_{s\leftarrow} = [0,\, s^* - \delta_s)$, the spectral gap of $H(s)$ satisfies*

$$g(s) \ge \frac{A_1(A_1+1)}{A_2}\,(s^* - s)\,. \tag{6.1.1}$$

Proof. We upper-bound $\lambda_0(s)$ via the variational principle and lower-bound $\lambda_1(s)$ from the eigenvalue equation.

The ansatz must live in the span of $\{|k\rangle : k \ge 1\}$, orthogonal to the ground-state component $|0\rangle$, and should concentrate amplitude on levels close to E_0 where the energy expectation is lowest. The natural weighting is the inverse energy gap, because levels near E_0 should carry more amplitude. Unit normalization then fixes the scale, so we define

$$|\phi\rangle = \frac{1}{\sqrt{A_2 N}} \sum_{k=1}^{M-1} \frac{\sqrt{d_k}}{E_k - E_0}\,|k\rangle\,. \tag{6.1.2}$$

This weighting also arises in first-order perturbation theory. The correction to the ground state $|E_0\rangle$ of sH_z due to the perturbation $-(1-s)\,|\psi_0\rangle\langle\psi_0|$ has coefficients proportional to $\langle E_k\rangle\,\psi_0/(E_k - E_0) = \sqrt{d_k/N}/(E_k - E_0)$, which matches the form above up to normalization. Normalization is immediate.

$$\langle\phi\rangle\,\phi = \frac{1}{A_2 N} \sum_{k=1}^{M-1} \frac{d_k}{(E_k - E_0)^2} = \frac{A_2}{A_2} = 1. \tag{6.1.3}$$

To compute $\langle\phi| H(s) |\phi\rangle$, decompose $H(s) = -(1-s)\,|\psi_0\rangle\langle\psi_0| + s(H_z - E_0) + sE_0$. Each term contributes separately.

The projector term gives

$$-(1-s)\left|\langle\psi_0\rangle\,\phi\right|^2 = -(1-s)\left(\frac{1}{\sqrt{A_2 N}}\sum_{k=1}^{M-1}\frac{d_k}{(E_k-E_0)\sqrt{N}}\right)^2 = -(1-s)\frac{A_1^2}{A_2}, \tag{6.1.4}$$

where $\langle\psi_0\rangle\,\phi = A_1/\sqrt{A_2}$ follows from $\langle\psi_0\rangle\,k = \sqrt{d_k/N}$ and the definition of A_1.

The shifted diagonal term gives

$$s\,\langle\phi|\,(H_z - E_0)\,|\phi\rangle = \frac{s}{A_2 N}\sum_{k=1}^{M-1}\frac{d_k}{(E_k-E_0)^2}\cdot(E_k-E_0) = \frac{s}{A_2 N}\sum_{k=1}^{M-1}\frac{d_k}{E_k-E_0} = \frac{s\,A_1}{A_2}. \tag{6.1.5}$$

The constant term contributes $sE_0\,\langle\phi\rangle\,\phi = sE_0$. Combining the three terms gives

$$\lambda_0(s) \le \langle\phi|\,H(s)\,|\phi\rangle = sE_0 - (1-s)\frac{A_1^2}{A_2} + s\frac{A_1}{A_2} = sE_0 + \frac{A_1}{A_2}\left(s(1+A_1) - A_1\right). \tag{6.1.6}$$

Since $s^*(1+A_1) = A_1$, we have $s(1+A_1) - A_1 = (1+A_1)(s-s^*) = (s-s^*)/(1-s^*)$, so

$$\lambda_0(s) \le sE_0 + \frac{A_1}{A_2}\cdot\frac{s-s^*}{1-s^*}. \tag{6.1.7}$$

For $s < s^*$, the second term is negative, confirming $\lambda_0(s) < sE_0$.

For the first excited state, the eigenvalue equation (Lemma 5.3.1) confines $\lambda_1(s)$ to the interval (sE_0, sE_1), so

$$\lambda_1(s) \ge sE_0. \tag{6.1.8}$$

The gap is therefore

$$g(s) = \lambda_1(s) - \lambda_0(s) \ge sE_0 - sE_0 - \frac{A_1}{A_2}\cdot\frac{s-s^*}{1-s^*} = \frac{A_1}{A_2}\cdot\frac{s^*-s}{1-s^*}. \tag{6.1.9}$$

Since $1/(1-s^*) = A_1 + 1$, we obtain $g(s) \ge A_1(A_1+1)(s^*-s)/A_2$. □

At the left boundary of the crossing window, $s = s^* - \delta_s$, the bound gives

$$g(s^* - \delta_s) \ge \frac{A_1(A_1+1)}{A_2}\cdot\delta_s = \hat{g}, \tag{6.1.10}$$

using $A_1(A_1+1)\delta_s/A_2 = \hat{g}$ from Eq. (5.4.10). Since $g_{\min} = (1 \pm O(\eta))\hat{g}$ from Eq. (5.4.9), the gap at the window boundary is $\Theta(g_{\min})$. The three-region decomposition is therefore tight because the left bound meets the window bound at the boundary rather than leaving a gap between them.

An alternative derivation uses concavity. Since $\lambda_0(s) = \min_{|\psi\rangle}\langle\psi|\,H(s)\,|\psi\rangle$ is the pointwise minimum of affine functions in s, it is concave. The Hellmann-Feynman theorem [16] gives the second derivative explicitly.

$$\ddot{\lambda}_0(s) = -2\sum_{j\ge 1}\frac{|\,\langle\phi_j(s)|\,\dot{H}\,|\phi_0(s)\rangle\,|^2}{\lambda_j(s)-\lambda_0(s)} \le 0,$$

where $\dot{H} = H_z + |\psi_0\rangle\langle\psi_0|$ and $|\phi_j(s)\rangle$ are the instantaneous eigenstates. Concavity implies that every tangent line lies above the function. In particular, the tangent at s^* gives $\lambda_0(s) \le \lambda_0(s^*) + \lambda_0'(s^*)(s-s^*)$, an upper bound of the same form as (6.1.7), though the variational approach gives slightly sharper constants.

When $M = 2$ ($d_0 = 1$, $d_1 = N-1$, $E_0 = 0$, $E_1 = 1$), the ansatz reduces to $|\phi\rangle = |1\rangle$, and the bound becomes

$$g(s) \ge \frac{(N-1)/N\cdot(2N-1)/N}{(N-1)/N}\left(\frac{1}{2}-s\right) = \frac{2N-1}{N}\left(\frac{1}{2}-s\right) \approx 2\left(\frac{1}{2}-s\right). \tag{6.1.11}$$

The exact gap $g(s) = \sqrt{(2s-1)^2 + 4s(1-s)/N}$ at $s = 1/4$ equals $\sqrt{1/4 + 3/(4N)} \approx 1/2$, while the bound gives $(2N-1)/(4N) \approx 1/2$. The bound is tight near s^* and only becomes loose as s approaches 0, where the true gap approaches 1 while the bound continues growing.

6.2 Gap to the Right of the Crossing

The variational principle cannot bound the gap to the right of s^*. It bounds ground energies from above, not excited energies from below, and what we need on the right is a lower bound on $\lambda_1(s) - \lambda_0(s)$ that captures the linear reopening of the gap.

The obstacle is structural. On the left, $\lambda_1(s)$ is bounded below by sE_0 from the eigenvalue equation, which gives a clean anchor point. On the right, $\lambda_1(s)$ still lies between sE_0 and sE_1, but now many higher branches pass through the same interval and generate their own avoided crossings. We need a method that controls spectral distance without tracking individual branches one by one. The eigenvalue equation (Lemma 5.3.1) characterizes the full spectrum implicitly, but it does not directly give the linear-in-$(s - s^*)$ lower bound we need.

The resolvent provides exactly this. For a self-adjoint operator A with spectrum $\sigma(A)$ and any $\lambda \notin \sigma(A)$, the resolvent

$$R_A(\lambda) = (\lambda I - A)^{-1} \tag{6.2.1}$$

is a bounded operator whose norm equals the inverse distance from λ to the spectrum:

$$\|R_A(\lambda)\| = \frac{1}{\operatorname{dist}(\lambda,\, \sigma(A))}. \tag{6.2.2}$$

This follows from the spectral theorem. In the eigenbasis of A with eigenvalues $\{\lambda_j\}$, the resolvent is diagonal with entries $1/(\lambda - \lambda_j)$, so its operator norm is $\max_j |1/(\lambda - \lambda_j)| = 1/\min_j |\lambda - \lambda_j|$. If a point γ lies between two consecutive eigenvalues λ_0 and λ_1, then $\operatorname{dist}(\gamma, \sigma(A)) = \min(\gamma - \lambda_0, \lambda_1 - \gamma) \leq g/2$, since the minimum of two non-negative numbers summing to g is at most $g/2$. Therefore $\|R_A(\gamma)\| = 1/\operatorname{dist}(\gamma, \sigma(A)) \geq 2/g$, and the useful contrapositive is

$$g(s) \geq \frac{2}{\|R_{H(s)}(\gamma)\|}. \tag{6.2.3}$$

The spectral-gap problem has become a norm problem. A lower bound on the gap is now an upper bound on a resolvent norm.

This resolvent approach to rank-one perturbations has precedent in spatial search. Childs and Goldstone [67] used it to prove $O(\sqrt{N})$ search time on the complete graph. Chakraborty, Novo, and Roland [68, 65] then extended the method to broad graph families via Sherman-Morrison.

The algebraic structure is the same as in our Hamiltonian $H(s) = sH_z - (1-s)\,|\psi_0\rangle\langle\psi_0|$, with a graph Laplacian replaced by a diagonal cost Hamiltonian. We therefore import the same mechanism, with graph parameters replaced by A_1 and A_2.

Spatial search via continuous-time quantum walks asks for a marked vertex in a graph G on N vertices by evolving $|s\rangle = (1/\sqrt{N})\sum_v |v\rangle$ under $H_{\text{search}} = -\gamma L - \sum_{v\in S} |v\rangle\langle v|$, where L is the graph Laplacian and $\gamma > 0$ is tunable [67]. When $|S| = 1$, the oracle term is rank one (and low rank more generally). The dictionary to our setting is direct. L plays the role of sH_z, the oracle projector plays the role of $(1-s)\,|\psi_0\rangle\langle\psi_0|$, the graph spectral gap corresponds to Δ, and effective resistance plays the role of A_2.

In both settings, one places a line $\gamma(s)$ between the two lowest eigenvalues, applies Sherman-Morrison to split the resolvent into a known diagonal part plus a correction term, and then bounds that correction. The method works because rank-one perturbations of diagonal operators always admit this inversion step, reducing the gap problem to one rational bound.

The constants $k = 1/4$ and $f(s^*) = 4$ are not accidents of this specific Hamiltonian. They come from the same line-placement optimization that appears whenever a rank-one perturbation is handled this way. The optimization balances denominator positivity against numerator growth in $f(s)$. In that sense the constants are structural. They do not depend on whether the unperturbed part is a graph Laplacian or a diagonal cost Hamiltonian.

Since $H(s) = sH_z - (1-s)\,|\psi_0\rangle\langle\psi_0|$ is a rank-one perturbation of sH_z, we can invert its resolvent explicitly. The Sherman-Morrison identity [66] states that for an invertible operator A and vectors $|u\rangle, \langle v|$,

$$(A + |u\rangle\langle v|)^{-1} = A^{-1} - \frac{A^{-1}\,|u\rangle\langle v|\,A^{-1}}{1 + \langle v|\,A^{-1}\,|u\rangle}, \tag{6.2.4}$$

provided $1 + \langle v|\,A^{-1}\,|u\rangle \neq 0$. Applying this to the resolvent of $H(s)$ decomposes it into the resolvent of sH_z (whose spectrum is known explicitly) and a correction from the rank-one term $-(1-s)\,|\psi_0\rangle\langle\psi_0|$. The triangle inequality then yields an upper bound on $\|R_{H(s)}(\gamma)\|$.

We choose a line $\gamma(s)$ between $\lambda_0(s)$ and $\lambda_1(s)$ for all $s \geq s^*$. Then we apply Sherman-Morrison, bound each contribution in terms of A_1 and A_2, and convert the resulting resolvent estimate into a linear lower bound on $g(s)$.

The simplest line starts at sE_0 when $s = s^*$ and ends between E_0 and E_1 at $s = 1$. Take $\beta(s) = a(s - s^*)/(1 - s^*)$ with $a < \Delta$, and set $\gamma(s) = sE_0 + \beta(s)$. For $a = \Delta/6$, one can show $f(s) \leq 1$ for all $s \geq s^*$. This yields $g(s) \geq \beta(s) = (\Delta/6)(s - s^*)/(1 - s^*)$. The bound is valid but too weak where the runtime is decided. At the window boundary $s = s^* + \delta_s$, it gives $g(s^* + \delta_s) \geq (\Delta/6) \cdot \delta_s/(1 - s^*) = (\Delta A_2)/(6A_1) \cdot g_{\min}$. Since $\Delta A_2 \leq A_1$, this is at most $g_{\min}/6$, and it can be polynomially smaller when $\Delta A_2 \ll A_1$. At $s = s^*$, the same estimate collapses to $g(s^*) \geq 0$, which misses the true minimum gap entirely.

The failure has a geometric explanation. At s^*, the ground energy $\lambda_0(s^*)$ sits $g_{\min}/2$ below s^*E_0. The line $\gamma(s)$ passes through s^*E_0 at $s = s^*$, so it has no safety margin from the lower branch. At a midpoint between two eigenvalues, the resolvent norm is $2/g$. At a point that touches one eigenvalue, it diverges. So the line must start at $O(g_{\min})$ distance from both branches.

The fix is to shift the line origin from s^* to a point $s_0 < s^*$ so that $\beta(s^*) = k\, g_{\min}$ for a constant $k < 1$. With $\beta(s) = a(s - s_0)/(1 - s_0)$, the constraint $\beta(s^*) = k\, g_{\min}$ determines

$$s_0 = s^* - \frac{k\, g_{\min}(1 - s^*)}{a - k\, g_{\min}}. \tag{6.2.5}$$

The line now passes through $\gamma(s^*) = s^*E_0 + k\, g_{\min}$, which lies between $\lambda_0(s^*)$ and $\lambda_1(s^*)$ when k is chosen appropriately. The price is that $s_0 < s^*$ introduces extra terms in the monotonicity analysis for $f(s)$. We therefore need a careful choice of a.

Lemma 6.2.1 (Gap to the right of the crossing)**.** *Assume $A_1 \geq 1/2$. Let $k = 1/4$, $a = 4k^2\Delta/3 = \Delta/12$, and s_0 as in Eq. (6.2.5). Then for all $s \geq s^*$, the spectral gap of $H(s)$ satisfies*

$$g(s) \geq \frac{\Delta}{30} \cdot \frac{s - s_0}{1 - s_0}. \tag{6.2.6}$$

Proof. Set $\gamma(s) = sE_0 + \beta(s)$ with $\beta(s) = a(s - s_0)/(1 - s_0)$. The argument reduces to showing that a certain ratio $f(s)$, built from the numerator and denominator of the Sherman-Morrison correction, is monotonically decreasing on $[s^*, 1]$. Once that is established, $\max_{s \geq s^*} f(s) = f(s^*) = O(1)$, and the resolvent bound $\|R_{H(s)}(\gamma)\| \leq (1/\beta)(1 + f(s))$ converts directly into a linear gap lower bound.

Since $H(s) = sH_z - (1 - s)\,|\psi_0\rangle\langle\psi_0|$, the resolvent of $H(s)$ at γ satisfies, via Eq. (6.2.4) and the triangle inequality,

$$\|R_{H(s)}(\gamma)\| \leq \|R_{sH_z}(\gamma)\| + (1 - s)\frac{\|R_{sH_z}(\gamma)\,|\psi_0\rangle\langle\psi_0|\,R_{sH_z}(\gamma)\|}{1 + (1 - s)\,\langle\psi_0|\,R_{sH_z}(\gamma)\,|\psi_0\rangle}. \tag{6.2.7}$$

The unperturbed resolvent $R_{sH_z}(\gamma)$ is diagonal in the $|k\rangle$ basis with entries $1/(\gamma - sE_k) = 1/(\beta - s(E_k - E_0))$ for $k \geq 1$ and $1/\beta$ for $k = 0$. The nearest eigenvalue of sH_z to γ is sE_0, at distance β, so $\|R_{sH_z}(\gamma)\| = 1/\beta$.

We now bound the numerator and denominator of the second term separately. Both bounds use $\beta(s) \leq s(E_k - E_0)/2$ for all $k \geq 1$, so the Taylor series in $\beta/(s(E_k - E_0))$ converges quickly. Here $\beta(s) \leq a = \Delta/12$, while $s(E_k - E_0) \geq s^*\Delta \geq \Delta/3$ because $s^* = A_1/(A_1 + 1) \geq 1/3$ when $A_1 \geq 1/2$. Therefore $\beta \leq \Delta/12 < \Delta/6 \leq s(E_k - E_0)/2$, as required. The condition $A_1 \geq 1/2$ also marks the nontrivial search regime. Since $A_1 \geq 1 - d_0/N$, the complementary case $A_1 < 1/2$ implies $d_0 > N/2$, where random sampling already succeeds with constant probability.

Numerator bound. The squared norm of $R_{sH_z}(\gamma)\,|\psi_0\rangle$ expands as

$$\|R_{sH_z}(\gamma)\,|\psi_0\rangle\|^2 = \frac{d_0}{N\beta^2} + \frac{1}{N}\sum_{k=1}^{M-1}\frac{d_k}{\big(s(E_k - E_0) - \beta\big)^2}. \tag{6.2.8}$$

Using $s(E_k - E_0) - \beta \geq s(E_k - E_0)/2$, each term in the sum is at most $4d_k/(Ns^2(E_k - E_0)^2)$, giving

$$\|R_{sH_z}(\gamma)\,|\psi_0\rangle\langle\psi_0|\,R_{sH_z}(\gamma)\| \leq \|R_{sH_z}(\gamma)\,|\psi_0\rangle\|^2 \leq \frac{d_0}{N\beta^2} + \frac{4A_2}{s^2}. \tag{6.2.9}$$

Denominator bound. Expanding the expectation value gives

$$\begin{aligned} 1 + (1 - s)\,\langle\psi_0|\,R_{sH_z}(\gamma)\,|\psi_0\rangle &= 1 + \frac{(1 - s)d_0}{N\beta} - \frac{1 - s}{N}\sum_{k=1}^{M-1}\frac{d_k}{s(E_k - E_0) - \beta} \\ &= 1 + \frac{(1 - s)d_0}{N\beta} - \frac{1 - s}{s}\sum_{k=1}^{M-1}\frac{d_k}{N(E_k - E_0)}\sum_{\ell=0}^{\infty}\left(\frac{\beta}{s(E_k - E_0)}\right)^{\ell}. \end{aligned} \tag{6.2.10}$$

Using $\beta/(s(E_k - E_0)) \le 1/2$ to bound the geometric series by $1 + 2\beta/(s(E_k - E_0))$ gives

$$1 + (1-s)\,\langle\psi_0|\,R_{sH_z}(\gamma)\,|\psi_0\rangle \ge 1 + \frac{(1-s)d_0}{N\beta} - (1-s)\left(\frac{A_1}{s} + \frac{2A_2\beta}{s^2}\right). \tag{6.2.11}$$

Collecting terms. Substituting the bounds (6.2.9) and (6.2.11) into (6.2.7) and factoring gives

$$\|R_{H(s)}(\gamma)\| \le \frac{1}{\beta}\,(1 + f(s))\,, \tag{6.2.12}$$

and

$$f(s) = \frac{\frac{d_0}{N}\,s^2(1-s) + 4A_2\beta^2(1-s)}{\frac{d_0}{N}\,s^2(1-s) + \beta\,s\,\dfrac{s-s^*}{1-s^*} - 2A_2\beta^2(1-s)}. \tag{6.2.13}$$

To obtain this form, multiply numerator and denominator of the second term in (6.2.7) by β, then multiply by $s^2(1-s)$ to clear fractions. The key step is rewriting the denominator's constant-plus-linear terms using $A_1 = s^*/(1-s^*)$:

$$1 - \frac{(1-s)A_1}{s} + \frac{(1-s)d_0}{N\beta} = \frac{s-s^*}{s(1-s^*)} + \frac{(1-s)d_0}{N\beta}, \tag{6.2.14}$$

since $1 - A_1(1-s)/s = (s - A_1(1-s))/s = (s - s^*(1-s)/(1-s^*))/s = (s(1-s^*) - s^*(1-s))/(s(1-s^*)) = (s-s^*)/(s(1-s^*))$. Multiplying through by $\beta s^2(1-s)$ and collecting the Taylor-bounded terms into the $A_2\beta^2$ contributions gives Eq. (6.2.13). The fraction d_0/N measures the density of ground states in the computational basis.

The numerator of $f(s)$ measures how strongly the rank-one perturbation can amplify the resolvent norm. The d_0/N term comes from the $|0\rangle$ component of $|\psi_0\rangle$, and the A_2 term comes from the excited components. The denominator records the opposing effect. As γ moves away from the crossing, the factor $\beta\,s(s-s^*)/(1-s^*)$ increases and pushes the resolvent back down. This is why $f(s^*)$ is only $O(1)$ near the crossing and why $f(s) \to 0$ as s approaches 1.

From (6.2.12) and (6.2.3), the spectral gap satisfies

$$g(s) \ge \frac{2\beta(s)}{1 + f(s)} \ge \frac{2\beta(s)}{1 + \max_{s \ge s^*} f(s)}. \tag{6.2.15}$$

If f is monotonically decreasing on $[s^*, 1]$, then $\max_{s\ge s^*} f(s) = f(s^*)$, and the bound becomes $g(s) \ge 2\beta(s)/(1+f(s^*))$, which is linear in $s - s_0$.

Monotonicity of f. We show $f'(s) < 0$ for $s \in [s^*, 1]$. Write $f = u/v$, so the sign of f' is the sign of $u'v - uv'$. The derivative algebra is long, so it helps to name the structure before expanding. After cancellation, three terms remain, which we label T_1, T_2, T_3. Terms T_1 and T_3 are negative. Term T_2 is positive and proportional to $(d_0/N)\,s_0$, which appears because the line origin is shifted below s^*. The real work is to show that T_1 alone dominates T_2 on all of $[s^*, 1]$. The argument factors $T_1 + T_2$ and compares a convex quadratic in s (from T_1) against a cubic $s(1-s)^2$ (from T_2). Both expressions are bounded by their values at s^*, and the spectral condition (Definition 5.2.2) ensures the quadratic term wins. Write $f = u/v$ with

$$\begin{aligned} u &= \frac{d_0}{N}\,s^2(1-s) + 4A_2\beta^2(1-s), \\ v &= \frac{d_0}{N}\,s^2(1-s) + \beta\,s\,\frac{s-s^*}{1-s^*} - 2A_2\beta^2(1-s). \end{aligned} \tag{6.2.16}$$

Then $f' = (u'v - uv')/v^2$, so the sign of f' is determined by $u'v - uv'$.

Computing u' and v' using $\beta' = a/(1-s_0)$:

$$\begin{aligned} u' &= \frac{4aA_2\beta}{1-s_0}(2 + s_0 - 3s) + \frac{d_0}{N}\,s(2-3s), \\ v' &= \frac{a(3s^2 - 2s(s^* + s_0) + s^*s_0)}{(1-s_0)(1-s^*)} - \frac{2aA_2\beta}{1-s_0}(2 + s_0 - 3s) + \frac{d_0}{N}\,s(2-3s). \end{aligned} \tag{6.2.17}$$

Expanding $u'v$ and uv' and taking the difference produces exact cancellation of two terms. The canceled terms are $(d_0/N)^2 s^3(2-3s)(1-s)$ and $8aA_2^2\beta^3(1-s)(2+s_0-3s)/(1-s_0)$. The remainder has three terms [10]:

$$u'v - uv' = \underbrace{-\frac{4aA_2\beta^2}{(1-s_0)(1-s^*)}\Big(s^2(1 + s_0 - s^*) - 2s\,s_0 + s^*s_0\Big)}_{T_1} \tag{6.2.18}$$

$$+\underbrace{\frac{12aA_2\frac{d_0}{N}\beta}{1-s_0}\,s(1-s)^2\,s_0}_{T_2}$$
$$\underbrace{-\frac{\frac{d_0}{N}\,s^2a}{(1-s_0)(1-s^*)}\Big(-s^2(s^*+s_0-1)+2s\,s_0s^*-s^*s_0\Big)}_{T_3}.$$

Terms T_1 and T_3 are negative, while T_2 is positive. The positive term T_2 is the only one that contains $(d_0/N)\,s_0$, so it is exactly the cost of shifting the line origin below s^*. We now show that T_1 alone controls T_2.

Factor out $-4aA_2\beta/(1-s_0)$ from T_1+T_2:

$$-\frac{4aA_2\beta}{1-s_0}\left(\frac{\beta}{1-s^*}\Big(s^2(1+s_0-s^*)-2s\,s_0+s^*s_0\Big)-\frac{3d_0}{N}\,s_0\,s(1-s)^2\right). \tag{6.2.19}$$

The quadratic $s^2(1+s_0-s^*)-2s\,s_0+s^*s_0$ is convex in s because $1+s_0-s^*>0$, and here $s_0<s^*$. Its minimizer lies at $s_m<s^*$, so throughout $[s^*,1]$ it stays above its value at s^*. At $s=s^*$ that value is $s^*(1-s^*)(s^*-s_0)>0$. The cubic $s(1-s)^2$ reaches its maximum at $s=1/3\le s^*$, so on $[s^*,1]$ it also stays below its value at s^*. Therefore the bracket in (6.2.19) is bounded below by its value at $s=s^*$:

$$\frac{a(s^*-s_0)^2}{1-s_0}-\frac{3d_0}{N}\,s_0(1-s^*)^2. \tag{6.2.20}$$

Using $s_0\le s^*$ and $s^*-s_0=k\,g_{\min}(1-s^*)/(a-k\,g_{\min})$, this is positive whenever

$$a<\frac{4}{3}k^2\frac{A_1}{A_2}. \tag{6.2.21}$$

Since $\Delta A_2\le A_1$ and $A_2\le\sum_{k\ge1}d_k/(N(E_k-E_0)^2)\le A_1/\Delta$, the choice $a=(4/3)k^2\Delta$ satisfies (6.2.21). With this choice, $u'v-uv'<0$ on $[s^*,1]$, so f is monotonically decreasing.

Evaluating $f(s^*)$. At $s=s^*$, $\beta(s^*)=k\,g_{\min}$. The term $\beta\,s(s-s^*)/(1-s^*)$ vanishes, so

$$f(s^*)=\frac{\frac{d_0}{N}\,s^{*2}(1-s^*)+4A_2k^2g_{\min}^2(1-s^*)}{\frac{d_0}{N}\,s^{*2}(1-s^*)-2A_2k^2g_{\min}^2(1-s^*)}. \tag{6.2.22}$$

Replacing $g_{\min}$ by its leading-order expression $\hat g=2s^*\sqrt{d_0/(NA_2)}$ from Eq. (5.4.9) (valid up to a $(1\pm O(\eta))$ factor that does not affect the final constant), we have $A_2k^2\hat g^2=4k^2s^{*2}d_0/N$. Substituting gives

$$f(s^*)=\frac{1+16k^2}{1-8k^2}. \tag{6.2.23}$$

For $k=1/4$, $f(s^*)=(1+1)/(1-1/2)=4$, so $1+f(s^*)=5$.

Final bound. From (6.2.15),

$$g(s)\ge\frac{2\beta(s)}{1+f(s^*)}=\frac{2a}{1+f(s^*)}\cdot\frac{s-s_0}{1-s_0}. \tag{6.2.24}$$

The prefactor evaluates to

$$\frac{2a}{1+f(s^*)}=\frac{2\cdot(4/3)k^2\Delta}{1+(1+16k^2)/(1-8k^2)}=\frac{4}{3}k^2\cdot\frac{1-8k^2}{1+4k^2}\cdot\Delta. \tag{6.2.25}$$

The function $P(k)=(4/3)k^2(1-8k^2)/(1+4k^2)$ is maximized at $k_{\rm opt}=\frac12\sqrt{\sqrt{3/2}-1}\approx0.237$, where $P(k_{\rm opt})=\frac13(5-2\sqrt6)\approx0.034$. For $k=1/4$:

$$P(1/4)=\frac{4}{3}\cdot\frac{1}{16}\cdot\frac{1/2}{5/4}=\frac{1}{30}. \tag{6.2.26}$$

Therefore $g(s)\ge(\Delta/30)(s-s_0)/(1-s_0)$. □

Specializing to $M=2$ and $\Delta=1$, the bound gives $g(s)\ge(1/30)(s-s_0)/(1-s_0)$, where $s_0=1/2-O(1/\sqrt N)$ is close to $s^*\approx1/2$ for large N. Near $s=3/4$, the exact gap from Eq. (5.3.15) is $g(3/4)=\sqrt{1/4+3/(4N)}\approx1/2$, while the bound gives approximately $(1/30)(1/4)/(1/2)=1/60$. The bound is conservative by a factor of approximately 30 but correctly captures the linear growth. This constant is the price of a clean, uniform bound valid for all problem Hamiltonians satisfying the spectral condition.

6.3 The Complete Gap Profile

Combining the results of this chapter with those of Chapter 5, the spectral gap $g(s)$ is bounded below across all of $[0, 1]$.

Theorem 6.3.1 (Complete gap profile)**.** *Let H_z satisfy the spectral condition (Definition 5.2.2) and assume $A_1 \geq 1/2$ (equivalently $s^* \geq 1/3$). The spectral gap of $H(s) = -(1-s)\,|\psi_0\rangle\langle\psi_0| + sH_z$ satisfies, for all $s \in [0, 1]$:*

$$g(s) \geq \begin{cases} \dfrac{A_1(A_1+1)}{A_2}\,(s^* - s)\,, & s \in \mathcal{I}_{s\leftarrow} = [0,\, s^* - \delta_s)\,, \\ g_{\min}\,, & s \in \mathcal{I}_{s^*} = [s^* - \delta_s,\, s^* + \delta_s]\,, \\ \dfrac{\Delta}{30} \cdot \dfrac{s - s_0}{1 - s_0}, & s \in \mathcal{I}_{s\rightarrow} = (s^* + \delta_s,\, 1]\,, \end{cases} \tag{6.3.1}$$

where $s_0 = s^* - k\,g_{\min}(1 - s^*)/(a - k\,g_{\min})$ with $k = 1/4$ and $a = \Delta/12$.

Proof. The three cases follow from Lemma 5.4.2 (window, proved in Chapter 5), Lemma 6.1.1 (left), and Lemma 6.2.1 (right). The right bound holds for all $s \geq s^*$ and therefore covers $\mathcal{I}_{s\rightarrow}$. The window bound $g(s) \geq g_{\min}$ is tighter than the right bound at s^* but weaker far from the crossing. □

The right branch uses $\frac{s-s_0}{1-s_0}$, while the published paper [10] writes $\frac{s-s^*}{1-s_0} + \frac{s^*-s_0}{1-s_0}$ as two separate terms. These are identical: $s - s_0 = (s - s^*) + (s^* - s_0)$. The single-fraction form absorbs the constant offset $s^* - s_0$ into the numerator, which simplifies the piecewise statement without changing the bound.

The bounds match across region boundaries. At the left boundary $s = s^* - \delta_s$,

$$\frac{A_1(A_1+1)}{A_2} \cdot \delta_s = \hat{g} = \Theta(g_{\min}), \tag{6.3.2}$$

so the left bound at the window boundary is $\Theta(g_{\min})$, consistent with the window bound. At $s = s^*$, the right bound gives $g(s^*) \geq 2\beta(s^*)/(1 + f(s^*)) = 2k\,g_{\min}/5 = g_{\min}/10$, which is below $g_{\min}$ by a constant factor but still $O(g_{\min})$. The window bound provides the tighter estimate $g(s^*) = g_{\min}$.

The piecewise bounds are intentionally asymmetric. The left arm is steep, and the right arm is shallower. The variational method tracks the left slope closely. The resolvent method gives a weaker slope but remains valid through the spectral congestion on the right. Geometrically, the profile is a broad V centered at s^* with a narrow rounded minimum of width about $2\delta_s$. The left slope is $A_1(A_1+1)/A_2$, which is $O(\mathrm{poly}(n))$ for Ising instances. The right slope is $\Delta/(30(1 - s_0))$, set by the problem gap Δ. At the endpoints, $g(0) = 1$ for H_0 and $g(1) = \Delta$ for H_z.

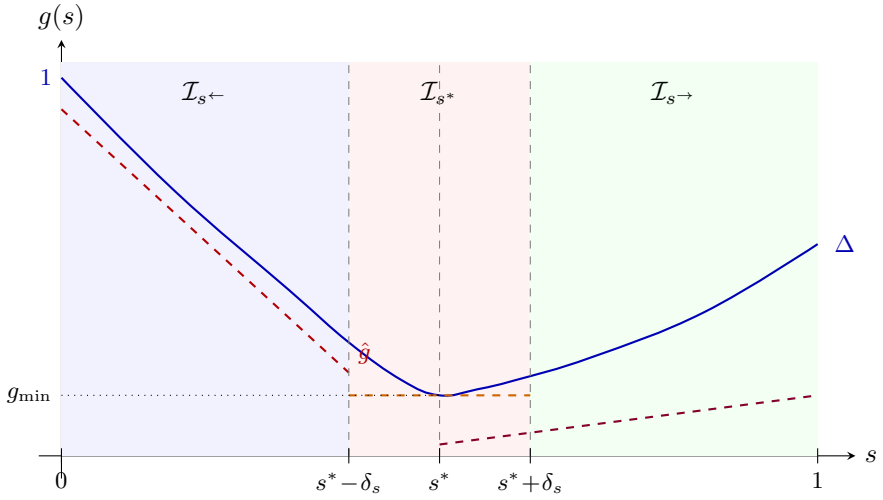

Figure 6.1: Schematic gap profile for $H(s)$. The solid curve shows the true spectral gap $g(s)$, which equals 1 at $s = 0$, dips to $g_{\min}$ at $s = s^*$, and recovers to Δ at $s = 1$. The left arm is steep (slope $A_1(A_1+1)/A_2$); the right arm is shallower (slope controlled by Δ). Dashed lines show the piecewise lower bounds from Theorem 6.3.1: linear on the left, constant $g_{\min}$ in the window, and linear on the right (reaching $\Delta/30$ at $s = 1$). The right bound is below $g_{\min}$ at s^* but remains $O(g_{\min})$.

Four parameters control the gap: A_1, A_2, d_0, and Δ. For any problem Hamiltonian H_z satisfying the spectral condition, Theorem 6.3.1 bounds $g(s)$ over all of $[0,1]$ up to constants. The minimum is $g_{\min} = \Theta(\sqrt{d_0/(NA_2)})$ at $s^* = A_1/(A_1+1)$, and it is exponentially small in n when $d_0 = O(1)$. The crossing location depends only on A_1. More solutions (larger d_0) widen the gap, while richer near-ground spectral structure (larger A_2) narrows it. At $s = 1$, the gap returns to Δ, the spectral gap of H_z itself.

For unstructured search, the exact gap $g(s) = \sqrt{(2s-1)^2 + 4s(1-s)/N}$ and the piecewise bound from Theorem 6.3.1 can be compared directly. The left bound has slope $(2N-1)/N \approx 2$, matching the asymptotic slope of the exact gap, which approaches $2(1-1/N) \approx 2$ away from s^*. The window bound $g_{\min} = 1/\sqrt{N}$ is exact. The right bound has slope approximately $1/15$ near s^*, weaker than the true slope by a factor of 30, but sufficient for the runtime integral since the window dominates.

The window dominates the runtime integral. $\int_0^1 g(s)^{-2}\,ds$ splits across the three regions. In the left and right regions, $g(s) \sim C|s - s^*|$ for constants C, and

$$\int_{\delta_s}^{s^*} \frac{du}{(Cu)^2} = \frac{1}{C^2}\left(\frac{1}{\delta_s} - \frac{1}{s^*}\right) \leq \frac{1}{C^2\delta_s}, \tag{6.3.3}$$

which is $O(1/(C^2\delta_s))$. In the window, $g(s) \geq g_{\min}$ gives $\int_{s^*-\delta_s}^{s^*+\delta_s} g(s)^{-2}\,ds \leq 2\delta_s/g_{\min}^2$. The window contribution $\delta_s/g_{\min}^2 = \Theta(A_2^{3/2}/(A_1(A_1+1)) \cdot \sqrt{N/d_0})$ dominates the outer regions. Once the Δ-dependent right-arm term is included, the full integral yields the runtime

$$T = O\left(\frac{\sqrt{A_2}}{A_1(A_1+1)\Delta^2}\sqrt{\frac{N}{d_0}}\right),$$

which Chapter 7 derives rigorously.

Chapter 7

Optimal Schedule

The spectral gap of $H(s)$ is now bounded from below on all of $[0,1]$. Theorem 6.3.1 shows a piecewise form. The gap reaches $g_{\min}$ at s^*, then reopens with slope $A_1(A_1+1)/A_2$ on the left and $\Delta/30$ on the right. Chapter 5 already identified the key runtime integral, $\int_0^1 g(s)^{-2}\,ds$ (Eq. (5.5.6)), and showed that the crossing window dominates. The remaining issue is the adiabatic theorem itself. Its error bound determines which power of g controls runtime.

With a constant-rate theorem, runtime is controlled by $\int_0^1 g(s)^{-3}\,ds$. For the profile of Theorem 6.3.1, the crossing window contributes $\delta_s/g_{\min}^3$. In the two-level case $M=2$ with $g_{\min}=1/\sqrt{N}$, this gives $T=O(N)$ and no speedup over classical search. An adaptive schedule with $K'(s)$ scaled to the gap replaces $\int g^{-3}\,ds$ with $\int g^{-p}\,ds$ for $p\in(1,2)$. The resulting runtime

$$T = O\left(\frac{\sqrt{A_2}}{A_1(A_1+1)\Delta^2}\sqrt{\frac{N}{d_0}}\frac{1}{\varepsilon}\right)$$

matches Grover scaling up to explicit spectral prefactors.

7.1 How Theorem Choice Sets Runtime

The gap profile alone does not determine runtime. Translating spectral data into evolution time requires an adiabatic theorem, and different theorems permit different schedules. That choice changes the gap dependence and, in the running example, is exactly the difference between $O(N)$ and $O(\sqrt{N})$.

The earliest rigorous bounds, due to Jansen, Ruskai, and Seiler [17], apply to a constant schedule $K'(s)=T$ and give a transition probability of order $O(1/T^2)$. Their Theorem 3 states that for a state $\psi\in P(0)$, the probability of leaving the ground space satisfies

$$(\psi,[1-P(s)]U_\tau(s)\psi)\le A(s)^2, \tag{7.1.1}$$

where $A(s)\le (1/T)(\|H'\|/g^2)|_{\text{bdry}}+(1/T)\int_0^s(7\sqrt{m}\,\|H'\|^2/g^3+\|H'\|/g^2)\,ds'$, with m the multiplicity of the ground eigenvalue and the boundary term evaluated at $s=0$ and s. Setting $A(s)=\varepsilon$ and solving for T gives

$$T = O\left(\frac{1}{\varepsilon}\int_0^1 \frac{\|H'\|^2}{g(s)^3}\,ds\right). \tag{7.1.2}$$

With $M=2$ and $\|H'\|=O(1)$, the integral $\int_0^1 g^{-3}\,ds$ is dominated by the $O(1/\sqrt{N})$-wide window where $g\approx 1/\sqrt{N}$. Its contribution is $(1/\sqrt{N})\cdot N^{3/2}=N$. Therefore the JRS bound gives $T=O(N/\varepsilon)$, which matches classical search. A constant schedule allocates the same physical time per unit of s whether the gap is $O(1)$ or $O(1/\sqrt{N})$. That uniform allocation forces the g^{-3} dependence, so the narrow crossing window dominates and the quantum speedup disappears.

The resolution is to let the schedule depend on the gap. Roland and Cerf [60] introduced a *local* adiabatic condition. Instead of enforcing adiabaticity with one global timescale T, they enforce it infinitesimally on each segment $[s,s+ds]$. The standard criterion gives

$$\left|\frac{ds}{dt}\right| \le \frac{\varepsilon\, g(s)^2}{|\langle e_1(s)|H'(s)|e_0(s)\rangle|},$$

where e_0, e_1 are the ground and first excited states. Inverting this inequality yields

$$K'(s) = \frac{dt}{ds} \geq \frac{|\langle e_1|H'|e_0\rangle|}{\varepsilon\, g(s)^2}.$$

For the running example, $|\langle e_1|H'|e_0\rangle| = O(1)$ because $H'(s) = |\psi_0\rangle\langle\psi_0| + H_z$ is constant. Thus $K'(s) \propto 1/g(s)^2$, and the runtime becomes

$$T = \frac{C}{\varepsilon}\int_0^1 g(s)^{-2}\, ds. \tag{7.1.3}$$

The integral can be evaluated explicitly. Writing $g(s)^2 = (2s-1)^2 + 4s(1-s)/N$ and substituting $u = 2s - 1$:

$$\int_0^1 g(s)^{-2}\, ds = \frac{1}{2}\int_{-1}^1 \frac{du}{u^2 + (1-u^2)/N} = \frac{1}{2}\int_{-1}^1 \frac{N\, du}{1 + (N-1)u^2}. \tag{7.1.4}$$

For large N, the substitution $v = \sqrt{N-1}\, u$ gives $\frac{N}{2\sqrt{N-1}}\int_{-\sqrt{N-1}}^{\sqrt{N-1}} \frac{dv}{1+v^2} = \frac{N}{2\sqrt{N-1}} \cdot 2\arctan\big(\sqrt{N-1}\big) = O(\sqrt{N})$, since $\arctan\big(\sqrt{N-1}\big) \to \pi/2$. Therefore $T = O(\sqrt{N}/\varepsilon)$, recovering the Grover speedup from a smooth, continuous-time evolution.

The Roland-Cerf construction requires exact knowledge of $g(s)$ at every point. For the running example with $M = 2$, this is feasible because the gap has the closed form in Eq. (5.3.15). For a general M-level problem Hamiltonian, the exact gap is unknown and only the piecewise bounds of Theorem 6.3.1 are available. If one substitutes a lower bound $g_0(s) \leq g(s)$, the schedule slows down conservatively because $1/g_0^2 \geq 1/g^2$, so the runtime increases only by constants. The difficulty shifts to error control: derivative terms in the adiabatic bound become sensitive to corners in g_0. The adaptive schedule of section 7.3 addresses this through the exponent $p \in (1, 2)$.

Several later results sharpened this picture. Boixo, Knill, and Somma [69] introduced eigenpath traversal, which replaces continuous evolution with projections onto ground states of intermediate Hamiltonians $H(s_0), H(s_1), \ldots, H(s_L)$. Their key ingredient is phase randomization between steps. It suppresses coherent accumulation of diabatic error, which otherwise recreates the usual $O(1/g_{\min}^2)$ behavior. Under the condition $\int g^{-p}\, ds = O(g_{\min}^{1-p})$, this gives $O(1/g_{\min})$ scaling. Cunningham and Roland [70] tightened constants and gave a continuous-time version that underlies section 7.2. Elgart and Hagedorn [18] followed a different route using Gevrey-smooth switching, obtaining superpolynomial suppression with runtime $T \geq K\, g^{-2}|\ln g|^{6\alpha}$. The schedule used here has a different practical advantage: it only needs a certified lower bound $g_0(s) \leq g(s)$, not the exact gap.

7.2 The Adiabatic Error Bound

The Schrödinger equation $i\, d|\psi\rangle/dt = H(s(t))|\psi\rangle$ governs the evolution under the time-dependent Hamiltonian $H(s)$, with $s : [0, T] \to [0, 1]$ parameterizing the interpolation. The density-matrix form $d\rho/dt = -i[H, \rho]$ is more convenient for the error analysis and also covers mixed states. We reparameterize time by $t = K(s)$, where $K : [0, 1] \to \mathbb{R}^+$ is differentiable and monotone increasing. The chain rule then gives

$$\frac{d\rho}{ds} = -iK'(s)[H(s), \rho(s)], \tag{7.2.1}$$

where $K'(s) = dK/ds > 0$ controls the instantaneous evolution rate. The total runtime is $T = K(1) = \int_0^1 K'(s)\, ds$. A large $K'(s)$ means slow evolution (long physical time per unit of s), allowing the state to track the ground state through a small-gap region. A small $K'(s)$ means fast evolution, appropriate where the gap is large and diabatic transitions are suppressed.

The error of the adiabatic evolution is the probability that the final state does not lie in the ground space of $H(1)$:

$$\varepsilon = 1 - \mathrm{Tr}[P(1)\rho(1)], \tag{7.2.2}$$

where $P(s)$ denotes the projector onto the ground eigenspace of $H(s)$ and $\rho(0) = P(0)$ (the system starts in the ground state of $H(0)$). The projector $P(s)$ and the ground energy $\lambda_0(s)$ are both functions of s, varying as the Hamiltonian interpolates from H_0 to H_z. The operator

$$(H(s) - \lambda_0(s))^+ = \sum_{j\geq 1} \frac{1}{\lambda_j(s) - \lambda_0(s)}\, |\phi_j(s)\rangle\langle\phi_j(s)| \tag{7.2.3}$$

is the pseudoinverse of $H(s) - \lambda_0(s)$: it acts as zero on the ground space and as $(\lambda_j - \lambda_0)^{-1}$ on the j-th excited eigenspace. Its operator norm is $1/g(s)$, so a small spectral gap amplifies the pseudoinverse.

Lemma 7.2.1 (Adiabatic error bound [10, 70])**.** *Let $H(s)$ be a twice-differentiable path of Hamiltonians with a continuous ground energy $\lambda_0(s)$ and a spectral gap $g(s) > 0$ for all $s \in [0,1]$. Let $K : [0,1] \to \mathbb{R}^+$ be a schedule with absolutely continuous derivative K'. Then the evolution (7.2.1) starting from $\rho(0) = P(0)$ satisfies*

$$\varepsilon \le \frac{1}{K'(1)} \left\| \left[P'(1),\, (H(1) - \lambda_0(1))^+\right] \right\| + \int_0^1 \frac{1}{K'} \left\| \left[P',\, (H - \lambda_0)^+\right]' \right\| ds + \int_0^1 \left| \left(\frac{1}{K'}\right)' \right| \left\| \left[P',\, (H - \lambda_0)^+\right] \right\| ds. \tag{7.2.4}$$

Proof. Since $\rho(0) = P(0)$, the error is $\varepsilon = \operatorname{Tr}[P(0)\rho(0)] - \operatorname{Tr}[P(1)\rho(1)] = |\operatorname{Tr}[P\rho]|_0^1$, so it suffices to track $\operatorname{Tr}[P(s)\rho(s)]$. Differentiating:

$$\frac{d}{ds}\operatorname{Tr}[P\rho] = \operatorname{Tr}[P'\rho] + \operatorname{Tr}[P\rho']. \tag{7.2.5}$$

The second term vanishes. Substituting the evolution equation (7.2.1): $\operatorname{Tr}[P\rho'] = -iK' \operatorname{Tr}[P[H,\rho]]$. Since $HP = \lambda_0 P$, the cyclic property gives $\operatorname{Tr}[P[H,\rho]] = \operatorname{Tr}[PH\rho - P\rho H] = \lambda_0 \operatorname{Tr}[P\rho] - \operatorname{Tr}[HP\rho] = 0$.

For $\operatorname{Tr}[P'\rho]$, write $Q = I - P$ and use the decomposition $P' = PP'Q + QP'P$, which holds because $PP'P = 0$ and $QP'Q = 0$.[i] Inserting $Q = (H - \lambda_0)^+(H - \lambda_0)$ and using the identities $(H - \lambda_0)\rho P = [H,\rho]P$ and $P\rho(H - \lambda_0) = -P[H,\rho]$ (both consequences of $HP = \lambda_0 P$), a cyclic rearrangement under the trace gives

$$\operatorname{Tr}[P'\rho] = \operatorname{Tr}\left[PP'(H - \lambda_0)^+[H,\rho]\right] - \operatorname{Tr}\left[(H - \lambda_0)^+ P'P[H,\rho]\right]. \tag{7.2.6}$$

Since $(H - \lambda_0)^+ P = P(H - \lambda_0)^+ = 0$ (the pseudoinverse annihilates the ground space), $PP'(H - \lambda_0)^+$ reduces to $P'(H - \lambda_0)^+$ and $(H - \lambda_0)^+ P'P$ reduces to $(H - \lambda_0)^+ P'$, so the two terms combine into a commutator:

$$\operatorname{Tr}[P'\rho] = \operatorname{Tr}\left[\left[P',\, (H - \lambda_0)^+\right][H,\rho]\right] = i(K')^{-1} \operatorname{Tr}\left[\left[P',\, (H - \lambda_0)^+\right]\rho'\right], \tag{7.2.7}$$

where the last equality substitutes $[H,\rho] = i(K')^{-1}\rho'$ from (7.2.1).

Integrating from 0 to 1 gives $\operatorname{Tr}[P\rho]\big|_0^1 = i\int_0^1 (K')^{-1} \operatorname{Tr}[[P',\, (H - \lambda_0)^+]\,\rho']\, ds$. Integration by parts, with $u = (K')^{-1}[P',\, (H - \lambda_0)^+]$ and $dv = \rho'\, ds$, transfers the derivative from ρ onto u:

$$\begin{aligned} \operatorname{Tr}[P\rho]\big|_0^1 = i(K'(1))^{-1} \operatorname{Tr}\left[\left[P'(1),\, (H(1) - \lambda_0(1))^+\right]\rho(1)\right] \\ - i\int_0^1 \operatorname{Tr}\left[\left((K')^{-1}\left[P',\, (H - \lambda_0)^+\right]' + \left((K')^{-1}\right)'\left[P',\, (H - \lambda_0)^+\right]\right)\rho\right] ds. \end{aligned} \tag{7.2.8}$$

The boundary term at $s = 0$ vanishes. Since $\rho(0) = P(0)$, the commutator trace expands as

$$\operatorname{Tr}\left[\left[P',\, (H - \lambda_0)^+\right] P\right] = \operatorname{Tr}[P'(H - \lambda_0)^+ P] - \operatorname{Tr}[(H - \lambda_0)^+ P'P].$$

For the first summand, $(H - \lambda_0)^+ P = 0$ (the pseudoinverse annihilates the ground-space projector), so $\operatorname{Tr}[P'(H - \lambda_0)^+ P] = 0$. For the second, cyclicity of the trace gives $\operatorname{Tr}[(H - \lambda_0)^+ P'P] = \operatorname{Tr}[P(H - \lambda_0)^+ P'] = 0$ by the same identity. Taking absolute values and bounding $|\operatorname{Tr}[A\rho]| \le \|A\|$ for any density matrix ρ yields (7.2.4). □

The error bound depends on $H(s)$ only through the commutator $[P', (H - \lambda_0)^+]$ and its derivative. The following bounds express these in terms of the Hamiltonian derivatives H', H'' and the spectral gap g, using the Riesz integral representation of the spectral projector introduced by Kato [16].

Lemma 7.2.2 (Projector derivative bounds [10])**.** *Under the conditions of Lemma 7.2.1:*

$$\|P'(s)\| \le \frac{2\|H'(s)\|}{g(s)}, \tag{7.2.9}$$

$$\left\| \left[P'(s),\, (H(s) - \lambda_0(s))^+\right] \right\| \le \frac{4\|H'(s)\|}{g(s)^2}, \tag{7.2.10}$$

$$\left\| \left[P'(s),\, (H(s) - \lambda_0(s))^+\right]' \right\| \le \frac{40\|H'(s)\|^2}{g(s)^3} + \frac{4\|H''(s)\|}{g(s)^2}. \tag{7.2.11}$$

Proof of (7.2.9). Let Γ be a circle in the complex plane centered at $\lambda_0(s)$ with radius $g(s)/2$. The Riesz integral representation gives

$$P(s) = \frac{1}{2\pi i} \oint_\Gamma R_{H(s)}(z)\, dz, \tag{7.2.12}$$

[i] Differentiating $P^2 = P$ gives $P'P + PP' = P'$. Left-multiplying by P: $PP'P + PP' = PP'$, so $PP'P = 0$. Then $QP'Q = P' - PP' - P'P + PP'P = P' - P' = 0$.

where $R_{H(s)}(z) = (zI - H(s))^{-1}$ is the resolvent. Differentiating with respect to s:

$$P'(s) = \frac{1}{2\pi i} \oint_\Gamma R_{H(s)}(z)\, H'(s)\, R_{H(s)}(z)\, dz, \tag{7.2.13}$$

using the resolvent identity $R'_H = R_H H' R_H$. On the contour Γ, every point z lies at distance exactly $g(s)/2$ from $\lambda_0(s)$ and at distance at least $g(s)/2$ from every other eigenvalue (since the nearest eigenvalue is $\lambda_1(s)$ at distance $g(s)$ from $\lambda_0(s)$). Therefore $\|R_{H(s)}(z)\| = 1/\mathrm{dist}(z, \sigma(H(s))) \le 2/g(s)$ on Γ. Bounding the integral:

$$\|P'(s)\| \le \frac{1}{2\pi} \oint_\Gamma \|R_H(z)\| \cdot \|H'(s)\| \cdot \|R_H(z)\|\, |dz| \le \frac{1}{2\pi} \left(\frac{2}{g}\right)^2 \|H'\| \cdot \pi g = \frac{2\|H'\|}{g}. \tag{7.2.14}$$

□

Bound (7.2.10) follows from (7.2.9): $\|[A, B]\| \le 2\|A\| \cdot \|B\|$ gives $\|[P', (H - \lambda_0)^+]\| \le 2 \cdot 2\|H'\|/g \cdot 1/g = 4\|H'\|/g^2$.

Bound (7.2.11) requires two intermediate results. Write $\widetilde{H} = H - \lambda_0$ for the shifted Hamiltonian. Its pseudoinverse satisfies

$$(\widetilde{H}^+)' = -\widetilde{H}^+ \widetilde{H}' \widetilde{H}^+ + P' \widetilde{H}^+ + \widetilde{H}^+ P', \tag{7.2.15}$$

where $\widetilde{H}' = H' - \lambda_0'$. To see this, split the difference quotient $(\widetilde{H}^+(s+h) - \widetilde{H}^+(s))/h$ using $Q = \widetilde{H}^+ \widetilde{H}$ and $P = I - Q$. The Q-part gives $\lim_{h\to 0} \widetilde{H}^+(s)(\widetilde{H}(s) - \widetilde{H}(s+h))\widetilde{H}^+(s+h)/h = -\widetilde{H}^+ \widetilde{H}' \widetilde{H}^+$, while the P-part, after adding and subtracting $P(s+h)\widetilde{H}^+(s+h)$ and $\widetilde{H}^+(s)P(s)$, yields $P'\widetilde{H}^+ + \widetilde{H}^+ P'$. Bounding the norm and using $|\lambda_0'| = |\langle \phi_0 | H' | \phi_0 \rangle| \le \|H'\|$ (Hellmann-Feynman):

$$\|(\widetilde{H}^+)'\| \le \frac{\|H'\| + |\lambda_0'|}{g^2} + \frac{4\|H'\|}{g^2} \le \frac{6\|H'\|}{g^2}. \tag{7.2.16}$$

The second intermediate result bounds P''. Differentiating $P' = (2\pi i)^{-1} \oint_\Gamma R_H H' R_H\, dz$ gives

$$P'' = \frac{1}{2\pi i} \oint_\Gamma (2R_H H' R_H H' R_H + R_H H'' R_H)\, dz, \tag{7.2.17}$$

where the two $R_H H' R_H H' R_H$ terms arise from differentiating each resolvent factor. Bounding by $\|R_H(z)\| \le 2/g$ on Γ and integrating over the contour of length πg:

$$\|P''\| \le \frac{1}{2\pi} \left(\frac{2}{g}\right)^3 2\|H'\|^2 \cdot \pi g + \frac{1}{2\pi} \left(\frac{2}{g}\right)^2 \|H''\| \cdot \pi g = \frac{8\|H'\|^2}{g^2} + \frac{2\|H''\|}{g}. \tag{7.2.18}$$

Now expand $[P', (H - \lambda_0)^+]' = [P'', (H - \lambda_0)^+] + [P', ((H - \lambda_0)^+)']$ and bound each commutator:

$$\|[P'', (H - \lambda_0)^+]\| \le \frac{2\|P''\|}{g} \le \frac{16\|H'\|^2}{g^3} + \frac{4\|H''\|}{g^2}, \tag{7.2.19}$$

and, using (7.2.9) and (7.2.16):

$$\|[P', ((H - \lambda_0)^+)']\| \le 2\|P'\| \cdot \|(\widetilde{H}^+)'\| \le 2 \cdot \frac{2\|H'\|}{g} \cdot \frac{6\|H'\|}{g^2} = \frac{24\|H'\|^2}{g^3}. \tag{7.2.20}$$

Summing gives $40\|H'\|^2/g^3 + 4\|H''\|/g^2$. A block-matrix decomposition of the commutator with respect to P and $Q = I - P$, tracking cross terms exactly rather than using submultiplicativity, replaces the coefficient 40 by ≈ 4.77 [10]; the asymptotic scaling is unchanged.

The simplest schedule is constant. It sets $K'(s) = T$, so evolution proceeds at a uniform rate regardless of the gap. Substituting the derivative bounds into the error bound (7.2.4) with $(1/K')' = 0$ gives the constant-rate result.

Theorem 7.2.3 (Constant-rate runtime)**.** *Under the conditions of Lemma 7.2.1, a constant schedule $K'(s) = T$ achieves error at most ε provided*

$$T \ge \frac{1}{\varepsilon} \left(\frac{4\|H'(1)\|}{g(1)^2} + \int_0^1 \frac{40\|H'(s)\|^2}{g(s)^3}\, ds + \int_0^1 \frac{4\|H''(s)\|}{g(s)^2}\, ds \right). \tag{7.2.21}$$

Proof. With constant K', the third term in (7.2.4) vanishes. Substituting bounds (7.2.10) and (7.2.11) into the remaining two terms:

$$\varepsilon \leq \frac{1}{T}\left(\frac{4\|H'(1)\|}{g(1)^2} + \int_0^1 \frac{40\|H'(s)\|^2}{g(s)^3}\,ds + \int_0^1 \frac{4\|H''(s)\|}{g(s)^2}\,ds\right). \tag{7.2.22}$$

Setting the right side equal to ε and solving for T gives (7.2.21). □

Since $H'' = 0$ for the linear interpolation $H(s) = -(1-s)\,|\psi_0\rangle\langle\psi_0| + sH_z$, and $H'(s) = |\psi_0\rangle\langle\psi_0| + H_z$ is constant with $\|H'\| = O(1)$, the dominant term in (7.2.21) is $\int_0^1 g(s)^{-3}\,ds$. From the gap profile of Theorem 6.3.1, the crossing window contributes

$$\int_{s^*-\delta_s}^{s^*} g(s)^{-3}\,ds \leq \frac{\delta_s}{g_{\min}^3} = \frac{A_2}{A_1(A_1+1)} \cdot g_{\min}^{-2}, \tag{7.2.23}$$

using $\delta_s = A_2 g_{\min}/(A_1(A_1+1))$ from Eq. (5.4.10). This gives $T_{\text{constant}} = O(\delta_s/(\varepsilon\, g_{\min}^3))$.

Specializing to $M = 2$ with $g_{\min} = 1/\sqrt{N}$, the exact gap $g(s) = \sqrt{(2s-1)^2 + 4s(1-s)/N}$ from Eq. (5.3.15) gives $\int_0^1 g(s)^{-3}\,ds = O(N)$. The dominant contribution comes from the $O(1/\sqrt{N})$ window where $g \approx 1/\sqrt{N}$. Hence $T_{\text{constant}} = O(N/\varepsilon)$, matching classical search. A constant-rate schedule therefore gives no quantum speedup. It wastes time where the gap is large and still moves too quickly near s^*.

7.3 The Adaptive Schedule

The constant schedule fails because it treats every value of s the same. The error bound (7.2.4) suggests the opposite strategy. Choose large $K'(s)$ where the gap is small and small $K'(s)$ where the gap is large. Since $K'(s) = dt/ds$, this means spending physical time where diabatic transitions are dangerous. The natural ansatz is $K'(s) \propto 1/g(s)^p$ for some $p \geq 1$. Then runtime scales as $T \propto \int_0^1 g(s)^{-p}\,ds$, while the error terms involve integrals of the form $\int g^{q-3}\,ds$.

The exponent p controls the runtime-error tradeoff. The family $K'(s) \propto 1/g_0(s)^p$ extends Roland-Cerf ($p = 2$) to a continuum of schedules. At $p = 1$, $\int g_0^{-1}\,ds$ is mild but the companion error integral $\int g_0^{-2}\,ds$ diverges for piecewise linear profiles. At $p = 2$, the scaling is favorable, but the schedule-variation term requires exact gap information. The useful regime is therefore $p \in (1,2)$. There, $\int g_0^{-p}\,ds = O(g_{\min}^{1-p})$ and $\int g_0^{p-3}\,ds = O(g_{\min}^{p-2})$, whose product is always $O(g_{\min}^{-1})$. This is exactly the range where a certified lower bound $g_0 \leq g$ suffices.

The adaptive rate theorem, extending the eigenpath traversal framework of [70] to the continuous-time setting, formalizes this trade-off.

Theorem 7.3.1 (Adaptive rate [10])**.** *Let $H(s)$ satisfy the conditions of Lemma 7.2.1, and let $g_0 : [0,1] \to \mathbb{R}^+$ be an absolutely continuous function satisfying $g_0(s) \leq g(s)$ for all s. Suppose there exist $1 < p < 2$ and constants $B_1, B_2 \geq 1$ such that*

$$\int_0^1 \frac{ds}{g_0(s)^p} \leq B_1\, g_{\min}^{1-p} \qquad \text{and} \qquad \int_0^1 \frac{ds}{g_0(s)^{3-p}} \leq B_2\, g_{\min}^{p-2}. \tag{7.3.1}$$

Assume additionally that $g_0(1) \geq g_{\min}$, that there exists $b \in (0,1]$ with $g_0(s) \geq b\, g_{\min}$ for all $s \in [0,1]$, and that $\sup_{s\in[0,1]} |g_0'(s)| < \infty$. Define

$$c = \sup_{s\in[0,1]} \left(4\|H'(s)\| + 40\|H'(s)\|^2 B_2 + 4\|H''(s)\| + 6p\,|g_0'(s)|\,\|H'(s)\|\,B_2\right). \tag{7.3.2}$$

The last term uses $|g_0'(s)|$ rather than $|g'(s)|$: since the schedule is defined in terms of g_0, the derivative $(K'^{-1})' \propto (g_0^p)'$ involves g_0'. Then the schedule

$$K'(s) = \frac{1}{\varepsilon} \cdot \frac{c}{g_0(s)^p \cdot g_{\min}^{2-p}} \tag{7.3.3}$$

achieves error at most ε, with total runtime

$$T = \int_0^1 K'(s)\,ds \leq \frac{c\,B_1}{\varepsilon\, g_{\min}}. \tag{7.3.4}$$

Proof. Let ε_0 denote the actual error. Substituting (7.3.3) into the error bound (7.2.4): $(K')^{-1} = \varepsilon\, g_0^p\, g_{\min}^{2-p}/c$, and $|((K')^{-1})'| = (\varepsilon\, g_{\min}^{2-p}/c) \cdot p\, g_0^{p-1}\, |g_0'|$. The three terms become

$$\varepsilon_0 \le \frac{\varepsilon}{c}\, g_{\min}^{2-p}\Bigg(g_0(1)^p \left\| \left[P'(1), (H(1)-\lambda_0(1))^+\right] \right\| + \int_0^1 g_0^p \left\| \left[P', (H-\lambda_0)^+\right]' \right\| ds + \int_0^1 p\, g_0^{p-1} |g_0'| \left\| \left[P', (H-\lambda_0)^+\right] \right\| ds \Bigg). \quad (7.3.5)$$

Boundary term. Using bound (7.2.10) with $g_0 \le g$:

$$g_{\min}^{2-p}\, g_0(1)^p \cdot \frac{4\|H'(1)\|}{g(1)^2} \le 4\|H'(1)\|\, g_{\min}^{2-p}\, g_0(1)^{p-2} \le 4\|H'\|, \quad (7.3.6)$$

since $g_0(1) \ge g_{\min}$ and $p-2<0$ imply $g_0(1)^{p-2} \le g_{\min}^{p-2}$.

Commutator derivative integral. Using bound (7.2.11) and splitting:

$$g_{\min}^{2-p} \int_0^1 g_0^p \cdot \frac{40\|H'\|^2}{g^3}\, ds \le 40\|H'\|^2\, g_{\min}^{2-p} \int_0^1 \frac{ds}{g_0^{3-p}} \le 40\|H'\|^2 B_2, \quad (7.3.7)$$

where $g_0^p/g^3 \le g_0^p/g_0^3 = 1/g_0^{3-p}$ since $g_0 \le g$, and the B_2 condition (7.3.1) absorbs $g_{\min}^{2-p} \cdot g_{\min}^{p-2} = 1$. Similarly, the H'' sub-term contributes

$$g_{\min}^{2-p} \int_0^1 g_0^p \cdot \frac{4\|H''\|}{g^2}\, ds \le 4\|H''\|\, g_{\min}^{2-p} \int_0^1 \frac{ds}{g_0^{2-p}} \le 4\|H''\|, \quad (7.3.8)$$

since $g_0 \ge b\, g_{\min}$ and $p-2<0$ imply $g_0^{p-2} \le b^{p-2} g_{\min}^{p-2}$, giving $\int g_0^{p-2}\, ds = O(g_{\min}^{p-2})$ with the constant b^{p-2} absorbed into the O-notation.

Schedule variation integral. Using bound (7.2.10):

$$\begin{aligned} g_{\min}^{2-p} \int_0^1 p\, g_0^{p-1} |g_0'| \cdot \frac{4\|H'\|}{g^2}\, ds &\le 4p\, \|H'\|\, g_{\min}^{2-p} \int_0^1 \frac{g_0^{p-1}\, |g_0'|}{g_0^2}\, ds \\ &= 4p\, \|H'\|\, g_{\min}^{2-p} \int_0^1 g_0^{p-3}\, |g_0'|\, ds. \end{aligned} \quad (7.3.9)$$

Using $\sup|g_0'| < \infty$, we have $\int g_0^{p-3} |g_0'|\, ds \le \sup|g_0'| \cdot \int g_0^{p-3}\, ds \le \sup|g_0'| \cdot B_2\, g_{\min}^{p-2}$. The resulting bound is $4p \sup|g_0'|\, \|H'\|\, B_2$. The constant c in (7.3.2) uses the factor $6p$ rather than $4p$; this is a valid overestimate that simplifies the expression without affecting the asymptotic result.

Collecting. Summing all contributions:

$$\varepsilon_0 \le \frac{\varepsilon}{c}\left(4\|H'\| + 40\|H'\|^2 B_2 + 4\|H''\| + 6p \sup|g_0'|\, \|H'\|\, B_2\right) \le \frac{\varepsilon}{c} \cdot c = \varepsilon. \quad (7.3.10)$$

Runtime. The total evolution time is

$$T = \int_0^1 K'\, ds = \frac{c}{\varepsilon}\, g_{\min}^{p-2} \int_0^1 \frac{ds}{g_0^p} \le \frac{c}{\varepsilon}\, g_{\min}^{p-2} \cdot B_1\, g_{\min}^{1-p} = \frac{c\, B_1}{\varepsilon\, g_{\min}}. \quad (7.3.11)$$

□

Three terms compose the error. The first is a boundary term that depends on $g_0(1)$ and is $O(1)$. The second is an integral that pairs g_0^p from the schedule with g^{-3} from the derivative bounds, producing $\int g_0^{p-3}\, ds$. The third is a schedule-variation term from the non-constant K'. The parameter p balances the two integrals. B_1 bounds $\int g_0^{-p}\, ds$ (the runtime cost), while B_2 bounds $\int g_0^{p-3}\, ds$ (the error cost). Their product with $g_{\min}^{-1}$ gives the final runtime.

Corollary 7.3.2. *If $\int_0^1 g(s)^{-p}\, ds = O(g_{\min}^{1-p})$ for all $p > 1$, and $\|H'\|$, $\|H''\|$, $|\lambda_0'|$, $|g'|$ are all $O(1)$, then $T = O(1/(\varepsilon\, g_{\min}))$.*

The runtime scales inversely with the minimum gap, which is optimal for quantum search [36]. The running example satisfies these conditions.

The integral $\int_0^1 g(s)^{-p}\, ds$ is dominated by the $O(1/\sqrt{N})$-wide window where $g \approx 1/\sqrt{N}$: the window's contribution is $(1/\sqrt{N}) \cdot N^{p/2} = N^{(p-1)/2}$, while outside the window $g = \Omega(|s-1/2|)$ and the integral converges. For any $p > 1$, this gives $O(g_{\min}^{1-p})$.

Lemma 7.3.3 (Grover gap integral)**.** *For the exact gap* $g(s) = \sqrt{(2s-1)^2 + 4s(1-s)/N}$ *of the running example* ($M = 2$, $d_0 = 1$, $d_1 = N-1$)*,*

$$\int_0^1 g(s)^{-p}\, ds = O\left(N^{(p-1)/2}\right) = O\left(g_{\min}^{1-p}\right) \qquad \text{for all } p > 1. \tag{7.3.12}$$

Proof. The gap is symmetric about $s = 1/2$ and achieves its minimum $g_{\min} = 1/\sqrt{N}$ there. Split the integral at $1/2 - 1/\sqrt{N}$. In the window $[1/2 - 1/\sqrt{N},\, 1/2]$, bound $g \geq g_{\min}$:

$$\int_{1/2-1/\sqrt{N}}^{1/2} g^{-p}\, ds \leq \frac{1}{\sqrt{N}} \cdot N^{p/2} = N^{(p-1)/2}. \tag{7.3.13}$$

Outside the window, $g(s) \geq c|s - 1/2|$ for a constant $c > 0$ (the gap grows linearly away from the minimum). The change of variable $u = g(s)$, with $|ds/du| = O(1)$ since $|g'(s)| \leq 2$, gives

$$\int_0^{1/2-1/\sqrt{N}} g^{-p}\, ds \leq C \int_{1/\sqrt{N}}^{O(1)} u^{-p}\, du = O\left(N^{(p-1)/2}\right). \tag{7.3.14}$$

Combining and using the symmetry about $1/2$ gives the result. □

The other conditions of Corollary 7.3.2 are immediate: $\|H'\| = \||\psi_0\rangle\langle\psi_0| + H_z\| \leq 2$, $H'' = 0$, $|\lambda_0'| \leq \|H'\| \leq 2$ by the Hellmann-Feynman theorem, and $|g'(s)| \leq 2$ (from $|g'| = |4(1 - 1/N)(1/2 - s)/g| \leq 2$, since the numerator is at most $2g$). Therefore $T = O(\sqrt{N}/\varepsilon)$ for the running example with an adaptive schedule, compared to $T = O(N/\varepsilon)$ with a constant schedule. The adaptive schedule recovers the full Grover speedup.

The schedule $K'(s) \propto 1/g(s)^p$ concentrates the evolution time near the crossing: at $s = 1/2$, where $g \approx 1/\sqrt{N}$, the schedule rate is $K' \propto N^{p/2}$, while far from $1/2$, where $g = O(1)$, it is $K' = O(1)$. The algorithm spends $O(\sqrt{N})$ physical time traversing the window and $O(1)$ time traversing the rest of $[0, 1]$.

7.4 Runtime of Adiabatic Quantum Optimization

Applying Theorem 7.3.1 to $H(s) = -(1-s)\,|\psi_0\rangle\langle\psi_0| + sH_z$ with the gap profile of Theorem 6.3.1 requires three concrete steps. We construct a continuous lower bound $g_0(s)$ from the piecewise bounds, compute B_1 and B_2 by splitting $\int g_0^{-p}\, ds$ across the three regions and showing each contributes $O(\mathrm{poly}(n) \cdot g_{\min}^{1-p})$, and then evaluate the constant c.

The bounds from Theorem 6.3.1 are valid on their regions but do not meet continuously at $s^* - \delta_s$ and s^*. The left bound is too high at $s^* - \delta_s$, and the right bound is too low at s^*. Since Theorem 7.3.1 requires g_0 to be absolutely continuous on $[0, 1]$, we shrink the left and window pieces by a constant factor b so the three branches join continuously.

Define

$$g_0(s) = \begin{cases} b\,\dfrac{A_1(A_1+1)}{A_2}\,(s^* - s)\,, & s \in [0,\, s^* - \delta_s), \quad (\text{i.e., } b\,\tfrac{A_1}{A_2} \cdot \tfrac{s^*-s}{1-s^*}) \\ b\, g_{\min}, & s \in [s^* - \delta_s,\, s^*), \\ \dfrac{\Delta}{30} \cdot \dfrac{s - s_0}{1 - s_0}, & s \in [s^*,\, 1], \end{cases} \tag{7.4.1}$$

where s_0 is given by Eq. (6.2.5) and the shrinking factor is

$$b = k \cdot \frac{2}{1 + f(s^*)} = \frac{1}{4} \cdot \frac{2}{1+4} = \frac{1}{10}, \tag{7.4.2}$$

using $k = 1/4$ and $f(s^*) = 4$ from Eq. (6.2.23).

Each piece of g_0 lies below its corresponding bound from Theorem 6.3.1. The left and window pieces are scaled by $b = 1/10$, while the right piece is unchanged. It remains to check continuity at both junctions. At $s = s^* - \delta_s$, the left branch gives $b \cdot A_1(A_1+1)\delta_s/A_2$. Using $\delta_s = A_2 g_{\min}/(A_1(A_1+1))$ from Eq. (5.4.10), this equals $b\, g_{\min} = g_{\min}/10$, exactly the window value. At $s = s^*$, the window value is again $b\, g_{\min} = g_{\min}/10$, while the right branch gives $(\Delta/30)(s^* - s_0)/(1 - s_0)$. Using $s^* - s_0 = k\, g_{\min}(1 - s^*)/(a - k\, g_{\min})$ and $1 - s_0 = (1 - s^*)a/(a - k\, g_{\min})$ from Eq. (6.2.5),

$$\frac{\Delta}{30} \cdot \frac{s^* - s_0}{1 - s_0} = \frac{\Delta}{30} \cdot \frac{k\, g_{\min}}{a} = \frac{\Delta}{30} \cdot \frac{g_{\min}/4}{\Delta/12} = \frac{g_{\min}}{10}, \tag{7.4.3}$$

which again matches the window value. The constants b, k, and a are therefore coupled exactly to enforce continuity. In particular, $b = 1/10$ absorbs both the $k = 1/4$ factor from the right-side resolvent bound and the value $f(s^*) = 4$ from the Chapter 6 monotonicity analysis.

The integral $\int_0^1 g_0^{-p}\,ds$ splits across the three regions. In the left region, $g_0(s) = b\,A_1(A_1+1)(s^*-s)/A_2$, so

$$\begin{aligned}\int_0^{s^*-\delta_s} g_0^{-p}\,ds &= \left(\frac{A_2}{b\,A_1(A_1+1)}\right)^p \int_{\delta_s}^{s^*} \frac{du}{u^p} = \frac{1}{b^p}\left(\frac{A_2}{A_1(A_1+1)}\right)^p \cdot \frac{1}{(p-1)\,\delta_s^{p-1}} \\ &= \frac{1}{b^p(p-1)} \cdot \frac{A_2}{A_1(A_1+1)} \cdot g_{\min}^{1-p}, \end{aligned} \tag{7.4.4}$$

where the last step uses $\delta_s^{p-1} = (A_2 g_{\min}/(A_1(A_1+1)))^{p-1}$. In the window, $g_0 = b\,g_{\min}$ is constant:

$$\int_{s^*-\delta_s}^{s^*} g_0^{-p}\,ds = \frac{\delta_s}{b^p\,g_{\min}^p} = \frac{1}{b^p} \cdot \frac{A_2}{A_1(A_1+1)} \cdot g_{\min}^{1-p}. \tag{7.4.5}$$

Combining the left and window contributions with $b^{-p} = 10^p$ gives

$$\frac{1/(p-1)+1}{b^p} = \frac{p\,10^p}{p-1},$$

so the combined term is $(p/(p-1)) \cdot 10^p \cdot A_2/(A_1(A_1+1)) \cdot g_{\min}^{1-p}$.

In the right region, $g_0(s) = (\Delta/30)(s-s_0)/(1-s_0)$, so

$$\begin{aligned}\int_{s^*}^1 g_0^{-p}\,ds &= \left(\frac{30(1-s_0)}{\Delta}\right)^p \int_{s^*-s_0}^{1-s_0} \frac{du}{u^p} = \left(\frac{30(1-s_0)}{\Delta}\right)^p \cdot \frac{1}{(p-1)(s^*-s_0)^{p-1}} \\ &= \frac{1}{p-1}\left(\frac{30}{\Delta}\right)^p \left(\frac{a}{k}\right)^{p-1} (1-s_0) \cdot g_{\min}^{1-p}, \end{aligned} \tag{7.4.6}$$

using $s^* - s_0 = k\,g_{\min}(1-s^*)/(a - k\,g_{\min})$ and $1 - s_0 = a(1-s^*)/(a-k\,g_{\min})$. Now set $a = (4/3)k^2\Delta$ and $k = 1/4$, so $a/k = \Delta/3$. This yields $(30/\Delta)^p(\Delta/3)^{p-1} = 30^p/(3\Delta)$, together with $(1-s_0) \le 1/(1+A_1)$. Hence the right contribution is $3 \cdot 10^p/((p-1)\Delta(1+A_1)) \cdot g_{\min}^{1-p}$.

Since $\Delta A_2 \le A_1$ (equivalently $A_2 \le A_1/\Delta$), the left-plus-window term satisfies $A_2/(A_1(1+A_1)) \le 1/(\Delta(1+A_1))$. Combining all three contributions gives

$$\int_0^1 g_0^{-p}\,ds \le \frac{(p+3)\cdot 10^p}{(p-1)(1+A_1)\Delta} \cdot g_{\min}^{1-p}, \qquad \text{so} \quad B_1 = O\!\left(\frac{1}{\Delta(1+A_1)}\right). \tag{7.4.7}$$

The integral $\int_0^1 g_0^{p-3}\,ds$ has the same three-region decomposition, now with exponent $3-p$. Because $p \in (1,2)$ implies $3-p \in (1,2)$, each region converges by the same change of variables used for B_1. For example, the window contribution is

$$\int_{s^*-\delta_s}^{s^*} (b\,g_{\min})^{p-3}\,ds = \delta_s\,b^{p-3} g_{\min}^{p-3} = b^{p-3}\frac{A_2}{A_1(A_1+1)} g_{\min}^{p-2} = O(g_{\min}^{p-2}),$$

with $b^{p-3} = 10^{3-p}$ absorbed into constants. The left and right pieces have the same order, so

$$B_2 = O\!\left(\frac{1}{\Delta(1+A_1)}\right). \tag{7.4.8}$$

For the adiabatic Hamiltonian $H(s) = -(1-s)\,|\psi_0\rangle\langle\psi_0| + sH_z$, we have

$$\|H'(s)\| = O(1), \qquad \|H''(s)\| = 0, \qquad |\lambda_0'(s)| = O(1), \tag{7.4.9}$$

because $H'(s) = |\psi_0\rangle\langle\psi_0| + H_z$ is constant and $\lambda_0'(s) = \langle\phi_0(s)|\,H'(s)\,|\phi_0(s)\rangle$ is bounded by $\|H'\|$ through Hellmann-Feynman. The derivative $|g_0'(s)|$ is piecewise bounded: $b\,A_1(A_1+1)/A_2$ on the left, 0 in the window, and $\Delta/(30(1-s_0))$ on the right. For piecewise linear g_0, this keeps $|g_0'|B_2$ bounded. The window contributes nothing because $g_0' = 0$ there. On each linear branch, $|g_0'|$ factors out and the substitution $u = g_0(s)$ gives

$$\int g_0^{p-3}|g_0'|\,ds = \int_{g_{\min}/10}^{O(1)} u^{p-3}\,du = O(g_{\min}^{p-2}),$$

independently of the slopes. Since $\|H''\| = 0$, the dominant term in (7.3.2) is $40\|H'\|^2 B_2$. Therefore

$$c = O(B_2). \tag{7.4.10}$$

Theorem 7.4.1 (Runtime of AQO: Main Result 1 [10]). *Let H_z satisfy the spectral condition (Definition 5.2.2) and assume $A_1 \geq 1/2$ (equivalently $s^* \geq 1/3$). For any $\varepsilon > 0$, the adaptive schedule (7.3.3) with the gap lower bound (7.4.1) prepares the ground state of H_z with fidelity at least $1-\varepsilon$ in time*

$$T = O\left(\frac{1}{\varepsilon} \cdot \frac{\sqrt{A_2}}{\Delta^2\, A_1(A_1+1)} \cdot \sqrt{\frac{N}{d_0}}\right). \tag{7.4.11}$$

Proof. By Theorem 7.3.1, $T \leq c\, B_1/(\varepsilon\, g_{\min})$. Substituting $c = O(B_2)$, $B_1 = O(1/(\Delta(1+A_1)))$, $B_2 = O(1/(\Delta(1+A_1)))$, and $g_{\min} = (2A_1/(A_1+1))\sqrt{d_0/(NA_2)}$ from Eq. (5.4.9):

$$T = O\left(\frac{1}{\varepsilon} \cdot \frac{B_1 B_2}{g_{\min}}\right) = O\left(\frac{1}{\varepsilon} \cdot \frac{1}{\Delta^2(1+A_1)^2} \cdot \frac{A_1+1}{2A_1}\sqrt{\frac{NA_2}{d_0}}\right) = O\left(\frac{1}{\varepsilon} \cdot \frac{\sqrt{A_2}}{\Delta^2\, A_1(A_1+1)} \cdot \sqrt{\frac{N}{d_0}}\right). \tag{7.4.12}$$

□

Remark (A_1^2 vs $A_1(A_1+1)$). *Our published work [10] states A_1^2 in Theorem 1. The expression $A_1(A_1+1)$ follows from the proof derivation in Appendix A-IV of [10], and is what the algebra above produces. For Ising Hamiltonians with $A_1 = O(\mathrm{poly}(n))$, the distinction is absorbed by $O(\cdot)$ notation, since $A_1(A_1+1) = A_1^2 + A_1 = \Theta(A_1^2)$.*

The runtime in (7.4.11) has five interpretable factors. The $1/\varepsilon$ term is linear in target error. The factor $\sqrt{A_2}$ measures spectral crowding near E_0, where larger $A_2 = (1/N)\sum d_k/(E_k - E_0)^2$ sharpens the minimum and narrows the crossing window. The denominator $A_1(A_1+1)$ encodes crossing location, since larger A_1 pushes s^* toward 1 and steepens the left arm. The term $1/\Delta^2$ is the cost of right-side control, with one $1/\Delta$ from B_1 and one from B_2. Finally, $\sqrt{N/d_0}$ is the Grover factor. In short, the speedup is quantum. The remaining terms are explicit spectral overheads of generality. Compared with the constant-rate theorem, the key gain is here. Time still scales linearly in the target error $1/\varepsilon$, and the minimum-gap scaling improves from $T = O(g_{\min}^{-2})$ to $T = O(g_{\min}^{-1})$. At the proof level, the improvement comes from replacing the g^{-3} corridor with power-law control centered on g^{-2}.

For Ising Hamiltonians H_σ (Eq. (5.1.4)) with $A_1, A_2 = O(\mathrm{poly}(n))$ and $\Delta \geq 1/\mathrm{poly}(n)$, this becomes $T = \widetilde{O}(\sqrt{N/d_0})$. That matches the lower bound of [36] up to polylogarithmic factors. When $d_0 = O(1)$, the adiabatic algorithm recovers the Grover $\sqrt{N}$ scaling.

For the canonical two-level case $M = 2$ with $A_1 \approx 1$, $A_2 \approx 1$, $\Delta = 1$, and $d_0 = 1$, we obtain

$$T = O\left(\frac{1}{\varepsilon} \cdot \frac{1}{1 \cdot 2} \cdot \sqrt{N}\right) = O\left(\frac{\sqrt{N}}{\varepsilon}\right), \tag{7.4.13}$$

matching the circuit-based Grover algorithm. The adaptive adiabatic approach achieves the same quadratic speedup through a smooth interpolation between two Hamiltonians, without relying on the discrete iterate structure of amplitude amplification.

Runtime is controlled by how much spectral information the schedule receives. The constant-rate schedule (Theorem 7.2.3) gives $T = O(N/\varepsilon)$ because the crossing window dominates. The Roland-Cerf schedule (section 7.1) sets $K'(s) \propto 1/g(s)^2$ and improves this to $T = O(\sqrt{N}/\varepsilon)$, but it needs the exact gap at every point. The adaptive schedule in Theorem 7.3.1 keeps the same $\sqrt{N}$ scaling while using only a certified lower bound $g_0(s) \leq g(s)$, namely the Chapter 6 profile bounds. That change, from exact gap to lower bound, is what makes the method usable for general spectral-condition instances. The discrete-time eigenpath route of Boixo et al. [69] reaches the same $O(1/g_{\min})$ scaling through a different mechanism, so this scaling is not tied to one proof template.

Guo and An [42] place this in a broader framework. They study interpolations $H(u(s)) = (1-u(s))H_0 + u(s)H_1$ under a measure condition. The set $\{s : \Delta(u(s)) \leq x\}$ has Lebesgue measure $O(x)$ as $x \to 0$. Under that condition, the power-law schedule with exponent $p = 3/2$ achieves $O(1/\Delta_*)$, a quadratic improvement over $O(1/\Delta_*^2)$. They also show that $p = 3/2$ is optimal for linear gap profiles. The profile in Theorem 6.3.1 satisfies their condition because it has one minimum at s^* and linear reopening on both sides. Equivalently, for small x, the set $\{s : g(s) \leq x\}$ is an interval around s^* of width $\Theta(x)$. Their theorem provides the existence-and-scaling layer; Chapters 5 and 6 add explicit constants, which is what turns (7.4.11) into a concrete runtime bound. This condition also separates narrow, sharp minima from broad, flat ones. Sharp minima satisfy it with a bounded constant, while broad flat minima force larger overhead.

Running the adaptive schedule still requires knowledge of $g_0(s)$, hence of s^*, δ_s, and $g_{\min}$. These all depend on A_1. Inside the window $[s^* - \delta_s, s^*)$, the schedule is constant, $K' = c/(\varepsilon\, b^p\, g_{\min}^2)$, so the main issue is not local slope but window placement. Because $s^* = A_1/(A_1+1)$, we must know A_1 to accuracy $O(\delta_s) = O(2^{-n/2})$

to center the slow segment correctly. Outside the window, placement errors change only constants. Inside this exponentially narrow window, the same error causes a real loss of fidelity.

Imprecision in A_2 and d_0 causes only polynomial slowdown. Replacing A_2 by the lower bound $1 - d_0/N$ (Eq. (5.2.3)) and taking $d_0 = 1$ changes runtime only by poly(n) factors, because these parameters appear through $\sqrt{A_2/d_0}$ and B_1. The critical quantity is A_1. It must be estimated to additive accuracy $O(\delta_s) = O(2^{-n/2})$ before evolution begins. That requirement is severe. Even though H_z has a poly(n)-bit description, the needed precision in A_1 is exponential in n. Chapter 8 shows that even approximating A_1 to much coarser precision $1/\text{poly}(n)$ is NP-hard, while exact computation is #P-hard.

Chapter 8

Hardness of Optimality

The optimal schedule from Chapter 7 achieves a quadratic speedup over classical brute-force search, but the schedule must be fixed before evolution begins. It depends on the spectral parameter A_1, the weighted sum of inverse gaps that determines where the avoided crossing occurs. This parameter must be known to additive accuracy $O(2^{-n/2})$. Given the $N = 2^n$ diagonal entries of H_z, brute-force computation of $A_1 = (1/N)\sum_{k=1}^{M-1} d_k/(E_k - E_0)$ by enumerating eigenvalues, sorting, and summing takes $O(N)$ time. That is the same cost as classical unstructured search. If pre-computation costs as much as the task itself, the speedup is only conditional.

The runtime of Theorem 7.4.1,

$$T = O\left(\frac{1}{\varepsilon} \cdot \frac{\sqrt{A_2}}{\Delta^2\, A_1(A_1+1)} \cdot \sqrt{\frac{N}{d_0}}\right),$$

makes this dependence explicit. [10] also states an A_1^2 denominator in its headline theorem form. We keep the proof-level $A_1(A_1+1)$ expression, which is the tighter form used in the derivation. In the normalized regime $E_k \in [0,1]$, $A_1 \geq 1 - d_0/N$, so both forms differ only by a constant-factor normalization for the asymptotic statements used here. The adaptive schedule places a slow phase in the window $[s^* - \delta_s,\, s^*)$ centered at $s^* = A_1/(A_1+1)$, where the gap is smallest, and accelerates elsewhere. The parameters A_2 and d_0 enter only through $\sqrt{A_2/d_0}$. Using conservative bounds ($A_2 \geq 1 - d_0/N$ from Eq. (5.2.3), and $d_0 = 1$ for worst-case search) changes only polynomial prefactors when $d_0 \ll N$. The decisive quantity is A_1. It sets crossing location, while $\delta_s = O(\sqrt{d_0 A_2/N}) = O(2^{-n/2})$ sets required precision. If the crossing estimate is wrong by more than δ_s, evolution passes too quickly through the minimum and loses ground-state fidelity. Throughout this chapter, we write $A_1(H)$ when dependence on the Hamiltonian matters.

The hardness of computing A_1 is not the only obstacle to adiabatic optimization for hard problems. Even if A_1 were known exactly, the single-crossing framework of Chapters 5–7 applies only to the rank-one projector $H_0 = -|\psi_0\rangle\langle\psi_0|$. For the transverse-field driver (Chapter 5), the multi-crossing regime makes this framework inapplicable. Knowing A_1 no longer helps there, because the schedule would need to navigate exponentially many crossings rather than one.

The two barriers are complementary. Computing A_1 is hard even in the rank-one setting, and the single-crossing method fails for other drivers even when spectral information is available.

NP-hardness already appears at precision $1/\mathrm{poly}(n)$. Two queries to an A_1-oracle then suffice to solve 3-SAT (section 8.1). At precision $2^{-\mathrm{poly}(n)}$, the problem becomes #P-hard because polynomial interpolation can recover all degeneracies from polynomially many queries (section 8.2).

The algorithmically relevant precision $2^{-n/2}$ sits strictly between these scales. It is fine enough to matter for scheduling, but not fine enough for either existing hardness proof to transfer directly. At this precision, a quantum algorithm uses $O(2^{n/2})$ queries, while any classical algorithm needs $\Omega(2^n)$. This is exactly a Grover-type quadratic separation (section 8.3).

8.1 NP-Hardness of Estimating A_1

The Hamiltonian H_z encodes an optimization problem whose ground energy E_0 determines whether a solution exists. For a 3-SAT instance, $E_0 = 0$ when a satisfying assignment exists and $E_0 \geq 1/\mathrm{poly}(n)$ otherwise. Distinguishing these two cases is the local Hamiltonian promise problem, known to be NP-hard [21]. The spectral parameter A_1 is not obviously tied to this decision problem, because it aggregates information across all

energy levels rather than only the ground energy. A modified Hamiltonian H' bridges the two tasks. Comparing $A_1(H')$ with $A_1(H)$ reveals whether E_0 vanishes.

Define the $(n+1)$-qubit Hamiltonian

$$H' = H \otimes \frac{I + \sigma_z}{2}. \tag{8.1.1}$$

The operator $(I+\sigma_z)/2$ is the projector onto $|0\rangle$ for the ancilla qubit. It has eigenvalue 1 on $|0\rangle$ and eigenvalue 0 on $|1\rangle$. On the $|0\rangle$ branch, H' has the same spectrum as H, with eigenvalues E_k and degeneracies d_k. On the $|1\rangle$ branch, H' annihilates every state, contributing 2^n eigenvalues at energy 0. The ground energy of H' is therefore always zero, regardless of $E_0(H)$.

This is the mechanism behind the reduction. $A_1(H')$ measures from the fixed reference point $E'_0 = 0$, while $A_1(H)$ measures from the instance-dependent reference $E_0(H)$. When $E_0(H) > 0$, the two values separate by a detectable amount.

Lemma 8.1.1 (Disambiguation [10])**.** *Let $\varepsilon, \mu_1, \mu_2 \in (0,1)$. Suppose $\mathcal{C}_\varepsilon$ is a procedure that accepts the description of a Hamiltonian H and outputs $\widetilde{A}_1(H)$ with $|\widetilde{A}_1(H) - A_1(H)| \le \varepsilon$. Let H be an n-qubit diagonal Hamiltonian with eigenvalues $0 \le E_0 < E_1 < \cdots < E_{M-1} \le 1$ and $M \in$ poly(n), such that either* (i) $E_0 = 0$ *or* (ii) $\mu_1 \le E_0 \le 1 - \mu_2$*. Then two calls to $\mathcal{C}_\varepsilon$ suffice to decide between* (i) *and* (ii)*, provided*

$$\varepsilon < \frac{\mu_1}{6(1-\mu_1)} - \frac{d_0}{6N} \cdot \frac{1}{\mu_1 \mu_2}. \tag{8.1.2}$$

Proof. Call $\mathcal{C}_\varepsilon$ on H and on H' defined by Eq. (8.1.1), obtaining estimates $\widetilde{A}_1(H)$ and $\widetilde{A}_1(H')$. The test statistic is $\widetilde{A}_1(H) - 2\widetilde{A}_1(H')$, where the factor 2 compensates for the doubling of the Hilbert space (H' acts on 2^{n+1} states, so $A_1(H')$ carries a normalization factor $1/2^{n+1}$ instead of $1/2^n$).

Case (i): $E_0 = 0$**.** The ground energy of H' is 0 with degeneracy $d_0 + 2^n$, and the excited levels of H' are $E_1, \ldots, E_{M-1}$ with degeneracies $d_1, \ldots, d_{M-1}$. Since $E_0 = 0$, both $A_1(H)$ and $A_1(H')$ sum over the same gaps $E_k - 0 = E_k$:

$$A_1(H) = \frac{1}{2^n} \sum_{k=1}^{M-1} \frac{d_k}{E_k}, \qquad A_1(H') = \frac{1}{2^{n+1}} \sum_{k=1}^{M-1} \frac{d_k}{E_k}.$$

Therefore $A_1(H) - 2A_1(H') = 0$, and by the triangle inequality the test statistic satisfies $|\widetilde{A}_1(H) - 2\widetilde{A}_1(H')| \le 3\varepsilon$.

Case (ii): $\mu_1 \le E_0 \le 1 - \mu_2$**.** The ground energy of H' is still 0 (from the $|1\rangle$ branch), but now $E_0, E_1, \ldots, E_{M-1}$ are all excited levels. Thus

$$A_1(H') = \frac{1}{2^{n+1}} \sum_{k=0}^{M-1} \frac{d_k}{E_k}.$$

Decompose $A_1(H)$ using the partial fraction identity $d_k/(E_k - E_0) = d_k/E_k + d_k E_0/(E_k(E_k - E_0))$:

$$\begin{aligned} A_1(H) &= \frac{1}{2^n} \sum_{k=1}^{M-1} \frac{d_k}{E_k - E_0} = \frac{1}{2^n} \sum_{k=1}^{M-1} \frac{d_k}{E_k} + \frac{E_0}{2^n} \sum_{k=1}^{M-1} \frac{d_k}{E_k(E_k - E_0)} \\ &= \frac{1}{2^n} \sum_{k=0}^{M-1} \frac{d_k}{E_k} - \frac{d_0}{2^n E_0} + \frac{E_0}{2^n} \sum_{k=1}^{M-1} \frac{d_k}{E_k(E_k - E_0)}. \end{aligned} \tag{8.1.3}$$

The first sum equals $2A_1(H')$. For the remainder sum, $E_k \le 1$ and $E_k - E_0 \le 1 - E_0$, so the product $E_k(E_k - E_0)$ is at most $1 - E_0$. Each fraction $d_k/(E_k(E_k - E_0))$ is therefore bounded from below:

$$\frac{E_0}{2^n} \sum_{k=1}^{M-1} \frac{d_k}{E_k(E_k - E_0)} \ge \frac{E_0}{1 - E_0} \cdot \frac{1}{2^n} \sum_{k=1}^{M-1} d_k = \frac{E_0}{1 - E_0} \left(1 - \frac{d_0}{N}\right).$$

Combining with Eq. (8.1.3):

$$\begin{aligned} A_1(H) - 2A_1(H') &\ge \frac{E_0}{1 - E_0} \left(1 - \frac{d_0}{N}\right) - \frac{d_0}{N E_0} \\ &= \frac{E_0}{1 - E_0} - \frac{d_0}{N} \cdot \frac{1 - E_0 + E_0^2}{E_0(1 - E_0)}. \end{aligned} \tag{8.1.4}$$

Since $1 - E_0 + E_0^2 \le 1$ and $E_0(1-E_0) \ge \mu_1\mu_2$ on the given range, the fraction $(1-E_0+E_0^2)/(E_0(1-E_0))$ is at most $1/(\mu_1\mu_2)$. The first term $E_0/(1-E_0)$ is increasing in E_0, so it is at least $\mu_1/(1-\mu_1)$. Therefore

$$A_1(H) - 2A_1(H') \ge \frac{\mu_1}{1-\mu_1} - \frac{d_0}{N}\cdot\frac{1}{\mu_1\mu_2},$$

and the test statistic satisfies

$$\widetilde{A}_1(H) - 2\widetilde{A}_1(H') \ge \frac{\mu_1}{1-\mu_1} - \frac{d_0}{N\mu_1\mu_2} - 3\varepsilon.$$

The two cases are distinguished when 3ε from case (i) is separated from the lower bound in case (ii), requiring $6\varepsilon < \mu_1/(1-\mu_1) - d_0/(N\mu_1\mu_2)$. □

The disambiguation succeeds whenever the positive correction $E_0/(1-E_0)$ from the partial fraction identity dominates the negative term $-d_0/(NE_0)$, which happens as long as d_0/N is small relative to $\mu_1^2\mu_2$. For the Ising Hamiltonians of interest, d_0/N is exponentially small in n, so the condition is easily satisfied.

Theorem 8.1.2 (NP-hardness of A_1 estimation [10])**.** *Computing $A_1(H)$ to additive accuracy*

$$\varepsilon < \frac{1}{72(n-1)}$$

for a 3-local Hamiltonian H on n qubits is NP-hard.

Proof. We reduce 3-SAT to ground-energy disambiguation, following the construction of [71, 10]. Let φ be a 3-SAT formula on n_{var} Boolean variables $x_0, \dots, x_{n_{\mathrm{var}}-1}$ with m clauses, each of the form $a_k \vee b_k \vee c_k$ where each literal is some x_l or $\bar{x}_l$. If $n_{\mathrm{var}} + m < 15$, solve by brute force. Otherwise, define the single-qubit projectors

$$P_{x_l} = \frac{I - \sigma_z^{(l)}}{2}, \qquad P_{\bar{x}_l} = \frac{I + \sigma_z^{(l)}}{2},$$

which project onto the $|1\rangle$ and $|0\rangle$ states of qubit l, respectively. For each clause k ($0 \le k < m$), introduce an auxiliary qubit at index $n_{\mathrm{var}} + k$ and define

$$\begin{aligned} H_k = {} & P_{\bar{a}_k} + P_{\bar{b}_k} + P_{\bar{c}_k} + P_{\bar{x}_{n_{\mathrm{var}}+k}} \\ & + P_{a_k}P_{b_k} + P_{a_k}P_{c_k} + P_{b_k}P_{c_k} \\ & + P_{\bar{a}_k}P_{x_{n_{\mathrm{var}}+k}} + P_{\bar{b}_k}P_{x_{n_{\mathrm{var}}+k}} + P_{\bar{c}_k}P_{x_{n_{\mathrm{var}}+k}}. \end{aligned} \tag{8.1.5}$$

Direct computation on the computational basis shows that the minimum eigenvalue of H_k is 3 when clause k is satisfied and 4 when it is not; the maximum eigenvalue is 6. The combined Hamiltonian on $2n_{\mathrm{var}} + 2m$ qubits is

$$H = \frac{1}{6m}\sum_{k=0}^{m-1} H_k + \frac{1}{2n_{\mathrm{var}}+2m}\sum_{j=n_{\mathrm{var}}+m}^{2n_{\mathrm{var}}+2m-1} P_{x_j} - \frac{1}{2}I. \tag{8.1.6}$$

The first sum normalizes the clause energies to $[1/2, 1]$; the second sum adds $n_{\mathrm{var}} + m$ free qubits whose projectors prefer $|0\rangle$; the identity shift places the eigenvalues in $[0, 1]$. When all clauses are satisfied, there exists an assignment making every H_k achieve its minimum, giving $E_0 = 0$. When some clause is unsatisfied, the minimum of $\sum H_k/(6m)$ increases by at least $1/(6m)$, giving $E_0 \ge 1/(6m)$.

Apply Lemma 8.1.1 with $\mu_1 = 1/(6m)$ and $\mu_2 = 1/2$. The number of eigenvalues is $N = 2^{2n_{\mathrm{var}}+2m}$ and the ground-state degeneracy satisfies $d_0 \le 2^{n_{\mathrm{var}}+m}$, so $d_0/N \le 2^{-(n_{\mathrm{var}}+m)}$. Substituting into Eq. (8.1.2), the right-hand side satisfies

$$\frac{1}{6}\cdot\frac{1}{6m-1} - \frac{12m}{6}\cdot\frac{d_0}{N} \ge \frac{1}{36(n_{\mathrm{var}}+m-1)} - \frac{2m}{2^{n_{\mathrm{var}}+m}}, \tag{8.1.7}$$

since $1/(6(6m-1)) \ge 1/(36(n_{\mathrm{var}}+m-1))$ for $n_{\mathrm{var}} \ge 1$ and $d_0/N \le 2^{-(n_{\mathrm{var}}+m)}$. For $n_{\mathrm{var}} + m \ge 15$, the second term satisfies $2m/2^{n_{\mathrm{var}}+m} \le 1/(72(n_{\mathrm{var}}+m-1))$, so the disambiguation succeeds whenever

$$\varepsilon < \frac{1}{72(n_{\mathrm{var}}+m-1)}.$$

The Hamiltonian H' from Eq. (8.1.1) acts on $n = 2n_{\mathrm{var}} + 2m + 1$ qubits and is 3-local (since H is 2-local and the tensor product with $(I+\sigma_z)/2$ adds one ancilla). Since $n_{\mathrm{var}} + m \le n$, the precision bound $\varepsilon < 1/(72(n-1))$ follows. □

When $M = 2$ (Grover search), the spectral parameter $A_1 = (N-1)/N$ is trivial to obtain from the instance description. There are only two levels, and their degeneracies are fixed by the number of marked items. NP-hardness appears only for Hamiltonians that encode combinatorial structure with polynomially many levels and exponentially small ground-energy gaps. In that regime, A_1 depends nontrivially on the full degeneracy profile.

Remark. The disambiguation technique extends beyond 3-SAT. The MaxCut decision problem (given a graph $G = (V, E)$ and integer k, does G have a cut of size at least k?) also reduces to A_1 estimation. The construction adds a weighted edge to G, creating an auxiliary Hamiltonian H' whose A_1 value differs from a reference by at least $1/(|E|(|E|-1))$ between the two cases. This yields NP-hardness at precision $2/(5n^4)$ with a 2-local Hamiltonian, sharpening the locality requirement from 3-local to 2-local at the cost of a slightly tighter precision bound.

8.2 #P-Hardness of Computing A_1 Exactly

NP-hardness captures a decision question, namely whether $E_0 = 0$. But A_1 carries more than a single decision bit. It is a weighted sum over all energy levels, and its exact value determines every degeneracy d_k. Recovering these degeneracies solves counting problems. For NP-complete Hamiltonians, for example, d_0 counts satisfying assignments. Counting is harder than deciding, and it is #P-complete [8].

The extraction uses a parametrized family of Hamiltonians that shifts the spectrum continuously, turning A_1 into a rational function whose poles carry the degeneracies as residues. For a parameter $x > 0$, define the $(n+1)$-qubit Hamiltonian

$$H'(x) = H \otimes I - \frac{x}{2} I \otimes \frac{I + \sigma_z^{(n+1)}}{2}. \tag{8.2.1}$$

On the $|0\rangle$ branch of the ancilla, the eigenvalues are $E_k - x/2$ with degeneracies d_k. On the $|1\rangle$ branch, the eigenvalues are E_k with degeneracies d_k. The ground energy is $E_0 - x/2$ (from the $|0\rangle$ branch, for $x > 0$). The gaps relative to this ground energy are $\Delta_k = E_k - E_0$ (extending the notation $\Delta = E_1 - E_0$ from earlier chapters to all levels) for the $|0\rangle$ branch and $\Delta_k + x/2$ for the $|1\rangle$ branch.

Computing $A_1(H'(x))$ from these gaps and defining $f(x) = 2A_1(H'(x)) - A_1(H)$ isolates the $|1\rangle$-branch contribution [10]:

$$f(x) = \frac{1}{N} \sum_{k=0}^{M-1} \frac{d_k}{\Delta_k + x/2}. \tag{8.2.2}$$

This function is a sum of M simple poles at $x = -2\Delta_k$. Each pole has residue $2d_k/N$, encoding the degeneracy of the corresponding energy level. The function f is a partial-fraction decomposition of the entire degeneracy spectrum. The extraction problem reduces to recovering these residues from evaluations of f.

Lemma 8.2.1 (Exact degeneracy extraction [10])**.** *Suppose $\mathcal{C}$ is a procedure that computes $A_1(H)$ exactly for any n-qubit diagonal Hamiltonian H. Let H_σ be an Ising Hamiltonian (Equation 5.1.4) with integer eigenvalues and known spectral gaps $\Delta_k = E_k - E_0$. Then $O(\text{poly}(n))$ calls to $\mathcal{C}$ suffice to compute all degeneracies $d_0, d_1, \ldots, d_{M-1}$.*

Proof. Each evaluation of $f(x_i)$ requires two calls to $\mathcal{C}$, one for $A_1(H)$ and one for $A_1(H'(x_i))$. Evaluate f at M distinct positive odd integers $x_i \in \{1, 3, \ldots, 2M-1\}$. These values avoid the poles. For each k, $\Delta_k + x_i/2 \geq 0 + 1/2 > 0$ because $\Delta_k \geq 0$ and $x_i \geq 1$. The total cost is $2M = O(\text{poly}(n))$ oracle calls.

Define the reconstruction polynomial

$$P(x) = \prod_{k=0}^{M-1} \left(\Delta_k + \frac{x}{2}\right) f(x) = \frac{1}{N} \sum_{k=0}^{M-1} d_k \prod_{\ell \neq k} \left(\Delta_\ell + \frac{x}{2}\right). \tag{8.2.3}$$

Multiplying $f(x)$ by the product of all denominators clears the poles, yielding a polynomial of degree at most $M-1$ in x. Since the gaps Δ_k are known integers, the values $P(x_i) = \prod_k (\Delta_k + x_i/2) \cdot f(x_i)$ are computable from oracle outputs. The M values $P(x_1), \ldots, P(x_M)$ determine P uniquely by Lagrange interpolation [72]. A polynomial of degree at most $M-1$ is fixed by M distinct evaluations.

The degeneracies are recovered by evaluating P at the poles. Setting $x = -2\Delta_k$ kills every factor $(\Delta_\ell + x/2)$ except the k-th, giving

$$d_k = \frac{N \cdot P(-2\Delta_k)}{\prod_{\ell \neq k} (\Delta_\ell - \Delta_k)}, \qquad k \in \{0, \ldots, M-1\}. \tag{8.2.4}$$

The denominator is nonzero because the eigenvalues are distinct. The entire computation (oracle calls, Lagrange interpolation, pole evaluation) runs in $O(\text{poly}(n))$ time. □

Extracting d_0 from an Ising Hamiltonian encoding a 3-SAT formula counts satisfying assignments and therefore solves #3-SAT. Since #3-SAT is #P-complete [8], an exact A_1 oracle would solve every problem in #P in polynomial time. The same degeneracy data also determines IQP output probabilities [73]. From d_k and Δ_k, one computes $|\langle 0^n|C_{\mathrm{IQP}}|0^n\rangle|^2 = |N^{-1}\sum_k d_k\, e^{i\Delta_k}|^2$, which is itself #P-hard. The NP-hardness result of section 8.1 uses a 3-local Hamiltonian because the ancilla raises locality by one. The #P-hardness statement already holds for 2-local Ising Hamiltonians, since Eq. (8.2.1) preserves 2-locality when H is 2-local.

The exact oracle is unrealistic. A robust version of Lemma 8.2.1 must tolerate additive noise ε in the oracle outputs. Paturi's amplification lemma gives the control we need.

Lemma 8.2.2 (Paturi [74])**.** *Let $P(x)$ be a polynomial of degree at most M satisfying $|P(i)| \le c$ for all integers $i \in \{0, 1, \ldots, M\}$. Then $|P(x)| \le c \cdot 2^M$ for all $x \in [0, M]$.*

Paturi's lemma bounds polynomial growth between sample points. If a polynomial is bounded by c at $M+1$ integer points, it can grow by at most a factor 2^M on the interval. Applied to the difference between exact and approximate reconstruction polynomials, this gives explicit control of interpolation error.

Error propagation has three stages: sample-point error, extrapolation amplification, and rounding threshold. Stage 1 itself has three algebraic sub-steps: oracle noise enters f as $|\tilde{f}(x_i) - f(x_i)| \le 3\varepsilon$ (three oracle calls contribute), then enters polynomial samples as $|\tilde{P}(x_i) - P(x_i)| \le 3\varepsilon \prod_k (\Delta_k + x_i/2)$, and the product is bounded by B^M with $B = \Delta_{\max} + M = \mathrm{poly}(n)$.

Lemma 8.2.3 (Approximate degeneracy extraction [10])**.** *Under the same hypotheses as Lemma 8.2.1, but with an oracle $\mathcal{C}_\varepsilon$ satisfying $|\widetilde{A}_1(H) - A_1(H)| \le \varepsilon$, all degeneracies d_k can be computed exactly by $O(\mathrm{poly}(n))$ calls to $\mathcal{C}_\varepsilon$ for sufficiently small $\varepsilon \in O(2^{-\mathrm{poly}(n)})$.*

Proof sketch. **Stage 1 (sample-point error).** The proof follows the same three-stage route. The approximate polynomial $\tilde{P}$ is the Lagrange interpolant through the noisy values $(\tilde{P}(x_1), \ldots, \tilde{P}(x_M))$. Its difference $D = \tilde{P} - P$ is a polynomial of degree at most $M-1$ bounded by $3\varepsilon B^M$ at the sample points. By Paturi's lemma (Lemma 8.2.2), $|D(x)| \le 3\varepsilon B^M \cdot 2^{M-1}$ on the interpolation interval.

Stage 2 (extrapolation amplification). At the pole evaluation points $x^* = -2\Delta_k$, which lie outside the interval $[1, 2M-1]$, the error is bounded by Lagrange-basis amplification:

$$|D(x^*)| \le 3\varepsilon B^M \cdot \Lambda_M(x^*),$$

where $\Lambda_M(x^*) = \sum_j \prod_{i \ne j} |x^* - x_i|/|x_j - x_i|$ is the Lebesgue function. For extrapolation outside the interval, $\Lambda_M(x^*)$ grows exponentially in M, but since $M = \mathrm{poly}(n)$, the total amplification is $2^{\mathrm{poly}(n)}$. Dividing by $\prod_{\ell \ne k} |\Delta_\ell - \Delta_k|$ (also at most $2^{\mathrm{poly}(n)}$ for integer gaps) and multiplying by $N = 2^n$, the degeneracy error satisfies

$$|d_k - \tilde{d}_k| \le 3\varepsilon \cdot 2^{\mathrm{poly}(n)}.$$

Stage 3 (rounding to exact degeneracies). For $\varepsilon = O(2^{-\mathrm{poly}(n)})$ with a sufficiently large polynomial, this is less than $1/2$. Since degeneracies are positive integers, rounding $\tilde{d}_k$ to the nearest integer recovers d_k exactly. □

The proof extends to probabilistic oracles. If $\mathcal{C}_\varepsilon$ succeeds with probability at least $3/4$, then $O(\mathrm{poly}(n))$ queries produce enough correct sample points to reconstruct P despite corrupted evaluations. The Berlekamp-Welch algorithm recovers a polynomial of degree d from k partially corrupted evaluations, provided at least $\max\{d+1, (k+d)/2\}$ evaluations are correct [73]. By the Chernoff bound, querying $k = O(\mathrm{poly}(n))$ times ensures that at least $(k + M - 2)/2$ evaluations are correct with high probability. Combining this with Lemma 8.2.3:

Theorem 8.2.4 (#P-hardness of A_1 estimation [10])**.** *Estimating $A_1(H)$ to additive accuracy $\varepsilon = O(2^{-\mathrm{poly}(n)})$ is #P-hard, even for 2-local Ising Hamiltonians. The result holds for both deterministic and probabilistic estimation algorithms.*

NP-hardness says that extracting even a single bit from A_1 is hard. The relevant bit is whether a satisfying assignment exists. #P-hardness says something stronger. The entire degeneracy spectrum $\{d_k\}$ is encoded in A_1 as a function of auxiliary parameters, and recovering any single d_k solves a counting problem. Computing the number of satisfying assignments of a 3-SAT formula, for instance, is #P-complete. The polynomial interpolation extracts all d_k simultaneously from $O(\mathrm{poly}(n))$ evaluations of A_1, which is why the required precision jumps from $1/\mathrm{poly}(n)$ to $2^{-\mathrm{poly}(n)}$.

With $M = 2$, the reconstruction polynomial $P(x) = (d_0/N)(1+x/2) + (d_1/N)(x/2)$ is linear. Two evaluations determine d_0 and d_1 exactly, and interpolation reduces to fitting a line through two points. The #P-hardness comes from Hamiltonians with $M = O(n^2)$ levels, where the reconstruction polynomial has high degree and tiny oracle errors amplify through the exponential Paturi factor. The next section quantifies this amplification as $2^{O(M \log n)}$.

8.3 The Intermediate Regime

The adiabatic algorithm requires A_1 to precision $O(2^{-n/2})$. NP-hardness holds at $1/\mathrm{poly}(n)$ (Theorem 8.1.2), and #P-hardness holds at $2^{-\mathrm{poly}(n)}$ (Theorem 8.2.4). The algorithmically relevant precision $2^{-n/2}$ lies strictly between these regimes. The interpolation method does not reach this precision. Braida et al. [10] therefore left this intermediate regime open.

The interpolation technique extracts exact integers from approximate real evaluations. At precision $2^{-n/2}$, the error amplification inherent in polynomial extrapolation makes this extraction impossible.

NP-hardness extends to $2^{-n/2}$ by monotonicity. An oracle at precision $2^{-n/2}$ is strictly more powerful than one at $1/\mathrm{poly}(n)$, so it still solves 3-SAT. The #P-hardness argument does not extend in the opposite direction. An oracle at precision $2^{-n/2}$ is *less* powerful than one at $2^{-\mathrm{poly}(n)}$, and the interpolation proof for that regime fails here.

The failure has a concrete source. Oracle noise at rate ε enters the polynomial samples scaled by $B^M = \mathrm{poly}(n)^M$ from the denominator-clearing step. The Lebesgue function $\Lambda_M(x^*)$ of the interpolation then amplifies this error by a factor of $2^{\Omega(M)}$ for extrapolation outside the sample interval. The amplified error must stay below $1/2$ for rounding to recover exact integers. At $\varepsilon = 2^{-n/2}$ and $M = \mathrm{poly}(n)$, the product $\varepsilon \cdot B^M \cdot \Lambda_M$ exceeds $1/2$, and rounding fails.

Theorem 8.3.1 (Interpolation barrier)**.** *The polynomial interpolation technique of section 8.2 requires oracle precision $\varepsilon = 2^{-n-O(M \log n)}$ to extract exact degeneracies, where $M = \mathrm{poly}(n)$ is the number of distinct energy levels. At $\varepsilon = 2^{-n/2}$, the amplified error exceeds $1/2$ and rounding fails. The #P-hardness argument does not extend to precision $2^{-n/2}$.*

Proof. We trace the same three-stage propagation from oracle noise to degeneracy error. Let ε denote the oracle accuracy, and let $B = \Delta_{\max} + M = \mathrm{poly}(n)$ bound the denominator factors, where $\Delta_{\max}$ is the largest spectral gap.

Stage 1 (sample-point error). The approximate function values satisfy $|\tilde{f}(x_i) - f(x_i)| \le 3\varepsilon$. The approximate polynomial samples are $\tilde{P}(x_i) = \prod_k (\Delta_k + x_i/2)\, \tilde{f}(x_i)$, with error

$$|\tilde{P}(x_i) - P(x_i)| \le 3\varepsilon \prod_{k=0}^{M-1} \left(\Delta_k + \frac{x_i}{2}\right) \le 3\varepsilon\, B^M. \tag{8.3.1}$$

Stage 2 (extrapolation amplification). The approximate degeneracies are computed from Eq. (8.2.4) with $\tilde{P}$ in place of P. Since $\tilde{P}$ is the Lagrange interpolant through the noisy samples, its value at any point x^* is $\tilde{P}(x^*) = \sum_j \tilde{P}(x_j) \prod_{i \ne j} (x^* - x_i)/(x_j - x_i)$. At $x^* = -2\Delta_k$,

$$|\tilde{P}(x^*) - P(x^*)| \le 3\varepsilon\, B^M \sum_{j=0}^{M-1} \prod_{i \ne j} \frac{|x^* - x_i|}{|x_j - x_i|} = 3\varepsilon\, B^M \cdot \Lambda_M(x^*), \tag{8.3.2}$$

where $\Lambda_M(x^*) = \sum_j \prod_{i \ne j} |x^* - x_i|/|x_j - x_i|$ is the Lebesgue function at x^*. It is the amplification factor for pointwise interpolation error. If each sample has error δ, the extrapolated value at x^* can incur error as large as $\delta \cdot \Lambda_M(x^*)$.

For extrapolation outside the sample interval, this amplification is exponential in M. Consider odd-integer nodes $x_j = 2j + 1$ and evaluation point $x^* = -2\Delta_k \le 0$, which lies outside $[1, 2M - 1]$. Each numerator factor obeys $|x^* - x_i| = 2\Delta_k + 2i + 1 \le 2B + 1$. For the denominator,

$$\prod_{i \ne j} |x_j - x_i| = \prod_{i \ne j} 2|j - i| = 2^{M-1}\, j!\, (M - 1 - j)!,$$

because the nodes are equally spaced with spacing 2. The sum over j becomes

$$\Lambda_M(x^*) \le \sum_{j=0}^{M-1} \frac{(2B+1)^{M-1}}{2^{M-1}\, j!\, (M-1-j)!} = \frac{(2B+1)^{M-1}}{(M-1)!}, \tag{8.3.3}$$

using $\sum_j \binom{M-1}{j} = 2^{M-1}$. The denominator in Eq. (8.2.4) satisfies $\prod_{\ell \ne k} |\Delta_\ell - \Delta_k| \ge k!(M-1-k)!$ for integer gaps (since $|\Delta_\ell - \Delta_k| \ge |\ell - k|$), with minimum over k at least $((M-1)/(2e))^{M-1}$ by Stirling's approximation.

Putting these bounds together, the total degeneracy error is

$$|d_k - \tilde{d}_k| \le \frac{3\varepsilon\, N\, B^M\, (2B+1)^{M-1}}{(M-1)!\, ((M-1)/(2e))^{M-1}}. \tag{8.3.4}$$

Since $B = \text{poly}(n)$ and $M = \text{poly}(n)$, the amplification factor is $2^{O(M \log n)}$.

Stage 3 (rounding threshold). To extract exact degeneracies by rounding, we need $|d_k - \tilde{d}_k| < 1/2$. This requires

$$\varepsilon < \frac{1}{6N \cdot 2^{O(M \log n)}} = 2^{-n-O(M \log n)}. \tag{8.3.5}$$

Consequence at $\varepsilon = 2^{-n/2}$. Set $\varepsilon = 2^{-n/2}$ and $M = n^c$ for some constant $c \geq 1$. The error bound from Eq. (8.3.4) evaluates to

$$|d_k - \tilde{d}_k| \leq 3 \cdot 2^{-n/2} \cdot 2^n \cdot 2^{O(n^c \log n)} = 3 \cdot 2^{n/2 + O(n^c \log n)} \gg 1.$$

Even for $c = 1$ (the most favorable case $M = n$), the exponent $n/2 + \Omega(n)$ diverges. The upper bound on the degeneracy error already exceeds $1/2$, so the rounding step cannot be guaranteed to succeed. □

The precision $\varepsilon = 2^{-n/2}$ is too coarse for interpolation but too fine for brute force. It sits in a window that existing techniques cannot reach from either side.

This amplification is not specific to the construction above. Exponential growth is intrinsic to polynomial extrapolation for any d nodes, any interval, and any evaluation point sufficiently far outside that interval.

Theorem 8.3.2 (Generic extrapolation barrier)**.** *Let $x_1, \ldots, x_d$ be any d distinct nodes in an interval $[a, b]$, and let x^* satisfy $\text{dist}(x^*, [a, b]) \geq b - a$. The Lebesgue function at x^* satisfies $\Lambda_d(x^*) \geq 2^{d-1}$. Consequently, any polynomial extrapolation scheme that evaluates a degree-$(d-1)$ interpolant at x^* from samples with pointwise error δ can incur worst-case error at least $\delta \cdot 2^{d-1}$ at x^*.*

Proof. Assume $x^* \leq a - (b - a)$ (the case $x^* \geq b + (b - a)$ follows by symmetry). Let $x_{(1)} = \min_j x_j \geq a$ be the leftmost node. The corresponding Lagrange basis polynomial satisfies

$$|\ell_{(1)}(x^*)| = \prod_{i:\, x_i \neq x_{(1)}} \frac{|x_i - x^*|}{|x_i - x_{(1)}|} = \prod_{i:\, x_i \neq x_{(1)}} \left(1 + \frac{x_{(1)} - x^*}{x_i - x_{(1)}}\right).$$

Each factor has numerator shift $x_{(1)} - x^* \geq a - (a - (b - a)) = b - a$ and denominator $x_i - x_{(1)} \leq b - a$, so every factor is at least 2. With $d - 1$ such factors, $|\ell_{(1)}(x^*)| \geq 2^{d-1}$. Since $\Lambda_d(x^*) = \sum_j |\ell_j(x^*)| \geq |\ell_{(1)}(x^*)|$, the bound follows. For perturbed samples $y_j = P(x_j) + e_j$ with $|e_j| \leq \delta$, the extrapolation error is

$$\tilde{P}(x^*) - P(x^*) = \sum_{j=1}^{d} e_j \, \ell_j(x^*).$$

Choosing adversarial signs $e_j = \delta \, \text{sign}(\ell_j(x^*))$ gives

$$|\tilde{P}(x^*) - P(x^*)| = \delta \sum_{j=1}^{d} |\ell_j(x^*)| = \delta \, \Lambda_d(x^*) \geq \delta \cdot 2^{d-1},$$

so the worst-case error can be at least $\delta \cdot 2^{d-1}$. □

Theorem 8.3.2 rules out rescuing the #P-hardness argument by tweaking interpolation details. Reordering nodes (equispaced, Chebyshev, or otherwise), changing polynomial bases, or reparameterizing variables cannot push amplification below 2^{d-1}. At $d = M = \text{poly}(n)$, the needed precision stays at $\varepsilon = 2^{-\Omega(n)}$, far below $2^{-n/2}$. The same obstacle appears in quantum-advantage hardness arguments. In each case, the proof reduces approximate sampling to an exact counting problem through polynomial interpolation, and the Lebesgue constant of that interpolation controls how much noise is amplified. For boson sampling [75], the interpolation runs over matrix permanents; for IQP circuits [76], over gap-amplified partition functions; for random circuit sampling [77], over output probabilities of random quantum circuits. All three face the same barrier. Pushing the error tolerance from exponentially small to the moderate regime $1/\text{poly}(n)$ requires taming a Lebesgue constant that grows as $2^{\Omega(n)}$, and no known rearrangement of the interpolation nodes avoids this.

The interpolation barrier does not rule out #P-hardness at $2^{-n/2}$ by other methods. A proof that avoids polynomial extrapolation, for example through direct algebraic reductions or information-theoretic arguments, might still work. The barrier identifies the pressure point. A proof of counting hardness at this precision must avoid recovering exact integers from approximate real values.

The hardness results above are computational. Given an explicit description of H_z, how hard is it to compute A_1? A different question asks about information. Given only black-box access to the diagonal entries of H_z,

how many queries are needed to estimate A_1 to precision ε? The query model isolates the information cost from the computational cost, and at precision $2^{-n/2}$ it reveals a clean quantum–classical separation that the computational model has not yet established.

We work in the query model where each call to a diagonal oracle $O_H\colon |x\rangle|0\rangle \mapsto |x\rangle|E_x\rangle$ reveals one diagonal entry of H_z at unit cost. A quantum algorithm can bypass polynomial interpolation entirely, using amplitude estimation to extract A_1 from interference rather than from reconstructed integers.

Theorem 8.3.3 (Quantum algorithm for A_1)**.** *There exists a quantum algorithm that estimates $A_1(H_z)$ to additive precision ε using*

$$O\left(\sqrt{N} + \frac{1}{\varepsilon\,\Delta_1}\right) \tag{8.3.6}$$

quantum queries to the diagonal oracle O_H, where $\Delta_1 = E_1 - E_0$ is the spectral gap of H_z.

Proof. The algorithm has two stages.

Stage 1: Finding E_0. The Hamiltonian H_z is diagonal in the computational basis, so computing E_x for a given $|x\rangle$ requires one query to O_H. Finding the minimum of E_x over all $x \in \{0,1\}^n$ is an instance of quantum minimum finding [32], which succeeds with high probability in $O(\sqrt{N})$ queries.

Stage 2: Amplitude estimation of A_1. Define the function

$$g(x) = \begin{cases} \dfrac{1}{E_x - E_0} & \text{if } E_x \neq E_0, \\ 0 & \text{if } E_x = E_0. \end{cases}$$

The spectral parameter is the mean $A_1 = (1/N)\sum_x g(x)$. Since the eigenvalues lie in $[0,1]$, the values of g on non-ground states are in $[1, 1/\Delta_1]$. Rescaling to $h(x) = \Delta_1 \cdot g(x)$ yields $h(x) \in [0,1]$, and $A_1 = \mu_h/\Delta_1$ where $\mu_h = (1/N)\sum_x h(x)$.

Construct a quantum oracle U_h acting as $U_h\colon |x\rangle|0\rangle \mapsto |x\rangle\left(\sqrt{1-h(x)}\,|0\rangle + \sqrt{h(x)}\,|1\rangle\right)$. The implementation queries O_H once to obtain E_x, performs classical arithmetic on an ancilla to compute $h(x) = \Delta_1/(E_x - E_0)$ (or 0 for ground states), executes a controlled rotation $R_y(2\arcsin\sqrt{h(x)})$ on a flag qubit, and uncomputes the ancilla. Each application uses $O(1)$ queries to O_H and $O(\mathrm{poly}(n))$ auxiliary gates.

Preparing the uniform superposition $|+\rangle^{\otimes n}$ and applying U_h, the probability of measuring the flag qubit in $|1\rangle$ is

$$p = \frac{1}{N}\sum_x h(x) = \mu_h.$$

Amplitude estimation [34] estimates p to additive precision δ using $O(1/\delta)$ applications of U_h and its inverse. Setting $\delta = \varepsilon\,\Delta_1$ ensures $|A_1 - \tilde{A}_1| = |\mu_h - \tilde{\mu}_h|/\Delta_1 \leq \varepsilon$. The number of U_h applications is $O(1/(\varepsilon\,\Delta_1))$.

Combining both stages gives $O(\sqrt{N})$ queries for Stage 1 and $O(1/(\varepsilon\,\Delta_1))$ queries for Stage 2, yielding Eq. (8.3.6). For $\varepsilon = 2^{-n/2}$ and $\Delta_1 = 1/\mathrm{poly}(n)$, this becomes $O(2^{n/2} + 2^{n/2}\,\mathrm{poly}(n)) = O(2^{n/2}\,\mathrm{poly}(n))$. □

To confirm that the quantum algorithm's $O(2^{n/2})$ query count is a genuine advantage, we need a classical lower bound. The natural route is information-theoretic. We ask how many samples a classical algorithm needs to distinguish two carefully chosen instances whose A_1 values differ by ε.

Theorem 8.3.4 (Classical lower bound for A_1 estimation)**.** *Any classical randomized algorithm estimating $A_1(H_z)$ to additive precision ε in the query model requires $\Omega(1/\varepsilon^2)$ queries in the worst case.*

Proof. We construct an adversarial pair of instances that are indistinguishable without sufficiently many queries.

Instance construction. Fix $t = \lceil \varepsilon N \rceil$. Instance H_0 has a hidden set $S \subseteq \{0,1\}^n$ with $|S| = N/2$, and eigenvalues $E_x = 0$ for $x \in S$, $E_x = 1$ otherwise. Instance H_1 has $|S'| = N/2 + t$ ground states. The spectral parameters are $A_1(H_0) = 1/2$ and $A_1(H_1) = (N/2 - t)/N = 1/2 - t/N$, differing by $t/N \geq \varepsilon$. An algorithm estimating A_1 to precision $\varepsilon/2$ must distinguish the two instances.

Information-theoretic bound. A classical query at string x reveals $E_x \in \{0,1\}$, which is equivalent to learning whether $x \in S$. Under a uniform prior on S (or S'), successive queries follow a hypergeometric sampling model. Conditioned on earlier outcomes, the j-th query is a Bernoulli trial. Under hypothesis H_i, x is a ground state with probability $p_j^{(i)} = (|S_i| - g_{j-1})/(N - j + 1)$, where g_{j-1} counts ground states already found. The difference $p_j^{(1)} - p_j^{(0)} = t/(N - j + 1)$ is independent of g_{j-1}. Since both parameters are $\Theta(1)$, a Taylor expansion of binary KL divergence $D(p\|p+\delta) = \delta^2/(p(1-p)) + O(\delta^3)$ with $\delta = t/(N-j+1)$ gives the conditional per-query divergence

$$D_j = O\left(\frac{t^2}{(N-j)^2}\right) = O\left(\frac{t^2}{N^2}\right)$$

when $q \leq N/2$. By the chain rule for KL divergence, the total information from q adaptive queries is

$$D_{\mathrm{KL}}^{(q)} \leq \sum_{j=1}^{q} D_j \leq q \cdot O\left(\frac{t^2}{N^2}\right).$$

By Le Cam's two-point method [78], reliable hypothesis testing requires $D_{\mathrm{KL}}^{(q)} \geq \Omega(1)$. Via Pinsker's inequality, total variation distance is at most $\sqrt{D_{\mathrm{KL}}/2}$, and reliable distinguishing needs total variation $\Omega(1)$. Therefore

$$q \geq \Omega\left(\frac{N^2}{t^2}\right) = \Omega\left(\frac{1}{\varepsilon^2}\right).$$

At $\varepsilon = 2^{-n/2}$, this gives $q \geq \Omega(2^n)$. □

Corollary 8.3.5 (Quadratic quantum-classical separation)**.** *In the query model, estimating $A_1(H_z)$ to precision $\varepsilon = 2^{-n/2}$ exhibits a quadratic quantum-classical separation, with quantum complexity $O(2^{n/2}\,\mathrm{poly}(n))$ and classical complexity $\Omega(2^n)$.*

Proof. The upper bound is Theorem 8.3.3 with $\Delta_1 = 1$ for the adversarial instance (or $\Delta_1 = 1/\mathrm{poly}(n)$ in general). The lower bound is Theorem 8.3.4. The separation ratio is $\Omega(2^{n/2}/\mathrm{poly}(n))$, matching Grover's quadratic speedup for unstructured search. □

At the precision the adiabatic algorithm needs, quantum computation offers exactly the speedup the algorithm achieves.

The quantum bound in Theorem 8.3.3 is not only an upper bound; it is tight. The tightness already appears on the simplest family, namely $M = 2$ with $\Delta_1 = 1$. There, estimating $A_1 = (N - d_0)/N$ to precision ε is exactly approximate counting at precision ε.

Write the Grover iterate as $G = (2\,|+\rangle\langle+| - I)(I - 2\Pi_S)$, where Π_S projects onto the d_0 ground states. Its eigenphases are $\pm 2\theta$ with $\sin^2\theta = d_0/N$. For $d_0 \approx N/2$, we have $dp/d\theta = \sin 2\theta = 1$, so precision ε in A_1 requires precision ε in θ. The Heisenberg limit for quantum phase estimation [79], together with the quantum Cramér-Rao inequality [80] and Fisher bound $F_Q \leq 4T^2$, gives $T \geq 1/(2\varepsilon)$ applications of G, each with $O(1)$ oracle cost. Combining this with the upper bound yields quantum query complexity $\Theta(2^{n/2})$ at precision $\varepsilon = 2^{-n/2}$. The next chapter formalizes this theorem and ties it to the information cost of the adiabatic approach.

Two complementary frameworks apply here. Computational complexity asks whether a classical computer can extract A_1 from an explicit Hamiltonian description (J_{ij}, h_j). Query complexity asks how many oracle evaluations are information-theoretically necessary when diagonal entries are hidden behind O_H. A problem can be easy in one model and hard in the other. For A_1 estimation, both frameworks show hardness, which supports the same conclusion: the pre-computation barrier is structural, not an artifact of one proof style.

In the computational model with an explicit Hamiltonian description, the precision-dependent hardness landscape is summarized below.

Precision ε	Hardness	Source
$1/\mathrm{poly}(n)$	NP-hard	Theorem 8.1.2
$2^{-n/2}$	NP-hard	monotonicity
$2^{-\mathrm{poly}(n)}$	#P-hard	Theorem 8.2.4

In the query model with a diagonal oracle at the algorithmically relevant precision $\varepsilon = 2^{-n/2}$, the comparison is:

Model	Complexity	Source
Quantum	$O(2^{n/2} \cdot \mathrm{poly}(n))$	Theorem 8.3.3
Classical	$\Omega(2^n)$	Theorem 8.3.4

The precision $2^{-n/2}$ is exactly the algorithmic target. The adiabatic schedule needs A_1 to precision $O(\sqrt{d_0/N})$, which is $O(2^{-n/2})$ in the worst case $d_0 = O(1)$. It is also where interpolation-based #P-hardness proofs break (Theorem 8.3.1), even though NP-hardness still follows by monotonicity. It is also where query complexity separates sharply. The quantum algorithm uses $O(2^{n/2})$ queries, while classical sampling requires $\Omega(2^n)$.

Classical sampling provides independent evidence for the hardness of A_1 estimation at the algorithmic precision. Given a procedure that samples eigenvalues E_x according to the distribution $\{d_k/N\}$, estimating the mean $A_1 = \mathbb{E}[1/(E_x - E_0)]$ to precision δ_s requires $O(1/\delta_s^2) = \widetilde{O}(2^n/d_0)$ samples by Chebyshev's inequality [81].

This matches the formal $\Omega(2^n)$ lower bound of Theorem 8.3.4 up to logarithmic factors, providing a consistency check between the query-complexity result and concrete sampling algorithms.

The information barrier is not specific to adiabatic evolution. Consider the time-independent Hamiltonian $H = -|\psi_0\rangle\langle\psi_0| + r\,H_\sigma$, where $r > 0$ is fixed and H_σ is the problem Hamiltonian. Evolving $|\psi_0\rangle$ under H for time t produces oscillations between $|\psi_0\rangle$ and the ground state of H_σ, with success probability controlled by r.

The oscillation frequency is set by the spectral gap of H, and this gap is maximized when r is tuned to the avoided crossing, namely $r = A_1$ (up to normalization). To keep success probability non-negligible, r must lie within $O(2^{-n/2})$ of A_1 [10]. So the same barrier appears in this model as well. One still needs A_1 to exponential precision, and computing it remains NP-hard. The obstacle comes from spectral structure, not from adiabatic formalism itself.

The results of this chapter create a tension. The adiabatic algorithm of Theorem 7.4.1 achieves Grover scaling $\widetilde{O}(\sqrt{N/d_0})$, matching the unstructured-search lower bound. Yet the schedule depends on a spectral parameter whose computation is NP-hard, even at much coarser precision than the algorithm ultimately needs. In the circuit model, Grover achieves the same speedup without any spectral pre-computation because oracle queries gather information adaptively during execution. In the adiabatic framework, by contrast, the schedule must be fixed before evolution begins.

What the adiabatic model pays in pre-computation, the circuit model avoids entirely. The gap between them is not computational power but computational knowledge. The next chapter formalizes this as an information-runtime tradeoff, proving a separation theorem for uninformed schedules and exploring whether adaptive measurements can bypass the classical pre-computation barrier.

Chapter 9

Information Gap

The adiabatic algorithm works. Chapter 7 proves it reaches the Grover speedup $\widetilde{O}(\sqrt{N/d_0})$ with an optimal local schedule. But the schedule passes through an avoided crossing at $s^* = A_1/(A_1+1)$, and Chapter 8 proves that computing A_1 from a classical description of H_z is NP-hard. Without s^*, the schedule designer does not know where the gap reaches its minimum and cannot concentrate the slowdown where it matters. In the circuit model, the Dürr-Høyer algorithm [32] achieves the same speedup without computing s^*, without A_1, without the gap profile, and without any spectral parameter at all. It does not traverse an interpolation path. It never encounters an avoided crossing.

The discrepancy between these two facts is the subject of this chapter. The adiabatic approach to unstructured search pays an information cost that the circuit approach does not. That cost turns out to have precise mathematical structure. An uninformed fixed schedule loses a factor of $\Omega(2^{n/2})$ in runtime. Each additional bit of A_1 knowledge halves the penalty, with no abrupt phase transition. Quantum measurement during evolution recovers the full speedup with $\Theta(n)$ binary probes. No instance-independent modification within the rank-one framework can eliminate the spectrum dependence. And the hardness of A_1 is counting hardness, not optimization hardness, connected to partition functions rather than satisfiability. The information gap is a property of the computational model, not of the computational task.

The same phenomenon may arise whenever a quantum algorithm navigates a parametrized energy landscape. The mechanism itself creates an information requirement absent from the raw problem specification. Variational algorithms need good initial parameters, quantum annealing needs an appropriate cooling schedule, and adiabatic algorithms need the crossing position. In each case, the bottleneck is not the hardness of the underlying problem but the cost of learning where, in parameter space, the algorithm must concentrate its effort. The rank-one unstructured search studied here is the setting where this cost admits exact quantification, and the results are sharp enough to yield a complete taxonomy.

9.1 The Cost of Ignorance

Throughout this chapter, asymptotic notation (O, Ω, Θ) refers to the limit $N \to \infty$ (equivalently $n \to \infty$ with $N = 2^n$). Unless stated otherwise, the spectral parameters d_0, M, Δ, A_1, A_2 and the target error ε are treated as fixed positive constants independent of n. When we write "$O(T_{\text{inf}})$," the hidden constant may depend on these spectral parameters but not on n.

A *fixed schedule* is chosen before the instance is revealed. It may depend on problem size n and target error ε, but not on instance-specific spectral data. An *instance-independent* algorithm uses the same Hamiltonian design for all energy assignments with the same degeneracy structure.

NP-hardness is a statement about worst-case classical computation. It does not directly tell us how much runtime an adiabatic algorithm loses by not knowing A_1. If a fixed schedule that ignores A_1 still achieved $O(\sqrt{N/d_0})$, the hardness of computing A_1 would be academic. It is not. The right way to quantify the loss is through a game. The schedule designer commits to a velocity profile $v(s)$ before seeing the instance. An adversary, knowing the schedule, then places the gap minimum at the worst possible position within an uncertainty interval. The separation between what the informed designer achieves and what the uninformed designer can guarantee is a minimax ratio, and it grows exponentially. To make this game precise, we need a class of gap functions that the adversary is allowed to play. The adversary's freedom is parametrized by three quantities: the endpoints s_L, s_R of the uncertainty interval (encoding what the schedule designer does not know) and the minimum gap value Δ_* (encoding what is fixed across instances). Requiring a unique minimum

avoids degenerate cases where multiple crossings interact, which is the generic situation for the rank-one family studied here.

Definition 9.1.1 (Gap class)**.** *The gap class $\mathcal{G}(s_L, s_R, \Delta_*)$ consists of all gap functions $g : [0,1] \to \mathbb{R}_{>0}$ such that the minimum $g(s^*) = \Delta_*$ is achieved at a unique point $s^* \in [s_L, s_R]$, and $g(s) > \Delta_*$ for all $s \neq s^*$.*

For the running example ($M = 2$, $d_0 = 1$, $N = 4$), $s^* = A_1/(A_1 + 1) = 3/7$ and $\Delta_* = g_{\min} = 1/\sqrt{4} = 1/2$. Any gap function in $\mathcal{G}(0, 1, 1/2)$ has minimum value $1/2$ somewhere in $[0, 1]$. The adversary controls where that minimum sits.

The schedule designer's constraint is the Roland-Cerf local condition, which ties velocity to the gap at each point. The schedule must traverse the gap slowly enough to maintain adiabaticity, and it must do so for every instance simultaneously, because the schedule is fixed before the instance is revealed.

Definition 9.1.2 (RC-admissible fixed schedules)**.** *Fix a family of Hamiltonian instances. A fixed schedule u with velocity profile $v(s) = |ds/dt|$ is* RC-admissible *on an instance if it satisfies the local Roland-Cerf condition*

$$v(s) \leq \frac{\varepsilon\, g(s)^2}{\|H'(s)\|} \qquad \forall s \in [0,1].$$

It is uniformly RC-admissible *on the family if this inequality holds for every instance in the family.*

The parameter Δ_* is the minimum of the abstract gap function g, distinct from the spectral gap $\Delta = E_1 - E_0$ of H_z and the rank-one minimum $g_{\min}$ of $H(s)$. For rank-one gap profiles, $\Delta_* = g_{\min} = \Theta(\sqrt{d_0/(NA_2)})$.

The schedule induces a velocity profile $v(s) > 0$ on $[0, 1]$, with total evolution time $T = \int_0^1 v(s)^{-1}\, ds$.

Within the uniformly RC-admissible class (Definition 9.1.2), the crossing velocity obeys a pointwise bound. Since $H'(s) = |\psi_0\rangle\langle\psi_0| + H_z$ with $H_z \succeq 0$ and $\||\psi_0\rangle\langle\psi_0|\| = 1$, we have $\|H'(s)\| \geq 1$ for all s. (Also $\|H'(s)\| \leq 2$ from $\|H_z\| \leq 1$.) Therefore RC-admissibility gives

$$v(s) \leq \varepsilon\, g(s)^2.$$

At a crossing point where $g = \Delta_*$, this yields $v \leq \varepsilon\, \Delta_*^2$.

The crossing window has width $\delta_s = \Theta(\Delta_*)$. More precisely, Chapter 5 gives $\delta_s = \hat{g}/c_L$ (Equation 5.4.10), where $\hat{g} = \frac{2A_1}{A_1+1}\sqrt{d_0/(NA_2)}$ and $g_{\min} = (1 \pm O(\eta))\hat{g}$. Since $c_L = A_1(A_1 + 1)/A_2$ is a positive constant independent of n, the proportionality $\delta_s = \Theta(g_{\min}) = \Theta(\Delta_*)$ holds with constants depending only on the fixed spectral parameters A_1, A_2, d_0.

Define the reference scale $v_{\text{slow}} = \varepsilon\, \Delta_*^2$. Since the family assumption $g_{\min} = \Theta(\Delta_*)$ means $g_{\min}$ and Δ_* differ by at most fixed multiplicative constants, all crossing velocities are comparable to v_{slow} up to constants independent of n. Both the uninformed and informed runtimes are computed under the same RC condition, so these constants cancel in the ratio $T_{\text{unf}}/T_{\text{inf}}$. The separation depends on the geometric factor $(s_R - s_L)/\Delta_*$ alone.

Lemma 9.1.3 (Adversarial gap construction)**.** *For any $s_{\text{adv}} \in [s_L, s_R]$ and $\Delta_* > 0$, the gap function $g_{\text{adv}}(s) = \Delta_* + (s - s_{\text{adv}})^2$ belongs to $\mathcal{G}(s_L, s_R, \Delta_*)$.*

Proof. The function satisfies $g_{\text{adv}}(s_{\text{adv}}) = \Delta_*$, $g_{\text{adv}}(s) > \Delta_*$ for $s \neq s_{\text{adv}}$, and $g_{\text{adv}}(s) > 0$ for all s. □

Lemma 9.1.4 (Velocity bound for uninformed schedules)**.** *Let u be a fixed schedule that is uniformly RC-admissible on the rank-one family in Theorem 9.1.5. Then there exists a constant $C_{\text{vel}} > 0$ independent of n such that $v(s) \leq C_{\text{vel}}\, v_{\text{slow}}$ for all $s \in [s_L, s_R]$, provided N is sufficiently large that $\Delta_* < \min(1 - s_R, s_L)$ (in particular, $\Delta_* \leq 1 - s'$ for all $s' \in [s_L, s_R]$, which makes the adversary's construction feasible).*

Proof. Suppose $v(s') > C_{\text{vel}}\, v_{\text{slow}}$ for some $s' \in [s_L, s_R]$. We construct a physical Hamiltonian in the rank-one family whose gap minimum occurs at s', then apply RC-admissibility on that instance.

The two-level family has two free parameters: excitation gap $\Delta > 0$ and solution fraction $\rho = d_0/N$. Since $s^* = A_1/(A_1 + 1)$ with $A_1 = (1 - \rho)/\Delta$, fixing the crossing at s' constrains $\Delta = (1 - \rho)(1 - s')/s'$, leaving ρ free. Substituting into the gap formula (Equation 5.4.9), which gives $\hat{g} = \frac{2A_1}{A_1+1}\sqrt{d_0/(NA_2)}$, and using the two-level simplifications $A_1 = (1 - \rho)/\Delta$, $A_2 = (1 - \rho)/\Delta^2$, $A_1/(A_1 + 1) = s'$, and $d_0/(NA_2) = \rho\Delta^2/(1 - \rho)$, yields $\hat{g} = 2(1 - s')\sqrt{\rho(1 - \rho)}$. Choosing ρ to satisfy $\hat{g} = \Delta_*$ requires $\rho(1 - \rho) = \Delta_*^2/(4(1 - s')^2)$, which is feasible for $\Delta_* \leq 1 - s'$ (holding asymptotically since $\Delta_* = \Theta(2^{-n/2})$ and $s' \leq s_R < 1$). The resulting Hamiltonian H_z has crossing at s' and $g_{\min} = \Theta(\Delta_*)$. The adversary in the minimax game selects this physical Hamiltonian, not merely an abstract gap function.

Because $g_{\min} = \Theta(\Delta_*)$ on the family, there exists $c_+ > 0$ (independent of n) such that $g_{\min} \le c_+ \Delta_*$. Uniform RC-admissibility on this Hamiltonian gives

$$v(s') \le \frac{\varepsilon\, g_{\min}^2}{\|H'(s')\|} \le \varepsilon\, c_+^2\, \Delta_*^2 = c_+^2\, v_{\text{slow}},$$

using $\|H'(s')\| \ge 1$. Choosing $C_{\text{vel}} = c_+^2$ contradicts $v(s') > C_{\text{vel}} v_{\text{slow}}$. The key point is that the adversary constructs a different physical Hamiltonian for each probe point s': the schedule must be simultaneously admissible on all of them. Because s' was arbitrary in $[s_L, s_R]$, the bound holds throughout the interval. □

Theorem 9.1.5 (Separation (uniformly RC-admissible class))**.** *Let T_{unf} be the minimum time over all fixed schedules that are uniformly RC-admissible for all rank-one instances whose gap minima satisfy $s^* \in [s_L, s_R]$ and $g_{\min} = \Theta(\Delta_*)$, and let T_{inf} be the corresponding optimal informed runtime (with known s^*) on the same rank-one family. Then*

$$\frac{T_{\text{unf}}}{T_{\text{inf}}} = \Omega\left(\frac{s_R - s_L}{\Delta_*}\right). \tag{9.1.1}$$

Proof. By Lemma 9.1.4, $v(s) \le C_{\text{vel}} v_{\text{slow}}$ for all $s \in [s_L, s_R]$. The uninformed time satisfies

$$T_{\text{unf}} = \int_0^1 \frac{ds}{v(s)} \ge \int_{s_L}^{s_R} \frac{ds}{v(s)} \ge \frac{s_R - s_L}{C_{\text{vel}}\, v_{\text{slow}}}. \tag{9.1.2}$$

The informed schedule knows s^* exactly and needs to be slow only in the crossing window of width $O(\Delta_*)$. For rank-one profiles, $\delta_s = \hat{g}/c_L = \Theta(g_{\min}) = \Theta(\Delta_*)$ by Equation 5.4.10, so Theorem 7.4.1 gives $T_{\text{inf}} = \Theta(\delta_s / v_{\text{slow}}) = \Theta(\Delta_* / v_{\text{slow}})$. The velocity factors cancel:

$$\frac{T_{\text{unf}}}{T_{\text{inf}}} = \Omega\left(\frac{s_R - s_L}{\Delta_*}\right). \tag{9.1.3}$$

□

Corollary 9.1.6 (Constant-width uncertainty family)**.** *For any n-qubit rank-one family in which the minimum gap scales as $\Delta_* = \Theta(2^{-n/2})$, the crossing uncertainty interval has constant width $s_R - s_L = \Theta(1)$, and the endpoints are bounded away from the boundaries ($\exists\, \gamma > 0$ independent of n with $\gamma \le s_L < s_R \le 1 - \gamma$), the minimax separation satisfies*

$$\frac{T_{\text{unf}}}{T_{\text{inf}}} = \Omega(2^{n/2}).$$

The ratio $(s_R - s_L)/\Delta_*$ has a direct geometric reading. The numerator measures how much of the schedule the designer must keep slow, because the crossing might be anywhere in $[s_L, s_R]$. The denominator measures the width of the region that actually needs to be slow around the true crossing. An informed designer slows down over a window of width $O(\Delta_*)$. An uninformed designer must slow down over the entire interval $[s_L, s_R]$. The ratio of the two windows is the overhead.

For the running example ($N = 4$, $d_0 = 1$), consider the toy geometry with $s_R - s_L = 1$ and $\Delta_* = 1/2$. The separation ratio is $2 = \sqrt{N}$, consistent with the general corollary. The corollary itself is a worst-case uncertainty statement. It does not apply to the standard Grover setting, where $s^* = 1/2 + O(1/N)$ is known a priori.

If classical preprocessing runs in polynomial time, NP-hardness forces a gap-uninformed model for fixed schedules. Inside the uniformly RC-admissible class, that model pays an $\Omega(2^{n/2})$ overhead from the adversarial geometry of Lemma 9.1.3. The penalty is geometric, not a byproduct of the hardness reduction.

9.2 Partial Knowledge and Hedging

The separation theorem gives the extremes. Perfect knowledge yields T_{inf}, and total ignorance yields $\Omega(2^{n/2}) \cdot T_{\text{inf}}$. But NP-hardness does not mean total ignorance. A polynomial-time heuristic might approximate A_1 to some finite precision. A brute-force search over a fraction of the state space might narrow the uncertainty. Partial knowledge must interpolate between the extremes, and the shape of that interpolation determines whether classical preprocessing is worth the effort.

Throughout this section, ε denotes precision in A_1 estimation (distinct from the adiabatic target error ε in Definition 9.1.2, which is fixed and absorbed into the implicit constants of Section 9.1).

Suppose an algorithm has access to an estimate $A_{1,\text{est}}$ satisfying $|A_{1,\text{est}} - A_1| \le \varepsilon$. The uncertainty propagates to the crossing position through the map $f(x) = x/(x+1)$, whose derivative is $f'(x) = 1/(x+1)^2$.

Lemma 9.2.1 (A_1-to-s^* precision propagation)**.** *If* $|A_{1,\text{est}} - A_1| \le \varepsilon$ *with* $|\varepsilon| \le (1 + A_1)/2$*, then* $|s^*_{\text{est}} - s^*| \le 2|\varepsilon|/(A_1 + 1)^2$.

Proof. Direct computation gives the exact identity

$$s^*_{\text{est}} - s^* = \frac{A_1 + \varepsilon}{1 + A_1 + \varepsilon} - \frac{A_1}{1 + A_1} = \frac{\varepsilon}{(1 + A_1)(1 + A_1 + \varepsilon)}. \tag{9.2.1}$$

Under $|\varepsilon| \le (1 + A_1)/2$, the denominator satisfies $1 + A_1 + \varepsilon \ge (1 + A_1)/2$, so

$$|s^*_{\text{est}} - s^*| \le \frac{|\varepsilon|}{(1 + A_1) \cdot (1 + A_1)/2} = \frac{2|\varepsilon|}{(1 + A_1)^2}. \tag{9.2.2}$$

□

Given A_1 precision ε, Lemma 9.2.1 places the true crossing within radius $2\varepsilon/(A_1 + 1)^2$ of the estimate. The uncertainty interval therefore has width $W(\varepsilon) = 4\varepsilon/(A_1 + 1)^2$. Define the ε-informed gap class as $\mathcal{G}_\varepsilon = \mathcal{G}(s_L(\varepsilon), s_R(\varepsilon), \Delta_*)$, where the endpoints come from this interval. Applying Theorem 9.1.5 gives the lower bound. A matching upper bound comes from a schedule that stays uniformly slow on this interval and fast outside it.

Theorem 9.2.2 (Interpolation)**.** *For additive* A_1 *precision* $0 < \varepsilon \le (1 + A_1)/2$*, the optimal adiabatic runtime satisfies*

$$T(\varepsilon) = \Theta\left(T_{\text{inf}} \cdot \max\left(1, \frac{\varepsilon}{\delta_{A_1}}\right)\right), \tag{9.2.3}$$

where $\delta_{A_1} = 2\sqrt{d_0 A_2/N}$ *is the precision threshold for optimality.*

Proof. Lower bound. For $\varepsilon \ge \delta_{A_1}$, Theorem 9.1.5 applied to $\mathcal{G}_\varepsilon$ gives $T(\varepsilon) \ge W(\varepsilon)/v_{\text{slow}}$. Taking the ratio with $T_{\text{inf}} = \Theta(\delta_s/v_{\text{slow}})$ and using the identity

$$(A_1 + 1)^2 \cdot \delta_s = (A_1 + 1)^2 \cdot \frac{2}{(A_1 + 1)^2}\sqrt{\frac{d_0 A_2}{N}} = 2\sqrt{\frac{d_0 A_2}{N}} = \delta_{A_1} \tag{9.2.4}$$

yields $T(\varepsilon)/T_{\text{inf}} \ge \Theta(\varepsilon/\delta_{A_1})$. For $\varepsilon < \delta_{A_1}$, the trivial bound $T(\varepsilon) \ge T_{\text{inf}}$ holds regardless of precision.

Upper bound. Let $J = [s_L(\varepsilon), s_R(\varepsilon)]$ with width $W(\varepsilon)$. For $\varepsilon \ge \delta_{A_1}$, use a fixed schedule that sets $v = v_{\text{slow}} = \Theta(\Delta_*^2)$ on J. Outside J, let $d(s, J) = \text{dist}(s, J)$ and set

$$v(s) = \kappa\big(\Delta_* + c_{\min} d(s, J)\big)^2$$

with $\kappa > 0$ chosen small enough for RC-admissibility. This is valid because for any true crossing $s^* \in J$, the Chapter 6 gap bounds imply $g(s) \ge \max(g_{\min}, c_{\min}|s - s^*|)$ with $c_{\min} := \min(c_L, c_R) > 0$ and $g_{\min} = \Theta(\Delta_*)$, hence $g(s) \ge \widetilde{c}(\Delta_* + c_{\min} d(s, J))$ with a constant $\widetilde{c} > 0$ independent of n, and $\|H'(s)\| \le 2$.

Time on J is

$$T_J = \Theta\left(\frac{W(\varepsilon)}{v_{\text{slow}}}\right).$$

Time outside J is bounded by

$$T_{\overline{J}} \le \frac{2}{\kappa}\int_0^1 \frac{dd}{(\Delta_* + c_{\min} d)^2} = O(1/\Delta_*) = O(T_{\text{inf}}),$$

since $\delta_s = \Theta(\Delta_*)$ and $T_{\text{inf}} = \Theta(\delta_s/v_{\text{slow}}) = \Theta(1/\Delta_*)$. Therefore

$$T = T_J + O(T_{\text{inf}}) = \Theta\left(T_{\text{inf}} \cdot \max\left(1, \frac{\varepsilon}{\delta_{A_1}}\right)\right),$$

using $W(\varepsilon) = \Theta((\varepsilon/\delta_{A_1})\delta_s)$. For $\varepsilon < \delta_{A_1}$, the informed schedule gives $T = O(T_{\text{inf}})$. □

The structure is a linear interpolation with a smooth crossover at $\varepsilon \sim \delta_{A_1}$, not a discontinuous phase transition. At precision $1/\text{poly}(n)$ (NP-hard to achieve), the overhead is $\Theta(2^{n/2}/\text{poly}(n))$, close to the full exponential penalty. At precision $2^{-n/2}$ (the algorithmically relevant scale from Equation 5.4.10), the overhead is $\Theta(1)$. Each additional bit of A_1 knowledge halves the runtime. The region between the NP-hard precision and the optimal precision is the "information gap," and the interpolation theorem maps it quantitatively. For the running example:

Precision ε	$T(\varepsilon)/T_{\text{inf}}$
$2^{-n/2}$	$\Theta(1)$
$2^{-n/4}$	$\Theta(2^{n/4})$
$1/n$	$\Theta(2^{n/2}/n)$
$1/\text{poly}(n)$	$\Theta(2^{n/2}/\text{poly}(n))$
1 (no knowledge)	$\Theta(2^{n/2})$

The last row ("1 (no knowledge)") is the fully uninformed limit from Corollary 9.1.6; it is included for context alongside the interpolation regime.

The interpolation theorem treats A_1 precision as a continuous resource. A complementary operational question asks for the best fixed schedule when s^* is only known to lie in an interval $[u_L, u_R]$. A hedging schedule spreads slowdown across that full interval instead of concentrating it at one point. It uses velocity v_{slow} on $[u_L, u_R]$ and v_{fast} outside. The total evolution time is $T = (u_R - u_L)/v_{\text{slow}} + (1 - u_R + u_L)/v_{\text{fast}}$; normalizing to $T = 1$ makes the error a function of velocity allocation alone.

Write $w = u_R - u_L$ for the interval width. The separation theorem used the Roland-Cerf local condition, which bounds error through $\int g^{-2}\, ds$. The JRS framework (Equation 7.1.1) has a stronger g^{-3} weighting and includes boundary/derivative terms (Chapter 7). When the velocity $v(s) = ds/dt$ is piecewise constant, the change of variables $dt = ds/v$ gives $\|dH/dt\|^2 g^{-3}\, dt = v\, \|H'\|^2 g^{-3}\, ds$, so v factors out of the JRS integrand on each segment. Isolating the dominant g^{-3} bulk term under this ansatz gives the schedule-allocation proxy

$$E_{\text{proxy}} := v_{\text{slow}} I_{\text{slow}} + v_{\text{fast}} I_{\text{fast}},$$

where $I_{\text{slow}} = \int_{u_L}^{u_R} g(u)^{-3}\, du$ and $I_{\text{fast}} = \int_{[0,1]\setminus[u_L,u_R]} g(u)^{-3}\, du$. This proxy captures the segment-wise weighting used for allocation, but it is not asserted to equal the full rigorous transition-probability bound. Because the crossing lies in the slow region, typically $I_{\text{slow}} \gg I_{\text{fast}}$.

Theorem 9.2.3 (Hedging (piecewise-constant proxy optimum))**.** *Fix an uncertainty interval $[u_L, u_R]$ with width $w = u_R - u_L$, and restrict to piecewise-constant schedules with velocity v_{slow} on $[u_L, u_R]$ and v_{fast} outside. Under runtime normalization $T = 1$, the proxy objective $E_{\text{proxy}} = v_{\text{slow}} I_{\text{slow}} + v_{\text{fast}} I_{\text{fast}}$ is minimized at*

$$v_{\text{slow}} = w + \sqrt{(1-w)w/R}, \qquad R := I_{\text{slow}}/I_{\text{fast}}.$$

Moreover, as $R \to \infty$,

$$\frac{E_{\text{proxy,opt}}}{E_{\text{proxy,unif}}} \to w = u_R - u_L.$$

Proof. Write $w = u_R - u_L$ for the interval width. The normalization constraint $w/v_{\text{slow}} + (1-w)/v_{\text{fast}} = 1$ fixes the total time $T = 1$, and the proxy objective is $E_{\text{proxy}} = v_{\text{slow}} I_{\text{slow}} + v_{\text{fast}} I_{\text{fast}}$. The constraint gives

$$v_{\text{fast}} = \frac{(1-w)\, v_{\text{slow}}}{v_{\text{slow}} - w}, \tag{9.2.5}$$

valid for $v_{\text{slow}} > w$. Substituting into the error gives

$$E_{\text{proxy}}(v_{\text{slow}}) = v_{\text{slow}}\, I_{\text{slow}} + \frac{(1-w)\, v_{\text{slow}}}{v_{\text{slow}} - w}\, I_{\text{fast}}. \tag{9.2.6}$$

Differentiating with respect to v_{slow} and setting to zero:

$$\frac{dE_{\text{proxy}}}{dv_{\text{slow}}} = I_{\text{slow}} - \frac{(1-w)\, w\, I_{\text{fast}}}{(v_{\text{slow}} - w)^2} = 0. \tag{9.2.7}$$

Solving yields $(v_{\text{slow}} - w)^2 = (1-w)\, w\, I_{\text{fast}}/I_{\text{slow}} = (1-w)\, w/R$, so

$$v_{\text{slow}} = w + \sqrt{(1-w)\, w/R}. \tag{9.2.8}$$

At this optimum, $v_{\text{fast}} = (1-w)\, v_{\text{slow}}/\sqrt{(1-w)\, w/R} = \sqrt{R\, w\, (1-w)} + (1-w)$. The optimal proxy value, substituting $v_{\text{slow}} - w = \sqrt{(1-w)\, w/R}$, is

$$E_{\text{proxy,opt}} = \left(w + \sqrt{(1-w)\, w/R}\right) I_{\text{slow}} + \left(\sqrt{R\, w\, (1-w)} + (1-w)\right) I_{\text{fast}}. \tag{9.2.9}$$

Since $R = I_{\text{slow}}/I_{\text{fast}} \gg 1$, the terms involving $\sqrt{R}$ contribute $2\sqrt{w\,(1-w)\, I_{\text{slow}}\, I_{\text{fast}}} = o(I_{\text{slow}})$, and the dominant term is $w\, I_{\text{slow}}$, while the uniform proxy value is $E_{\text{proxy,unif}} = I_{\text{slow}} + I_{\text{fast}} \approx I_{\text{slow}}$. Therefore $E_{\text{proxy,opt}}/E_{\text{proxy,unif}} \to w = u_R - u_L$ as $R \to \infty$. □

For an uncertainty interval $[0.4, 0.8]$ (so $w = 0.4$), the hedging ratio $E_{\text{proxy,opt}}/E_{\text{proxy,unif}}$ approaches 0.4 in the large-R regime, i.e. a 60% reduction in the allocation proxy.

Corollary 9.2.4 (Conditional fidelity improvement at fixed runtime)**.** *Assume that in the operating regime and schedule class under comparison, transition error is asymptotically proportional to the proxy: $\eta = \kappa E_{\text{proxy}}(1 + o(1))$ with the same $\kappa > 0$ for hedged and uniform schedules at fixed T. Then*

$$\eta_{\text{hedge}} \sim w \cdot \eta_{\text{unif}}.$$

Consequently, for success fidelity $\mathcal{F} = 1 - \eta$,

$$\mathcal{F}_{\text{hedge}} - \mathcal{F}_{\text{unif}} \sim \eta_{\text{unif}}(1 - w).$$

Proof. By hypothesis,

$$\frac{\eta_{\text{hedge}}}{\eta_{\text{unif}}} = \frac{E_{\text{proxy,hedge}}}{E_{\text{proxy,unif}}} \cdot (1 + o(1)).$$

Apply Theorem 9.2.3 to get $E_{\text{proxy,hedge}}/E_{\text{proxy,unif}} \to w$, hence $\eta_{\text{hedge}} \sim w\,\eta_{\text{unif}}$. Then

$$\mathcal{F}_{\text{hedge}} - \mathcal{F}_{\text{unif}} = \eta_{\text{unif}} - \eta_{\text{hedge}} \sim \eta_{\text{unif}}(1 - w). \qquad \square$$

The hedging and separation theorems answer different questions, and the distinction matters. The separation theorem (Theorem 9.1.5) is a worst-case adversarial statement. The adversary places the gap minimum anywhere in $[s_L, s_R]$ after seeing the schedule, and the resulting overhead is $\Omega((s_R - s_L)/\Delta_*)$, which grows exponentially in n. The hedging theorem assumes a fixed (but unknown) crossing position within $[u_L, u_R]$ and optimizes piecewise-constant velocity allocation for the proxy objective above. The exponential factor in the separation ratio comes from the denominator $\Delta_* = \Theta(2^{-n/2})$; the hedging ratio $w = u_R - u_L$ is a constant independent of n. Both are correct, but they measure different quantities. The separation measures the cost of total ignorance about Δ_*-scale placement, while hedging measures the benefit of knowing the crossing's coarse location.

Several caveats are in order. The hedging theorem establishes the optimal velocity allocation for piecewise-constant schedules with respect to E_{proxy}, but whether piecewise-constant is optimal among all fixed schedules with the same uncertainty interval (and under full JRS bounds) remains open. A smoother velocity profile that transitions gradually between slow and fast regions might achieve a better constant, though the improvement cannot change the $\Theta(w)$ scaling at proxy level. The asymptotic ratio w is valid in the regime $R = I_{\text{slow}}/I_{\text{fast}} \gg 1$, which holds whenever the gap minimum lies well inside the uncertainty interval. For crossings near the boundary of $[u_L, u_R]$, the improvement degrades. Finally, the analysis treats single avoided crossings; systems with multiple gap minima would require a multi-region hedging strategy.

These limitations suggest natural directions. Is w the optimal constant for hedging, or can non-piecewise-constant fixed schedules do better? If the crossing position has a known prior distribution rather than just a support, can distribution-aware hedging improve on worst-case allocation? For multi-crossing systems, does the hedging overhead grow with the number of crossings or can a single slow region cover multiple minima?

Bounded uncertainty about s^* therefore yields a constant-factor reduction of the hedging proxy at fixed runtime, and (under the proportionality assumption of Corollary 9.2.4) a matching fidelity improvement proportional to interval width, rather than the exponential runtime overhead of the worst-case adversarial model. In the taxonomy of Section 9.7, this is the same information setting as Level 2; however, that table measures runtime overhead T/T_{inf}, not fixed-runtime fidelity gain.

9.3 Quantum Bypass

The separation and interpolation theorems characterize the cost of ignorance within the fixed-schedule model, where the designer commits to a velocity profile before the evolution begins. But an adiabatic device is a physical system. It can be measured during execution. Measurements yield information about the spectrum, and that information can be used to adjust the schedule on the fly. The question, posed in [10], is whether this adaptive access can close the information gap entirely.

It can. Han, Park, and Choi [82] independently proposed a constant geometric speed (CGS) schedule that traverses the eigenstate path at uniform arc length, setting $v(s)$ so that the instantaneous eigenstate moves at a constant rate in Hilbert space. Near the crossing, where the eigenstate changes rapidly, this automatically slows the evolution. Overlap estimates from quantum Zeno Monte Carlo measurements provide the needed feedback during evolution. Their method improves the runtime scaling from $O(1/\Delta_*^2)$ to $O(1/\Delta_*^1)$ and numerically preserves the quadratic speedup without prior spectral knowledge. The binary-search protocol below uses a

different mechanism. Rather than adapting continuously, it first locates the crossing through discrete branch probes and then runs the informed schedule. In the ideal decision-probe model, it achieves $O(T_{\text{inf}})$.

The key distinction is between *computing* and *detecting*. Computing s^* from the classical description of H_z is NP-hard. Detecting s^* by probing the quantum system $H(s)$ at selected parameter values can be efficient, because each probe extracts a bit of information about the spectrum at a cost proportional to the inverse gap at the probe point. We model this with a binary decision-probe oracle. A probe at parameter s returns whether s is at or left of the true crossing, and costs $O(1/g(s))$.

Definition 9.3.1 (Binary decision probe)**.** *For an instance H, let $D_H : [0,1] \to \{0,1\}$ be the idealized oracle*

$$D_H(s) = \begin{cases} 0, & s \le s^*(H), \\ 1, & s > s^*(H), \end{cases}$$

with probe cost $O(1/g_H(s))$.

Definition 9.3.2 (Adaptive adiabatic protocol)**.** *The protocol operates in two phases.*

Phase 1 (Location). *Initialize $s_{\text{lo}} = 0$, $s_{\text{hi}} = 1$. For $i = 1, \ldots, \lceil n/2 \rceil$:*

1. *Set $s_{\text{mid}} = (s_{\text{lo}} + s_{\text{hi}})/2$.*
2. *Query $D_H(s_{\text{mid}})$.*
3. *If $D_H(s_{\text{mid}}) = 0$ (at or left of crossing), set $s_{\text{lo}} = s_{\text{mid}}$.*
4. *If $D_H(s_{\text{mid}}) = 1$ (right of crossing), set $s_{\text{hi}} = s_{\text{mid}}$.*

After $\lceil n/2 \rceil$ iterations, s^* is located to precision $O(2^{-n/2})$.

Phase 2 (Execution). *Reset the state to $|\psi_0\rangle$. Evolve from $s = 0$ to $s = 1$ using the informed local schedule of Theorem 7.4.1, with the crossing position estimated in Phase 1.*

Each call to $D_H(s_{\text{mid}})$ costs $O(1/g(s_{\text{mid}}))$ by Definition 9.3.1, since the branch test resolves a spectral question about $H(s_{\text{mid}})$ and the required evolution time scales inversely with the gap at the probe point.

Lemma 9.3.3 (Phase 1 cost)**.** *The total time for Phase 1 is $O(T_{\text{inf}})$.*

Proof. Let $d_i = |s_{\text{mid},i} - s^*|$ be the distance from the i-th midpoint to the true crossing. Chapter 6 gives two complementary bounds. Outside the crossing window ($|s - s^*| > \delta_s$), the gap satisfies

$$g(s) \ge c_{\min} |s - s^*|,$$

where $c_{\min} = \min(c_L, c_R)$ with $c_L = A_1(A_1+1)/A_2$ and $c_R = \Delta/30$. Both constants are positive and independent of n. Inside the crossing window ($|s - s^*| \le \delta_s$), the gap satisfies $g(s) \ge g_{\min}$. Because $g_{\min}$ is the global minimum, these two bounds combine to

$$g(s_{\text{mid},i}) \ge \max(g_{\min},\ c_{\min} \cdot d_i). \tag{9.3.1}$$

The probe cost at iteration i is therefore

$$O\left(\frac{1}{g(s_{\text{mid},i})}\right) \le O\left(\min\left(\frac{1}{g_{\min}},\ \frac{1}{c_{\min} \cdot d_i}\right)\right). \tag{9.3.2}$$

The two bounds in (9.3.2) cross at $d_i = g_{\min}/c_{\min}$. Since $g_{\min} = c_L \delta_s \cdot (1 - O(\eta))$ and $c_{\min} \le c_L$, the crossover distance satisfies

$$d_{\text{cross}} = g_{\min}/c_{\min} = (c_L/c_{\min})\, \delta_s \ge \delta_s.$$

The ratio $c_L/c_{\min}$ is a positive constant independent of n because $c_L = A_1(A_1+1)/A_2$ and $c_R = \Delta/30$ are fixed by spectral parameters. Therefore $c_{\min} = \min(c_L, c_R) > 0$ is also fixed. At most $O(\log(c_L/c_{\min}) + 1) = O(1)$ binary-search midpoints can fall in the near regime $d_i \le d_{\text{cross}}$.

Group the $\lceil n/2 \rceil$ iterations by the distance d_i in dyadic shells $S_j = [2^{-j-1}, 2^{-j}]$. Let $L_i = 2^{-i+1}$ be the binary-search interval width at step i. Since the next interval is the half containing s^*, the midpoint distances obey

$$d_{i+1} = \left| d_i - \frac{L_i}{4} \right| = \left| d_i - 2^{-i-1} \right|.$$

This recurrence gives $O(1)$ occupancy per shell: for $i > j+1$, $d_i \le L_i/2 = 2^{-i} < 2^{-j-1}$, so $d_i \notin S_j$; and for $i \le j$, if $d_i \in (2^{-j-1}, 2^{-j})$, then $d_{i+1} \notin (2^{-j-1}, 2^{-j})$. Thus the shell interior is visited at most once, with only

a dyadic-rational edge case where the boundary value 2^{-j-1} can appear twice consecutively. Hence each shell contributes $O(1)$ midpoint queries.

Far shells ($j < \log_2(1/\delta_s) \approx n/2$): here $d_i > \delta_s$, so the binding bound in (9.3.2) is $O(1/(c_{\min} \cdot d_i)) = O(2^j/c_{\min})$, where $c_{\min}$ enters the implicit constant.

Near shells ($j \geq n/2$): here $d_i \leq \delta_s$, so the binding bound is $O(1/g_{\min}) = O(1/\Delta_*) = O(2^{n/2})$.

There are $O(1)$ near shells because at most $O(1)$ midpoints can satisfy $d_i \leq d_{\text{cross}}$ in a binary search. The total cost is

$$\sum_{j=0}^{n/2-1} O(1) \cdot O(2^j) + O(1) \cdot O(2^{n/2}) = O(2^{n/2}) + O(2^{n/2}) = O(2^{n/2}) = O(T_{\text{inf}}). \tag{9.3.3}$$

The state preparation cost is $O(n)$ per iteration and $O(n)$ iterations, giving $O(n^2) = o(T_{\text{inf}})$. □

Theorem 9.3.4 (Adaptive adiabatic optimality in the decision-probe model)**.** *The adaptive protocol of Definition 9.3.2 achieves runtime $T_{\text{adapt}} = O(T_{\text{inf}})$ with $\Theta(n)$ measurements.*

Proof. Phase 1 locates s^* to precision $O(2^{-n/2}) = O(\delta_s)$ using total time $O(T_{\text{inf}})$ by Lemma 9.3.3. This precision is within the crossing window width $\delta_s = O(\Delta_*)$. Phase 2 has time $O(T_{\text{inf}})$ by Theorem 7.4.1, since the estimate of s^* is accurate to $O(\delta_s)$. The total is $O(T_{\text{inf}}) + O(T_{\text{inf}}) = O(T_{\text{inf}})$. □

Theorem 9.3.5 (Measurement lower bound)**.** *For rank-one families where the crossing location is a priori uncertain in an interval of width $\Theta(1)$ and $\delta_s = \Theta(2^{-n/2})$ (the same regime as Corollary 9.1.6), any adaptive protocol in the binary decision-probe model that guarantees localization of s^* to precision $O(\delta_s)$ requires $\Omega(n)$ measurements. In particular, any locate-then-execute strategy that first localizes s^* and then runs the informed schedule in $O(T_{\text{inf}})$ has measurement cost $\Omega(n)$.*

Proof. The prior uncertainty interval has width $\Theta(1)$, while the required final uncertainty is $O(\delta_s) = \Theta(2^{-n/2})$. Therefore the protocol must distinguish among $K = \Omega(1/\delta_s) = \Omega(2^{n/2})$ disjoint location bins. In the binary decision-probe model, each measurement returns one bit, so after m measurements there are at most 2^m possible transcripts. To identify one of K bins in the worst case we need $2^m \geq K$, hence $m \geq \log_2 K = \Omega(n)$. □

The three adiabatic regimes are:

Strategy	Runtime	Measurements
Fixed, uninformed	$\Omega(2^{n/2} \cdot T_{\text{inf}})$	0
Adaptive	$O(T_{\text{inf}})$	$\Theta(n)$
Fixed, informed	$O(T_{\text{inf}})$	0

For the running example ($N = 4$, $d_0 = 1$, $n = 2$), Phase 1 performs $\lceil 1 \rceil = 1$ probe at $s_{\text{mid}} = 0.5$, so the location stage already achieves width $1/2 = O(2^{-n/2})$. The gap at that point is $g(0.5) = 1/\sqrt{N} = 1/2$, which gives probe cost $O(1/g) = O(2) = O(T_{\text{inf}})$.

Implementation note. A physical instantiation of D_H uses phase-estimation-based branch tests on $H(s_{\text{mid}})$, which distinguish the ground and excited branches at cost $O(1/g(s_{\text{mid}}))$ per probe. The theorem above is stated in the ideal decision-probe model; the open question is whether constant-probability probes with standard amplification introduce only polylogarithmic overhead, preserving the $O(T_{\text{inf}})$ scaling. The key observation is that each probe requires only constant-probability correctness, so standard amplification keeps the overhead logarithmic.

The adaptive protocol acquires A_1 through measurement, while the circuit model bypasses A_1 entirely. The Dürr-Høyer minimum-finding algorithm [32] achieves $\Theta(\sqrt{N/d_0})$ by maintaining a threshold and iteratively lowering it with Grover search. It never traverses an adiabatic path and never encounters an avoided crossing. Its mechanism is amplitude amplification with iterative thresholding and no spectral inputs. It needs no A_1, no s^*, no Δ, and no gap profile.

Proposition 9.3.6 (A_1-blindness)**.** *Let X_{DH} denote the output of the amplified Dürr-Høyer algorithm (with $r = \Theta(n)$ repetitions). Then $I(X_{\text{DH}}; A_1 \mid S_0, E_0) \leq 2^{-\Omega(n)}$. Conditioned on success ($X_{\text{DH}} \in S_0$), the mutual information is exactly zero.*

Proof. Two problem Hamiltonians H_z, H_z' are ground-equivalent if they share the same ground energy E_0 and ground space S_0. By symmetry of Grover's algorithm applied to the uniform initial state, the output distribution

conditioned on success is Uniform(S_0), regardless of the excited spectrum. Since A_1 depends only on the excited spectrum (via $\{d_k, E_k\}_{k\geq 1}$), we have

$$I(X_{\mathrm{DH}};\, A_1 \mid \text{success}, S_0, E_0) = 0.$$

Let F be the failure indicator of the amplified routine, and fix any prior over ground-equivalent instances conditioned on (S_0, E_0). With $r = \Theta(n)$ repetitions using Boyer-Brassard-Høyer-Tapp amplification [33], the per-trial success probability is at least 2/3, so

$$p_f := \Pr[F = 1] \leq (1/3)^r = 2^{-\Omega(n)}.$$

Using chain rule and the fact that F is a function of X_{DH}:

$$\begin{aligned} I(X_{\mathrm{DH}};\, A_1 \mid S_0, E_0) &\leq I(X_{\mathrm{DH}}, F;\, A_1 \mid S_0, E_0) \\ &= I(F;\, A_1 \mid S_0, E_0) + I(X_{\mathrm{DH}};\, A_1 \mid F, S_0, E_0) \\ &= I(F;\, A_1 \mid S_0, E_0) + p_f\, I(X_{\mathrm{DH}};\, A_1 \mid F = 1, S_0, E_0) \\ &\leq H(F) + p_f\, H(X_{\mathrm{DH}} \mid F = 1, S_0, E_0). \end{aligned} \tag{9.3.4}$$

The $F = 0$ term vanishes by the conditional independence established above. Now $H(F) \leq h_2(p_f)$, where $h_2(p) = -p \log p - (1-p)\log(1-p)$ is the binary entropy, and $H(X_{\mathrm{DH}} \mid F = 1, S_0, E_0) \leq \log N = n$, so Eq. (9.3.4) gives

$$I(X_{\mathrm{DH}};\, A_1 \mid S_0, E_0) \leq h_2(p_f) + p_f n = 2^{-\Omega(n)}.$$

□

The circuit model does not merely avoid computing A_1. It is provably blind to it. Two problem Hamiltonians that share the same ground space but have entirely different excited spectra, and therefore different A_1 values, produce output distributions that are exponentially close in total variation. Conditioned on success, the distributions coincide exactly (uniform on S_0), and all discrepancy is confined to failure events of probability $2^{-\Omega(n)}$, so $\|P_{H_z} - P_{H'_z}\|_{\mathrm{TV}} \leq p_f(H_z) + p_f(H'_z) = 2^{-\Omega(n)}$. No measurement on the output of Dürr-Høyer, no matter how clever, can reliably distinguish two such instances. The fixed adiabatic model has the opposite property. A schedule tuned to one value of A_1 performs poorly on ground-equivalent instances with different excited spectra, because the crossing position shifts and the gap minimum moves away from the schedule's slowdown region.

The three models form a hierarchy of spectral information usage. The circuit model is blind to A_1 and does not need it. The adaptive adiabatic model acquires A_1 through $O(n)$ measurements during execution, paying $O(T_{\mathrm{inf}})$ to do so. The fixed adiabatic model requires A_1 as classical input and faces NP-hard recovery. This hierarchy captures the "information gap" operationally. The same computational task admits three qualitatively different information profiles depending on the model.

The adaptive protocol's efficiency rests on a structural feature of the rank-one gap profile. The gap grows linearly away from the crossing ($\alpha = 1$), so a probe at distance d costs $O(1/d)$ and the geometric sum converges. But the rank-one case is special. Flatter gap profiles widen the danger zone, and the degradation turns out to be continuous rather than binary.

9.4 Gap Geometry and Schedule Optimality

If the gap approaches its minimum more gently than the rank-one linear growth, the danger zone where the schedule must be slow widens, and the runtime degrades. How much depends on the geometry of the approach.

To make the scaling statements precise, this section analyzes the model profile

$$g_{\alpha,c,\Delta_*}(s) = \Delta_* + c|s - s^*|^\alpha, \qquad c > 0,$$

on $[0, 1]$, with c independent of Δ_*. The flatness exponent α parametrizes the gap shape. A V-shaped minimum ($\alpha = 1$) is the rank-one case. Flatter approaches ($\alpha > 1$) create wider regions where the gap stays close to its minimum, forcing the schedule to be slow over a wider interval.

Guo and An [42] identified a measure condition that guarantees $O(1/g_{\min})$ for the $p = 3/2$ power-law schedule, which they show is variationally optimal within the JRS error functional. The condition asks that sublevel sets of the gap grow at most linearly: $\mu(\{s : g(s) \leq x\}) \leq Cx$ for all $x > 0$, with C independent of Δ_*. This section proves three things. First, the measure condition holds if and only if $\alpha \leq 1$. Second, when $\alpha > 1$, the optimal power-law schedule degrades from $T = O(1/\Delta_*)$ to $T = O(1/\Delta_*^{3-2/\alpha})$, forming a continuous

spectrum of scaling exponents rather than a binary dichotomy between "easy" and "hard" gap profiles. Third, the rank-one framework forces $\alpha = 1$, placing it exactly at the boundary where the measure condition holds.

Whether some non-power-law fixed schedule can recover $O(1/\Delta_*)$ when $\alpha > 1$ remains open. The constant geometric speed approach of Han, Park, and Choi [82] achieves $O(1/g_{\min})$ by adaptive gap measurements, but that method uses runtime feedback during evolution and is therefore not a fixed schedule. The open question is whether there exists a fixed (non-adaptive) schedule family, not necessarily a power law, that achieves $O(1/\Delta_*)$ for gap profiles with $\alpha > 1$. No such family is currently known.

Theorem 9.4.1 (Geometric characterization)**.** *For the model profile $g_{\alpha,c,\Delta_*}(s)$, the measure condition $\mu(\{s : g(s) \le x\}) \le Cx$ with C independent of Δ_* holds if and only if $\alpha \le 1$.*

Proof. For $x \ge \Delta_*$, write $y = (x - \Delta_*)/c$. The sublevel set has measure

$$\mu(x) = \mu(\{s : g(s) \le x\}) \le \min(1,\, 2y^{1/\alpha}).$$

Case $\alpha \le 1$. For $x \in [\Delta_*, 1]$,

$$\frac{\mu(x)}{x} \le \frac{2}{c^{1/\alpha}} \frac{(x - \Delta_*)^{1/\alpha}}{x} \le \frac{2}{c^{1/\alpha}} x^{1/\alpha - 1} \le \frac{2}{c^{1/\alpha}},$$

because $1/\alpha - 1 \ge 0$ and $x \le 1$. For $x \ge 1$, $\mu(x)/x \le 1$. Thus $\sup_{x>0} \mu(x)/x \le \max(1, 2/c^{1/\alpha})$, independent of Δ_*.

Case $\alpha > 1$. At $x = 2\Delta_*$, one side of the sublevel interval always contributes length at least $(\Delta_*/c)^{1/\alpha}$, so $\mu(x) \ge (\Delta_*/c)^{1/\alpha}$. Therefore

$$\frac{\mu(2\Delta_*)}{2\Delta_*} \ge \frac{1}{2c^{1/\alpha}} \Delta_*^{1/\alpha - 1},$$

which diverges as $\Delta_* \to 0$ since $1/\alpha - 1 < 0$. Hence no finite C independent of Δ_* can satisfy the measure condition. □

The gap integral $\int_0^1 g(s)^{-\beta}\, ds$ controls the runtime for power-law schedules. A substitution $u = c|s - s^*|^\alpha/\Delta_*$ gives the following scaling.

Lemma 9.4.2 (Gap integral)**.** *For the model profile g_{α,c,Δ_*} and $\beta > 1/\alpha$,*

$$\int_0^1 g(s)^{-\beta}\, ds = \Theta(\Delta_*^{1/\alpha - \beta}). \tag{9.4.1}$$

For $\beta = 1/\alpha$, the integral is $\Theta(\log(1/\Delta_*))$. For $\beta < 1/\alpha$, the integral is $\Theta(1)$.

Proof. The substitution $u = (c|s - s^*|^\alpha)/\Delta_*$ transforms the near-minimum contribution to

$$\Delta_*^{1/\alpha - \beta} \int_0^U u^{1/\alpha - 1} (1 + u)^{-\beta}\, du,$$

where $U = \Theta(1/\Delta_*)$. As $u \to \infty$, the integrand behaves like $u^{1/\alpha - 1 - \beta}$.

If $\beta > 1/\alpha$, the exponent is strictly less than -1, so the u-integral converges to a finite constant, yielding $\Theta(\Delta_*^{1/\alpha - \beta})$.

If $\beta = 1/\alpha$, the integrand is asymptotically u^{-1}, so the integral contributes $\Theta(\log U) = \Theta(\log(1/\Delta_*))$.

If $\beta < 1/\alpha$, the integral grows as $U^{1/\alpha - \beta}$, which cancels the prefactor $\Delta_*^{1/\alpha - \beta}$, giving $\Theta(1)$.

The contribution from outside a neighborhood of s^* is always $O(1)$. For fixed δ, if $|s - s^*| \ge \delta$ then $g(s) \ge g_0 > 0$ independently of Δ_*, so $\int_{|s-s^*| \ge \delta} g(s)^{-\beta} ds \le g_0^{-\beta}$. □

Theorem 9.4.3 (Scaling spectrum)**.** *For the model profile g_{α,c,Δ_*} with flatness exponent $\alpha > 2/3$, the adiabatic runtime with the $p = 3/2$ power-law schedule (variationally optimal in the JRS framework [42]) satisfies*

$$T = \Theta(1/\Delta_*^{3 - 2/\alpha}). \tag{9.4.2}$$

Proof. The power-law schedule $u'(s) = c_p\, g(u(s))^p$ has normalization constant $c_p = \int_0^1 g(v)^{-p}\, dv$. The JRS error functional becomes

$$\eta \le \frac{1}{T}\, c_p \int_0^1 g(v)^{p-3}\, dv. \tag{9.4.3}$$

By Lemma 9.4.2, $c_p = \Theta(\Delta_*^{1/\alpha-p})$ (requiring $p > 1/\alpha$) and the second integral is $\Theta(\Delta_*^{1/\alpha+p-3})$ (requiring $3-p > 1/\alpha$). Together these require $1/\alpha < p < 3 - 1/\alpha$, an interval of width $3 - 2/\alpha$, which is positive if and only if $\alpha > 2/3$. The symmetric choice $p = 3/2$ lies in this interval for all $\alpha > 2/3$. Their product is

$$c_p \int g^{p-3}\, dv = \Theta(\Delta_*^{(1/\alpha-p)+(1/\alpha+p-3)}) = \Theta(\Delta_*^{2/\alpha-3}). \tag{9.4.4}$$

Setting $\eta = O(1)$ gives $T = \Omega(\Delta_*^{-(3-2/\alpha)}) = \Omega(1/\Delta_*^{3-2/\alpha})$. The $p = 3/2$ power-law schedule achieves this scaling, giving a matching upper bound $T = O(1/\Delta_*^{3-2/\alpha})$. □

α	Exponent $\gamma = 3 - 2/\alpha$	Measure condition	Runtime
1	1	Holds	$\Theta(1/\Delta_*)$
2	2	Fails	$\Theta(1/\Delta_*^2)$
3	7/3	Fails	$\Theta(1/\Delta_*^{7/3})$
∞	3	Fails	$\Theta(1/\Delta_*^3)$

The exponents in the table are specific to the JRS-optimal $p = 3/2$ schedule; other schedule families produce different curves. In particular, the exponent $\gamma = 3$ at $\alpha = \infty$ is not universal. The Roland-Cerf schedule ($p = 2$) gives $T = O(1/\Delta_*^2)$ for flat gaps via a tighter adiabatic condition. The table shows the JRS-optimal scaling as the gap flattens.

The runtime exponent $\gamma = 3 - 2/\alpha$ interpolates continuously from 1 (V-shaped gap, best case) to 3 (flat gap, worst case). There is no sharp boundary between "easy" and "hard" gap profiles, only a gradual degradation as the minimum flattens. For the running example ($M = 2$, $d_0 = 1$, $N = 4$), $\alpha = 1$, and $\gamma = 1$, confirming the optimal $T = \Theta(1/\Delta_*)$ scaling. The formula $\gamma = 3 - 2/\alpha$ also explains why the transition is one-sided. As $\alpha \to \infty$ (perfectly flat gap), $\gamma \to 3$ and the exponent saturates. As $\alpha \to 2/3$ from above, the interval of valid power-law exponents shrinks to zero and the variational framework loses its grip entirely.

Proposition 9.4.4 (Structural $\alpha = 1$)**.** *For the rank-one Hamiltonian $H(s) = -(1-s)\,|\psi_0\rangle\langle\psi_0| + sH_z$ under the spectral-condition regime of Chapters 5–6 (with $d_1 \geq 1$ and $\Delta > 0$), the effective crossing geometry is linear: $g(s) = \Theta(|s - s^*|)$ for $|s - s^*| \gg \delta_s$. Equivalently, the flatness exponent is $\alpha = 1$.*

Proof. Chapter 5 gives the crossing-window form

$$g(s) = (1 \pm O(\eta))\frac{s(A_1+1)}{A_2(1-s)}\sqrt{(s-s^*)^2 + \Theta(\delta_s^2)}.$$

In the window, the prefactor $s/(1-s)$ is bounded above and below by positive constants (depending only on fixed spectral parameters), so for $|s - s^*| \gg \delta_s$ the square-root term is $\Theta(|s - s^*|)$ and hence $g(s) = \Theta(|s - s^*|)$. This is exactly $\alpha = 1$. □

The linearity is structural. The coupling between the ground and first excited branches is proportional to $|\langle\psi_0|\,\phi_1|^2 = d_1/N > 0$, so the avoided crossing is simple. A higher-order tangency ($\alpha > 1$) would require this coupling to vanish, which cannot happen when $d_1 > 0$. To get different values of α, one must change the interpolation scheme. Examples include quantum phase transitions with $H(s)$ nonlinear in s or systems with symmetry-enforced higher-order crossings. This structural $\alpha = 1$ explains why both the Roland-Cerf analysis and the Guo-An framework achieve the same asymptotic runtime.

Braida et al. [10] and Guo and An [42] are independent works on the same problem class. The former provides the spectral analysis (A_1, s^*, piecewise gap bounds), while the latter provides the variational optimization (power-law schedule, measure condition).

Theorem 9.4.5 (Measure condition for the rank-one gap profile)**.** *Under the spectral condition of Chapter 5, for all sufficiently large n the piecewise-linear gap profile satisfies the measure condition with*

$$C \leq \frac{3A_2}{A_1(A_1+1)} + \frac{30(1-s_0)}{\Delta}, \tag{9.4.5}$$

where s_0 is the right-arm basepoint defined in Chapter 6.

Proof. Fix $x > 0$. For $x < g_{\min}$, the sublevel set is empty. For $x \geq g_{\min}$, bound each region of the piecewise gap profile separately.

The left arm satisfies $g(s) \geq c_L(s^* - s)$, but it contributes only when $x \geq \hat{g}$ (because its minimum at the window boundary is $\hat{g}$). Hence its contribution is at most x/c_L for $x \geq \hat{g}$ and 0 for $x < \hat{g}$. The crossing window

has width $2\delta_s = 2\hat{g}/c_L$. If $x \geq \hat{g}$, the window contributes at most $2\hat{g}/c_L \leq 2x/c_L$. If $g_{\min} \leq x < \hat{g}$, use $g_{\min} \geq (1-2\eta)\hat{g}$ and $x \geq g_{\min}$ to get $\hat{g} \leq x/(1-2\eta)$. For $\eta \leq 1/6$, this implies $\hat{g} \leq 3x/2$, so the window contribution is at most $2\hat{g}/c_L \leq 3x/c_L$. The condition $\eta \leq 1/6$ holds asymptotically because $\eta = O(\sqrt{d_0/(NA_2)}) \to 0$.

Thus left-arm plus window contribution is at most $3x/c_L$ in both regimes ($x \geq \hat{g}$ and $g_{\min} \leq x < \hat{g}$). The right arm satisfies $g(s) \geq c_R(s-s_0)/(1-s_0)$ and contributes at most $x \cdot 30(1-s_0)/\Delta$. Adding these contributions and substituting $c_L = A_1(A_1+1)/A_2$ gives the stated bound. □

Corollary 9.4.6 (Grover measure constant)**.** *For Grover ($M = 2$, $d_0 = 1$, $d_1 = N-1$, $E_0 = 0$, $E_1 = 1$), the exact measure constant is $C = 1$.*

Proof. The exact gap is $g(s)^2 = (2s-1)^2(1-1/N) + 1/N$. Solving $g(s) \leq x$ gives

$$\mu(\{g \leq x\}) = \sqrt{\frac{Nx^2 - 1}{N-1}}$$

for $x \in [1/\sqrt{N}, 1]$, with $\mu = 1$ for $x > 1$. The ratio μ/x is increasing on $[1/\sqrt{N}, 1]$ and equals 1 at $x = 1$. □

For the Grover problem, the exact gap integral is $\int_0^1 g(s)^{-2}\,ds = (N/\sqrt{N-1}) \arctan\sqrt{N-1} \to (\pi/2)\sqrt{N}$ as $N \to \infty$. This closed-form evaluation confirms the $O(\sqrt{N})$ runtime from the piecewise analysis and provides the exact constant. For the running example ($N = 4$), $\int_0^1 g(s)^{-2}\,ds = (4/\sqrt{3}) \arctan\sqrt{3} = 4\pi/(3\sqrt{3}) \approx 2.42$, consistent with the runtime $T_{\text{inf}} = O(\sqrt{4}) = O(2)$.

Both the Roland-Cerf $p = 2$ schedule and Guo-An's $p = 3/2$ schedule achieve the same asymptotic runtime $T = O(\sqrt{N/d_0}/\varepsilon)$. As declared at the start of this chapter, all spectral parameters A_1, A_2, and Δ are absorbed into the implicit constant. The RC runtime involves the integral $I = \int_0^1 g(s)^{-2}\,ds$, while Guo-An's bound involves $C^2/g_{\min}$.

Theorem 9.4.7 (Constant comparison)**.** *Write $a = 3/c_L$ and $r = 30(1-s_0)/\Delta$. Define the surrogate constants $C_{\text{up}} := a + r$ (from the measure-constant upper bound) and $I_{\text{sur}} := a + r^2 c_L$ (the matching two-arm surrogate for the RC integral). Then*

$$I_{\text{sur}} - C_{\text{up}}^2 = (c_L - 1)r^2 - 2ar + a(1-a).$$

In the right-arm-dominated regime ($r \gg a$) with $c_L > 1$, we have $C_{\text{up}}^2/I_{\text{sur}} \to 1/c_L = A_2/(A_1(A_1+1)) < 1$.

Proof. With $C_{\text{up}} = a + r$ and $I_{\text{sur}} = a + r^2 c_L$, we obtain

$$I_{\text{sur}} - C_{\text{up}}^2 = (c_L - 1)r^2 - 2ar + a(1-a).$$

For $c_L > 1$ and $r \gg a$, the leading term $(c_L - 1)r^2$ dominates, so $I_{\text{sur}} > C_{\text{up}}^2$ and $C_{\text{up}}^2/I_{\text{sur}} \to 1/c_L$. □

The framework comparison extends across gap geometries. For $1/2 < \alpha < 1$, the Roland-Cerf integral $\int g^{-2}\,ds = \Theta(g_{\min}^{1/\alpha - 2})$ grows slower than $1/g_{\min}$, making the RC analysis tighter. At $\alpha = 1/2$, the same integral is $\Theta(\log(1/g_{\min}))$; for $\alpha < 1/2$, it is $\Theta(1)$. For $\alpha = 1$, both frameworks give $\Theta(1/g_{\min})$, and the surrogate comparison of Theorem 9.4.7 identifies regimes where the JRS prefactor can be smaller than the RC prefactor. For $\alpha > 1$, the measure constant $C \to \infty$ as $g_{\min} \to 0$, so the JRS framework degrades and only the RC analysis applies. The structural $\alpha = 1$ (Proposition 9.4.4) sits at the exact boundary where both frameworks are valid and neither uniformly dominates.

For the Grover problem, $c_L \to 2$ as $N \to \infty$. Using the exact values $C_{\text{exact}} = 1$ and $I_{\text{exact}} \to (\pi/2)\sqrt{N}$ gives $C^2/I \to 2/(\pi\sqrt{N}) \to 0$, so the JRS certification is asymptotically tighter. This comparison is unusually explicit because the Grover gap has a closed form.

For structured Hamiltonians with richer spectra, exact constants are rarely analytic, and Theorem 9.4.7 becomes the practical tool. Exact numerical diagonalization of the open ferromagnetic Ising chain (Equation 5.1.4, $J = h = 1$, computed in the thesis experiment pipeline `src/experiments/11_schedule_optimality/`) gives $C^2/I = 0.7273$ at $n = 8$, $C^2/I = 0.7122$ at $n = 10$, and $C^2/I = 0.6908$ at $n = 12$, while the Grover benchmarks at matching N are 0.6042, 0.6033, and 0.6031 respectively. The JRS advantage is stable across system sizes. The inequality $C^2 < I$ persists, but the ratio decreases toward the Grover benchmark as n grows. Varying the uniform field strength at fixed $n = 10$ ($h \in \{1, 2, 3, 4\}$) gives $C^2/I = 0.7122$, 0.7098, 0.7531, 0.7793, each above the Grover value and below 1. The non-monotonicity in h reflects competing effects. Increasing the field strength concentrates the spectrum near the ground state (decreasing C) but also reshapes the gap profile (changing I), and neither effect dominates uniformly.

The two frameworks are best viewed as complementary. The spectral analysis [10] identifies A_1, s^*, and the piecewise gap structure, while the variational analysis [42] identifies the optimal power-law exponent. Together

they give a complete account of the rank-one $\alpha = 1$ case, which sits exactly at the boundary where both frameworks apply and the measure condition remains bounded.

This complementarity persists under partial spectral knowledge. The RC framework ($p = 2$) builds the schedule from crossing position s^*, so its runtime degrades on the crossing-localization scale:

$$T_{\mathrm{RC}}(\varepsilon_{A_1}) = T_{\mathrm{RC},\infty} \cdot \Theta\left(\max\left(1, \frac{\varepsilon_{A_1}}{\delta_{A_1}}\right)\right),$$

where $\delta_{A_1} = 2\sqrt{d_0 A_2/N}$ is the threshold from Theorem 9.2.2. The JRS framework ($p = 3/2$) instead uses certified bounds (C_+, g_-) on the measure constant and minimum gap, leading to multiplicative overhead

$$\frac{(1 + \delta_C/C)^2}{1 - \delta_g/g_{\min}},$$

where δ_C and δ_g are estimation errors. The sensitivity profiles are therefore different. The RC framework needs exponentially precise localization of s^*, while JRS needs only constant relative accuracy in C and $g_{\min}$. In the partial-information regime forced by NP-hardness, this can make JRS more robust in practice even though both methods share the same asymptotic scaling.

The gap geometry and optimality analysis above assumes the rank-one interpolation

$$H(s) \;=\; -(1-s)\,|\psi_0\rangle\langle\psi_0| + s\,H_z.$$

The structural $\alpha = 1$, the crossing at $s^* = A_1/(A_1 + 1)$, and the measure condition all follow from this specific path. The rank-one structure is a design choice, not a physical constraint. A different initial state, ancilla qubits, a multi-segment path, or a higher-rank projector might avoid the A_1 dependence entirely. The next section shows that none of these modifications succeed.

9.5 Anatomy of the Barrier

The barrier theorems above apply to fixed schedules on rank-one Hamiltonians. A natural objection is that the designer has more freedom: ancilla qubits, different initial states, coupled interactions, multi-segment paths, higher-rank projectors. If any of these modifications eliminated the A_1 dependence, the information gap would be an artifact of a restrictive model rather than a structural limitation. We now show that none of them succeed, proceeding from the weakest modification (adding uncoupled ancillas) to the most general path redesign (multi-segment interpolation with higher-rank projectors), then combining the four obstructions into a single no-go theorem.

Recall from Chapter 5 that for any initial state $|\psi\rangle \in \mathbb{C}^N$, the weights $w_k(\psi) = \sum_{z\in\Omega_k} |\langle z|\psi\rangle|^2$ determine $A_1^{\mathrm{eff}}(\psi) = \sum_{k\geq 1} w_k(\psi)/(E_k - E_0)$ and therefore $s^*(\psi) = A_1^{\mathrm{eff}}(\psi)/(A_1^{\mathrm{eff}}(\psi) + 1)$. For the uniform superposition $|\psi_0\rangle$, we recover $w_k = d_k/N$ and $A_1^{\mathrm{eff}} = A_1$.

Theorem 9.5.1 (Product ancilla invariance)**.** *For any product initial state $|\Psi\rangle = |\psi_0\rangle \otimes |\phi\rangle$ and uncoupled final Hamiltonian $H_f = H_z \otimes I_{2^m}$, the extended Hamiltonian $H_{\mathrm{ext}}(s) = -(1-s)\,|\Psi\rangle\langle\Psi| + s(H_z \otimes I_{2^m})$ has the same crossing position $s^* = A_1/(A_1 + 1)$ as the bare system.*

Proof. Decompose the extended Hilbert space $\mathbb{C}^N \otimes \mathbb{C}^{2^m}$ into the subspace $\mathcal{V}_\phi = \mathbb{C}^N \otimes |\phi\rangle$ and its orthogonal complement. States $|z\rangle \otimes |a\rangle$ with $\langle\phi|a = 0$ satisfy $\langle\Psi|z, a = 0$, so they are exact eigenstates of $H_{\mathrm{ext}}(s)$ with eigenvalue $sE(z)$. These $N(2^m - 1)$ states do not participate in the avoided crossing. On $\mathcal{V}_\phi$, the restriction of $H_{\mathrm{ext}}(s)$ is unitarily equivalent to the bare Hamiltonian $H(s)$ via the map $|\psi\rangle \otimes |\phi\rangle \mapsto |\psi\rangle$. □

Remark (Gap degradation from ancillas)**.** *The crossing position is invariant, but the gap of $H_{\mathrm{ext}}(s)$ is strictly smaller than the bare gap. For $d_0 = 1$, the extra eigenvalues at sE_0 (from states $|z\rangle \otimes |a\rangle$ with $z \in \Omega_0$, $a \perp |\phi\rangle$) sit between the ground eigenvalue $\lambda_0(s) < sE_0$ and the crossing branch. Uncoupled ancillas make the gap worse, not better.*

Extra qubits by themselves do not move the bottleneck. They add spectators and can even shrink the usable gap, because the ancilla's excited states crowd the spectrum near the crossing. If the hardware cannot help, perhaps the initial state can. The rank-one framework uses the uniform superposition $|\psi_0\rangle$ because it is the natural starting point for unstructured search. But any state $|\psi\rangle$ defines weights $w_k(\psi)$ and hence a crossing position $s^*(\psi)$. A state whose crossing position does not depend on the spectrum would bypass the barrier entirely.

Theorem 9.5.2 (Universality of uniform superposition)**.** *Among all states $|\psi\rangle \in \mathbb{C}^N$, the uniform superposition $|\psi_0\rangle$ is the unique state (up to per-basis-element phases) for which the weights $w_k(\psi)$ depend only on $\{E_k, d_k\}$ and not on the specific assignment of energies to computational basis states.*

Proof. An energy assignment is a function $\sigma : \{0, \ldots, N-1\} \to \{E_0, \ldots, E_{M-1}\}$ with $|\sigma^{-1}(E_k)| = d_k$. The weights under assignment σ are $w_k(\psi, \sigma) = \sum_{z:\sigma(z)=E_k} |\langle z|\psi\rangle|^2$. We require $w_k(\psi, \sigma) = w_k(\psi, \sigma')$ for all assignments σ, σ' with the same degeneracies.

Any two such assignments are related by a permutation π of $\{0, \ldots, N-1\}$. The condition becomes $\sum_{z\in\Omega_k} |\langle z|\psi\rangle|^2 = \sum_{z\in\Omega_k} |\langle \pi^{-1}(z)|\psi\rangle|^2$ for all k and all permutations π.

Necessity. Consider two-level spectra with $d_0 = 1$. For any two basis states z_a, z_b, the transposition swapping them maps the assignment σ (with $\sigma(z_a) = E_0$) to σ' (with $\sigma'(z_b) = E_0$). The condition forces $|\langle z_a|\psi\rangle|^2 = |\langle z_b|\psi\rangle|^2$. Since z_a, z_b are arbitrary, $|\langle z|\psi\rangle|^2 = 1/N$ for all z.

Sufficiency. If $|\langle z|\psi\rangle|^2 = 1/N$ for all z, then $w_k = d_k/N$ regardless of the assignment. □

Corollary 9.5.3. *Within the rank-one initial-projector framework above (same Hamiltonian form for all energy assignments with the same degeneracy structure), any instance-independent adiabatic algorithm must use the uniform superposition as initial state, fixing the crossing at $s^* = A_1/(A_1+1)$.*

The uniform superposition is the only instance-independent choice. Any other state would assign unequal weight to at least two basis elements, and a permutation of energy levels would then produce different weights and a different crossing. Changing the initial state requires giving up instance independence, which amounts to knowing the spectrum in advance.

A more aggressive route is to keep the uniform state but add a fixed ancilla coupling V. The coupling might shift energy levels in a way that cancels the instance-dependent contribution to A_1^{eff}.

Theorem 9.5.4 (Coupled ancilla limitation)**.** *Consider an extended Hamiltonian $H_{\text{ext}}(s) = -(1-s)\,|\Psi\rangle\langle\Psi| + s(H_z \otimes I + V)$ where $|\Psi\rangle = |\psi_0\rangle \otimes |\phi\rangle$ and V is instance-independent. No fixed V makes A_1^{eff} constant across all problem instances.*

Proof. Consider the two-level family parametrized by $\Delta > 0$, with $E_0 = 0$, $E_1 = \Delta$, $d_0 = 1$, and $d_1 = N-1$. For $\Delta > 2\|V\|$, Weyl's inequality implies that each eigenvalue of $H_f(\Delta) = H_z(\Delta) \otimes I + V$ lies within $\|V\|$ of an eigenvalue of $H_z(\Delta) \otimes I$. The spectrum therefore splits into two separated clusters, one near energy 0 and one near energy Δ. For each eigenvalue E_j in the excited cluster, $|E_j - \Delta| \le \|V\|$. Hence the excited contribution to A_1^{eff} is

$$\sum_{j\in\text{excited}} \frac{|\langle\Psi|\,\phi_j\rangle|^2}{E_j - E_0} = \frac{1 - d_0/N}{\Delta + O(\|V\|)} = \Theta(1/\Delta)$$

for $\Delta \gg \|V\|$. Because $\|V\|$ is fixed independently of Δ, this contribution varies with Δ, so $A_1^{\text{eff}}(\Delta)$ cannot be constant. □

Coupling shifts energy levels but cannot make the excited contribution constant across all spectra. For large excitation energy Δ, the coupling V is a fixed perturbation against a growing gap, and Weyl's inequality bounds its effect to $O(\|V\|/\Delta)$. The last escape route within the rank-one design is to break the path into multiple segments and hope that an intermediate stage can absorb the spectrum dependence before the final segment encounters it.

Theorem 9.5.5 (Multi-segment rigidity)**.** *Consider a two-segment path where segment 2 has Hamiltonian $H_2(t) = -(1-t)\,|\psi_{\text{mid}}\rangle\langle\psi_{\text{mid}}| + tH_z$, and segment 1 is generated by an instance-independent Hamiltonian that does not involve H_z. Then the intermediate state $|\psi_{\text{mid}}\rangle$ must be the uniform superposition, giving the same crossing $B_1 = A_1$.*

Proof. Segment 2 is a rank-one adiabatic Hamiltonian with initial state $|\psi_{\text{mid}}\rangle$. Its crossing position is $t^* = B_1/(B_1+1)$ where $B_1 = \sum_{k\ge1} w_k(\psi_{\text{mid}})/(E_k - E_0)$. Because segment 1 does not involve H_z, $|\psi_{\text{mid}}\rangle$ is determined entirely by an instance-independent Hamiltonian and is therefore the same for all energy assignments with the same degeneracy structure. Theorem 9.5.2 then forces $w_k = d_k/N$, so $B_1 = A_1$. □

These four modifications exhaust the natural instance-independent designs where spectral information is not injected by measurement before the final rank-one segment: the Hilbert-space dimension (ancillas), the initial state (universality), fixed ancilla coupling, and path segmentation with an H_z-free preparation stage. Each fails for a different reason: ancillas decouple and leave the crossing invariant, the uniform superposition is forced by instance independence, coupling is a finite perturbation against a variable gap, and segmentation inherits the same constraint through the intermediate state. Together they close off the space.

Theorem 9.5.6 (No-go)**.** *For any adiabatic algorithm in this design class (rank-one initial Hamiltonian, final Hamiltonian whose ground state encodes the solution, instance-independent design, and no H_z dependence before the final rank-one segment), the crossing position cannot be made independent of the problem spectrum.*

Proof. Combine Theorems 9.5.1–9.5.5. Theorem 9.5.2 forces the uniform superposition. Theorem 9.5.1 shows that uncoupled ancillas preserve s^*. Theorem 9.5.4 shows that coupled ancillas can shift s^* but cannot make it constant. Theorem 9.5.5 then rules out escape through multi-segment paths within the class. □

For the running example ($N = 4$, $d_0 = 1$), product ancilla invariance (Theorem 9.5.1) implies that appending any number of ancilla qubits in a product state leaves the crossing at $s^* = 3/7$. Universality (Theorem 9.5.2) means that any other initial state would break instance independence on this family. Coupled ancillas (Theorem 9.5.4) can perturb the crossing but cannot pin it to a constant, because the perturbation is bounded while the excitation gap varies freely.

The no-go is best understood as a structural constraint rather than an engineering failure. The crossing position $s^* = A_1/(A_1 + 1)$ is determined by the secular equation of $H(s)$, which depends algebraically on the overlap between the initial state and each energy eigenspace. Instance independence forces those overlaps to be uniform, and uniform overlaps make s^* a nontrivial function of the spectrum through the weighted harmonic mean $A_1 = \sum_{k\geq 1}(d_k/N)/(E_k - E_0)$. Within this design class, no instance-independent transformation can break this dependence, because the secular equation encodes spectral data into the crossing position, and no design that treats all energy assignments equally can undo the encoding.

We have now exhausted this rank-one design class under instance independence. The natural objection is that rank one may simply be too narrow. We next move to rank-k projectors and show that the same dependence persists.

For rank-k projectors $P = UU^\dagger$, the secular equation becomes a $k \times k$ determinant condition

$$\det(I_k - (1 - s)G(\lambda, s)) = 0, \qquad G(\lambda, s) = U^\dagger(sH_z - \lambda I)^{-1}U.$$

On the two-level family ($E_0 = 0$, $E_1 = \Delta$), this reduces to

$$\det(I_k - (x/\Delta)B) = 0, \qquad B = U_{\text{exc}}^\dagger U_{\text{exc}}, \quad x = (1 - s)/s.$$

Each positive eigenvalue μ of B gives a crossing branch $s(\Delta) = 1/(1+\Delta/\mu)$, and this branch is non-constant in Δ.

Proposition 9.5.7 (Rank-k two-level obstruction)**.** *Fixed rank-k projectors cannot make crossing positions spectrum-independent on fixed-degeneracy two-level families unless the projector has zero support on excited states.*

Proof. On the two-level family ($E_0 = 0$, $E_1 = \Delta$), each positive eigenvalue μ of $B = U_{\text{exc}}^\dagger U_{\text{exc}}$ gives a crossing branch at $s(\Delta) = 1/(1 + \Delta/\mu)$, which is non-constant in Δ whenever $\mu > 0$. If the projector has zero support on excited states, then $B = 0$ and there are no crossing branches, but also no gap closing. □

The two-level obstruction already blocks constant crossings in the simplest nontrivial family. For general multilevel spectra, a trace argument gives an even sharper obstruction.

Proposition 9.5.8 (Trace no-go)**.** *For a rank-k projector $P = UU^\dagger$ and the multilevel family with gaps $\Delta_1, \ldots, \Delta_{M-1}$, if $B_j = U_j^\dagger U_j \neq 0$ and Δ_j varies, then at least one crossing position must change with Δ_j.*

Proof. Define the reduced matrix $A(\Delta) = \sum_{\ell=1}^{M-1} B_\ell/\Delta_\ell$ where $B_\ell = U_\ell^\dagger U_\ell \succeq 0$ collects the excited-level contributions. The trace $\operatorname{tr}(A(\Delta)) = \sum_\ell \operatorname{tr}(B_\ell)/\Delta_\ell$ is non-constant in Δ_j because $\operatorname{tr}(B_j) > 0$. By Weyl's eigenvalue monotonicity theorem, each eigenvalue of $A(\Delta)$ is a continuous function of Δ_j, and their sum equals $\operatorname{tr}(A)$. Since the trace changes, at least one positive eigenvalue, and hence at least one crossing position $s_r = G_r/(1 + G_r)$, must change with Δ_j. □

Remark. *When the excited blocks commute ($[B_\ell, B_m] = 0$ for all ℓ, m), the reduced crossing equation can be simultaneously diagonalized. This gives explicit per-branch formulas. For each active branch r with $G_r(\Delta) = \sum_\ell \mu_{\ell r}/\Delta_\ell > 0$, the crossing position is $s_r = G_r/(1 + G_r)$. Varying any gap Δ_j yields*

$$\frac{\partial s_r}{\partial \Delta_j} = -\frac{\mu_{jr}}{\Delta_j^2(1 + G_r)^2} \leq 0,$$

with strict inequality whenever $\mu_{jr} > 0$. So the commuting case gives explicit quantitative non-constancy for each branch, complementing the trace argument's aggregate statement. Even this most tractable version of the generalized secular equation cannot produce spectrum-independent crossings.

At this point the pattern is hard to miss. The barrier is structural inside the rank-one framework and survives the move to higher-rank projectors. It may still be possible to escape with genuinely different control models, such as time-dependent couplings or non-rank-one intermediate Hamiltonians, but those lie outside the present theorem. This distinction matters because once we drop the monotone-schedule restriction, constant controls already recover the Grover timescale on the restricted two-level family.

Proposition 9.5.9 (Constant-control optimality on two-level family [83])**.** *For $H_z = I - P_0$ where P_0 projects onto the d_0-dimensional ground space, the continuous-time rank-one Hamiltonian $H = -|\psi_0\rangle\langle\psi_0| + H_z$ with constant controls achieves $p_0(t^*) = 1$ at $t^* = (\pi/2)\sqrt{N/d_0}$, with controls independent of A_1.*

Proof. Let $\mu = d_0/N$, $|G\rangle = d_0^{-1/2}\sum_{x\in S_0}|x\rangle$, and $|B\rangle = (N-d_0)^{-1/2}\sum_{x\notin S_0}|x\rangle$. The initial state is $|\psi_0\rangle = \sqrt{\mu}\,|G\rangle + \sqrt{1-\mu}\,|B\rangle$. Dropping the global identity term, the effective Hamiltonian in the $(|G\rangle, |B\rangle)$ basis is

$$\widetilde{H} = -\begin{pmatrix} \mu & \sqrt{\mu(1-\mu)} \\ \sqrt{\mu(1-\mu)} & -\mu \end{pmatrix}, \tag{9.5.1}$$

which satisfies $\widetilde{H}^2 = \mu\, I_2$. The matrix exponential is $e^{-it\widetilde{H}} = \cos(\sqrt{\mu}\,t)\, I_2 - i\sin(\sqrt{\mu}\,t)\,\widetilde{H}/\sqrt{\mu}$. Applying to $|\psi_0\rangle$ and computing the ground-state probability:

$$p_0(t) = |\langle G|\, e^{-it\widetilde{H}}\,|\psi_0\rangle|^2 = \mu + (1-\mu)\sin^2(\sqrt{\mu}\,t). \tag{9.5.2}$$

At $t^* = (\pi/2)/\sqrt{\mu} = (\pi/2)\sqrt{N/d_0}$, $\sin^2(\sqrt{\mu}\,t^*) = 1$, so $p_0(t^*) = 1$. □

On the two-level family, the Hamiltonian self-calibrates. The dynamics reduce to a Rabi oscillation at frequency $\sqrt{\mu} = \sqrt{d_0/N}$, independent of A_1. The time-independent Hamiltonian $H_r = -|\psi_0\rangle\langle\psi_0| + r\cdot H_z$ with $r = 1$ is optimal without explicit knowledge of A_1 [83]. The monotone-schedule barrier is a barrier for schedules, not for continuous-time dynamics. Dropping the monotonicity constraint allows a qualitatively different mechanism (resonance instead of adiabatic passage) that does not require the crossing position. For general spectra, the resonance shifts to $r^* = A_1$ [83], and the calibration problem changes from classical computation of A_1 to quantum detection of a resonance.

Remark (Non-adiabatic barrier extension)**.** *The A_1 barrier extends beyond the adiabatic framework. For the time-independent Hamiltonian $H_r = -|\psi_0\rangle\langle\psi_0| + r\cdot H_z$, the resonance condition $r = A_1$ depends on the problem spectrum. Since A_1 varies across instances (Theorem 9.5.4), no instance-independent choice of r achieves resonance universally. The same structural ingredients used above apply to the oscillation parameter r exactly as they apply to the crossing position s^*. Uniform instance-independent driver weights and secular-equation dependence on spectral data govern both settings. Thus the barrier governs both adiabatic schedules (which need $s^* = A_1/(A_1+1)$) and non-adiabatic oscillation (which needs $r \approx A_1$).*

A natural approach is Loschmidt-echo measurement. Evolve under H_r and measure return probability $|\langle\psi_0|\, e^{-iH_r t}\psi_0|^2$, which oscillates with large amplitude near resonance and stays close to 1 away from resonance. On two-level families this works cleanly. Binary search over r with $O(n)$ probe measurements, each costing $O(1/g_{\min})$, locates r^* with polynomial overhead (details in [83]). For general multilevel spectra, additional excited-state frequencies can mask the resonance signal. Whether one can efficiently deconvolve this multilevel echo, or replace it with a better observable, remains open.

The constant-control counterexample applies only to the two-level family $H_z = I - P_0$. Under normalized controls, the barrier reappears.

Proposition 9.5.10 (Normalized-control lower bound)**.** *Under normalized controls $|g(t)| \le 1$ and the scaled family $H_z^{(\delta)} = \delta(I - P_0)$ with minimum excitation $0 < \delta \le 1$, any instance-independent algorithm achieving success probability $\ge 2/3$ requires $T = \Omega(\sqrt{N/d_0}/\delta)$.*

Proof. The oracle-dependent term $g(t)H_z^{(\delta)} = \delta g(t)(I - P_0)$ has instantaneous oracle strength $\delta|g(t)|$. The total oracle action is $\mathcal{A} = \int_0^T \delta|g(t)|\,dt \le \delta T$. The continuous-time query lower bound for unstructured search with d_0 marked items among N gives $\mathcal{A} = \Omega(\sqrt{N/d_0})$ [84], so $T = \Omega(\sqrt{N/d_0}/\delta)$. □

For $\delta = N^{-1/2}$, this yields $T = \Omega(N/\sqrt{d_0})$, the same exponential penalty as the fixed-schedule adiabatic model. The barrier reappears whenever controls are normalized. The scope of the obstruction is now precise. It comes from bounded, instance-independent controls on rank-one Hamiltonians. It does not come from continuous-time quantum computation itself, as the constant-control counterexample on two-level families demonstrates. The gap between these statements, general spectra with unbounded controls, remains open.

9.6 Computational Nature of A_1

The barrier survives every design modification within the rank-one framework and extends to higher-rank projectors. It cannot be engineered away. The next question is what kind of computational object A_1 actually is. The NP-hardness of Chapter 8 comes from a reduction that maps satisfiability to spectral estimation. But $A_1 = (1/N)\sum_{k\geq 1} d_k/(E_k - E_0)$ is a weighted sum over the entire excited spectrum, not a decision problem about the ground state. Its hardness turns out to be counting hardness, inherited from the partition-function structure of the energy landscape. This distinction matters because it separates the tractability of A_1 from the tractability of the underlying optimization problem.

The quantity A_1 aggregates the full spectrum, not just the gap edge. A minimal example makes this concrete. Consider three energy levels with $E_0 = 0$ ($d_0 = 1$), $E_1 = 1/n$ ($d_1 = 1$), and $E_2 = 1$ ($d_2 = N - 2$). Then $\Delta = 1/n \to 0$ but $A_1 = (n + N - 2)/N \to 1$, so $1/\Delta \to \infty$ while $A_1 = \Theta(1)$. The tail of $N - 2$ states at energy 1 contributes $(N - 2)/N \approx 1$ to A_1, while the single state at the gap edge contributes only $n/N \approx 0$. So the crossing position $s^* = A_1/(A_1 + 1) \approx 1/2$ is determined by the bulk of the spectrum, not by the minimum gap. In this sense A_1 is a whole-spectrum quantity that Δ alone cannot predict.

The distinction between NP-hardness at precision $1/\mathrm{poly}(n)$ (Theorem 8.1.2) and #P-hardness exactly (Theorem 8.2.4) matters because A_1 is fundamentally a counting quantity.

Proposition 9.6.1 (A_1 hardness is counting hardness)**.** *For Boolean CSPs where counting satisfying assignments is #P-hard (including k-SAT for $k \geq 2$), computing A_1 of the clause-violation Hamiltonian is #P-hard even restricted to satisfiable instances.*

Proof. Encode the CSP as $H_z = \sum_{j=1}^{m} C_j$ where each $C_j(x) = 1$ if assignment x violates clause j. The interpolation argument (Theorem 8.2.4) recovers all degeneracies d_k from polynomially many evaluations of A_1 with shifted parameters, via Lagrange interpolation on the rational function $f(x) = \sum_k d_k/(\Delta_k + x/2)$. For satisfiable CSPs, d_0 counts satisfying assignments, and counting is #P-hard by hypothesis. □

The connection between A_1 and the partition function makes this precise and reveals why the hardness is counting rather than optimization. Shifting energies so that $E_0 = 0$ and defining the Laplace partition function $Z(\beta) = \sum_x e^{-\beta E(x)}$, the spectral parameter admits the integral representation

$$A_1 = \frac{1}{N}\int_0^\infty (Z(\beta) - d_0)\, d\beta. \tag{9.6.1}$$

For integer spectra with $E(x) \in \{0, 1, \ldots, m\}$, the ordinary generating function $Z(t) = \sum_x t^{E(x)}$ gives

$$A_1 = \frac{1}{N}\int_0^1 \frac{Z(t) - d_0}{t}\, dt.$$

At first glance both formulas seem to require d_0, which is itself counting-hard for many CSPs. For additive approximation, however, one can replace d_0 by a single low-temperature sample $Z(\tau)$ with small $\tau > 0$. Define the τ-truncated proxy

$$A_1^{(\tau)} = \frac{1}{N}\int_\tau^1 \frac{Z(t) - Z(\tau)}{t}\, dt. \tag{9.6.2}$$

The additive error satisfies $0 \leq A_1 - A_1^{(\tau)} \leq \tau(1 + \ln(1/\tau))$. To see this, write $Z(t) - d_0 = \sum_{q\geq 1} d_q t^q$ and compute

$$(A_1 - A_1^{(\tau)})N = \int_0^\tau \sum_{q\geq 1} d_q t^{q-1}\, dt + \Big(\sum_{q\geq 1} d_q \tau^q\Big)\ln\frac{1}{\tau} = \sum_{q\geq 1} d_q \tau^q\Big(\frac{1}{q} + \ln\frac{1}{\tau}\Big).$$

All terms are nonnegative, giving the lower bound. For the upper bound, use $\tau^q \leq \tau$ and $1/q \leq 1$ to get $(A_1 - A_1^{(\tau)})N \leq (N - d_0)\tau(1 + \ln(1/\tau)) \leq N\tau(1 + \ln(1/\tau))$. The bound is tight: for the two-level Grover spectrum, equality holds up to the factor $(N - d_0)/N$. Choosing $\tau = O(\eta/\ln(1/\eta))$ therefore gives an η-approximation to A_1 without direct access to d_0.

When E_0 is known, this coarse form is already useful. Boltzmann sampling at inverse temperature β gives unbiased estimators of observables under the Boltzmann law; combining such samples across temperatures (for example via partition-function ratio estimation / thermodynamic integration) yields estimates of $Z(\beta)/Z(0) = Z(\beta)/N$. Integrating those estimates through Eq. (9.6.1) gives an additive approximation to A_1 without explicitly counting d_0. In this way, computing A_1 becomes a partition-function task, and tractability of A_1 tracks tractability of counting.

The truncated proxy $A_1^{(\tau)}$ works for integer spectra. For general nonnegative energies, the Laplace identity (9.6.1) requires an analogous truncation. Define the *anchored proxy* at inverse temperature $B > 0$:

$$A_1^{[B]} := \frac{1}{N} \int_0^B \big(Z(\beta) - Z(B)\big)\, d\beta. \tag{9.6.3}$$

Anchoring at $Z(B)$ instead of d_0 removes the ground-degeneracy dependence, and truncation at B avoids the infinite tail.

Proposition 9.6.2 (Laplace-side proxy error)**.** *For all $B > 0$,*

$$0 \le A_1 - A_1^{[B]} \le e^{-B\Delta_{\min}} \left(B + \frac{1}{\Delta_{\min}} \right).$$

Proof. Write $Z(\beta) - d_0 = \sum_{x:E(x)>0} e^{-\beta E(x)}$ and compute

$$(A_1 - A_1^{[B]})N = \sum_{x:E(x)>0} e^{-BE(x)} \left(\frac{1}{E(x)} + B \right),$$

which is nonnegative. Since $E(x) \ge \Delta_{\min}$, we have $e^{-BE(x)} \le e^{-B\Delta_{\min}}$ and $1/E(x) \le 1/\Delta_{\min}$, so the sum is at most $N\, e^{-B\Delta_{\min}}(B + 1/\Delta_{\min})$. □

The tail decays as $Be^{-B\Delta_{\min}}$, so additive error η requires $B = \Theta((1/\Delta_{\min}) \log(1/\eta))$. At schedule-relevant precision $\eta = 2^{-n/2}$, this forces $B = \Theta(n/\Delta_{\min})$. Low-temperature partition functions are unavoidable.

When E_0 and a lower bound $\Delta_{\min}$ are both known, even the simplest estimator suffices at coarse precision.

Remark (BPP coarse approximation)**.** *Define $G(x) = 0$ if $E(x) = E_0$ and $G(x) = 1/(E(x) - E_0)$ otherwise. Then $A_1 = \mathbb{E}_{x\sim\mathrm{Unif}}[G(x)]$ with $0 \le G(x) \le 1/\Delta_{\min}$. By Hoeffding's inequality [85], the empirical mean of T i.i.d. uniform samples satisfies $\Pr\big[|\widehat{A}_1 - A_1| > \eta\big] \le \delta$ for $T \ge (1/(2\eta^2\Delta_{\min}^2)) \ln(2/\delta)$. In particular, additive inverse-polynomial approximation of A_1 is in* BPP *under the promise that E_0 and $\Delta_{\min}$ are known and inverse-polynomially bounded.*

This stands in sharp contrast to the NP-hardness of A_1 estimation without the E_0 promise (Theorem 8.1.2). The promise boundary is the ground energy itself. Once the counting problem is partially solved by revealing E_0, the remaining estimation is a standard mean-estimation task.

The proxies above reduce A_1 to a weighted integral of partition-function values. An approximate partition-function oracle therefore yields an approximate A_1.

Proposition 9.6.3 (Partition-function oracle reduction)**.** *Assume integer energies in $\{0, 1, \dots, m\}$ with $E_0 = 0$. Fix $\varepsilon \in (0, 1)$ and suppose an oracle returns $\widehat{Z}(t)$ with $|\widehat{Z}(t) - Z(t)| \le \alpha N$ for any $t \in [\varepsilon, 1]$. The midpoint-rule estimator with K quadrature points satisfies*

$$\big|\widehat{A}_1^{(\varepsilon)} - A_1^{(\varepsilon)}\big| \le 2\alpha \ln \frac{1}{\varepsilon} + \frac{m \ln^2(1/\varepsilon)}{2K}.$$

Choosing $\alpha \le \eta/(8 \ln(1/\varepsilon))$ and $K \ge 4m \ln^2(1/\varepsilon)/\eta$ ensures the right-hand side is at most $\eta/2$, so combined with Eq. (9.6.2) the total error is at most η.

Proof. Change variables $u = \ln t$, so $A_1^{(\varepsilon)} = (1/N) \int_{\ln\varepsilon}^0 (Z(e^u) - Z(\varepsilon))\, du$. The oracle error at each point is at most $2\alpha N$ (triangle inequality on the difference $\widehat{Z}(t) - \widehat{Z}(\varepsilon)$), contributing $2\alpha \ln(1/\varepsilon)$ after integration and normalization. For the quadrature error, define $F(u) = Z(e^u) - Z(\varepsilon)$. Since $Z'(t) = \sum_{q\ge1} q\, d_q\, t^{q-1} \le mN$ for $t \in [0, 1]$, we have $|F'(u)| = |e^u Z'(e^u)| \le mN$. The midpoint rule on K intervals of width $h = \ln(1/\varepsilon)/K$ incurs total error at most $(mN/2) \cdot h \cdot \ln(1/\varepsilon)$. Dividing by N gives the quadrature term. □

Whenever a model family admits a polynomial-time partition-function approximation scheme, the oracle reduction converts it into a polynomial-time A_1 estimator at the same precision. The ferromagnetic Ising model provides a concrete instantiation.

Proposition 9.6.4 (Ferromagnetic Ising tractability at coarse precision)**.** *Consider a ferromagnetic Ising model with nonnegative couplings J_{ij} and fields h_i, energy range $R \le 1$, and minimum excitation $\Delta_{\min} \ge 1/W$ where $W = \sum J_{ij} + \sum h_i$. If a multiplicative FPRAS for $Z(\beta)$ is available on $\beta \in [0, B]$ [86], then A_1 admits an additive-η approximation in time* $\mathrm{poly}(n, W, 1/\eta, \log(1/\delta))$ *for any inverse-polynomial η.*

Proof. Apply Proposition 9.6.2 with $B = O(W \log(W/\eta))$ to make the tail at most $\eta/3$. The midpoint-rule quadrature with $K = \Theta(RB^2/\eta)$ points introduces error at most $\eta/3$. At each point, the FPRAS provides multiplicative accuracy $\mu = O(\eta/B)$, contributing at most $2\mu B \le \eta/3$. The FPRAS runtime per query is $\mathrm{poly}(n, 1/\mu, \log(1/\delta_q))$, and union-bounding over $K+1$ queries gives overall success probability $1-\delta$. □

The tractability does not survive at schedule-relevant precision. At $\eta = \Theta(2^{-n/2})$, the required multiplicative accuracy $\mu = O(2^{-n/2}/B)$ forces FPRAS runtime $\mathrm{poly}(1/\mu) = 2^{\Omega(n)}$, restoring the exponential cost. This is a precision barrier, not a model barrier. The algorithmic machinery works at every precision, but the cost crosses the polynomial-to-exponential boundary exactly at the schedule-relevant scale.

The partition-function chain above handles the generic case. For structured families, stronger results are possible. The most direct positive example is bounded treewidth, where variable elimination computes A_1 exactly without any precision limitation.

Proposition 9.6.5 (Bounded-treewidth tractability)**.** *Consider local integer-valued energy functions $E(x) = \sum_j E_j(x_{S_j})$ with bounded locality $|S_j| \le k$ and total range $E(x) - E_0 \in \{0, 1, \ldots, m\}$, given a tree decomposition of the primal graph of width w, the quantity A_1 is computable exactly in $\mathrm{poly}(n, m) \cdot 2^{O(w)}$ time.*

Proof. Write the partition-function polynomial as $Z(t) = \sum_x t^{E(x)} = \sum_{q=0}^{m} d_q t^q$, and also in factor-graph form as $Z(t) = \sum_x \prod_j t^{E_j(x_{S_j})}$. Variable elimination on the tree decomposition then computes $Z(t)$ exactly. At each elimination step, factor tables have at most 2^{w+1} entries, each a polynomial of degree at most m. Multiplying factors convolves polynomials at cost $O(m^2)$ per entry, and summing out a variable adds two polynomials at cost $O(m)$. After n elimination steps, we recover $Z(t) = \sum_q d_q t^q$, and then $A_1 = (1/N) \sum_{q > E_0} d_q/(q - E_0)$. □

The treewidth condition is sufficient, not necessary. A simpler criterion applies when the spectrum itself is simple. If H_z has at most $\mathrm{poly}(n)$ distinct energy levels with known energies and degeneracies, then $A_1 = (1/N) \sum_{k \ge 1} d_k/(E_k - E_0)$ is directly computable in $\mathrm{poly}(n)$ time from its defining sum. This criterion is complementary to bounded treewidth and applies whenever the spectrum is structurally simple, regardless of the interaction graph. For example, Hamming-distance costs $E(x) = |x \oplus z_0|$ have $M = n+1$ levels, degeneracies $d_k = \binom{n}{k}$, and energies $E_k = k$. Then $A_1 = (1/N) \sum_{k=1}^{n} \binom{n}{k}/k$ depends only on n and is trivial to compute.

The bridge between A_1 and Z is one-directional. Tractable Z implies tractable A_1, because the integral representations above reduce A_1 to a weighted integral of partition-function values. But exact A_1 does not determine low-temperature $Z(\beta)$. The single number A_1 compresses the entire degeneracy sequence $\{d_k\}$ into one weighted sum, losing the individual terms.

Proposition 9.6.6 (Reverse bridge obstruction)**.** *There exist two diagonal Hamiltonians H_z, H'_z on $N = 2^n$ states with the same ground degeneracy ratio d_0/N, same minimum excitation $\Delta_{\min}$, and $A_1(H_z) = A_1(H'_z)$ exactly, yet $|Z_{H_z}(\beta) - Z_{H'_z}(\beta)|/N \ge 1/100$ at $\beta = O(1/\Delta_{\min})$.*

Proof. Fix an integer $B \ge 3$. Define two spectra with the same $d_0/N = 1/2$ and $\Delta_{\min} = 1/B$. The first has $N/8$ states at energy $1/B$ and $3N/8$ states at energy B. The second has $N/16$ states at energy $1/B$ and $7N/16$ states at energy $c_B = 7B/(B^2+6)$. Direct computation gives the same value $A_1 = (B^2+3)/(8B)$ for both. At $\beta = B$, however,

$$\frac{Z_1(B)}{N} = \frac{1}{2} + \frac{e^{-1}}{8} + \frac{3e^{-B^2}}{8}, \qquad \frac{Z_2(B)}{N} = \frac{1}{2} + \frac{e^{-1}}{16} + \frac{7}{16} e^{-7B^2/(B^2+6)}.$$

Since $7B^2/(B^2+6) \ge 4.2$ for $B \ge 3$, the difference is at least $e^{-1}/16 - (7/16)e^{-4.2} > 1/100$. □

Three natural conjectures about easy instances of A_1 computation are all false.

One might expect that unique solutions simplify the spectral structure enough to make A_1 tractable, since a single ground state leaves less room for combinatorial complexity in the excited spectrum.

Proposition 9.6.7 (Unique solution does not imply easy A_1)**.** *There exist instances with $d_0 = 1$ for which computing A_1 is #P-hard.*

Proof. The proof of Proposition 9.6.1 applies directly to satisfiable instances with $d_0 = 1$. The interpolation reduction recovers $d_1, \ldots, d_{M-1}$ from A_1 evaluations, and counting assignments at each violation level remains #P-hard. Concretely, for a satisfiable 3-SAT instance with m clauses and a unique satisfying assignment, the clause-violation Hamiltonian $H_z = \sum_j C_j$ has $d_0 = 1$ and

$$A_1 = \sum_{k=1}^{m} \frac{d_k}{kN},$$

where d_k counts assignments that violate exactly k clauses. Recovering these counts from shifted A_1 evaluations is therefore #P-hard. □

If all excited degeneracies are small, the spectrum is spread thin. A natural guess is that A_1 simplifies because each term $d_k/(E_k - E_0)$ contributes little.

Proposition 9.6.8 (Bounded degeneracy is vacuous)**.** *If $d_k \leq \mathrm{poly}(n)$ for all excited levels $k \geq 1$, and $M \leq \mathrm{poly}(n)$, then $d_0 \geq N - \mathrm{poly}(n)^2$, and the optimization problem is trivially solvable by random sampling.*

Proof. The total state count satisfies $\sum_{k=0}^{M-1} d_k = N = 2^n$. If $d_k \leq \mathrm{poly}(n)$ for all $k \geq 1$ and $M \leq \mathrm{poly}(n)$, then $\sum_{k\geq 1} d_k \leq (M-1)\cdot \mathrm{poly}(n) \leq \mathrm{poly}(n)^2$, so $d_0 \geq N - \mathrm{poly}(n)^2$. For n large enough, $d_0/N \geq 1 - o(1)$, and a random sample finds a ground state with probability $1 - o(1)$. □

Hard optimization problems have complex energy landscapes, so one might expect A_1 to be hard precisely when optimization is hard.

Proposition 9.6.9 (Hard optimization does not imply hard A_1)**.** *The tractability of A_1 is independent of optimization hardness. 2-SAT is in P but #2-SAT is #P-complete [8], giving easy optimization with hard A_1. In the reverse direction, Grover search with a promised ground degeneracy d_0 gives hard optimization but trivial $A_1 = (N - d_0)/(N\Delta)$, computable in $O(1)$ from the promise.*

Proof. For the first direction, use the 2-SAT clause-violation Hamiltonian $H_z = \sum_j C_j$. Optimization (finding whether the minimum is 0 and producing an optimal assignment) is polynomial-time because 2-SAT is in P, while computing A_1 remains #P-hard by Proposition 9.6.1 together with #2-SAT completeness [8]. Thus easy optimization can coexist with hard A_1.

For the reverse direction, consider the two-level Grover family $H_z = \Delta(I - P_0)$ with promised $d_0 = \mathrm{rank}(P_0)$. In this family,

$$A_1 = \frac{1}{N}\frac{N - d_0}{\Delta} = \frac{N - d_0}{N\Delta},$$

so A_1 is computable in constant time from (N, d_0, Δ). Yet the associated optimization/search task is unstructured search with d_0 marked items, which is hard in the black-box model (query complexity $\Theta(\sqrt{N/d_0})$ quantum). Hence hard optimization can coexist with easy A_1. □

The tractability boundary for A_1 is therefore orthogonal to the standard complexity-theoretic divisions. Unique solutions do not help. Bounded degeneracies trivialize the problem for the wrong reason (the optimization itself becomes easy). Easy optimization can coexist with hard A_1 (2-SAT), and hard optimization can coexist with easy A_1 (Grover with a promise). The parameter that controls A_1 tractability is the partition-function structure of the energy landscape, specifically treewidth of the interaction graph, availability of polynomial-time sampling algorithms, and the algebraic properties of the degeneracy sequence. This is a counting-theoretic boundary, not an optimization-theoretic one.

9.7 Complexity Landscape

We now have the full cost structure of ignorance within the adiabatic framework. Uninformed schedules pay exponentially, partial knowledge helps linearly, adaptive measurement restores optimality, and the barrier is structural. The tight complexity bounds at the algorithmically relevant precision $\varepsilon = 2^{-n/2}$ pin down the information cost of fixed-schedule optimization in both the query model and the computational model.

Theorem 9.7.1 (Tight quantum query complexity at schedule precision)**.** *At the schedule-relevant precision $\varepsilon = \Theta(2^{-n/2})$, the quantum query complexity of A_1 estimation is $\Theta(2^{n/2}) = \Theta(1/\varepsilon)$. The lower bound is witnessed by two-level instances with $\Delta_1 = 1$.*

Proof. For $\varepsilon = \Theta(2^{-n/2})$ and $\Delta_1 = 1$, Theorem 8.3.3 gives $O(\sqrt{N} + 1/\varepsilon) = O(2^{n/2})$.

For the lower bound, restrict to $M = 2$ instances with $\Delta_1 = 1$. Then estimating $A_1 = (N - d_0)/N$ to precision ε is exactly additive approximate counting for d_0/N. By the standard quantum query lower bound for approximate counting on this two-level family [34, 35], this requires $\Omega(1/\varepsilon)$ queries (e.g., at the worst-case operating point $d_0 = \Theta(N)$ with density bounded away from $0, 1$). Hence at $\varepsilon = \Theta(2^{-n/2})$ we obtain $\Omega(2^{n/2})$.

Combining upper and lower bounds gives $\Theta(2^{n/2}) = \Theta(1/\varepsilon)$. □

The lower bound is inherited directly from approximate counting on the two-level subclass. Metrology-style Fisher-information arguments give compatible intuition for the same scaling, but are not needed for the query-complexity proof.

The tight bound $\Theta(2^{n/2})$ for quantum A_1 estimation at schedule precision connects directly to the adaptive protocol of section 9.3. The adaptive strategy achieves $T_{\text{adapt}} = O(T_{\text{inf}}) = O(2^{n/2})$, matching the estimation complexity. Both tasks require resolving $\Omega(2^{n/2})$ alternatives from quantum measurements that each reveal $O(1)$ bits. The adaptive protocol and the A_1 estimation algorithm operate at the same scale because they face the same information-theoretic bottleneck: the Heisenberg limit for sequential quantum sensing.

In the high-precision regime relevant to schedule placement, the quadratic quantum advantage persists.

Proposition 9.7.2 (Precision phase diagram)**.** *For two-level instances with $\Delta_1 = 1$ and precision $\varepsilon \leq c/\sqrt{N}$ (constant c), the query complexity of A_1 estimation is $\Theta(1/\varepsilon)$ quantum and $\Theta(1/\varepsilon^2)$ classical. Equivalently, the classical-to-quantum overhead factor is $\Theta(1/\varepsilon)$ (quadratic quantum advantage).*

Proof. In this regime, $1/\varepsilon \geq \sqrt{N}/c$, so the upper bound of Theorem 8.3.3 becomes $O(\sqrt{N}+1/\varepsilon) = O(1/\varepsilon)$. The matching quantum lower bound is the standard two-level approximate-counting lower bound $\Omega(1/\varepsilon)$ [34, 35]. The classical lower bound $\Omega(1/\varepsilon^2)$ follows from Theorem 8.3.4, and Monte Carlo sampling gives the matching upper bound $O(1/\varepsilon^2)$. □

The previous proposition is still a query statement. The next theorem asks what happens when we account for total computation time under a standard complexity assumption.

Theorem 9.7.3 (ETH computational complexity)**.** *Under the Exponential Time Hypothesis (ETH), any classical algorithm computing A_1 at precision $2^{-n/2}$ requires $2^{\Omega(n)}$ time.*

Proof sketch. The NP-hardness reduction (Theorem 8.1.2) maps 3-SAT on n_{var} variables to A_1 estimation of a 3-local Hamiltonian on $n = O(n_{\text{var}})$ qubits at precision $1/\text{poly}(n)$. By the Impagliazzo-Paturi-Zane sparsification lemma [87], 3-SAT on n_{var} variables can be reduced to instances with $O(n_{\text{var}})$ clauses, giving $n = O(n_{\text{var}})$ qubits. Any algorithm computing A_1 at precision $2^{-n/2}$ can, in particular, compute A_1 at the coarser precision $1/\text{poly}(n)$ (since $2^{-n/2} < 1/\text{poly}(n)$ for large n), and thus solves 3-SAT by the reduction. Under ETH, 3-SAT on $n_{\text{var}} = \Omega(n)$ variables requires $2^{\Omega(n_{\text{var}})} = 2^{\Omega(n)}$ time. The linear clause-to-qubit correspondence guaranteed by sparsification is essential: without it, the exponential lower bound on variable count would not transfer to qubit count. □

Under ETH, the quadratic quantum advantage extends from the query model to the computational model.

Corollary 9.7.4 (Quantum pre-computation cost)**.** *Estimating A_1 to the schedule-relevant precision $\delta_{A_1} = \Theta(2^{-n/2})$ via quantum amplitude estimation costs $\Theta(2^{n/2} \cdot \text{poly}(n))$ time, matching the adaptive protocol's runtime. In the same oracle-query model, classical estimation at this precision requires $\Theta(2^n)$ queries by Proposition 9.7.2; under unit-cost oracle access this implies $\Omega(2^n)$ pre-computation time (consistent with Theorem 9.7.3's $2^{\Omega(n)}$ lower bound).*

The information cost of fixed-schedule adiabatic optimization is exactly the Grover scale. Recovering the missing $n/2$ bits of A_1 costs $\Theta(2^{n/2})$ quantum time, the same order as Grover search and informed adiabatic evolution. A quantum pre-computation step followed by informed adiabatic evolution costs $\Theta(2^{n/2})$ in total. In the query model, a classical pre-computation step requires $\Theta(2^n)$ oracle queries, quadratically worse. The circuit model avoids the pre-computation entirely because amplitude amplification solves the search task without traversing the adiabatic path. From a parameterized-complexity viewpoint, A_1 estimation at precision $2^{-n/2}$ sits in FBQTIME$(2^{n/2} \cdot \text{poly}(n))$: not polynomial-time, but at the Grover scale.

These bounds assume that A_1 is estimated directly. One might hope that polynomial extrapolation from coarse-precision evaluations could bypass the exponential cost. The generic extrapolation barrier (Theorem 8.3.2) rules this out. The mechanism is the Lebesgue constant $\Lambda_d(x^*) = \sum_{j=0}^{d} |\ell_j(x^*)|$, which measures how much evaluation noise is amplified when extrapolating from $d+1$ nodes in $[a, b]$ to a point x^* outside the interval. When x^* lies at least $b-a$ away from $[a, b]$, all Lagrange basis polynomials $\ell_j(x^*)$ have the same sign, so $\Lambda_d(x^*) \geq 2^{d-1}$, meaning each additional node doubles the noise amplification rather than improving accuracy. For A_1 estimation, coarse evaluations at $d = \text{poly}(n)$ nodes achieve polynomial precision, but the exponential Lebesgue constant means extrapolating to schedule-relevant precision $2^{-n/2}$ requires each node evaluation to have precision $2^{-\Omega(n)}$, no better than direct estimation.

Proposition 9.7.5 (Two-level worst-case reduction)**.** *The two-level family ($M = 2$) is a worst-case subclass for A_1 estimation at schedule-relevant precision. Any worst-case lower bound for approximate counting on this subclass applies to general A_1 estimation.*

Proof. Worst-case complexity over all instances is at least the complexity on any subclass. Restricting to $M = 2$ gives

$$A_1 = \frac{N - d_0}{N\Delta_1},$$

so for fixed $\Delta_1 = 1$, estimating A_1 to additive precision ε is exactly approximate counting for d_0/N at precision ε. Therefore, any lower bound for approximate counting on this subclass is automatically a lower bound for general A_1 estimation. □

The worst-case hardness of A_1 estimation does not hide in complex spectra. Simple two-level instances, where A_1 reduces to counting, already saturate the query lower bound. Algorithms exploiting the sum-of-reciprocals structure of A_1 for multilevel spectra cannot beat algorithms for plain mean estimation.

At schedule-level precision, bounded-treewidth instances remain tractable for exact A_1 computation (Proposition 9.6.5). The partition-function methods of the previous section show that ferromagnetic Ising models admit polynomial-time A_1 approximation at coarse precision (Proposition 9.6.4), but the required multiplicative accuracy forces exponential FPRAS runtime at the schedule-relevant precision $\delta_{A_1} = \Theta(2^{-n/2})$.

The interpolation theorem gives a quantitative law relating information to runtime. The sharpest formulation is a communication game.

Alice has the full classical description of H_z: all eigenvalues and degeneracies. Bob has a quantum computer with oracle access to H_z, and Alice may send C classical bits to Bob. Bob must find a ground state in at most T queries.

In the circuit model, Bob needs no message. He runs Dürr-Høyer and achieves $T = O(\sqrt{N/d_0})$ at $C = 0$. In the fixed-schedule adiabatic model, Bob must place the schedule's slowdown at the crossing, which requires knowing s^* to precision $O(2^{-n/2})$. This is $n/2$ bits of information. Each bit Alice sends cuts the adiabatic runtime in half. If Alice sends C bits encoding A_1 to precision $\varepsilon = \Theta(2^{-C})$, then

$$T(C) = T_{\text{inf}} \cdot \Theta(\max(1, 2^{n/2-C})).$$

Theorem 9.7.6 (Bit-runtime information law)**.** *The classical communication cost for the adiabatic model to achieve target runtime T satisfies*

$$C^*(T) = \max\left(0,\ \frac{n}{2} - \log_2 \frac{T}{T_{\text{inf}}}\right) + O(1),$$

while $C^*_{\text{circuit}}(T) = 0$ for all $T = \Omega(T_{\text{inf}})$.

Proof. From $T(C) = T_{\text{inf}} \cdot \Theta(\max(1, 2^{n/2-C}))$, there exist constants $a, b > 0$ with

$$a\, T_{\text{inf}} \max(1, 2^{n/2-C}) \le T(C) \le b\, T_{\text{inf}} \max(1, 2^{n/2-C}).$$

Inverting these inequalities gives $C = \max(0,\ n/2 - \log_2(T/T_{\text{inf}})) + O(1)$. The circuit statement follows because Dürr-Høyer achieves $T = O(T_{\text{inf}})$ with zero message. □

The complete model comparison, synthesizing this chapter with Chapter 8, is given below.

Model	Info needed	Runtime	Communication
Circuit (Dürr-Høyer)	None	$\Theta(\sqrt{N/d_0})$	0 bits
Fixed AQO, informed	A_1 to $2^{-n/2}$	$O(\sqrt{N/d_0})$	$\Theta(n)$ bits
Fixed AQO, C bits	A_1 to 2^{-C}	$T_{\text{inf}} \cdot \Theta(\max(1, 2^{n/2-C}))$	C bits
Fixed AQO, uninformed	None	$\Omega(2^{n/2}\, T_{\text{inf}})$	0 bits
Adaptive AQO	$O(n)$ measurements	$O(\sqrt{N/d_0})$	0 bits
Constant-control, two-level	None	$\Theta(\sqrt{N/d_0})$	0 bits
Quantum A_1 estimation	$\varepsilon = 2^{-n/2}$	$\Theta(2^{n/2})$ queries	—
Classical A_1 estimation	$\varepsilon = 2^{-n/2}$	$\Theta(2^n)$ queries	—

The table reveals a clean separation. The circuit model and the adaptive adiabatic model both achieve optimal performance with zero classical communication. The fixed adiabatic model traces a diagonal, with each missing bit of A_1 doubling the runtime. The $\Theta(n)$-bit gap between the fixed adiabatic model and the circuit model is exactly the information content of A_1 at schedule-relevant precision. This gap is a property of the computational model, not of the computational task. The circuit model does not somehow extract A_1 at zero cost. It does not need A_1 at all, because its mechanism (amplitude amplification) does not traverse the interpolation path where A_1 controls the crossing position.

The running example makes the tradeoff concrete. With $N = 4$, $d_0 = 1$, and $n = 2$, the circuit model uses $O(2)$ queries at $C = 0$. The informed adiabatic model also uses $O(2)$ queries, but only after receiving $C = 1$ bit encoding the crossing position. Without that bit, the fixed adiabatic model requires $\Omega(4)$ queries. The factor-of-two slowdown is exactly the cost of one missing bit.

These results organize into a five-level taxonomy of ignorance, measured by the multiplicative overhead T/T_{inf}:

Level	Information available	Overhead T/T_{inf}
0	None (uninformed fixed schedule)	$\Omega(2^{n/2})$
1	A_1 to precision ε	$\Theta(\max(1, \varepsilon/\delta_{A_1}))$
2	s^* in known interval $[u_L, u_R]$	$\Theta(\max(1,\ (u_R - u_L)/\delta_s))$
3	Quantum measurement access	$O(1)$ via $O(n)$ probes
4	Circuit model (no spectral info)	1

Levels 0 through 3 are monotone within the adiabatic framework. Each strictly refines the previous one by adding information about the spectrum. Level 4 is qualitatively different because it reflects a change in computational model rather than additional spectral information, so its inclusion in the hierarchy represents a model comparison rather than a refinement.

The adiabatic approach to unstructured search works, reaches Grover scaling, and is optimal within its schedule class. Its information requirements are a structural consequence of the rank-one interpolation path. The crossing position s^* encodes $\Theta(n)$ bits of spectral data, that data is NP-hard to compute classically, and no instance-independent design within the framework can eliminate the dependence. These are not fundamental limits of quantum computation. They are limits of this specific model. The circuit model, which does not traverse an interpolation path, neither needs nor reveals the spectral parameter A_1. The adaptive adiabatic model, which does traverse the path but can measure during evolution, acquires the missing information at the Grover scale. The fixed-schedule model, forced to commit before execution, pays for ignorance at a rate of one bit per factor of two in runtime.

The "information gap" is therefore three things at once. It is a spectral gap: the minimum of $g(s)$ along the interpolation path, which sets the adiabatic timescale and whose geometry controls the runtime spectrum of Section 9.4. It is an epistemic gap: the $\Theta(n)$ bits of A_1 that separate the informed schedule from the uninformed one, quantified by the interpolation theorem of Section 9.2 and the bit-runtime law of Theorem 9.7.6. And it is a model gap: the qualitative separation between computational models that need spectral information and those that do not, made precise by the no-go theorems of Section 9.5 and the A_1-blindness of the circuit model in Section 9.3. The next chapter translates these results into machine-checked formal proofs.

Chapter 10

Formalization

Formalization entered this thesis as a way to learn the subject. The UAQO argument is long. Spectral statistics feed gap geometry, gap geometry feeds runtime, and runtime pairs with hardness reductions. I did not trust my own understanding of how the pieces fit together. Reading the paper convinced me that each step was correct. It did not convince me that I could reproduce the argument, modify it, or find its weak points. I wanted a setting where I could take the argument apart and put it back together, and where mistakes would surface immediately instead of hiding in the comfort of informal prose.

Lean 4 [88] with Mathlib [89] gave me that setting. I encoded the main UAQO paper [10] as a Lean development, not to certify the results but to see what happens when every dependency is typed, every hypothesis is named, and the difference between "proved" and "assumed" is decided by a kernel rather than by authorial emphasis. That process changed how I understood the argument. Statements that looked like single claims split into independent results with different hypotheses. Definitions that seemed equivalent turned out to carry different side conditions. Proof decompositions that seemed natural on paper failed in Lean because they required transporting conditions across interfaces that did not match. Other decompositions that looked awkward on paper turned out to be the clean ones, because they aligned with how the mathematics actually factors.

The formal artifact lives in `src/lean/UAQO`. Restricting to the main-paper scope (excluding `Experiments` and `Test`), it contains 32 Lean files, 11,596 lines, zero active `sorry` terms, 15 explicit axioms, and 330 theorem and lemma declarations. It builds with `lake build`. The rest of this chapter describes what I learned from writing it.

10.1 What Formalization Taught Me

UAQO has the structure of a relay. The spectral parameters A_1 and A_2 determine where the avoided crossing sits and how sharp it is. The gap profile $g(s)$ along the adiabatic path is built from those parameters. The runtime comes from $\int g(s)^{-2}\,ds$. And the hardness results connect A_1 to NP and #P through reductions that use the spectral structure. Each handoff between these layers carries hypotheses, and in prose those hypotheses can drift. A condition established in one section gets applied three sections later with a slightly different scope, and nobody notices because the prose never forced the connection to be explicit.

Lean makes the connection explicit. Every hypothesis a theorem uses appears in its type. If a gap bound requires the eigenvalues to be strictly ordered, that requirement is a function argument. If a runtime statement needs a spectral condition, any theorem that calls it must supply evidence for that condition. I found this useful in a specific way. It showed me where I had been mentally bundling independent claims. Results that I read as a single argument on paper turned out to have components with genuinely different hypotheses. Lean would not let me state the combined version, so I had to find the correct factoring. That factoring improved the mathematics.

A concrete example illustrates this separation. The spectral analysis in the paper treats the eigenvalue characterization and the gap bounds as parts of one argument. In Lean, they separate cleanly. The theorem `eigenvalue_condition` (in `Spectral/GapBounds.lean`) is fully proved from the spectral structure. It characterizes when λ is an eigenvalue of $H(s)$ via the secular equation, and needs only that $M > 0$ and $s \in (0, 1)$. The regional gap bounds `gap_bound_left`, `gap_at_avoided_crossing`, and `gap_bound_right`, all in the same file, additionally require `FullSpectralHypothesis`, which packages a spectral regularity condition ($A_1 > 1$ and $\sqrt{d_0 A_2/N} < (A_1 + 1)/2$) that the eigenvalue condition does not need. The paper uses both the eigenvalue condition and the gap bounds together without separating their hypotheses. In Lean, a result that uses only the

secular equation cannot accidentally import the spectral hypothesis, and a change to the gap analysis cannot break the eigenvalue characterization. This is the kind of structural insight that I could not have found by reading alone.

The bigger payoff was that Lean let me experiment. I could try a candidate theorem shape, see whether it type-checked, and learn from the failure when it did not. On paper, discovering the right decomposition of a proof takes many failed attempts that leave no trace. In Lean, the failures are immediate and specific. A statement that looked elegant failed because a side condition could not be transported across a module boundary. A formulation that looked unnecessarily verbose turned out to be the right one because it matched a Mathlib interface I could reuse. I tested alternate decompositions of the secular equation analysis, tried different ways to package the spectral data, and ended up with interfaces that I would not have found without the type checker pushing back.

Some of that experimentation lives in dedicated experiment modules outside the main scope. The experiment files explore directions beyond the paper: coupled schedules, structured tractability, circumventing the interpolation barrier. This chapter stays focused on the main-paper formalization, but the experiments were part of the same learning process.

The idea that mathematical proofs should be fully explicit is old. Hilbert wanted it [90]. Homotopy type theory gave it computational content [91]. Lean 4 is a modern instance: a dependently typed language with a small trusted kernel and a growing mathematical library [88, 89]. Large formalizations have already been carried through in other proof assistants. The odd-order theorem was proved in Coq [92] and the Kepler conjecture in HOL Light and Isabelle [93]. Those projects showed that the method scales to substantial mathematics.

For UAQO, the formalization helps most at the interface between spectral analysis and complexity reductions. That interface is where the dependency chain is longest and where assumptions are hardest to track by hand. The spectral parameters feed into gap bounds, gap bounds feed into runtime, and runtime feeds into the hardness reductions. Each handoff carries conditions that must match, and in a typed system, mismatches surface as type errors rather than as silent bugs in a published proof.

10.2 Lean in Brief

In Lean, a proposition is a type and a proof is a term inhabiting that type. The trusted kernel checks that terms are well-typed. Tactics, automation, and elaboration must all produce a kernel-accepted term before they count as proved. Four pieces are enough to read the formal artifacts in this chapter. The *kernel* is the final checker. The *elaborator* fills in implicit arguments and typeclass instances. *Tactic mode* builds proof terms incrementally, with each tactic transforming a goal into simpler subgoals. And *definitional equality* lets some identities reduce by computation, so that proofs of equalities between unfolded definitions can collapse to `rfl`.

What makes this useful for mathematics is that every theorem carries its dependencies in its type. If a result needs an eigenvalue ordering, that ordering is a function argument. If a downstream theorem consumes a gap bound, it must supply the hypotheses that the gap bound requires. A change to the spectral data model breaks every theorem that depends on it, and the break shows up immediately. In UAQO, the same spectral interfaces get reused in gap bounds, runtime wrappers, and hardness reductions, so a single well-chosen interface saves a lot of repeated work.

What makes Lean painful is the overhead. Typeclass search can fail far from the source of the problem. Elaboration errors are often nonlocal. Coercing between `Nat`, `Int`, and `Real` is tedious in analysis-heavy files. I kept an abstraction only when it reduced total proof effort across the development. When it did not, I removed it.

A reader who wants to check any claim in this chapter can do so independently.

Listing 10.1: Rebuilding the development and inspecting axiom dependencies.

```
-- From the repository root:
cd src/lean
lake update
lake build

#print axioms UAQO.Complexity.mainResult2
#print axioms UAQO.Complexity.mainResult3
#print axioms UAQO.Adiabatic.adiabaticTheorem
```

The `#print axioms` command lists every axiom a theorem depends on, transitively. A theorem with no domain axioms is fully kernel-checked. A theorem that lists domain axioms depends on exactly those assumptions and no others.

10.3 How the Encoding Is Organized

The first design I tried was wrong. I modeled Hamiltonians at the matrix level, carrying full operator data through every theorem. This was faithful to the linear-algebraic picture but useless for the proofs I actually needed. Gap bounds, crossing positions, and runtime integrals depend on eigenvalues and degeneracies, not on matrix entries. Carrying matrix-level detail through spectral arguments added clutter without content and made it hard to reuse lemmas across modules.

The design that worked models instances through spectral structure. The central record is `EigenStructure`. It packages ordered eigenvalues, degeneracies, an assignment map from basis states to energy levels, and consistency invariants.

Listing 10.2: Core spectral data model reused across UAQO modules.

```
structure EigenStructure (n : Nat) (M : Nat) where
  eigenvalues : Fin M -> Real
  degeneracies : Fin M -> Nat
  assignment : Fin (qubitDim n) -> Fin M
  eigenval_bounds : forall k, 0 <= eigenvalues k /\ eigenvalues k <= 1
  eigenval_ordered : forall i j, i < j -> eigenvalues i < eigenvalues j
  ground_energy_zero : (hM : M > 0) -> eigenvalues (Fin.mk 0 hM) = 0
  deg_positive : forall k, degeneracies k > 0
  deg_sum : Finset.sum Finset.univ degeneracies = qubitDim n
  deg_count : forall k, degeneracies k =
    (Finset.filter (fun z => assignment z = k) Finset.univ).card
```

Eigenvalues are bounded in $[0, 1]$ and strictly ordered. Ground energy is zero. Degeneracies are positive and sum to $N = 2^n$. The assignment map and count field enforce that every basis state belongs to exactly one level. These invariants are checked once at construction time. Every downstream theorem inherits them for free, which eliminates a class of errors where a proof silently assumes an ordering that was never verified.

This interface turned out to be a genuine improvement over what I started with. Theorem statements got shorter. Hypotheses transported cleanly across modules. Complexity lemmas could reuse spectral facts without re-establishing them. The spectral parameters A_1, A_2, and the gap quantities are defined directly on `EigenStructure`, and bridge theorems connect them to alternative representations.

Listing 10.3: Direct encoding of A_1 with bridge theorem to partial representation.

```
noncomputable def spectralParam {n M : Nat} (es : EigenStructure n M)
    (hM : M > 0) (p : Nat) : Real :=
  let E0 := es.eigenvalues (Fin.mk 0 hM)
  let N := qubitDim n
  (1 / N) * Finset.sum (Finset.filter (fun k => k.val > 0) Finset.univ)
    (fun k => (es.degeneracies k : Real) / (es.eigenvalues k - E0)^p)

noncomputable def A1 {n M : Nat} (es : EigenStructure n M) (hM : M > 0) : Real :=
  spectralParam es hM 1

theorem A1_partial_eq_A1 {n M : Nat} (es : EigenStructure n M) (hM : M > 0) :
    A1_partial es.toPartial hM = A1 es hM := by
  simp only [A1_partial, A1, spectralParam, EigenStructure.toPartial, pow_one]
```

The bridge theorem `A1_partial_eq_A1` is typical. Two representations of A_1 are defined independently and proved equal. One uses the full spectral definition and the other a partial-information variant. The proof is a single-line simplification, meaning the equality holds by unfolding definitions. Downstream code uses whichever representation is more convenient, and the bridge guarantees that results transfer.

Table 10.1 gives the size of the main-paper development.

Table 10.1: Main-paper scope in `src/lean/UAQO` (excluding `Experiments` and `Test`).

Component	Files	Approx. LOC	Role in proof architecture
Foundations	5	1,067	Hilbert-space and operator preliminaries consumed by later layers
Spectral	4	1,348	A_p definitions, crossing quantities, and gap-facing interfaces
Adiabatic	4	1,254	Schedule and runtime interfaces for adiabatic statements
Complexity	5	2,428	SAT and counting encodings, hardness interfaces, extraction contracts
Proofs	14	5,499	Lemma layer for secular analysis, interpolation, combinatorics, and verification support
Total	32	11,596	Zero active `sorry` terms and 15 explicit `axiom` declarations

Within this scope, the development contains 330 theorem and lemma declarations. The five components mirror the dependency structure of the UAQO argument itself: foundations feeds spectral, spectral feeds adiabatic and complexity, and proofs supports all four.

Table 10.2 pairs each headline claim of the chapter with the Lean artifacts that back it and their epistemic status.

Table 10.2: Claim-to-artifact map for the Chapter 10 argument.

Chapter claim	Primary Lean artifact	Epistemic status
Paper formulas for A_p, s^*, δ_s, $g_{\min}$ are represented faithfully	`Spectral/SpectralParameters`, `Test/Verify`	Definitional equality checks (`rfl`)
Two-query NP-hardness core is formally encoded	`Complexity/Hardness` (`mainResult2`)	Proved modulo `gareyJohnsonEncoding` axiom
Counting extraction bridge to #P statement is formalized	`Complexity/Hardness` (`mainResult3`)	Machine-checked theorem core
Global gap-profile runtime claims require additional spectral interface	`Proofs/Spectral/GapBoundsProofs`	Conditional via `FullSpectralHypothesis`
Adiabatic transfer theorems are wrappers over explicit physics interfaces	`Adiabatic/Theorem`	Axiom-mediated

Rows mentioning `Test/Verify` refer to audit wrappers, not to the proofs themselves. The definitions and proofs live in the main-scope modules listed in the same row.

10.4 Two Proof Paths

Tables describe what is proved. To see how a proof moves through the formal system, it helps to trace two concrete paths: the NP reduction from Chapter 8, and the counting bridge behind the #P extraction.

The theorem `mainResult2` formalizes the two-query reduction. Given a 3-CNF formula f, it constructs a Garey-Johnson encoding, computes the two-query difference D, and proves $D = 0$ if and only if f is satisfiable.

Listing 10.4: Proof skeleton of `mainResult2`.

```
theorem mainResult2 (f : CNFFormula) (hf : is_kCNF 3 f) :
    let enc := gareyJohnsonEncoding f hf
    let D := twoQueryDifference enc.es enc.hLevels
    (D = 0) <-> isSatisfiable f := by
```

```
  intro enc D
  constructor
  intro hD
  by_contra hunsat
  have hE0_pos := enc.unsat_ground_pos hunsat
  have hexcited := enc.unsat_excited_pop hunsat
  have hD_pos := twoQuery_unsat enc.es enc.hLevels hE0_pos enc.excited_pos hexcited
  linarith
  intro hsat
  have hE0_zero := enc.sat_ground_zero hsat
  exact twoQuery_sat enc.es enc.hLevels hE0_zero
```

The script is short because the work lives in helper lemmas. The satisfiable branch: `sat_ground_zero` shows a satisfying assignment forces $E_0 = 0$, then `twoQuery_sat` shows $D = 0$. The unsatisfiable branch: `unsat_ground_pos` gives $E_0 > 0$, `unsat_excited_pop` gives populated excited levels, `twoQuery_unsat` gives $D > 0$, and `linarith` closes the contradiction. The only axiom in the chain is the Garey-Johnson encoding interface, which packages a classical graph-coloring reduction that Mathlib does not yet cover. Once that interface is fixed, everything else is checked.

The second path is the counting bridge behind #P extraction. Informal proofs compress the step from satisfying assignments to a counting identity into a sentence. I made it a separate theorem.

Listing 10.5: Bridge theorem from semantic satisfiability to counting identity.

```
private theorem countZeroUnsatisfied_eq_numSatisfying (f : CNFFormula) :
    countAssignmentsWithKUnsatisfied f 0 = numSatisfyingAssignments f := by
  simp only [countAssignmentsWithKUnsatisfied, numSatisfyingAssignments]
  congr 1
  ext z
  simp only [Finset.mem_filter, Finset.mem_univ, true_and]
  rw [<- satisfies_iff_countUnsatisfied_zero]
  rfl
```

The statement looks trivial: assignments with zero unsatisfied clauses are satisfying assignments. But formally, the two filtering predicates must be shown extensionally equal, which requires unfolding both definitions and using a separately proved equivalence. Once this bridge exists, every downstream theorem imports it mechanically instead of re-arguing the point. The extraction chain from satisfiability to counting polynomial to #P is stabilized because each link is a named, proved artifact.

Both paths have the same shape. High-level scripts are five to fifteen lines. The real work is in interface lemmas with explicit hypotheses. The type checker enforces that hypotheses match at every call site. If they do not match, the proof fails to compile. This is the main reason formalization was worth the effort. The value is not that it makes proofs more clever, but that it catches mismatches I would have missed.

The type checker enforces what is proved. The next question is what is not proved, and how the development marks that boundary.

10.5 Assumptions and Boundaries

The formalization does not prove the full UAQO argument from first principles. It proves the NP-hardness and #P-hardness reductions in full (modulo one classical encoding axiom), and it proves the spectral parameter identities by definitional equality. But the resolvent-based gap analysis from Sections 2–3 of the paper, which connects spectral parameters to runtime bounds, is not formalized. Instead, it enters the development through `FullSpectralHypothesis`, which is carried as an explicit hypothesis rather than buried as an axiom.

Listing 10.6: Explicit hypothesis for full spectral-gap profile claims.

```
structure FullSpectralHypothesis {n M : Nat} (es : EigenStructure n M) (hM : M >= 2) : Prop where
  cond : spectralConditionForBounds es hM
  gap : forall (s : Real) (hs : 0 <= s /\ s <= 1) (E0 E1 : Real),
    IsEigenvalue (adiabaticHam es s hs) E0 ->
    IsEigenvalue (adiabaticHam es s hs) E1 ->
    E0 < E1 -> E1 - E0 >= minimumGap es hM
```

It packages a spectral regularity condition and a uniform gap lower bound. Any theorem that needs the full gap profile must supply this hypothesis. Any reader can check whether a given theorem actually supplies it or only assumes it.

The development declares 15 explicit axioms, grouped in Table 10.3.

Table 10.3: Axiom groups in the UAQO main-paper formalization.

Group	Count	Representative content
Primitive interfaces	3	Polynomial-time predicate, Schrodinger-evolution predicate, degeneracy-count interface
Standard complexity interfaces	3	Membership and hardness interfaces for 3-SAT and #3-SAT classes
Quantum dynamics interfaces	6	Adiabatic transfer bounds, local-schedule transfer, phase-randomization transfer, unstructured-search lower-bound interface
Paper-specific interfaces	3	Garey-Johnson encoding and reduction bridges used in UAQO hardness statements
Total	15	Every assumption is declared by `axiom` and inspectable via `#print axioms`

The primitive interfaces axiomatize concepts that current Lean libraries cannot define natively: polynomial-time computation, Schrodinger evolution, degeneracy counting. The complexity interfaces encode standard results such as Cook-Levin for 3-SAT [6] and Valiant for #3-SAT [8]. The quantum dynamics interfaces package results like the Jansen-Ruskai-Seiler adiabatic bound [17]. As Lean libraries grow, individual axioms can be discharged and replaced by proofs. The development is structured so that discharging an axiom narrows the trust boundary without requiring any downstream theorem to be rewritten.

AI helped with the exploratory phase. I used it to propose theorem shapes, suggest decompositions, and draft bridge lemmas. But AI suggestions needed checking, because they often solved a local goal by importing stronger assumptions than necessary. A tactic script that closes the current goal is not the same as a tactic script that closes it under the right hypotheses. The discipline was simple: temporary `sorry` during design, no `sorry` in the delivered code, and `#print axioms` on every result before accepting it. Anything that could not be proved became a named axiom with a citation.

Formal methods for quantum computing have mostly focused on circuit-level verification: QWIRE [94] and SQIR [95] verify gate-level programs, CoqQ [96] reasons about quantum program semantics, and Isabelle-based work [97] targets quantum protocols. None of these tools handle spectral analysis or complexity reductions. They operate at the circuit abstraction, where the relevant objects are gates and registers rather than eigenvalues and spectral gaps. This development works at a different layer. It carries spectral structure through to hardness reductions in a single typed system. The cost is that the quantum dynamics (the adiabatic theorem, the transfer bounds) enter as axioms rather than as proved results, because formalizing the resolvent calculus underlying those bounds is a separate project. The approach follows the pattern of earlier large formalizations [92, 93]: quantitative scope, reproducible build, explicit assumption ledger, honest boundary between proved and assumed.

The mathematics in the source paper belongs to its authors [10]. The Lean code, the experiments, and the workflow described here are my path through their argument. A reader who finishes this chapter can rebuild the artifact, inspect any theorem's dependencies, and start extending the formal interfaces for new problems in adiabatic quantum optimization.

Chapter 11

Conclusion

Bibliography

[1] Lov K. Grover. A fast quantum mechanical algorithm for database search. In *Proceedings of the 28th Annual ACM Symposium on Theory of Computing*, pages 212–219, 1996. doi:10.1145/237814.237866.

[2] Charles H. Bennett, Ethan Bernstein, Gilles Brassard, and Umesh Vazirani. Strengths and weaknesses of quantum computing. *SIAM Journal on Computing*, 26(5):1510–1523, 1997. doi:10.1137/S0097539796300933.

[3] Sanjeev Arora and Boaz Barak. *Computational Complexity: A Modern Approach*. Cambridge University Press, 2009.

[4] David Deutsch. Quantum theory, the Church-Turing principle and the universal quantum computer. *Proceedings of the Royal Society A*, 400(1818):97–117, 1985. doi:10.1098/rspa.1985.0070.

[5] Ethan Bernstein and Umesh Vazirani. Quantum complexity theory. *SIAM Journal on Computing*, 26(5): 1411–1473, 1997. doi:10.1137/S0097539796300921.

[6] Stephen A. Cook. The complexity of theorem-proving procedures. In *Proceedings of the Third Annual ACM Symposium on Theory of Computing (STOC)*, pages 151–158, 1971. doi:10.1145/800157.805047.

[7] Richard M. Karp. *Reducibility among Combinatorial Problems*, pages 85–103. Springer US, 1972. doi:10.1007/978-1-4684-2001-2_9.

[8] Leslie G. Valiant. The complexity of enumeration and reliability problems. *SIAM Journal on Computing*, 8(3):410–421, 1979. doi:10.1137/0208032.

[9] Seinosuke Toda. PP is as hard as the polynomial-time hierarchy. *SIAM Journal on Computing*, 20(5): 865–877, 1991. doi:10.1137/0220053.

[10] Arthur Braida, Shantanav Chakraborty, Alapan Chaudhuri, Joseph Cunningham, Rutvij Menavlikar, Leonardo Novo, and Jérémie Roland. Unstructured adiabatic quantum optimization: Optimality with limitations. *arXiv preprint arXiv:2411.05736*, 2024.

[11] F. Barahona. On the computational complexity of Ising spin glass models. *Journal of Physics A: Mathematical and General*, 15(10):3241–3253, 1982. doi:10.1088/0305-4470/15/10/028.

[12] Andrew Lucas. Ising formulations of many NP problems. *Frontiers in Physics*, 2:5, 2014. doi:10.3389/fphy.2014.00005.

[13] Edward Farhi, Jeffrey Goldstone, Sam Gutmann, and Michael Sipser. Quantum computation by adiabatic evolution. *arXiv:quant-ph/0001106*, 2000. doi:10.48550/arXiv.quant-ph/0001106.

[14] Edward Farhi, Jeffrey Goldstone, Sam Gutmann, Joshua Lapan, Andrew Lundgren, and Daniel Preda. A quantum adiabatic evolution algorithm applied to random instances of an NP-complete problem. *Science*, 292(5516):472–475, 2001. doi:10.1126/science.1057726.

[15] Max Born and Vladimir Fock. Beweis des adiabatensatzes. *Zeitschrift für Physik*, 51:165–180, 1928. doi:10.1007/BF01343193.

[16] Tosio Kato. On the adiabatic theorem of quantum mechanics. *Journal of the Physical Society of Japan*, 5 (6):435–439, 1950.

[17] Sabine Jansen, Mary-Beth Ruskai, and Ruedi Seiler. Bounds for the adiabatic approximation with applications to quantum computation. *Journal of Mathematical Physics*, 48(10):102111, 2007. doi:10.1063/1.2798382.

[18] Alexander Elgart and George A. Hagedorn. A note on the switching adiabatic theorem. *Journal of Mathematical Physics*, 53(10), 2012. doi:10.1063/1.4748968.

[19] Lev D. Landau. Zur theorie der energieubertragung. ii. *Physikalische Zeitschrift der Sowjetunion*, 2: 46–51, 1932.

[20] Clarence Zener. Non-adiabatic crossing of energy levels. *Proceedings of the Royal Society A*, 137(833): 696–702, 1932. doi:10.1098/rspa.1932.0165.

[21] Julia Kempe, Alexei Kitaev, and Oded Regev. The complexity of the local Hamiltonian problem. *SIAM Journal on Computing*, 35(5):1070–1097, 2006. doi:10.1137/S0097539704445226.

[22] Scott Kirkpatrick, C. Daniel Gelatt, and Mario P. Vecchi. Optimization by simulated annealing. *Science*, 220(4598):671–680, 1983. doi:10.1126/science.220.4598.671.

[23] Nicholas Metropolis, Arianna W. Rosenbluth, Marshall N. Rosenbluth, Augusta H. Teller, and Edward Teller. Equation of state calculations by fast computing machines. *The Journal of Chemical Physics*, 21 (6):1087–1092, 1953. doi:10.1063/1.1699114.

[24] Elizabeth Crosson and Aram W. Harrow. Simulated quantum annealing can be exponentially faster than classical simulated annealing. In *2016 IEEE 57th Annual Symposium on Foundations of Computer Science (FOCS)*, pages 714–723, 2016. doi:10.1109/FOCS.2016.81.

[25] Paul A. M. Dirac. *The Principles of Quantum Mechanics*. Oxford University Press, 1930.

[26] John von Neumann. *Mathematical Foundations of Quantum Mechanics*. Princeton University Press, 1955. English translation by Robert T. Beyer; original German 1932.

[27] Michael A. Nielsen and Isaac L. Chuang. *Quantum Computation and Quantum Information*. Cambridge University Press, 10th anniversary edition, 2010. doi:10.1017/CBO9780511976667.

[28] Adriano Barenco, Charles H. Bennett, Richard Cleve, David P. DiVincenzo, Norman Margolus, Peter Shor, Tycho Sleator, John A. Smolin, and Harald Weinfurter. Elementary gates for quantum computation. *Physical Review A*, 52(5):3457–3467, 1995. doi:10.1103/PhysRevA.52.3457.

[29] Alexei Yu. Kitaev, Alexander H. Shen, and Mikhail N. Vyalyi. *Classical and Quantum Computation*, volume 47 of *Graduate Studies in Mathematics*. American Mathematical Society, 2002.

[30] Christopher M. Dawson and Michael A. Nielsen. The Solovay-Kitaev algorithm. *Quantum Information and Computation*, 6(1):81–95, 2006.

[31] John Watrous. Quantum computational complexity. *Encyclopedia of Complexity and Systems Science*, pages 7174–7201, 2009. doi:10.1007/978-0-387-30440-3_428.

[32] Christoph Dürr and Peter Høyer. A quantum algorithm for finding the minimum. *arXiv preprint quant-ph/9607014*, 1996.

[33] Michel Boyer, Gilles Brassard, Peter Høyer, and Alain Tapp. Tight bounds on quantum searching. *Fortschritte der Physik*, 46(4-5):493–505, 1998. doi:10.1002/(SICI)1521-3978(199806)46:4/5<493::AID-PROP493>3.0.CO;2-P.

[34] Gilles Brassard, Peter Høyer, Michele Mosca, and Alain Tapp. Quantum amplitude amplification and estimation. *Contemporary Mathematics*, 305:53–74, 2002. doi:10.1090/conm/305/05215.

[35] Ashwin Nayak and Felix Wu. The quantum query complexity of approximating the median and related statistics. In *Proceedings of the 31st Annual ACM Symposium on Theory of Computing (STOC)*, pages 384–393, 1999. doi:10.1145/301250.301349.

[36] Edward Farhi, Jeffrey Goldstone, Sam Gutmann, and Daniel Nagaj. How to make the quantum adiabatic algorithm fail. *International Journal of Quantum Information*, 6(03):503–516, 2008. doi:10.1142/S021974990800358X.

[37] Dorit Aharonov, Wim van Dam, Julia Kempe, Zeph Landau, Seth Lloyd, and Oded Regev. Adiabatic quantum computation is equivalent to standard quantum computation. *SIAM Journal on Computing*, 37 (1):166–194, 2007. doi:10.1137/S0097539705447323.

[38] Jeremie Roland and Nicolas J. Cerf. Quantum search by local adiabatic evolution. *Physical Review A*, 65 (4):042308, 2002. doi:10.1103/PhysRevA.65.042308.

[39] Boris Altshuler, Hari Krovi, and Jérémie Roland. Anderson localization makes adiabatic quantum optimization fail. *Proceedings of the National Academy of Sciences*, 107(28):12446–12450, 2010. doi:10.1073/pnas.1002116107.

[40] Tameem Albash and Daniel A. Lidar. Adiabatic quantum computation. *Reviews of Modern Physics*, 90: 015002, 2018. doi:10.1103/RevModPhys.90.015002.

[41] W. van Dam, M. Mosca, and U. Vazirani. How powerful is adiabatic quantum computation? In *Proceedings 42nd IEEE Symposium on Foundations of Computer Science*, pages 279–287, 2001. doi:10.1109/SFCS.2001.959902.

[42] Xi Guo and Dong An. Improved gap dependence in adiabatic state preparation by adaptive schedule. *arXiv preprint arXiv:2512.10329*, 2025.

[43] Dorit Aharonov and Amnon Ta-Shma. Adiabatic quantum state generation and statistical zero knowledge. In *Proceedings of the 35th Annual ACM Symposium on Theory of Computing*, pages 20–29, 2003. doi:10.1145/780542.780546.

[44] Hari Krovi, Maris Ozols, and Jérémie Roland. Adiabatic condition and the quantum hitting time of Markov chains. *Physical Review A*, 82:022333, 2010. doi:10.1103/PhysRevA.82.022333.

[45] Rolando D. Somma, Daniel Nagaj, and Mária Kieferová. Quantum speedup by quantum annealing. *Physical Review Letters*, 109:050501, 2012. doi:10.1103/PhysRevLett.109.050501.

[46] Silvano Garnerone, Paolo Zanardi, and Daniel A. Lidar. Adiabatic quantum algorithm for search engine ranking. *Physical Review Letters*, 108:230506, 2012. doi:10.1103/PhysRevLett.108.230506.

[47] Yiğit Subaşı, Rolando D. Somma, and Davide Orsucci. Quantum algorithms for systems of linear equations inspired by adiabatic quantum computing. *Physical Review Letters*, 122:060504, 2019. doi:10.1103/PhysRevLett.122.060504.

[48] Dong An and Lin Lin. Quantum linear system solver based on time-optimal adiabatic quantum computing and quantum approximate optimization algorithm. *ACM Transactions on Quantum Computing*, 3(2), 2022. doi:10.1145/3498331.

[49] Dominic W. Berry, Andrew M. Childs, Yuan Su, Xin Wang, and Nathan Wiebe. Time-dependent Hamiltonian simulation with l^1-norm scaling. *Quantum*, 4:254, 2020. doi:10.22331/q-2020-04-20-254.

[50] Yimin Ge, Jordi Tura, and J. Ignacio Cirac. Faster ground state preparation and high-precision ground energy estimation with fewer qubits. *Journal of Mathematical Physics*, 60(2):022202, 2019. doi:10.1063/1.5027484.

[51] Lin Lin and Yu Tong. Near-optimal ground state preparation. *Quantum*, 4:372, 2020. doi:10.22331/q-2020-12-14-372.

[52] Alexander M. Dalzell, Nicola Pancotti, Earl T. Campbell, and Fernando G.S.L. Brandão. Mind the gap: Achieving a super-Grover quantum speedup by jumping to the end. In *Proceedings of the 55th Annual ACM Symposium on Theory of Computing*, pages 1131–1144, 2023. doi:10.1145/3564246.3585203.

[53] Matthew B. Hastings and Michael H. Freedman. Obstructions to classically simulating the quantum adiabatic algorithm. *Quantum Information and Computation*, 13(11–12):1038–1076, 2013.

[54] Mark W Johnson, Mohammad HS Amin, Suzanne Gildert, Trevor Lanting, Firas Hamze, Neil Dickson, Richard Harris, Andrew J Berkley, Jan Johansson, Paul Bunyk, et al. Quantum annealing with manufactured spins. *Nature*, 473(7346):194–198, 2011. doi:10.1038/nature10012.

[55] Ben W. Reichardt. The quantum adiabatic optimization algorithm and local minima. In *Proceedings of the 36th Annual ACM Symposium on Theory of Computing*, pages 502–510, 2004. doi:10.1145/1007352.1007428.

[56] Vicky Choi. Different adiabatic quantum optimization algorithms for the NP-complete exact cover and 3SAT problems. *Quantum Information and Computation*, 11(7–8):638–648, 2011.

[57] Adam Callison, Nicholas Chancellor, Florian Mintert, and Viv Kendon. Finding spin glass ground states using quantum walks. *New Journal of Physics*, 21(12):123022, 2019. doi:10.1088/1367-2630/ab5ca2.

[58] Matthew B. Hastings. The power of adiabatic quantum computation with no sign problem. *Quantum*, 5: 597, 2021. doi:10.22331/q-2021-12-06-597.

[59] András Gilyén, Matthew B. Hastings, and Umesh Vazirani. (sub)exponential advantage of adiabatic quantum computation with no sign problem. In *Proceedings of the 53rd Annual ACM SIGACT Symposium on Theory of Computing*, pages 1357–1369, 2021. doi:10.1145/3406325.3451060.

[60] Jeremie Roland and Nicolas J. Cerf. Quantum search by local adiabatic evolution. *Physical Review A*, 65 (4):042308, 2002. doi:10.1103/PhysRevA.65.042308.

[61] Marko Žnidarič and Martin Horvat. Exponential complexity of an adiabatic algorithm for an NP-complete problem. *Physical Review A*, 73:022329, 2006. doi:10.1103/PhysRevA.73.022329.

[62] Itay Hen. Continuous-time quantum algorithms for unstructured problems. *Journal of Physics A: Mathematical and Theoretical*, 47(4):045305, 2014. doi:10.1088/1751-8113/47/4/045305.

[63] Arthur Braida. *Analog Quantum Computing for NP-Hard Combinatorial Graph Problems*. PhD thesis, Université d'Orléans, 2024.

[64] Gene H. Golub. Some modified matrix eigenvalue problems. *SIAM Review*, 15(2):318–334, 1973. doi:10.1137/1015032.

[65] Shantanav Chakraborty, Leonardo Novo, and Jérémie Roland. Optimality of spatial search via continuous-time quantum walks. *Physical Review A*, 102:032214, 2020. doi:10.1103/PhysRevA.102.032214.

[66] Jack Sherman and Winifred J. Morrison. Adjustment of an inverse matrix corresponding to a change in one element of a given matrix. *The Annals of Mathematical Statistics*, 21(1):124–127, 1950. doi:10.1214/aoms/1177729893.

[67] Andrew M. Childs and Jeffrey Goldstone. Spatial search by quantum walk. *Physical Review A*, 70: 022314, 2004. doi:10.1103/PhysRevA.70.022314.

[68] Shantanav Chakraborty, Leonardo Novo, Andris Ambainis, and Yasser Omar. Spatial search by quantum walk is optimal for almost all graphs. *Physical Review Letters*, 116:100501, 2016. doi:10.1103/PhysRevLett.116.100501.

[69] Sergio Boixo, Emanuel Knill, and Rolando Somma. Eigenpath traversal by phase randomization. *Quantum Information and Computation*, 9(9&10):833–855, 2009.

[70] Joseph Cunningham and Jérémie Roland. Eigenpath traversal by Poisson-distributed phase randomisation. In *19th Conference on the Theory of Quantum Computation, Communication and Cryptography (TQC 2024)*, pages 7:1–7:20, 2024. doi:10.4230/LIPIcs.TQC.2024.7.

[71] M.R. Garey, D.S. Johnson, and L. Stockmeyer. Some simplified NP-complete graph problems. *Theoretical Computer Science*, 1(3):237–267, 1976. doi:10.1016/0304-3975(76)90059-1.

[72] George M. Phillips. *Interpolation and Approximation by Polynomials*, volume 14. Springer Science & Business Media, 2003. doi:10.1007/b97417.

[73] Ramis Movassagh. The hardness of random quantum circuits. *Nature Physics*, 19(11):1719–1724, 2023. doi:10.1038/s41567-023-02131-2.

[74] Ramamohan Paturi. On the degree of polynomials that approximate symmetric Boolean functions. In *Proceedings of the 24th Annual ACM Symposium on Theory of Computing*, pages 468–474, 1992. doi:10.1145/129712.129758.

[75] Scott Aaronson and Alex Arkhipov. The computational complexity of linear optics. In *Proceedings of the 43rd Annual ACM Symposium on Theory of Computing*, pages 333–342, 2011. doi:10.1145/1993636.1993682.

[76] Michael J. Bremner, Ashley Montanaro, and Dan J. Shepherd. Achieving quantum supremacy with sparse and noisy commuting quantum computations. *Quantum*, 1:8, 2017. doi:10.22331/q-2017-04-25-8.

[77] Adam Bouland, Bill Fefferman, Chinmay Nirkhe, and Umesh Vazirani. On the complexity and verification of quantum random circuit sampling. *Nature Physics*, 15(2):159–163, 2019. doi:10.1038/s41567-018-0318-2.

[78] Lucien Le Cam. Convergence of estimates under dimensionality restrictions. *The Annals of Statistics*, 1 (1):38–53, 1973. doi:10.1214/aos/1176342150.

[79] Vittorio Giovannetti, Seth Lloyd, and Lorenzo Maccone. Quantum metrology. *Physical Review Letters*, 96:010401, 2006. doi:10.1103/PhysRevLett.96.010401.

[80] Samuel L. Braunstein and Carlton M. Caves. Statistical distance and the geometry of quantum states. *Physical Review Letters*, 72(22):3439–3443, 1994. doi:10.1103/PhysRevLett.72.3439.

[81] Leonid Gurvits. On the complexity of mixed discriminants and related problems. In *Proceedings of the 30th International Conference on Mathematical Foundations of Computer Science*, pages 447–458. Springer-Verlag, 2005. doi:10.1007/11549345_39.

[82] Mancheon Han, Hyowon Park, and Sangkook Choi. The constant geometric speed schedule for adiabatic state preparation: Towards quadratic speedup without prior spectral knowledge, 2025.

[83] Eduardo Araújo, Shantanav Chakraborty, and Leonardo Novo. Advantages and limitations of analog quantum search methods. *In preparation*, 2025.

[84] Edward Farhi and Sam Gutmann. Analog analogue of a digital quantum computation. *Physical Review A*, 57(4):2403–2406, 1998. doi:10.1103/PhysRevA.57.2403.

[85] Wassily Hoeffding. Probability inequalities for sums of bounded random variables. *Journal of the American Statistical Association*, 58(301):13–30, 1963. doi:10.1080/01621459.1963.10500830.

[86] Mark Jerrum and Alistair Sinclair. Polynomial-time approximation algorithms for the ising model. *SIAM Journal on Computing*, 22(5):1087–1116, 1993.

[87] Russell Impagliazzo, Ramamohan Paturi, and Francis Zane. Which problems have strongly exponential complexity? *Journal of Computer and System Sciences*, 63(4):512–530, 2001. doi:10.1006/jcss.2001.1774.

[88] Leonardo de Moura and Sebastian Ullrich. The Lean 4 theorem prover and programming language. In *Proceedings of the 28th International Conference on Automated Deduction (CADE-28)*, volume 12699 of *Lecture Notes in Computer Science*, pages 625–635. Springer, 2021. doi:10.1007/978-3-030-79876-5_37.

[89] The mathlib Community. The Lean mathematical library. *Proceedings of the 9th ACM SIGPLAN International Conference on Certified Programs and Proofs*, pages 367–381, 2020. doi:10.1145/3372885.3373824.

[90] David Hilbert. Mathematical problems. *Bulletin of the American Mathematical Society*, 8(10):437–479, 1902. doi:10.1090/S0002-9904-1902-00923-3.

[91] The Univalent Foundations Program. *Homotopy Type Theory: Univalent Foundations of Mathematics*. Institute for Advanced Study, 2013. URL `https://homotopytypetheory.org/book`.

[92] Georges Gonthier, Andrea Asperti, Jeremy Avigad, Yves Bertot, Cyril Cohen, Francois Garillot, Stephane Le Roux, Assia Mahboubi, Russell O'Connor, Sidi Ould Biha, Ioana Pasca, Laurence Rideau, Alexey Solovyev, Enrico Tassi, and Laurent Théry. A machine-checked proof of the odd order theorem. In *Interactive Theorem Proving*, volume 7998 of *Lecture Notes in Computer Science*, pages 163–179. Springer, 2013. doi:10.1007/978-3-642-39634-2_14.

[93] Thomas Hales, Mark Adams, Gertrud Bauer, Tat Dat Dang, John Harrison, Le Truong Hoang, Cezary Kaliszyk, Victor Magron, Sean McLaughlin, Tat Thang Nguyen, Quang Truong Nguyen, Tobias Nipkow, Steven Obua, Josef Pleso, Jason Rute, Alexey Solovyev, Thi Hoai An Ta, Nam Trung Tran, Trieu Thi Diep, Josef Urban, Ky Vu, and Roland Zumkeller. A formal proof of the kepler conjecture. *Forum of Mathematics, Pi*, 5:e2, 2017. doi:10.1017/fmp.2017.1.

[94] Robert Rand, Jennifer Paykin, and Steve Zdancewic. QWIRE practice: Formal verification of quantum circuits in Coq. In *Proceedings of the 14th International Conference on Quantum Physics and Logic (QPL)*, volume 266 of *Electronic Proceedings in Theoretical Computer Science*, pages 119–132, 2018. doi:10.4204/EPTCS.266.8.

[95] Kesha Hietala, Robert Rand, Shih-Han Hung, Xiaodi Wu, and Michael Hicks. A verified optimizer for quantum circuits. *Proceedings of the ACM on Programming Languages*, 5(POPL):1–29, 2021. doi:10.1145/3434318.

[96] Li Zhou, Gilles Barthe, Pierre-Yves Strub, Junyi Liu, and Mingsheng Ying. CoqQ: Foundational verification of quantum programs. *Proceedings of the ACM on Programming Languages (POPL)*, 7 (POPL):833–865, 2023. doi:10.1145/3571222.

[97] Jaap Boender, Florian Kammüller, and Rajagopal Nagarajan. Formalization of quantum protocols using Coq. *Electronic Proceedings in Theoretical Computer Science*, 195:71–83, 2015. doi:10.4204/EPTCS.195.6.